

**COMPUTATIONAL NEURAL MODELS AT MOLECULAR,
CELLULAR AND BEHAVIORAL LEVELS
- THREE CASE STUDIES**

A Dissertation presented to the Faculty of the Graduate School
University of Missouri

In Partial Fulfillment
Of the Requirement for the Degree

Doctorate in Philosophy

by
ASHWIN MOHAN

Dr. Satish S. Nair, Dissertation Supervisor

DECEMBER 2009

The undersigned, appointed by the Dean of the Graduate School, have examined the dissertation
entitled

COMPUTATIONAL NEURAL MODELS AT MOLECULAR,
CELLULAR AND BEHAVIORAL LEVELS
- THREE CASE STUDIES

Presented by Ashwin Mohan

A candidate for the degree of Doctor of Philosophy

And hereby certify that in their opinion it is worthy of acceptance.

Dr. Satish S. Nair

Dr. Dominic Ho

Dr. Robert McLaren

Dr. Reginald Cocroft

Dr. Jyotsna Nair

To my wife, Svaathi, for her unconditional love and commitment

To my parents, Bhamini and Mohan, for their unequivocal dedication towards my education and having provided the foundation on which I could come this far

To Mutha and Manni, for providing the vision to undertake this journey

To my in-laws, Subramanian and Revathi for their patience

To Prabha and Ravi, for the love and support

To Santhosh and Renu, for their friendship

To Kishore, Venkat and Zhivago, for never giving up on me

To my extended family, for their affection

To Ajja, Patti and Jayanth, who shall forever be in my thoughts

ACKNOWLEDGEMENTS

I wish to express my gratitude to Dr. Satish S. Nair for introducing me to the world of computational neuroscience. The Ph.D. research work was one of the most enjoyable experiences. I am confident the cross-training received under you will serve me well in the years to come.

I wish to thank Dr. Reginald Cocroft for co-advising on the agent based modeling project studying antipredator signals in treehoppers. I wish to thank Dr. Peter Kalivas, for his input and encouragement while modeling neuroplasticity due to cocaine. I have learnt immensely about interacting and collaborating with scientists from you both.

I thank Dr. Robert McLaren who advised me during the initial part of the Ph.D. research. Special thanks to the committee members Dr. Dominic Ho and Dr. Jyotsna Nair for taking the time out to review my research work.

I thank all my colleagues, especially Sandeep, Marianne and Russell, with whom I enjoyed working so much. Charlie and Henry for working relentlessly with me in these last few months. Guoshi, John, and Ali, it was fun working with you. To all involved, thank you.

TABLE OF CONTENTS

ACKNOWLEDGMENTS	ii
LIST OF ILLUSTRATIONS	vi
LIST OF TABLES	ix
LIST OF NORMENCLATURE	xi
ABSTRACT	xiv
CHAPTER 1: Introduction and Objectives	
1.1 Background and Motivation	1
1.2 Chapter Overview and Objectives	2
<u>MOLECULAR LEVEL – Modeling neuroplasticity due to cocaine</u>	
CHAPTER 2: Computational models of neuronal networks — Modeling neuroplasticity in PFC-NAc glutamate transmission due to cocaine	
2.1 Introduction and Overview.....	7
2.2 Systems approaches in neuroscience	8
2.3 Computational research in cocaine addiction	30
2.4 Conclusions	62
2.5 References	63
2.6 Tables	69
2.7 Figures	71
CHAPTER 3: Molecular diffusion model of glutamate homeostasis in nucleus accumbens neuropil incorporates neuroadaptations due to chronic cocaine	
3.1 Abstract	80
3.2 Introduction	80
3.3 Methods	82

3.4 Results	91
3.5 Discussions	97
3.6 Conclusions	101
3.7 References	102
3.8 Tables	107
3.9 Figures	110

NETWORK LEVEL – Modeling the fear circuit in mammals

CHAPTER 4: Computational model predicts formation of distinct groups of neurons in the basal amygdala with fear conditioning

4.1 Abstract	115
4.2 Introduction	116
4.3 Methods	119
4.4 Results	125
4.5 Discussions	126
4.6 Conclusion	127
4.7 References	128
4.8 Tables	130
4.9 Figures	136

BEHAVIORAL LEVEL – Modeling social behavior in an insect colony

CHAPTER 5: Computational model of rapid transmission of information in a group-living insect predicts underlying rules for emergent behavior in the antipredator signals

5.1 Abstract	146
5.2 Introduction	147
5.3 Methods	149

5.4 Results	160
5.5 Discussions	165
5.6 References	168
5.7 Tables	170
5.8 Figures	173
CHAPTER 6: Conclusions and Future Research	
6.1 Summary	181
<u>APPENDIX</u>	
APPENDIX A: Other Technical Publications	
A.1 Computational model of extracellular glutamate in the nucleus accumbens incorporates neuroadapatations by chronic cocaine	184
A.2 Role of perisynaptic parameters in neurotransmitter homeostasis—Computational study of a general synapse.....	219
APPENDIX B: Non Technical Publications	
B.1 Professional Skills in the Engineering Curriculum	247
APPENDIX C: K-12 Lesson Plans and Outreach Activities	
C.1 Are we like Robots?	274
C.2 How do human sensors work?	284
C.3 Development of LEGO robotics camps and activities	291
APPENDIX D: Publications and Presentations	
VITA	307

LIST OF ILLUSTRATIONS

Figure		Page
<i>Chap 1</i>		
1.	Cocaine-induced cellular adaptations in the glutamatergic projections from the Prefrontal Cortex (PFC) to the Nucleus Accumbens	4
2.	Schematic of various regions involved in the fear circuit	5
3.	A typical colony of the treehopper insect colony (<i>Umbonia crassicornis</i>) in the wild with the mother at the end of the aggregation .	6
<i>Chap 2</i>		
1.	Model of a standard RC circuit	71
2.	Simplified circuit model of a neuron	72
3.	A model for the glutamate-activated signaling network	72
4.	Bifurcation diagram showing how CaMKII activity changes as Ca ²⁺ varies	73
5.	Scheme of MAPK cascade	73
6.	Different firing patterns produced by the two-compartment model	74
7.	Hypothesized cellular adaptations in PFC-NAc Glu pathway in cocaine withdrawal	75
8.	Preliminary action potential predictions for an in vitro single PFC cell for control and cocaine cases	76
9.	Model for Glu neuroplasticity in pyramidal cell terminals projecting to NAc	76
10.	Model predictions of the concentration of synaptic Glu at the PFC-NAc synapse	77
11.	Glial configuration in the perisynaptic space around the PFC-NAc	

	synapse	78
12.	Neural circuit mediating drug seeking	79
<i>Chap 3</i>		
1.	Glial configuration of the example case cortico-accumbens synapse used to study glutamate homeostasis	110
2.	Normalized contributions of synaptic and non-synaptic glutamate to transient and steady state control basal concentrations	111
3.	Percentage receptor occupancy characteristics for AMPA and NMDA during the control basal, natural reward seeking, cocaine basal and drug seeking based on synaptic and non-synaptic sources	112
4.	Three distinct types of glial configurations used to characterize diffusion path length and synaptic isolation for a general synapse	113
5.	Comparison of $[Glu]_{syn}$ and $[Glu]_{ex}$ under control conditions for various glial configurations	114
<i>Chap 4</i>		
1.	Two compartment pyramidal cell and interneuron models with ionic and synaptic currents	135
2.	Schematic of BA network model and simulation schedule showing tone and shock during sensitization, conditioning and extinction phases	135
3.	Responses of various cell types in the Basal Amygdala network	136
4.	Response of units to intracellular current pulses	137
5.	Preliminary results from the network model	138

Chap 5

1.	Nymph location on stem with mother at the end of the aggregation	173
2.	Flowchart depicting schematic of the agent based computational model	174
3.	Comparison of biological and model results for a particular family used to compute error	175
4.	Validation results for experiment that considered neighborhood equal to the size of the aggregation	176
5.	Variation in training and testing for individual error components across trials	177
6.	Comparison of total error (ET) for training vs. testing based on two initial conditions	178
7.	Convergence of parameters across two trials	179
8.	Comparing the influence of varying global information on spatio-temporal properties	180

LIST OF TABLES

Table	Page
<i>Chap 2</i>	
1. Parameters for the illustrative RS, IB, CH and FS cell models	69
2. Parameter adjusted in Glu release model with cocaine	69
3. Initial estimates of plasticity effects on extrasynaptic neurotransmitter concentrations for model	69
4. Reported ranges for some of the parameters used in the synapse model	70
5. Model predictions for control and two extreme cases	71
<i>Chap 3</i>	
1. Ranges for parameter values for configuration in figure 1	107
2. Glutamate receptor occupancy during transient and steady state conditions	108
3. Normalized sensitivity analysis to rank the parameters for configuration in figure 1.....	109
<i>Chap 4</i>	
1. Gating variables for ion channels and interneurons used in the network model	130
2. Maximal conductance densities	131
3. Model parameters for network connections and inputs	131
4. How to develop the basal amygdala model	132

5.	Expected behavior of components in the BA model	133
----	---	-----

Chap 5

1.	Input parameters and ranges	170
----	-----------------------------------	-----

2.	Input parametric set and error	171
----	--------------------------------------	-----

3.	Normalized values showing change in error per unit change in input parameters	172
----	---	-----

LIST OF NORMENCLATURE

AA, Arachidonic Acid;

AGS3, Activator of G-Protein Signaling 3;

AMPA, Alpha-Amino-3-Hydroxy-5-Methyl-4-Isoxazolepropionic Acid;

cAMP, Cyclic Adenosine Monophosphate;

CaMKII, Calcium/Calmodulin-dependent Protein Kinase II;

Cl, Chloride;

CREB, Ca²⁺/cAMP-responsive element-binding protein;

DR, Delayed Rectifying;

D_{syn}, D_{sh} and D_{ex}, Diffusion Coefficient in the Synapse, between the Sheath and Extracellular Space;

EAAT, Excitatory Amino Acid Transporter;

ECS, Extracellular Space;

G_i, Glial Sheath;

GABA, γ -Aminobutyric Acid;

GLT-1, Glutamate Transporter Protein;

GPi, Globus Pallidus Internal Segment;

GPw, Globus Pallidus External Segment;

HVA, High Voltage Activated Calcium;

IB, Intrinsically Bursting;
K, Potassium;
KS, Slowly Inactivating Potassium;
LTD, Long-Term Depression;
LTP, Long-Term Potentiation;
MAPK, Mitogen Activated Protein Kinase;
mGluR2/3, Metabotropic Glutamate Receptors;
Na, Sodium;
NaP, Persistent Sodium;
NAc, Nucleus Accumbens;
NMDA, N-methyl-D-aspartic acid;
 P_{syn} , P_{mGluR} , and P_{ex} , Glutamate Concentrations at synapse, mGluR and Extracellular Space;
PF, Prefrontal;
PFC, Prefrontal Cortex;
PKA, Protein Kinase A;
PKC, Protein Kinase C;
PLA₂, Phospholipase A₂;
PP1, Protein Phosphatase 1;
PSC, Post Synaptic Currents;

SNc, Substantia Nigra compact;

STN, Subthalamic Nucleus;

TTX, Tetrodoxin;

VTA, Ventral Tegmental Area;

XAG, Glutamate Transporters;

xc-, Cystine-Glutamate Exchange;

COMPUTATIONAL NEURAL MODELS AT MOLECULAR, CELLULAR AND BEHAVIORAL LEVELS - THREE CASE STUDIES

Ashwin Mohan

Dr. Satish S. Nair, Dissertation Supervisor

ABSTRACT

Biologists and physiologists acquire data at all scales ranging from molecular and cellular to network and behavioral levels. Biological experiments are typically very focused, and integrating findings from different levels to understand functions can become difficult using present experimental paradigms. Computational tools and systems concepts facilitate integration of information across levels to further understanding of functional level issues. This integration is eventually formalized as experimentally accessible models that facilitate visualization of the system as a whole. This dissertation focuses on the modeling and analysis of a set of biological phenomenon at the molecular (chapters 2 and 3) and cellular/network (chapter 4) and behavior (chapter 5) levels.

The second chapter (Molecular level) outlines the methods used to develop a computational model of elements in the PFC–NAc glutamatergic pathway to study cellular adaptations during withdrawal from cocaine. The study helped identify various parameters and their ranges that were eventually used to constrain the computational model of a single synapse to biological experiments. The third chapter (Molecular level) outlines a molecular diffusion model of the PFC–NAc that was developed to characterize molecular level interactions including stimulation of synaptic receptors. This model was

then used to propose other feasible glial geometries to study the role of diffusion path length on synaptic isolation.

At the network level, the fourth chapter outlines a systematic approach to understand learning mechanisms in an important unit of the fear circuit, the basal amygdala (BA). A biophysical network model of the basal amygdala was developed to investigate possible interconnectivity to produce three different types of cells reported recently in the literature, after auditory fear conditioning: fear cell, extinction-resistant cells, and extinction cells.

At the behavior level, the fifth chapter outlines an approach to study group behavior emerging from social interactions amongst individuals using an agent based model. We develop a computational model of rapid signaler-receiver interactions in this group-living insect. We use the model to study the emergence of informative global patterns by providing interacting nymphs with limited locally available information. Specifically, the model predicted that for a nymph to consider signaling, at least two nymphs has to be signaling within a neighborhood for it to elicit an signal. The model was also used to predict the influence of local and global cues on signaling behavior, which could eventually be verified by biologists using controlled experiments.

CHAPTER 1

Introduction and objectives

1.1. BACKGROUND AND MOTIVATION

Computational neuroscience provides tools to abstract and generalize principles of brain function using mathematics, with applicability to the entire neuroscience spectrum including molecular, cellular, systems, and translational levels (NIH Neuroscience Blueprint 2004). Computational techniques and tools are being developed to model several pathways and brain mechanisms with increasing accuracy and are found to be essential to generate an understanding of the underlying functions in this case (Koch and Segev, 2001; Mauk, 2000). Indeed, computational models based on the real anatomy and physiology of the nervous system already constitute what is, in effect, a compact and self-correcting database of neurobiological facts and functional relationships (Bower and Bolouri, 2001).

The best computational work is both informed by and subsequently contributes to a biological understanding of the nervous system. Computational approaches also allow us to fine tune hypotheses before testing them in biological systems, streamlining the discovery process and decreasing the volume of the use of animal models. Therefore, computational neuroscientists and biological neuroscientists are interdependent groups – neither can reach the full capabilities of their work without the other.

Systems biology aims at system-level understanding of biology in terms of structure, dynamics, control, and design (Hartwell et al., 1999, Kitano, 2002) through the integration of all types of biological information at all levels of order and definition of the interactions of individual elements with one another. This integration is eventually

formalized as experimentally accessible models that facilitate visualization of the system as a whole. Ideas developed in engineering and computer science such as amplification, adaptation, robustness, insulation, error correction and coincidence detection have been studied in biology for specific systems.

Typically, systems engineers work on dynamical modeling for a wide spectrum of applications ranging from human behavior and weather modeling, to very accurate models for aircraft and automobiles. Interestingly, the process of modeling is the same for all the models in the spectrum, except for the level of complexity and uncertainties involved. Computational models help transition from the ‘real world’ to the ‘math world’ where systems from all levels of the spectrum described above look similar. Thus, for systems and control engineers, the techniques of modeling and control are ubiquitous throughout nature, and seem similar. However, control of a system requires that the system be understood ‘adequately’. The term ‘adequately’ implies that the level of understanding of the system is related to the accuracy of control or understanding required. This requirement on control or understanding, typically takes the process of mathematical modeling, for most systems.

1.2 OVERVIEW OF THESIS AND OBJECTIVES

This thesis focuses on the modeling and analysis of certain brain circuits at the molecular (chapters 2 and 3) and cellular/network (chapter 4) and behavior (chapter 5) levels. Each of the chapters 2–5 are in the form of stand-alone journal papers. The specific objectives of the thesis are listed below under descriptions for chapters 2–5, with the key point being posed as a question in quotes.

Chapter 2 – “What are specific cellular adaptations in and around the PFC-NAc synapse after chronic cocaine?” Two important structures involved in the circuit for cocaine abuse and dependence are the nucleus accumbens (NAc) and pre-frontal cortex (PFC) (Kalivas and Volkow, 2005). NAc is part of part of the pleasure system, or reward circuit and is traditionally studied for its role in addiction. The cardinal features of cocaine addiction include uncontrollable urges to obtain drugs and reduced behavioral responding to biological rewards. The fact that these characteristics persist after years of drug abstinence points to enduring neuroplasticity due to cocaine abuse in brain circuitry responsible for processing motivationally relevant stimuli. Augmented responding for drug-associated stimuli and reduced responding for natural rewards arise from cocaine-induced cellular adaptations. Cocaine-induced reduction in cystine-glutamate (xc-) exchange and metabotropic glutamate receptors (mGluR2/3) signaling is shown in figure 1.

The goal was to develop a computational model of elements in the PFC-NAc glutamatergic pathway to study cellular adaptations during withdrawal from cocaine. The overall model for the PFC-NAc pathway functioned as follows: the PFC pyramidal cell fired causing an action potential which resulted in release of neurotransmitter glutamate (Glu) in the PFC-NAc synapse, and the release subsequently being modulated by a feedback loop involving mGluR's present on the pre-synapse. The Glu released inside the synaptic cleft diffused out of the synapse and was largely taken up via Glu transporters on the glial sheath that surrounds the synapse. We modeled Glu homeostasis in the perisynaptic region considering synaptic Glu release, transporter dynamics, tortuosity, and the xc- exchangers, to highlight the importance of the various mechanisms

involved.

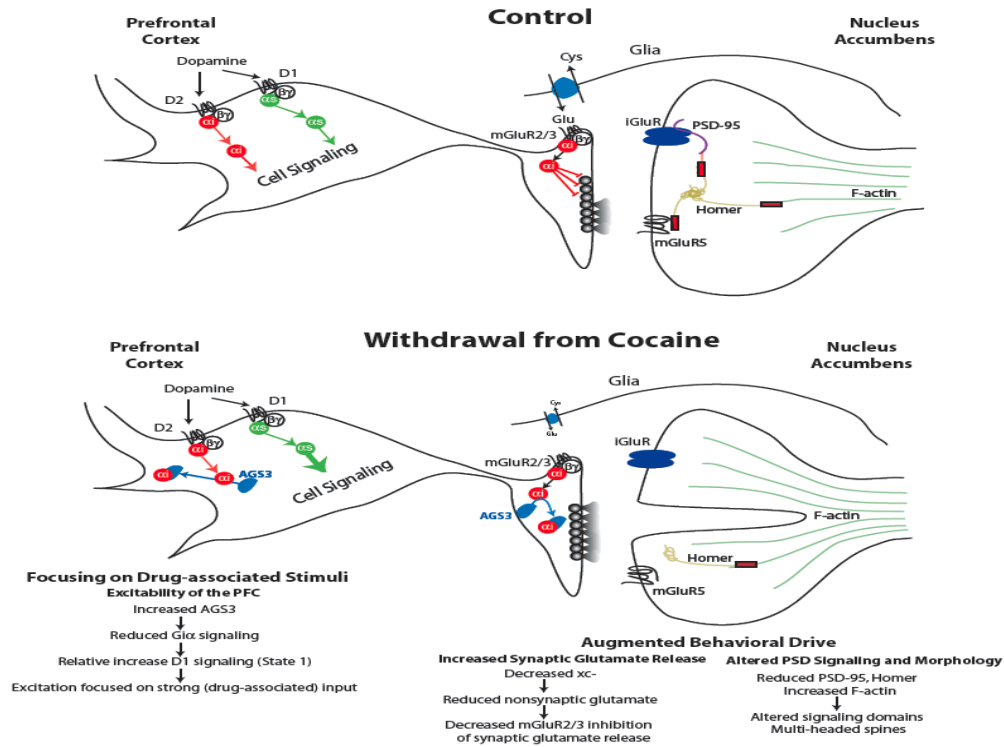


Figure 1. Cocaine-induced cellular adaptations in the glutamatergic projections from the Prefrontal Cortex (PFC) to the Nucleus Accumbens (NAc) (Kalivas et al. 2005).

Chapter 3 – “Molecular diffusion model to study what are possible glial configurations around a PFC-NAc synapse?” Synapses are specialized junctions through which the neuronal cells communicate with each other by releasing neurotransmitters such as glutamate. Diffusion of neurotransmitter is critical in chemical synapses. Synapse and their characteristics are being studied by numerous research groups around the world. The perisynaptic region comprised of glial sheaths that hold glutamate removal proteins called transporters (XAG), and cystine glutamate exchangers that produce glutamate. Even with specialized equipment and extensive research, the perisynaptic space (region around the synapse) remains poorly characterized presently. Chapter 3 focused on developing a synaptic diffusion model of the PFC - NAc, to gain finer molecular insights

into the various mechanism involved in glutamate homeostasis, and to better characterize the perisynaptic region, in particular the role of the glial sheaths in maintaining synaptic isolation.

Chapter 4 – “What is the network connectivity in the basal amygdala nuclei after a fear conditioning protocol?” A biologically realistic network model of the Basal Amygdala (BA) was proposed to study the underlying mechanisms in the formation of three distinct types of cells in BA after auditory fear conditioning. Hebbian synaptic plasticity was implemented into the excitatory and inhibitory receptor-mediated synapses to model learning, using electrophysiology and imaging data from rats. The network model was trained and tested using the Pavlovian fear conditioning paradigm, and the mechanisms how the three distinct populations of cells (fear, extinction-resistant, and extinction types) emerged were identified.

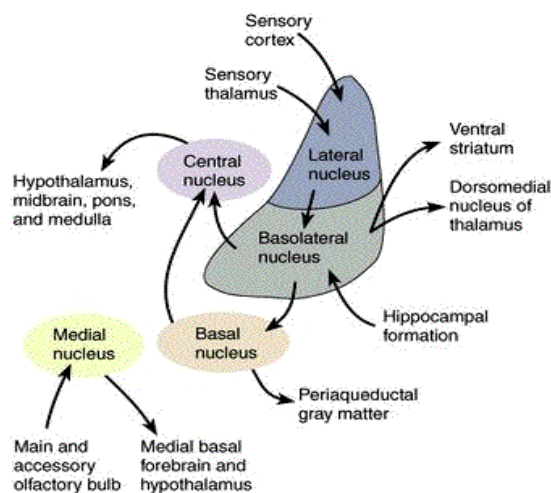


Figure 2. Schematic of various regions involved in the fear circuit.

Chapter 5 – “Studying cause and effect responsible for emergent behavior.” The study of group behavior emerging from social interactions amongst individuals using agent based models has gained momentum in recent years. Although most of the individuals in the insect group of *Umbonia crassicornis* do not have information about where the predator is, the signaling behavior of the group yields an emergent pattern that provides the defending adult with information about predator presence and location. Offspring signal synchronously to warn a defending parent of a predator attack. We develop a computational model of rapid signaler-receiver interactions in this group-living insect. We test the emergence of informative global patterns by providing interacting nymphs with limited locally available information with this agent based model. Known parameters such as size of the aggregation and spatial distribution are estimated from experimental recordings. Further, the model investigates the behavioral rules underlying group signaling patterns that reveal the predator’s location.



Figure 3. A typical colony of *Umbonia crassicornis* nymphs in the wild with mother at the end of the aggregation protecting her brood.

CHAPTER 2

Computational Models of Neuronal Networks—Modeling neuroplasticity in Prefrontal Cortex—Nucleus Accumbens Glutamate Transmission due to cocaine addiction

2.1. INTRODUCTION AND OVERVIEW

Computational Neuroscience provides tools to abstract and generalize principles of brain function using mathematics, with applicability to the entire neuroscience spectrum including molecular, cellular, systems, and translational levels (NIH Neuroscience Blueprint, 2004). Researchers are investigating brain organization at specific levels of scale, ranging from molecular to behavioral levels, each of which provides important insights into the specific sub-system. However, improved understanding of the functional organization typically requires connection of multiple levels, something that can be facilitated by computational models (Koch and Segev, 2001). For instance, recent technical advances have resulted in a rapid accumulation of information on intracellular signaling pathways and relationships to long-term neuronal changes (Byrne and Roberts, 2004). Computational techniques and tools are being developed to model such mechanisms with increasing accuracy and are found to be essential to generate an understanding of the underlying functions in this case (Koch and Segev, 2001; Mauk, 2000). Indeed, computational models based on the real anatomy and physiology of the nervous system already constitute what is, in effect, a compact and self-correcting database of neurobiological facts and functional relationships (Bower and Bolouri, 2001).

There is increasing belief (Koch and Segev, 2001) that laboratories and researchers will rely on models and modeling software to check the significance and accuracy of their data, and that these models will enhance collaboration and communication within neuroscience.

The best computational work is both informed by and subsequently contributes to a biological understanding of the nervous system. As cited, one of the reasons computational approaches to questions about the nervous system have the potential to be so valuable is that these approaches span the spectrum of neuroscience from molecular to behavioral levels. Computational approaches also allow us to fine tune hypotheses before testing them in biological systems, streamlining the discovery process and decreasing the volume of the use of animal models. Therefore, computational neuroscientists and biological neuroscientists are interdependent groups—neither can reach the full capabilities of their work without the other. This chapter reviews principles of computational modeling in brain circuits (section 2.2) and illustrates the utility of computational approaches in the case of neuroplasticity due to cocaine in the glutamatergic pathway from the prefrontal cortex (PFC) to the nucleus accumbens (NAc) (section 2.3).

2.2. SYSTEM APPROACHES IN NEUROSCIENCE

2.2.1. Systems Principles in Modeling

Systems theory and concepts facilitate understanding of biology in terms of structure, dynamics, control, and design (Hartwell et al., 1999; Kitano, 2002) through the integration of all types of biological information at all levels of order and definition of the

interactions of individual elements with one another. This integration is eventually formalized as experimentally accessible models that facilitate visualization of the system as a whole. There is an increasing belief (Hartwell et al., 1999) that general 'design' principles that govern the structure and function of modules in biology naturally link it to system concepts, developed in engineering and computer science, such as amplification, adaptation, robustness, insulation, error correction and coincidence detection, all of which have been studied in biology for specific systems. Some of the design principles familiar to engineers that are relevant to biology include positive feedback loops (these drive rapid transitions between two different stable states of a system), negative feedback loops (these maintain an output parameter within a narrow range), coincidence detection systems, amplifiers (to minimize noise relative to signal), and parallel (backup) circuits that allow an electronic device to survive failures in one circuit (fail-safe systems).

The 'classic' computational model for action potential generation by Hodgkin and Huxley (1952) for which they won the Nobel prize in 1963 is often cited as the key development that highlighted the role of modeling in neuroscience. Box 1 below provides a brief description of the modeling details that show clearly that an action potential can be generated by a set of ordinary differential equations.

Box 1. Action potential using a set of ordinary differential eqns

Standard resistor–capacitor (RC) circuit. The standard RC circuit is shown in Figure 1. R_m is the resistance, C_m is the capacitance and E_m is the voltage of the battery.

Circuit Model. Current conservation indicates that $-I_{cm} - I_m = 0$. Using the capacitance relations, this results in

$$C_m \frac{dV_m}{dt} + \frac{V_m - E_m}{R_m} = 0 \quad (2.1)$$

Or,

$$R_m C_m \frac{dV_m}{dt} + V_m = E_m$$

A Neuronal Cell (V_m depends on the time varying conductances R_j which are either voltage(V_m) dependent or neurotransmitter dependent)

1. Na, K and leakage (R_m —typically Cl) channels
2. V_m is membrane potential, with m representing ‘membrane’; E_j , R_j represent reversal potential and channel resistance for ion j (R_m is typically the same as Cl channel resistance which does not change)
3. The active Na–K pump is also shown, which becomes part of the current source in the model, would result in a model similar to the one above!

Neuron Model. Again, current conservation leads to $-I_{cm} - I_m - I_k - I_{Na} + I_{inject} = 0$.

Using the capacitance relations again, this gives

$$C_m \frac{dV_m}{dt} + I_m + I_k + I_{Na} = I_{inject} \quad (2.2)$$

Or,

$$C_m \frac{dV_m}{dt} + \frac{V_m - E_m}{R_m} + \frac{V_m - E_k}{R_k} + \frac{V_m - E_{Na}}{R_{Na}} = I_{inject}$$

Or,

$$C_m \frac{dV_m}{dt} + G_m(V_m - E_m) + G_k(V_m - E_k) + G_{Na}(V_m - E_{Na}) = I_{inject}$$

where G_m , G_k and G_{Na} are the channel conductances which are the reciprocals of corresponding resistances, and I_{inject} represents any external injection of current one may provide (as in neurophysiology expts.).

How does one determine the varying conductances? The conductances G_k and G_{Na} changes dynamically as a function of membrane voltage, while G_m is constant. Hodgkin and Huxley (1952) determined forms for G_k and G_{Na} as follows:

$$G_k = \bar{g}_k h^4 \quad (2.3)$$

$$\frac{dn}{dt} = \alpha_n(V_m)(1-n) - \beta_n(V_m)n$$

$$\alpha_n(V_m) = \frac{0.01(10-V_m)}{\exp\left(\frac{10-V_m}{10}\right)-1}; \quad \beta_n(V_m) = 0.125\exp(-V_m/80)$$

$$G_{Na} = \bar{g}_{Na} m^3 h \quad (2.4)$$

$$\frac{dm}{dt} = \alpha_m(V_m)(1-m) - \beta_m(V_m)m$$

$$\frac{dh}{dt} = \alpha_h(V_m)(1-h) - \beta_h(V_m)h$$

$$\alpha_m(V_m) = \frac{0.1(25-V_m)}{\exp\left(\frac{25-V_m}{10}\right)-1}; \quad \beta_m(V_m) = 4\exp(-V_m/18)$$

$$\alpha_h(V_m) = 0.07\exp(-V_m/20); \quad \beta_h(V_m) = \frac{1}{\exp\left(\frac{30-V_m}{10}\right)+1}$$

where \bar{g}_k and \bar{g}_{Na} are the normalization constants that determine the maximum possible conductances.

Hodgkin and Huxley (1952) showed how this simple electrical circuit model could

simulate action potentials, a ‘computational’ finding for which they were awarded the Nobel prize in 1963! The electrical circuit model shown in Figure 2 is for a single compartment. If we use more than one compartment to model a neuron, we will have to connect many such circuits together. The computer then solves many coupled model equations (Eqns. 2.2–2.4) in parallel. This is what computer packages such as GENESIS and NEURON are designed to perform, so that the user has to only ‘define’ the problem using the basic ideas above and then let the software do the ‘number crunching’ and display the results in a form that is familiar to the neuroscientist.

2.2.2. Modeling at the Molecular Level

An intracellular signaling pathway is a sequence of biochemical reactions that relays information from extracellular stimuli to targets in the cytoplasm or nucleus (Smolen et al., 2004). These biochemical reactions are carried out by enzymes and second messengers. Intracellular pathways determine the response of a neuron to neurotransmitters, growth factors, and other signaling molecules. Examples of signals include calcium influx and binding of hormones, neurotransmitters, and growth factors to receptors. These signals incite effectors that alter the rates of specific cellular processes and can also regulate long-term processes such as neuronal growth and long-term potentiation.

Mathematical modeling gives us a conceptual view of the structure and operation of pathways by taking complex data and displaying it in a concise format (Smolen et al., 2004). In addition, these model equations can be used to develop computer simulations to help understand and predict systems-level behavior and emergent properties of complex biochemical systems. For instance, if the reaction rate varies in a nonlinear manner,

computer simulations of these equations commonly display unexpected and complex behaviors that cannot be guessed intuitively. Models also help reveal the effects of interactions within intracellular signaling pathways. Intracellular models of pathways being developed by researchers (including the authors, Li et al., 2005) are too numerous and span a very large range, and so are not reviewed here in detail. Instead we highlight some general principles and include an example which involves signaling via glutamate, the neurotransmitter involved in the study on cocaine neuroplasticity we report in section 2.3.

2.2.3. Modeling Levels

A central issue in all forms of modeling is that of how much biological detail to include, which could be in form of complexity of the signaling network, or in terms of greater precision in specifying what occurs within each pathway (Bhalla, 2004). In neuronal systems, neuromodulators act through intracellular second messenger pathways to influence the electrical properties of neurons, integration of synaptic inputs, spatio-temporal firing dynamics of neuronal networks, and, eventually, system behavior (Blackwell, 2005). Intracellular signals can be carried by ions such as Ca^{2+} , by small molecules such as cAMP, or by movement of macromolecules such as enzymes and transcription factors (Smolen et al., 2004). It is of great importance to model intracellular transport of these species to discover the underlying coordination principles of signaling pathways and this process can be modeled at several levels of detail. Consider modeling the diffusion of an important specific ion, Ca^{2+} . The simplest approach considers only Ca^{2+} exchanges across membranes that separate intracellular compartments while in a more computationally intensive method, the spaces within intracellular compartments are

modeled as small volume elements, with the ability to vary the Ca^{2+} concentration in each element independently (Smolen et al., 2004). To model the intracellular diffusion of Ca^{2+} more realistically, the intracellular space must be discretized, or divided into small volume elements and Ca^{2+} concentration within each element must be modeled. This, in fact, is the standard approach to simulate the partial differential equation that describes diffusion within an extended region (Smolen et al., 2004).

2.2.4. Modeling Methods

Modules. The first step in building complex models of biochemical pathways is to identify the “connection map” and then to organize the connection into modules that can be constrained by experimental data and analyzed computationally (Eungdamrong and Iyengar, 2004). Module definition has the advantages of limiting the number of components in an individual unit and constraining the overall behavior of the module by experimentally obtained input–output relationships (Neves and Iyengar, 2002). Such a bottom–up approach was found to be very beneficial in constructing signaling network models with interaction between different pathways (Bhalla and Iyengar, 1999, 2001). By analyzing the complex network formed by combining each module together, one can identify emergent properties which do not appear in individual modules (Bhalla and Iyengar, 1999). It is even suggested that all biological studies may be moving from a molecular to modular approach (Hartwell et al., 1999; also Saez–Rodriguez, 2004 who report a criterion for defining ‘modules’ based on the absence of retroactivity).

Modeling framework. The appropriate modeling methodology depends on the biology of the network and the phenomena (Eungdamrong and Iyengar, 2004). The three most commonly used modeling frameworks are chemical kinetics models, compartmental

models and diffusion–reaction models (Eungdamrong and Iyengar, 2004). Chemical kinetics models are developed by rate equations based on the law of conservation of mass, resulting in nonlinear ordinary differential equations (ODEs) that usually can only be solved numerically. While chemical kinetics models assume that molecular concentration is only a function of time, compartmental models treat molecules in different compartment as separate species. Partial differential equations (PDEs) are needed for compartmental models since concentration is dependent on both the time and space. Diffusion–reaction equations are used to model spatially restricted biochemical reactions where the rate of change of concentration of a molecule at any location depends on diffusion, active transport or convection, and on biochemical reactions (Eungdamrong and Iyengar, 2004). The PDE based diffusion–reaction models usually have to deal with a large set of coupled, nonlinear partial differential equations which require many more parameters, much greater computational resources and time than the ODE–based chemical kinetics models.

Parameter selection. Computational models should be based on and fully constrained by experimental data (Neves and Iyengar, 2002). Models of signaling pathways usually require parameter information such as concentrations of each species, kinetic rate constants for reactions and diffusion rates. Some parameter values such as enzyme Michaelis constants can be estimated by standard experiments *in vitro* while other parameters are difficult to measure (Smolen et al., 2004). A crucial step in model development is to compile biological parameters from published literature. If the parameters are not directly available in the literature, quantitative information may have to be manually extracted from the primary literature and entered into the database (Neves

and Iyengar, 2002). If parameter information is not available or incomplete, an alternative is to create models that will fit the observed input–output relationship data (Neves and Iyengar, 2002).

After reasonable “baseline” parameter values are obtained, simulations can be conducted and the evolution of concentrations is then compared with experimental data. After adjusting parameters, the simulation is repeated until optimal agreement is achieved between model predictions and experimental data. Computer programs are typically more efficient in optimizing parameters compared to the time–consuming trial–and–error approach. Due to the uncertainties in parameter values and activity coefficients, models of biochemical pathways should most commonly not be thought of as quantitative, but as qualitative descriptions (Smolen et al., 2004).

2.2.5. Model Prediction

A critical step in model development is the step from explaining observations to making predictions (Bhalla, 2004). The authors consider the system in Figure 3, where the activation of cyclic adenosine monophosphate (cAMP) elevates PKA level which leads to CaMKII disinhibition via a protein phosphatase 1 (PP1). CaMKII is capable of autophosphorylation following Ca^{2+} influx. If a stimulus causing Ca^{2+} influx can increase the cAMP level at the time, the CaMKII activity will have a great chance of becoming self–sustaining. Model simulations (Bhalla and Iyengar, 1999) predicted that sustained activity of CaMKII can only be obtained by stimuli which drive both Ca^{2+} and cAMP past threshold levels. The importance of this dual threshold of Ca^{2+} and cAMP levels in determining the degree of synaptic modification in hippocampal neurons have been supported by experiments (Brown et al., 2000). Strong CaMKII activation was produced

by the addition of a cAMP analog along with electrical stimulation and neither of the stimuli was able to generate this strong activation which induces LTP.

2.2.6. Model Analysis

Robustness . After a model is constructed and validated against experimental data, it is necessary to investigate the robustness of the model by performing parametric studies. Due to evolved compensatory mechanisms, the qualitative behavior of a biochemical pathway is usually preserved (Smolen et al., 2004). Most biological signaling networks are generally robust within an order of magnitude variation in kinetics parameters (Eungdamrong and Iyengar, 2004). Thus, the qualitative properties of the model should not change with modest variations in parameter values. Nevertheless, some components in the signaling pathways may be sensitive to biochemical parameters. As discussed above, PKC plays an important role in the persistent activation of MAPK in a positive feedback loop. It was shown that the switching behavior of the loop was sensitive to two-fold variations in PKC (Bhalla and Iyengar, 1999).

Bifurcation. Bifurcation analysis is a powerful dynamical tool for analyzing behaviors of a network as well as analyzing their sensitivity and robustness to parameter variations (Schmidt and Jacobsen, 2004). In a bifurcation diagram, the stable or unstable steady states of a equilibrium points in a model are plotted as parameters are varied, which allows easy visualization of model behavior in parameter space. As an example, the bifurcation diagram showing how the activity of CaMKII changes as $[Ca^{2+}]$ varies is shown in Figure 4 (Smolen et al., 2004). Point 1 corresponds to a low stable activity state when $[Ca^{2+}]$ is low. As $[Ca^{2+}]$ increases to a certain level with external stimulus, concentration of CaMKII will jump to a higher stable state (point 3). When $[Ca^{2+}]$

gradually decreases back to a lower level, concentration of CaMKII may still remain in the high activity state (point 4). The dashed line in Figure 4 corresponds to an unstable intermediate state where a small variation in $[Ca^{2+}]$ will move CaMKII up or down to the two stable states (Smolen et al., 2004). Note also that two stable states exist in the blue region (region of bistability). An extensive discussion of bifurcation is provided by Izhikevich (2007).

2.2.7. Emergent Properties of Signaling Networks

One of the important goals of modeling signaling networks is to identify the system-level properties which underlie the operational principles of the cell. Again, as an example, we list the emergent properties of a biochemical network studied by Bhalla and Iyengar (1999), which include integration of signals across multiple time scales, generation of distinct outputs depending on input strength and duration, and self-sustaining feedback loops. The glutamate-activated signaling network they modeled included four signaling pathways at dendritic synapses of hippocampal pyramidal neurons, where the postsynaptic protein kinases CaMKII, protein kinase C (PKC), protein kinase A (PKA), and mitogen activated protein kinase (MAPK) are activated following Ca^{2+} influx through the NMDA receptor. All these four pathways are linked together to form the network described (Figure 3). A self-sustaining feedback loop and one that involves ultrasensitivity are listed next as examples of emergent properties.

Self-sustaining feedback loop and bistability. Here we focus on a positive feedback loop between PKC and MAPK where some noteworthy features have been identified. MAPK can phosphorylate and activate phospholipase A_2 (PLA₂) which increases the level of arachidonic acid (AA), resulting in PKC activation. PKC in turn activates Raf,

the most-upstream protein kinase in the MAP-kinase cascade, leading to MAPK activation which closes the feedback loop. The positive feedback loop was shown to behave as a bistable switch with two distinct steady-states in simulation, where a brief glutamate exposure results in sustained activation of MAPK. In neurons, this behavior may have a significant implication: a large change in synaptic strength might occur from a long-lasting activation of MAPK and PKC induced by glutamate, dependent on a prolonged phosphorylation by MAPK or PKC of transcription factors such as Ca²⁺/cAMP-responsive element-binding protein (CREB) (Smolen et al., 2004).

The model of Figure 3 was able to distinguish stimulus patterns responsible for the induction of long-term potentiation (LTP) and long-term depression (LTD), as shown in a compartmental model simulation (Bhalla, 2002). Eight different stimulus patterns were simulated for the activation of the MAPK-PKC feedback loop, among which is a pattern used to produce LTP and a pattern used to induce LTD in experiments. The LTD stimulus pattern could lead to prolonged activation of the MAPK feedback loop even at low stimulus amplitude, while a higher amplitude was required to activate the loop using the LTP stimulus pattern.

Ultrasensitivity. When applied to signaling pathways, ultrasensitivity indicates that a response is more sensitive to extracellular stimulation than the normal hyperbolic response (Neves and Iyengar, 2002). Ultrasensitive responses are common in cellular information transfer because they allow cells to decode extracellular stimuli in an all-or-none manner (Legewie et al., 2005). Such switch-like behavior can be generated by zero-order ultrasensitivity or a mechanism which relies on an enzyme in a cooperative fashion (Smolen et al., 2004). Ultrasensitive responses are best illustrated in a well-

known MAPK pathway which begins from hormonal or neurotransmitter receptor and involves activation of several protein kinases, forming a cascade (Figure 4).

MAPK are activated through a dual phosphorylation by another kinase termed MAPK kinase (MAPKK or MEK), which is in turn activated by the MAPKK kinase (MAPKKK). Modeling of this cascade has shown that a small increase in the activity of MAPKK could cause a large increase in phosphorylated and active MAPK under physiological conditions through zero-order ultrasensitivity (Ferrell, 1996; Huang and Ferrell, 1996). This is because of the partial saturation of the enzymes as well as the dual phosphorylation mechanism of the kinases. The different levels also add the ultrasensitivity (Ferrell, 1997).

2.2.8. Challenges and Future Directions

Despite much progress being made in signaling network modeling, several issues remain to be addressed. Although large amounts of high-throughput biological data are available, the kinetics data have not been determined for many biochemical reactions. The concentration of endogenous proteins is hard to measure accurately in their environment (Eungdamrong and Iyengar, 2004). Besides, the rate constants are usually measured from *in vitro* experiments with purified components and their values may differ greatly *in vivo*. It will be helpful to obtain quantitative kinetics data with the fluorescence probes under development (Dundr et al., 2002).

Besides experimental barriers, computational challenges also exist. With the advances in high throughput technology, data on new protein-protein interactions and added details for signaling pathways are accumulating at an exponential rate (Eungdamrong and Iyengar, 2004). The organization and management of huge amounts of such data for

model development poses a big challenge since the role which these interactions play in the biological system is not clear. Fortunately, signaling databases are being constructed to aid modelers in generating “connection maps”, identifying network architecture and kinetic properties of each pathway. Some useful databases include Science’s STKE connection map (<http://stke.sciencemag.org>), the Molecule Pages (<http://www.signaling-gateway.org>) and the SigPath database (www.SigPath.org) (Eungdamrong and Iyengar, 2004).

The success of computational modeling of signaling networks is largely dependent on the coupling between the model and the experiment. More biological realism will be required as models tie closer to experiments and simple chemical models should be expanded to include space, stochasticity, and even mechanical effects (Bhalla, 2004). With rapid advancement in the generation of high-throughput data processing and closer interdisciplinary interactions, signaling models can become meaningfully powerful tools for biologists. This will also facilitate the long-term goal of integrating signaling network output to functional outcomes.

2.2.9. Modeling at the Cellular, Systems and Higher Levels

Neurons have evolved sophisticated means of generating electrical and chemical signals to encode, process, store, and transmit information (Baxter et al., 2004). To understand the functional consequences of particular neuronal features and the complex dynamics in neuronal systems, detailed physiological and anatomical data alone are not enough and quantitative approaches are needed (Bower and Beeman, 2003). The fundamental pioneering work by Hodgkin and Huxley (Hodgkin and Huxley, 1952; See Box. 1) provided an influential mathematical framework for modeling neuronal

excitability, and is still widely used over fifty years since its introduction. The reader is referred to excellent texts including Byrnes and Roberts (2004), Izhikevitch (2007), and Keener and Sneyd (1998) that describe in detail how the various channels are modeled and how their combined action results in the generation of an action potential. The focus of research at the cellular level has been largely to characterize/discover the various channels in different types of cells, and to determine their role in modulating firing patterns (Izhikevitch, 2007 provides an excellent overview). Since the Hodgkin–Huxley model (Box. 1), significant advances have been made to include additional ‘control’ channels that help shape the finer features of cellular firing patterns such as spike frequency adaptation. Here we provide a somewhat advanced example case of a two–compartment single cell model to illustrate how combinations of four different currents (‘control’ currents from a systems point of view) can produce a rich variety of firing patterns.

2.2.10. Cellular Level–Modeling Various Cell Types Using a Two–Compartment Model

Our basic Hodgkin–Huxley model has two compartments representing the soma (radius of 15 μm ; length of 30 μm) and the major dendrite (radius of 5 μm ; length of 200 μm) of the neuron. Each compartment contains a leakage current (I_L), a spike–generating sodium current (I_{Na}), a delay rectifier potassium current (I_{DR}), a high–voltage activated Ca^{2+} current (I_{Ca}) and a Ca^{2+} –activated, voltage–independent “afterhyperpolarization” K^+ current (I_{AHP}). The current–balance equations for the two compartments are given as

$$\begin{aligned}
C_m \frac{dV_s}{dt} &= -I_L - I_{Na} - I_{DR} - I_{Ca} - I_{AHP} + g_c(V_d - V_s) + I_s \\
C_m \frac{dV_d}{dt} &= -I_L - I_{Na} - I_{DR} - I_{Ca} - I_{AHP} + g_c(V_s - V_d) + I_d
\end{aligned} \tag{2.5}$$

where V_s and V_d are the somatic and dendritic membrane potentials (mV), I_s (I_d) is the electrode current applied to the soma (dendrite), C_m is the membrane capacitance, g_c is the coupling conductance. $R_m = 15 \text{ K}\Omega\text{-cm}^2$, $C_m = 1.0 \text{ }\mu\text{F/cm}^2$, and $R_i = 150 \text{ }\Omega\text{-cm}$.

Ionic Currents. The formulation of I_{Na} , I_{DR} , and I_{Ca} are taken from Durstewitz et al. (2000) and the kinetics of I_{AHP} is taken from Warman et al. (1994). The ionic currents are given by standard Hodgkin–Huxley expressions:

$$I_L = g_L(V - E_L); I_{Na} = g_{Na} m^3 h (V - E_{Na}); I_{DR} = g_{DR} n^4 (V - E_K);$$

$I_{Ca} = g_{Ca} u^2 v (V - E_{Ca}); I_{AHP} = g_{AHP} q (V - E_K)$ where V can be V_s or V_d , E_{Na} , E_K and E_{Ca} are the reversal Na^+ , K^+ and Ca^{2+} potentials, $E_{Na} = 55 \text{ mV}$, $E_K = -80 \text{ mV}$ and $E_{Ca} = 120 \text{ mV}$. The kinetic equation for each of the gating variables m , h , n , u , v and q takes the form

$$\frac{dx}{dt} = \frac{x_\infty(V, [Ca^{2+}]_i) - x}{\tau_x(V, [Ca^{2+}]_i)} \tag{2.6}$$

where $[Ca^{2+}]_i$ is the intracellular Ca^{2+} concentration, x_∞ is the voltage– (or Ca^{2+} –) dependent steady state and τ_x is a voltage– (or Ca^{2+} –) dependent time constant. x_∞ and

τ_x are given by the rate function, α_x and β_x , for the gating variables m , h , n

$$x_\infty = \alpha_x / (\alpha_x + \beta_x) \tag{2.7}$$

$$\tau_x = 1 / (\alpha_x + \beta_x) \tag{2.8}$$

For the gating variable q , x_∞ is also given by Eqn. (2.4) and τ_x is a constant. All the rate functions, steady states and time constants are listed later in this section.

Calcium Dynamics The extracellular calcium is assumed to be constant ($[Ca^{2+}]_o = 2$ mmol/l), whereas the intracellular calcium is regulated by a simple first-order differential equation of the form (Warman et al., 1994)

$$\frac{d[Ca^{2+}]_i}{dt} = -f \frac{I_{Ca}}{wzFA} + \frac{[Ca^{2+}]_{rest} - [Ca^{2+}]_i}{\tau_{Ca}} \quad (2.9)$$

f is the fraction of the Ca^{2+} influx ($f=0.024$), w is the shell thickness ($1\mu m$), A is the dendritic area, F is the Faraday constant, τ_{Ca} is the Ca^{2+} removal rate ($\tau_{Ca2}=100$ ms). The resting Ca^{2+} concentration is $[Ca^{2+}]_{rest} = 50$ nmol/l, which is the same as the initial concentration (Durstewitz et al., 2000). In Eqn. (2.9), the unit of the Ca^{2+} concentration is $\mu m/l$.

Regular spiking: With a constant current injections, these excitatory neurons fire a few spikes, with short interspike period and then the period increases. This is called the spike frequency adaptation. Increasing the strength of the injected dc-current increases the interspike frequency, though it never becomes too fast because of large spike-afterhyperpolarizations.

Intrinsically bursting: These excitatory neurons fire a stereotypical burst of spikes followed by repetitive single spikes. During the initial burst, variable u builds up and eventually switches the dynamics from bursting to spiking.

Chattering: These excitatory neurons can fire stereotypical bursts of closely spaced spikes. The inter-burst frequency can be as high as 40 Hz.

Fast spiking: These are inhibitory neurons that can fire periodic trains of action potentials with extremely high frequency practically without any adaptation (slowing down).

It should be noted that in the particular example, the channels modified as well as the model parameter values themselves have been selected primarily for illustrative purposes. So, it should be possible to obtain similar changes in patterns with inclusion of various other channels such as the I_h current (Pape, 1996).

2.2.12. Rate Functions, Steady States and Time Constants of the Two-Compartment Cell Model

$$\alpha_m = \frac{-0.2816(V + 28)}{\exp(-(V + 28)/9.3) - 1}; \beta_m = \frac{0.2464(V + 1)}{\exp((V + 1)/6) - 1};$$

$$\alpha_h = 0.098 \times \exp(-(V + 43.1)/20)$$

$$\beta_h = \frac{1.4}{\exp(-(V + 13.1)/10) + 1}; \alpha_n = \frac{-0.018(V - 13)}{\exp(-(V - 13)/25) - 1}; \beta_n = \frac{0.0054(V - 23)}{\exp((V - 23)/12) - 1}$$

$$\alpha_q = \frac{0.0048}{\exp(-(10 \log[Ca^{2+}]_i - 35)/2)}; \beta_q = \frac{0.012}{\exp((10 \log[Ca^{2+}]_i + 100)/5)}; \quad (2.10)$$

$$\tau_q = 48 \text{ ms}$$

$$u_\infty = \frac{1}{\exp(-(V + 24.6)/11.3) + 1}; \tau_u = 1.25 \times \text{sec}h(-0.031(V + 37.1));$$

$$v_\infty = \frac{1}{\exp((V + 12.6)/18.9) + 1}; \tau_v = 420.0 \text{ ms}$$

2.2.13. Modeling at the Higher Levels

For a network/systems level model to be complete, it must account for known neuroanatomy, network electrophysiology, pharmacology, pathophysiology, and

behavioral findings. Although the vast interconnectedness of the brain makes the formulation of a complete model computationally restrictive, scaled models of anatomical subsystems have offered new insights into brain function (Voytek, 2006). An example case system that has been well-studied is the basal ganglia which includes four main subnuclei: striatum, globus pallidus [internal segment (GPi) and external segment (GPe)], subthalamic nucleus (STN), and substantia nigra compact (SNc) and reticular (SNr)]. Movement disorders such as Parkinson's disease (PD) have been traced to basal ganglia dysfunction (Voytek, 2006, Bevan et al., 2006, and others). Bevan et al. (2006) integrate anatomical, physiological and computational studies to show how oscillatory processes at the levels of single neurons and neuronal networks in the subthalamic nucleus (STN) and external globus pallidus (GPe) are associated with the operation of the basal ganglia in both normal and in Parkinson's disease. Autonomous oscillation of STN and GPe neurons underlies tonic activity and is important for synaptic integration, whereas with Parkinson's disease, it results in abnormal low-frequency rhythmic bursting in the STN and GPe. They suggest that this finding supports the view that the basal ganglia use both the pattern and the rate of neuronal activity to encode information (Bevan et al., 2006).

As another example, Izhikevitch (2007) developed a large-scale model of the mammalian thalamo-cortical system with 10^{11} neurons with 10^{15} synapses. The model exhibited alpha and gamma rhythms, moving clusters of neurons in up- and down-states, and other interesting phenomena (see also <http://www.nsi.edu/users/izhikevitch/> and Scholarpedia-<http://www.scholarpedia.org/>). To develop this, he used simple models for spiking neurons combining the computational efficiency of the integrate-and-fire and

resonate-and-fire models and the biological properties of the Hodgkin-Huxley models. He shows how relatively simple models can provide detailed insights into the bifurcation mechanisms involved in the generation of action potentials and shows how the type of bifurcation affects the neuro-computational properties of the cells. His book provides extensive information about the modeling process, but is limited to the integrate-and-fire and resonate-and-fire model types. Thus, after justifying the use of the simple model, he develops the complex large-scale model, which is truly one of the very few to study higher level phenomena such as alpha and gamma rhythms.

The studies at the network and systems level are, however, few at the present time, primarily due to lack of information about the neurobiology. But with the increasing amounts of information being generated at the molecular and cellular levels, more such network/system level models will be developed. Systems scientists and engineers are predicted to play an increasing role in the development of such higher level models since they have developed a rich and large body of system theoretic concepts and models related to complex networks, learning and adaptation, optimization, and control which could be effectively used in the area of neuroscience, as more information emerges at molecular and cellular levels about the dynamics of pathways and their linkage to 'functions', including pathology.

Translational neuroscience is an important area that studies the impact of animal research on the understanding and treatment of human brain disorders. The animals used in such research include vertebrates and invertebrates. Translational neuroscience includes neuroethology, a growing area within neuroscience which emphasizes the study of neural mechanisms of natural behavior, as opposed to artificial conditions. The

expectation is that the study of neural mechanisms underlying a specific behavior in a particular animal will provide insights in a general sense to other species. For instance, the specializations of owls for hearing have provided insights into how sounds can be localized. Neuronal networks in insects and invertebrates are simpler to model and analyze. This has led to the emergence of a large group studying the stomato–gastric–ganglion, for instance, using computational modeling techniques (e.g., Marder and Goaillard, 2006). Similarly, simpler spinal cords of lampreys have provided rich information about the connectivity and pharmacology of neurons involved in generating locomotion. The expectation is that modeling smaller networks of this type will continue to reveal unexpected mechanisms that provide insights into the functioning of more complex brains. In addition to information about how such brain circuits implement various ‘functions’, research at the systems/network level has the potential to highlight the salient functions conserved across species in the nervous system, and, for instance, the role of neural adaptation in speciation. A multi–institutional project ‘Blue Brain’ is underway to develop a large scale model of a cortical column and structures (Sejnowski in Wikipedia–[http://en.wikipedia.org/wiki/ Computational_neuroscience](http://en.wikipedia.org/wiki/Computational_neuroscience)). Proceeding up in the modeling levels, researchers are beginning to use modeling tools to investigate the neural correlates of consciousness where most of the findings are speculative at the present time (Koch and Crick, 2003).

2.2.14. Computational Tools

Once the mathematical model for the neurobiological phenomenon has been developed (example of Hodgkin Huxley model shown in Box. 1 earlier), the values of the biophysical parameters have to be determined systematically. In addition to research

articles, sources for such information include databases such as CellPropDB, NeuronDB and ModelDB (<http://neuron.duke.edu/>). These websites also host entire computational models provided by authors of peer-reviewed articles, and the models themselves are available for download in many cases. After collecting information pertaining to biophysical parameters from various sources, one can proceed to the simulation phase.

Several computational modeling platforms are available depending on the expertise of the researcher. These range from general purpose software such as Matlab/Simulink (<http://www.mathworks.com/>) and XPP (<http://www.math.pitt.edu/~bard/xpp/xpp.html>) which permit the user to directly model the equations with parameters, to special purpose ones such as GENESIS (Bower and Beeman, 2003; <http://www.genesis-sim.org/GENESIS/>), and NEURON (Carnevale and Hines, 2006; <http://neuron.duke.edu/>) which are being designed for biologists with minimal understanding of the underlying mathematics. Both GENESIS and NEURON (and XPP) are available for free download from the sites listed. The websites also provide several tutorials for the beginning modeler. The packages can perform simulations of single neurons and of large networks of many abstract neuronal components. For example, a cerebellar Purkinje cell has been modeled in GENESIS with 4550 compartments and 8021 ionic conductances (De Schutter and Bower, 1994). Similarly Leblois et al. (2006) report a model to explain the pathology in basal ganglia with Parkinson's disease using a NEURON model. These packages can also be used to study cellular/network properties and biophysical properties of biochemical signaling pathways (Bhalla and Iyengar, 1999). However, the packages do not presently include biological knowledge or systems concepts.

2.3. COMPUTATIONAL RESEARCH IN COCAINE ADDICTION

2.3.1. Neurobiology of Cocaine Addiction

The neural structures involved in the circuit for cocaine abuse and dependence include the NAc core and shell, ventral pallidum, amygdala, hippocampus, PFC, and anterior cingulate gyrus (Everitt and Wolf, 2002; Koob et al., 2004; Kalivas et al., 2005). The cardinal features of cocaine addiction include uncontrollable urges to obtain drugs and reduced behavioral responding to biological rewards (Goldstein and Volkow, 2002). The fact that these characteristics persist after years of drug abstinence points to enduring neuroplasticity due to cocaine abuse in brain circuitry responsible for processing motivationally relevant stimuli (Kalivas et al., 2005). The primary adaptations produced by withdrawal from cocaine modeled in this proposal are outlined in Figure 7.

In rats trained to self administer cocaine, increased Glu release in the PFC–NAc projection (McFarland et al., 2004) and D1 receptor stimulation in the PFC (Capriles et al., 2003; McFarland et al., 2004; Sun and Rebec, 2005) are critical for reinstatement. One key cellular adaptation in the PFC pyramidal cells is an elevation in AGS3 that reduces signaling via D2 receptors (Bowers et al., 2004). The result is a heightened state of D1 tone that only allows the PFC cells to fire in response to strong (cocaine associated) stimuli, but limits output from relatively weaker stimuli (Seamans and Yang, 2004). Following withdrawal from cocaine, there is a reduction in basal extracellular Glu in the PFC–NAc synapse due to down–regulation of the cystine–glutamate exchange system (xc-), a mechanism contributing to the homeostatic regulation of extracellular Glu (Baker et al., 2003). The coincident increase in release probability for synaptic Glu and

drug reward seeking is reduced by restoring basal extracellular Glu levels (Baker et al., 2003). The increase in synaptic release probability may occur from a reduction in mGluR2/3 (Dietrich et al., 2002) signaling, a result occurring in part from the effects of increased AGS3 in the pre-synapse and in part from decreased cystine–glutamate exchange (Kalivas et al., 2005).

A number of potential cellular models of addiction have emerged over the last five years (Nestler, 2001; Koob et al., 2004; Kalivas et al., 2005). However, the systematic mathematical modeling of these adaptations to evaluate physiological impact on relevant circuitry (i.e. the PFC to NAc projection) is non-existent.

We report preliminary work related to computational modeling of elements in the PFC–NAc glutamatergic pathway to study cellular adaptations during withdrawal, within a larger modeling framework described below. The overall model for the PFC–NAc pathway functions as follows: the PFC pyramidal cell fires which results in release of Glu in the PFC–NAc synapse, with the release itself being modulated by a feedback loop involving mGluRs on the pre-synapse. The Glu released into the synapse diffuses out of the synapse and is largely transported via Glu transporters on the glial sheath that surrounds the synapse. We have modeled Glu homeostasis in the perisynaptic region considering the Glu release, transporter dynamics, tortuosity, and the xc- pump to highlight the importance of the various mechanisms involved.

We start with the morphology of the PFC pyramidal cell, followed by the mathematical details of channels, membrane potentials, and a compartmental model for a single cell, and their predictions. The simplified single cell model facilitates analytical study of the mechanisms involved, as illustrated below in the model for Glu release from

the PFC efferents. A discussion of on-going work on network level modeling similar to that in Durstewitz et al. (2000) is then reported.

2.3.2. Computational Model of Elements in the PFC–NAc Pathway

We report a computational modeling framework for the PFC–NAc glutamatergic pathway developed by our team which consists of ‘modules’ at the molecular and cellular levels, with a modeling approach for each module as described in an earlier section. The framework thus facilitates viewing the overall problem as a set of modules with each serving particular functions. The modules, in turn, are described by ODEs or PDEs. Such a framework permits the modules to be updated continuously as new data and information about neurobiology become available, e.g., new estimates of kinetic constants. The models reported in the following should thus be taken as being continually evolving since their structure facilitates incorporation of emerging information related to mechanisms and parameters in the pathway.

2.3.3. Excitability of the PFC Pyramidal Cell–Single Cell and Network Models

For the PFC–NAc pathway, we begin with an intrinsically bursting (IB) cortical layer V pyramidal cell as in Durstewitz et al. (2000). Within the deep cortical layers, IB neurons comprise greater than 60% of the neuronal content (Yang et al., 1996), including those that project to the NAc (Yang and Seamans, 1996). The model for such a pyramidal cell has one spherical soma and three cylindrical dendrite compartments with the same dimensions as in Durstewitz et al. (2000). The dendrite compartments are identified as basal, proximal apical, and distal apical. Durstewitz et al. (2000) considered an additional 92% increase in surface area from spines by increasing the effective membrane

capacitance and leakage conductance, and we consider a similar alteration in the passive electrical properties.

Modeling Ion Channels. The compartment model with linear current equations yields the following governing equation for the pyramidal cell (Keener and Sneyd, 1998):

$$C_m \frac{dv}{dt} = \sum g_r x y (v - v_r) + g_{leak} (v - v_{leak}) \quad (2.11)$$

where C_m is membrane capacitance, g is maximal conductance; x , y are activation/deactivation gating variables; v is membrane potential; and v_r is the reversal potential for channel r .

The Durstewitz et al. (2000) created model included spike generating sodium (Na) and persistent (NaP) sodium channels, a high voltage activated calcium channel (HVA), as well as delayed rectifying (DR), slowly inactivating (KS), and C-type potassium channels.

$$\begin{aligned} I_{NaP} &= g_{NaP} m^3 h (v - v_{Na}) & I_{DR} &= g_{DR} n^4 (v - v_K) \\ I_{Na} &= g_{Na} m h (v - v_{Na}) & I_{KS} &= g_{KS} a b (v - v_K) \\ I_{HVA} &= g_{HVA} u^2 v (v - v_C) & I_C &= g_C c^2 (v - v_K) \end{aligned} \quad (2.12)$$

Synaptic currents are simulated using the set of equations labeled (3.3). N-methyl-D-aspartate (NMDA) and alpha-amino-3-hydroxy-5-methyl-4-isoxazole propionate (AMPA) currents are modeled by dual exponential functions with NMDA containing an additional gating term for the magnesium block, while the GABA_A synaptic current is modeled by an alpha function.

$$\begin{aligned}
I_{AMPA} &= g_{AMPA} [\tau_{1A} \tau_{2A} / (\tau_{2A} - \tau_{1A})] \times [\exp(-t / \tau_{2A}) - \exp(-t / \tau_{1A})] (v - v_{AMPA}) \\
I_{NMDA} &= g_{NMDA} \times \frac{1.50265}{1 + 0.33 \exp(-0.06v)} \times [\tau_{1N} \tau_{2N} / (\tau_{2N} - \tau_{1N})] \times [\exp(-t / \tau_{2N}) - \exp(-t / \tau_{1N})] (v - v_{NMDA}) \\
I_{GABA} &= g_{GABA} \times t / \tau_{GABA} \times \exp(t / \tau_{GABA} + 1) (v - v_{GABA})
\end{aligned}
\tag{2.13}$$

where τ_{1A} and τ_{2A} , in the dual exponential function for AMPA represent time constants for the subsequent post synaptic currents (PSCs) elicited by each incoming spike event, and τ_{1N} and τ_{2N} represent the same for NMDA receptor mediated currents. The term v_{GABA} in the GABA alpha function is the time constant for the PSCs that are produced via this ionotropic inhibitor. The parameters used for this part are the same as in Durstewitz et al. (2000) and the changes to some of these due to cocaine are described below. Readers interested in additional mathematical details related to these equations are referred to recent modeling textbooks (e.g., Byrne and Roberts, 2004, Keener and Sneyd, 1998). Values for the various channel parameters for this part are the same as in Durstewitz (2000).

Modulation of excitability by cocaine. Several recent papers have investigated causes for the changes in excitability due to cocaine. These involves effects due to changes in AGS3 levels, and changes in K^+ and Ca^{2+} channels, which are discussed next.

In modeling a pyramidal cell, Durstewitz et al. (2000) consider two states for dopamine signaling: ‘State 1’ which has dominant dopamine signaling via D2, and ‘state 2’ with dominant D1 signaling (Trantham–Davidson et al., 2004). Kalivas et al. (2005) hypothesize the adaptation occurring in activator of G protein signaling–3 (AGS3) with withdrawal as shifting the pyramidal cell toward state 2, since elevation in AGS3 levels reduces signaling via D2 receptors (Bowers et al., 2004). Kalivas et al. (2005)

hypothesize that this reduction in D2 receptor signaling shifts the pyramidal cell toward state 2 (from the naturally dominant state 1).

Durstewitz et al. (2000) consider a linear variation in dopamine neuromodulation of several channel conductances with D1 receptor activation, shifting from the state 1 behavior with low D1 activation to state 2 behavior with high D1 activation. Specifically, they model the shift to state 2 with marked decreases in I_{NaP} threshold, I_{Ks} conductance, and AMPA channel conductance, and an increase in NMDA channel conductance. The reduction in AMPA makes it more difficult for weak inputs to drive the cell to its spike threshold, while spikes are potentiated for strong inputs. Since AGS3 alters D2 signaling, we propose the use of the dopamine signaling model for the cocaine case, using AGS3 levels instead of that of dopamine, i.e., AGS3 plays the same role as dopamine in altering the properties of the channels cited.

Dong et al. (2005) report that dopamine signaling via D1 selectively reduces potassium currents by about 35% in the chronic cocaine withdrawal case, predominantly through the slowly inactivating current I_{Ks} . The authors have modeled the reduction in channel conductance over the entire cell as the dopamine is increased from a low to a high state as approximately 50%. The same group (Nasif et al., 2005) also report an increase in calcium currents due to elevated dopamine levels in for the same case. They have attributed this phenomenon to an approximately 20% increase in L-type conductance in the neuron's soma. Both these changes contribute to an increase in the excitability of the PFC cell due to cocaine, as our preliminary results in Figure 8 show. Note that there is strong adaptation in the PFC firing implying that background input and network connectivity is important in determining the firing frequency. Apparently at odds

with these findings, Lavin et al. (2006) report in-vivo single cell recordings indicating that in the chronic cocaine withdrawal case, there is a reduction in action potentials with current-evoked case. The spontaneous state did not show any reduction in action potentials, though. They suggest that intrinsic channels other than the calcium and potassium ones may be modulated by cocaine. In addition to the possibly of other channels being involved, another explanation for the different findings could be the changes in ‘background’ input to a cell caused by the network, including GABA inhibition, as described next. A computational model could be very useful to reconcile such differences, and determine the underlying channel adaptations.

Network model. Heightened D1 renders the single cell model more excitable principally by lowering the persistent sodium threshold, while in a network sense, the effect of increasing NMDA also contributes to excitation. Further, the reduction in AMPA depolarization current prevents weaker signals from eliciting an action potential. The functional importance of GABA to this attenuation is also critical, and so interneurons providing inhibitory inputs need to be considered. The next step in PFC modeling efforts will be to model a network of pyramidal cells and interneurons to improve the predictions of PFC cell firings, compared to that of the single cell model described. In the meantime, we use a 2 Hz firing for the control case and 4 Hz for the cocaine case in the model in section 2.3.4.

Activation of mGluR2/3 receptors. The role that the mGluR2/3 autoreceptor plays in the firing rate of the pyramidal neuron is to regulate synaptic release probability, where increased activation creates suppression of subsequent release; an example model illustrating this phenomenon at the calyx of Held synapse in the auditory pathway is

reported in Billups et al. (2005). A reduction in activation of mGluR2/3 associated with cocaine withdrawal, could lead to increased release probability from the PFC pyramidal neuron, resulting in increased glutamate in the PFC–NAc synapse. Peters et al. (2005) have reported an increase in firing frequency with expected cocaine reward in rat nucleus accumbal neurons, which may be a direct result of such an increase in Glu in the PFC–NAc synapse. No previous modeling efforts to quantify these neuroplasticity mechanisms have examined this synaptic release and its regulation. We propose next a simplified model to investigate the regulation of Glu release by mGluRs, including plasticity in release probability due to cocaine.

2.3.4. Simplified Model for Synaptic Glu Release from PFC Pyramidal Cell Axon Terminals in NAc

A simplified model for the release of synaptic Glu from the PFC terminals in the NAc is proposed, with input as the number of action potentials along the PFC pyramidal cell axon and output as the Glu release in number of molecules, as shown in Figure 9. The nominal value of `Glu_release_per_spike` is constant for a fixed release probability. Cellular adaptations due to cocaine change this release probability through a series of downstream events, each of which is listed below using the blocks in Figure 9:

Presynaptic cell. Exocytosis is modeled (9 differential equations not listed here) using a two–pool model for estimating the number of releasable vesicles (Billups et al., 2005) and release probability. This release probability is modified by the cellular adaptations as described below. In the model below, `N_Glu_release_per_spike` is multiplied by the number of spikes per second `n_spikes`, to calculate `N_Glu_in`, the rate of Glu release into the synapse by exocytosis.

Perisynaptic space. The two mechanisms affecting Glu concentration in the synapse and perisynaptic space are diffusion and re-uptake, both modeled as being proportional to the synaptic Glu concentration, with gains $k_{\text{diffusion}}$ and k_{uptake} , respectively. A gain k_4 is included in the re-uptake model to characterize possible changes in that process due to cocaine, while diffusion is not affected by cocaine.

Cystine glutamate exchanger. The xc- exchanger generates glutamate outside the synapse (more details in the next section) and influences the Glu concentration at the mGluRs located on the presynaptic cell. These mGluRs regulate release probability. The gain k_3 models the plasticity in the xc- exchanger due to cocaine.

Regulation of release probability. The term $\text{Glu_release_per_spike}$ is modulated by *changes* in the mGluR receptor tone and in AGS3 signaling in the terminals, represented by the gains k_1 and k_2 respectively in Figure 9; the gain K is for scaling purposes only. The suppression term in the model is obtained by multiplying these gains with the concentration of extracellular Glu.

The output of the block to the right in Figure 9, $N_{\text{Glu_syn}}$, the concentration of Glu in the synapse, can then be represented by Eqn. 2.14.

$$N_{\text{Glu_syn}}(t+\Delta t) = N_{\text{Glu_syn}}(t) + [N_{\text{Glu_in}} - N_{\text{Glu_syn}}(t) * k_{\text{diffusion}} - N_{\text{Glu_syn}}(t) * k_{\text{uptake}} * k_4] * \Delta t \quad (2.14)$$

The other variables in this simplified model can be obtained using the expressions and logic in the schematic of Figure 9.

Experimental data for modeling. Estimates of glutamate levels are available for the extracellular space. We consider 4 micro-molar (μM) concentration within the extracellular space for the nominal case, and a 2 μM concentration for the withdrawal

case (Table 2), a consequence of the functional down regulation by the xc- exchanger. Previous simulations have considered a very low or negligible level of background glutamate in the synapse (Diamond, 2005). We use a concentration value of 10 millimolar (mM) in the synapse after a normal vesicular release (Grewer and Rauen, 2005).

For this simplified model, starting with nominal values for the gains, the objective is to determine alterations in Glu release by changing the gains, to simulate neuroplasticity in the mechanisms. Since our interest is in determining the *change* in Glu release, the gains are selected (see Table 2) to provide reasonable values for the concentrations in the synapse. The two blocks for diffusion and uptake in Figure 9 were modeled using constant gains $K_{\text{diffusion}}$ and K_{uptake} in this simplified model (see section 2.3.6 for more detailed models for these blocks), and values for these were selected to give the clearance times in Rusakov and Kullmann (1998). As indicated in Table 2, we assume that uptake is not affected by cocaine, i.e., k_4 does not change with cocaine.

2.3.5. Predictions of Synaptic Glu Release

As mentioned earlier, the single cell model was simulated for both control and cocaine cases, assuming a current injection input to the pyramidal cell. The firing of the PFC cell provides the value for n_{spikes} which is used as an input for this simplified model.

For the proposed simplified model for Glu release from the terminals (Figure 9), the decreased tone on the mGluR2/3 receptors with chronic cocaine is modeled (Table 2) by a 50% reduction (Xi et al., 2002) in gain k_1 , and the down-regulation of the xc-exchanger is modeled by a 70% reduction in gain k_2 (Baker et al., 2003). In addition, the extracellular level of Glu reduces by 50% due to cocaine. The net result of these

adaptations is that, with the same level of input to the PFC pyramidal cell, there is an increase in the level of glutamate released into the synapse, i.e., each spike elicits a greater release of Glu for the withdrawal case.

After the model comes to steady state in 1500s (Ca dynamics), an injection current of 70 pA is applied to the PFC cell soma in both cases to simulate identical inputs. The cocaine case includes the combined effect of the signaling change due to cellular adaptations in the PFC (which increases the number of spikes n_{spikes} , for the same level of current injection), and of all the cellular adaptations at the terminals cited above. Using the parameters in Table 2, the amount of glutamate released into the synapse is found to nearly double with each spike for the withdrawal case, as compared to the control case (Figure 10). This result is consistent with initial observations that the glutamate release levels are nearly doubled with chronic cocaine (Table 3).

Figure 10A shows that with an increased excitability found in the cocaine case, there is a reduction in release probability due a decrease in the size of the releasable pool. Figure 10B shows this reduction in the available fractional level of releasable transmitter pool size with increased spiking. The reduction in the gains k_1 and k_2 (Table 2) due to cocaine causes a lowering of this suppression of release probability, compared to the control case which has higher gains and higher suppression. So, suppression due to mGluR2/3 is blunted, diminishing this reduction. As shown in Figure 10C, this reduction in suppression helps maintain output levels despite a reduction in the number of vesicles available for release.

The overall effect can be described as follows: with normal release, the release of glutamate in the synapse is approximately 10 mM/spike. This per spike value decreases

for the cocaine case due to fewer vesicles being available for release; however, the blunting of mGluR receptors which cause suppression of release, and the increase in spike frequency causes a greater overall release. As indicated earlier, the increase in spike frequency for the PFC cell due to cocaine is still not clearly established and this model will have to be further refined as the PFC model is updated.

There are more overall spikes in the cocaine case in our present model for the same level of intrinsic excitation (Figure 10C; as noted, this itself is still under study). However, we would expect fewer spikes for a general excitation of NMDA and AMPA receptors in the PFC due to inhibition of AMPA via D1 receptor activation, while the cell would remain more excitable to those inputs that are able to elicit an action potential (such as cocaine seeking), due to increased NMDA activation and adaptations in other currents. Such synaptic mechanisms indicate the need for a network model and an increased level of detail in modeling the mechanisms to accurately determine their effects on release probability. The need for a network model has been mentioned earlier, and is an important future step in our study. Another part of the overall framework which involves a more detailed model for the block labeled ‘perisynaptic space’ in Figure 9, is described in the next section.

2.3.6. Modeling Glu Homeostasis in the PFC–NAc Perisynaptic Region

The previous component model provides a prediction for Glu release into the synaptic space with each spike, assuming a feedback mechanism involving mGluRs in simplified form (Figure 10). Here we attempt to model the three blocks of Figure 10 labeled ‘perisynaptic space’, ‘cystine glutamate exchanger’, and ‘Regulation of release probability’ in more detail using a discretized version of partial differential equations for

diffusion, and Michaelis–Menten equations for binding and transport. This will provide improved predictions of both transient and steady state Glu levels in the perisynaptic and extracellular spaces. The information will also enable us to model the feedback mechanism via excitation of the mGluR autoreceptors more realistically. The geometry and the equations used for this modeling are described next. Specific values of the parameters used in the model are listed in Table 4 later.

Box 2. Neurobiology information relevant to model development

Glial sheath

- Occurrence of glia (CA1 and PFC) on the post synaptic side is more than three fold of that of the presynaptic side (Lehre and Rusakov, 2002)
- Glia volume fraction: 10% (CA1); Glia surface area : $1.88 \mu\text{m}^2 / \mu\text{m}^3$ (Lehre and Rusakov, 2002)
- 100 nm of glia sheath is the minimum width observed in 3D profiles (Rusakov, 2001)
- Glia occupies 32% of the tissue volume near PFC synapses. The occurrence of glial membranes adjacent to these synapses was calculated to be 67% (Lehre and Rusakov, 2002)
- Most of the synapse could be covered by glia (95% glia coverage) (Rusakov, 2001)
- Glia could be made present in the periphery of the synapse. This could be justified by glial presence to prevent cross talk (Danbolt, 2001)
- The composition of the tissue (neuropil part) is so complex that a cube of gray

matter, e.g. (hippocampus CA1) measuring $1 \times 1 \times 1 \mu\text{m}$ contains total plasma membrane with a surface area of $14 \mu\text{m}^2$, of which 10% is due to astroglia (Danbolt, 2001)

- Diffusion out of the synaptic cleft is limited by size and tortuosity. Diffusion of glutamate is limited by glial covering, and partly by binding to glutamate transporters (Rusakov, 2001)
- Transporters that play a major role in glutamate removal in the brain have been identified and characterized, including two main glial transporters EAAT1–2, also known as GLAST/GLT and one neuronal type, EAAT4 (Lehre and Rusakov, 2002)
- It has been shown that there are between 15000 to 21000 glia glutamate transporter molecules are present/ μm^3 in the tissue of hippocampus (Danbolt, 2001)
- Near PF synapses, the glia volume and cell surface fractions are 3.4 to 2.7 times higher than CA1(Lehre and Rusakov, 2002)
- For unrestricted diffusion, tortuosity and volume fraction = 1; For restricted diffusion, tortuosity ≥ 1 , and volume fraction ≤ 1 (Barbour and Hausser, 1997)
- K_1 for mGluR = $10^7 \text{ m}^{-1}\text{s}^{-1}$ [$k_1\text{mglur}=7000$] used for calculation; K_{-1} for mGluR = $50 \text{ (s}^{-1}\text{)}$; [used value 0.007] (Barbour and Hausser, 1997)
- Varied k_{-1} and k_2 values to prove hypothesis that glutamate transporter binding is followed by fast translocation step; it was argued that this enhances glutamate removal(Lehre and Rusakov, 2002)

- Glial coverage of synapses directly regulates activation of extrasynaptic metabotropic receptors in the hypothalamus (Lehre and Rusakov, 2002)

Glutamate

- Brains produces huge amount of glutamate. 5–15 mmol per kg wet weight depending on the region. Glutamate is released from a variety of sources and a variety of mechanisms (Danbolt, 2001)
- Brain tissue has a remarkable ability to accumulate glutamate. This ability is due to glutamate transporter proteins present in the plasma membranes of both glia and neurons (Danbolt, 2001)
- Concentration gradient of glutamate across the plasma membranes is several thousand folds. The highest concentration is found inside the nerve terminals (Danbolt, 2001)
- There is no enzyme extracellularly that metabolizes glutamate; hence, the only rapid way to remove glutamate from the extracellular fluid surrounding the receptors is by cellular uptake (Danbolt, 2001)
- Diffusion can only work quickly over very short distances and it can be an efficient synaptic removal mechanism as long as the glutamate concentration in the extracellular fluid outside the synapse is kept low (Danbolt, 2001)
- Glutamate uptake is essential in controlling excitatory action of glutamate. It is the mechanism for maintaining low extracellular glutamate concentration in the long term (Danbolt, 2001)
- Release of glutamate, densities of glutamate transporters and receptors are

regulated in part by glutamate itself (Danbolt, 2001)

- The concentration of Glu in the extracellular space and the cerebrospinal fluid are around 3-4 μM and around 10 μM respectively (Danbolt, 2001)
- Astrocytes also contain the machinery for exocytotic release of glutamate (Danbolt, 2001)
- The fact that glutamate can be released by a number of different mechanisms and from both neurons and glia imply that there is release of glutamate not only into synaptic clefts, but also other parts of extracellular space (Danbolt, 2001)
- Transporters located inside the synaptic cleft can directly interfere with the glutamate concentration there (Danbolt, 2001)
- The pattern of activation of various receptor and transporter protein populations and the effect of the released glutamate depends on the glutamate concentrations achieved at the various locations from the release site and well as how quickly the concentrations change (Danbolt, 2001)
- The removal of glutamate from the cleft depends upon uptake, diffusion which again depends on concentration of water, tortuosity of extracellular space, and the interaction with glutamate binding sites. None of these parameters are known (Danbolt, 2001)
- Steady state value of Glu concentration was measured at 5 μM (Rusakov, 2001)

Presynaptic vesicle release and release probability

- Glutamate is transported into synaptic vesicles by a vesicular glutamate transporter and released by exocytosis (Danbolt, 2001)

- Concentration of glutamate inside vesicles is believed to be 0.1M (Danbolt, 2001)
- Vesicle diameter ranges from 25 nm to 45 nm. (Danbolt, 2001)
- Vesicle diameter of 45 nm and glutamate concentration of 150 mM = 4300 molecules (Danbolt, 2001)
- The synaptic release probability depends on the size of the readily releasable pool of vesicles (Danbolt, 2001)
- An average central synapse has about 20 release sites which need about 10s to refill (Danbolt, 2001)
- Average sustainable release capacity is approximately two vesicles per μm^3 of tissue per second (Danbolt, 2001)
- Average density of glutamatergic synapses are about 0.9–1.3 per μm^3 in CA-1 (Danbolt, 2001)
- In many synapses, release probability increases during two or three stimulations in a train due to facilitation (Trommerhauser et al., 2003)
- The calyx of Held synapse is a fast–excitatory, glutamate–mediated connection and contains hundreds of individual active zones which operate in parallel when activated by an action potential (Trommerhauser et al., 2003)
- There are about 550 active zones in the calyx of Held synapses (Trommerhauser et al., 2003)
- Each site is occupied by either an empty or a readily releasable vesicle (Trommerhauser et al., 2003)
- Depleting the pool of vesicles by strong stimulation led to estimates that the total

number of releasable pool of vesicles is in the range of 1800– 3000 (Trommerhauser et al., 2003)

- Average probability of release from single active zones is only 0.25–0.4 for single action potential under physiological conditions (Trommerhauser et al., 2003)
- The low number for release probability with the large number of releasable vesicles indicates that depletion of the pool of releasable vesicles during short trains of action potentials cannot be expected, unless such depletion is restricted to a subset of more readily releasable vesicles (Trommerhauser et al., 2003)
- Number of vesicles released is proportional to the respective pool occupancy and the release probability (Trommerhauser et al., 2003)

mGluR

- The NMDA and AMPA/kainate receptors are glutamate gated ion channels and are referred to as ionotropic glutamate receptors (Danbolt, 2001)
- The third family of glutamate receptors consists of G–protein coupled receptors, so called metabotropic receptors (mGluR 1–8), which are subdivided into 3 groups (Danbolt, 2001)
- Group III mGluRs are expressed presynaptically in many brain regions and pharmacological activation by agonists generally leads to inhibition of transmitter release (Lopez, Humbel, Pflimlin and Kew, 2003)
- The functional characteristics of excitatory synapses differ significantly between pathways and regions (Castro–Alamancos and Connors, 1997)
- There are several forms of short term plasticity such as facilitation, depression,

augmentation and potentiation that involve presynaptic mechanisms (Castro–Alamancos and Connors, 1997)

- Facilitation is caused by a transient increase in the probability of transmitter release following synaptic activation and apparently depends on a small residual increase in presynaptic internal Ca^{+} concentration (Castro–Alamancos and Connors, 1997)
 - Synapses that have a low probability of release tend to have large facilitation, because the second stimulus in a pair will evoke release (Castro–Alamancos and Connors, 1997)
 - Synapses with high probability of release tend to display depression, because of
 - the pool of vesicles available for release becomes depleted after an initial successful release (Castro–Alamancos and Connors, 1997)
 - Localization of presynaptic receptors related to transmitter release sites is of high functional importance (Castro–Alamancos and Connors, 1997)
 - While group II mGluRs are generally found at perisynaptic sites or without an obvious correlation to the glutamate release sites, group III mGluRs are concentrated at presynaptic active zones (Lorez, Humbel, Pflimlin and Kew, 2003)
 - There is convincing evidence that group II mGluR's serve as auto inhibitory feedback receptors during short term synaptic processing in the hippocampus (Lorez, Humbel, Pflimlin and Kew, 2003)
-

Perisynaptic geometry. The geometry of the perisynaptic space is not very well understood at the present time. We consider one typical configuration shown in Figure 11. The ‘production’ terms for glutamate in the model come from xc- pumps and by vesicular Glu release in the synapse. The glial sheath, with its particular geometry and transporters that ‘consume’ glutamate, act as the ‘control’ to regulate glutamate levels in the perisynaptic space within physiological limits. In this section we seek answers to ‘Using the laws of diffusion, binding, and transport, what glial geometry, and transporter and xc- concentrations, satisfying known neurobiology (Box 2), will predict reported physiological levels of Glu within the perisynaptic space?’

Consider the configuration in Figure 11. The synaptic disc, denoted as *region I*, has a radius of 160 nm (Rusakov and Kullmann, 1998) with a thickness of 20 nm. The two hemispherical regions around the cleft representing the pre and post-synaptic terminals are assumed rigid permitting no diffusion (Rusakov and Kullmann, 1998; Rusakov, 2001, Diamond, 2005). Upon release from the synapse, glutamate molecules diffuse into the perisynaptic space (Barbour and Hausser, 1997), where glutamate transporter dense glial astrocytes reduce glutamate spillover (Danbolt, 2001). A thin spherical layer of free space (region R_a , described below) encloses the edge of the synapse. Outside this is a region of porous neuropil, which is considered isotropic and is reduced in complexity via the use of tortuosity and volume fraction constants (regions G_1 , G_2 and the porous neuropil indicated in yellow). The tortuosity factor λ represents the increase in mean free path to diffusing glutamate molecules due to obstacles in the porous medium (Rusakov and Kullmann, 1998). The factor scales the diffusion coefficient for glutamate in free medium from D to D/λ^2 . The volume fraction α increases the diffusion source strength by $1/\alpha$

(Rusakov and Kullmann, 1998).

High levels of extracellular glutamate are harmful, and removal of extracellular glutamate by Excitatory Amino Acid Transporters (EAAT) is critical to prevent glutamate toxicity (Danbolt, 2001). As mentioned, the PFC–NAc synapse is assumed to be covered by a glial sheath (Lehre et al., 1995) to absorb glutamate overflowing the synapse. Indeed, astroglial membranes facing neuropil are more likely to include a higher density of transporters (Danbolt, 2001) than membranes that appose glia. The principal EAAT glutamate transporter in the CNS is GLT which includes the striatum (Danbolt, 2001, Furuta et al., 1997). GLT is commonly expressed in glial astrocytes, such as those that often completely surround corticostriatal afferents (Lehre et al., 1995). The density of GLT transporters is nonuniform, and glial membranes that face neuropil have a higher expression of GLT than membrane surface facing other glia. In a model of synaptic release, Rusakov (2001) considered transporter concentration as adjacent to a spherical or semispherical glial sheath that surround the neuron. EAATs (which includes both GLAST and GLT, though GLT is prominent) are expressed with a high density in the hippocampus, with a surface density of 5000–10000/ μm^2 (Lehre and Danbolt, 1998). Transporter labeling is high in hippocampus and cortex regions (GLT is expressed at 93% of the hippocampal density), moderate in the striatum, and low in the cerebellum (GLT is expressed at 24% of the hippocampal density).

Experimentation on CA1 hippocampal astrocytes (Diamond, 2005) suggests that their concentration is between 75 and 150 μM , corresponding to 6500–13000/ μm^2 . Our model assumes that the concentration of GLT in the cortex is also in this range. Colombo (2005) has shown the rate of glutamate uptake in striatum to be approximately 22–35% of that in

the cortex.

Region Ra represents free space outside the spherical synaptic apposition zone where no transporters are present, a transition space between the free synaptic medium and the porous neuropil, a morphology adapted from that for hippocampal pyramidal neuron synapses from Rusakov (2001). This region, which is 25 nm thick, has mGluR2/3 autoreceptors at $\theta = 20^\circ$ from the vertical in Figure 11 (100 nM concentration) that are ‘sensors’ in the negative feedback loop controlling Glu release from the PFC terminals.

Region G₁ and G₂ represents the transporter rich glial membranes. This region is subdivided into two parts: region G₁, with a high density of transporters, and G₂, which contains a reduced concentration of transporters (Table 5). xc- exchangers are located on the outer surface of the glial membranes of G₂, with an exchange velocity of 0.6 nM/ms. For achieving physiological levels of extracellular Glu (Danbolt, 2001), the reported configuration required a production rate of 10^{-4} femtomoles of Glu per second by xc-pumps, and these xc- pumps were distributed in eight sectors of the outer regions of glial membrane G₂.

Region R_b is the extracellular space containing diffused Glu but has no transporters or xc- pumps. Glu concentration in this region is thus controlled passively by a balance between the xc- pumps located on G₂, by Glu release in the synapse, and by glutamate uptake through transporters. This region extends up to 1 μm from the edge of the synapse. The outer boundary of this region has a point P_b where concentration measurements are made as indicated in Figure 11.

Diffusion, binding and transport dynamics. The principal mechanisms involved in transient glutamate dynamics in the perisynaptic region are glutamate diffusion out of the

synapse after release, binding to transporters and uptake in the glial sheath, production of glutamate by the xc- pumps, and activation of mGluR2/3 autoreceptors.

We begin by discretizing the extracellular space into small compartments which are assumed to have uniform concentrations of Glu and transporters within them at any particular instant. Glu concentration in each compartment is then updated each integration interval based on the diffusion, transport and production rates, as applicable. Regions R_a , R_b , G_1 , G_2 , in the extracellular space are discretized into $i = (1 \dots N_i)$ concentric spherical elements each of thickness dR , and each spherical element is divided into $j = (1 \dots N_j)$ annular sections where N_j is determined by $d\phi$. A mass balance for Glu each compartment yields Eqn. 2.15 (Rusakov, 2001),

$$Glu(i, j, t) = Glu(i, j, t - dt) + (\Sigma(J_R)S_R + \Sigma(J_T)S_T) \frac{dt}{V(i, j)} + (v_+ - v_-) \quad (2.15)$$

where $S_{Ri,j} = 2\pi R_i^2(\cos\phi_j - \cos\phi_{j-1})$ is the surface area between adjacent volume elements in the radial direction, and $S_{Ti,j} = 2\pi R_i \sin\phi_j (dR)$ is the surface area shared by adjacent volume elements in the tangential direction. The radial and tangential fluxes into the compartment are denoted by J_R and J_T respectively. Each compartment has a volume of $V(i,j) = 0.5(S_{Ri,j} + S_{Ri-1,j})dR$. For our simulation runs, $dR = 25$ nm and $d\phi = \pi/9$ radians. The term v_+ accounts for the production of Glu by the xc- exchanger and unbinding of Glu from the transporters, while the term v_- accounts for reduction in Glu due to transporter binding.

2.3.7. Nomenclature

k_1	forward reaction rate for glutamate binding with transporters
k_2	forward reaction rate for glutamate binding with transporters
k_{-1}	backward reaction rate for glutamate binding with transporters

$[Glu]$	concentration of free glutamate
$[T]$	transporter concentration
$[GluT]$	concentration of bound glutamate
$[R]$	Receptor concentration
$[Glu_{bo}]$	concentration of glutamate bound to receptors
k_{Im}	forward reaction rate, glutamate binding with receptors
k_{-Im}	backward reaction rate, glutamate binding with receptors

The synaptic cleft volume is discretized into $m = (1 \dots N_m)$ segments where dR_m is the radius of the cylindrical elements with a volume $\pi(R_m^2 - R_{m-1}^2) \cdot (\text{synaptic thickness})$, and contact surface between adjacent elements is $S_m = 2\pi R_m \cdot (\text{synaptic thickness})$. Eq. 1 was then applied to diffusion through the cleft, with no transporters present in this space, i.e., $v_+ = v_- = 0$. The parameter $dR_m = 40$ nm for the simulation.

The glutamate flux J between adjacent volume elements A and B is computed by Eqn. 2.16,

$$J_{AB}(t) = -D\nabla(Glu) = -\frac{D}{ds}(Glu_A(t-dt) - Glu_B(t-dt)) \quad (2.16)$$

where ds is the spatial distance between compartment centroids. For each compartment, this flux is calculated considering two others connected to it radially, and two connected in the tangential direction. Within a compartment, binding of glutamate with transporters is governed by the law of mass action (Rusakov and Kullmann 1998),



The differential equation form for this reaction, Eqn. set 2.18, gives the rate balance terms using the fact that the total transporter concentration in a compartment is conserved:

$$\begin{aligned}
\frac{d[Glu]}{dt} &= -k_1[Glu][T] + k_{-1}[GluT] \\
\frac{d[GluT]}{dt} &= k_1[Glu][T] - k_{-1}[GluT] - k_2[GluT] \\
[T_{total}] &= [T] + [GluT]
\end{aligned} \tag{2.18}$$

The discrete form of Eqn. set 2.18 is as follows (Rusakov, 2001):

$$\begin{aligned}
[Glu]_t &= [Glu]_{t-dt} + (-k_1[Glu]_{t-dt}[T]_{t-dt} + k_{-1}[Glu - T]_{t-dt})dt \\
[Glu - T]_t &= [Glu - T]_{t-dt} + (k_1[Glu]_{t-dt}[T]_{t-dt} - k_{-1}[Glu - T]_{t-dt} - k_2[Glu - T]_{t-dt})dt \\
[Glu - T]_t + [T]_t &= [Glu - T]_{t-dt} + [T]_{t-dt} = [T_{total}]
\end{aligned} \tag{2.19}$$

The diffusion coefficient D is taken as $.3 \mu\text{m}/\text{ms}$ (Diamond 2005, Rusakov, 2001). The tortuosity factor $\lambda=1.4$, and volume fraction $\alpha = 0.12$, are from hippocampal neuropil (Rusakov, 2001). The parameters for glutamate uptake dynamics are estimated from experiments (Bergles and Jahr 1998, Wadiche et al., 1995) as $k_1 = 10^4 \text{M}^{-1}\text{ms}^{-1}$, $k_{-1} = 0.2\text{ms}^{-1}$, and $k_2 = 0.1\text{ms}^{-1}$.

Binding of glutamate to the mGluR2/3 autoreceptors follows similar dynamics (Rusakov, 2001),



The reaction kinetics result in Eqn. set 2.21, of which the discretized version is given by Eqn. set 2.22 (Rusakov, 2001),

$$\begin{aligned}
\frac{dGlu_{bo}}{dt} &= k_{1m}[Glu_{free}][R] - k_{-1m}[Glu_{bo}] \\
\frac{dGlu_{free}}{dt} &= k_{-1m}[Glu_{bo}] - k_{1m}[Glu_{free}][R]
\end{aligned} \tag{2.21}$$

$$\begin{aligned}
[Glu_{bo}]_t &= [Glu_{bo}]_{t-dt} + (k_{1m}[Glu_{free}]_{t-dt}[R]_{t-dt} - k_{-1m}[Glu_{bo}]_{t-dt})dt \\
[R]_t + [Glu_{bo}]_t &= [R_{tot}]
\end{aligned}
\tag{ 2.22}$$

This leads to Eqn. 2.23, which assumes there is no significant alteration in the concentration of glutamate associated with receptor binding.

$$[Glu_{bo}]_t = [Glu_{bo}]_{t-dt} + (k_{1m}[Glu_{free}]_{t-dt}([R_{tot}] - [Glu_{bo}]_{t-dt}) - k_{-1m}[Glu_{bo}]_{t-dt})dt
\tag{ 2.23}$$

The kinetic constants $k_{1m}=7 \times 10^3$ M/ms, and $k_{-1m}=0.007$ /ms corresponding to high affinity glutamate receptors (Rusakov, 2001). The concentration of mGluRs is assumed to be 100 nM (Kalivas 2006, personal communication). Extracellular glutamate concentration plays a role in the activation of the mGluR2/3 autoreceptors (Kalivas et al.,2005), as described later.

2.3.8. Predictions Related to Glu Homeostasis in the Perisynaptic Space

The computational model includes equations relating to geometry, and to diffusion, binding and transport of Glu. We report preliminary results from the geometry in Figure 11. As mentioned earlier, region R_a is just outside the synapse and has no transporters; G denotes the glial sheath, with G_1 representing the glial sheath shown in blue in Figure 11, region G_2 representing another glial sheath shown in green with a different transporter density. The region shown in white represents free space for diffusion of Glu, without transporters. This includes regions R_a and R_b , with the latter extending up to a distance of 1 μ m from the edge of the synapse. Location P_b is at the outer boundary of outer region R_b , along $\theta = 90^\circ$, where the experimental measurement of Glu concentration is assumed to occur. The model thus has a total of 40 shells outside the synaptic region, each with a thickness of 25 nm.

Model inputs and baseline values. For the control case, we assume a PFC firing rate of 2 Hz, and 5000 molecules of Glu per vesicle (Diamond 2005, Rusakov, 2001, Rusakov and Kullmann 1998) with four vesicular release sites per pre-synaptic terminal. A probability of release of 0.24 for the control case (based on Trommerhauser et al.,2003) results in a release of 5000 molecules per PFC firing in the control case. Concentration of extracellular Glu is reported by Baker et al. (2003) as 5.6 μM in the control case and 2.89 μM with chronic cocaine in the withdrawn state.

For a given geometry, with the inputs just described, we systematically vary transporter and xc- concentrations within known physiological bounds, to determine whether reported experimental levels of steady state Glu concentrations can be obtained in the various regions of the perisynaptic space, for the cases considered.

Preliminary results. Three preliminary cases are investigated to help iteratively determine appropriate transporter concentrations (Table 5) in the various glial sheaths (at locations P_a , P_{G1} , P_{G2} , P_m , P_b in Figure 11) so as to have known Glu levels: (i) control case with PFC firing rate of 2 Hz and a release probability of 0.24 at 1 μM concentration of Glu near the mGluRs, (ii) ‘extreme case 1’ with no PFC firing and the xc- exchanger velocity at nominal levels, and (iii) ‘extreme case 2’ with PFC firing at 2 Hz and xc- exchanger velocity set to zero. For the control case, Glu concentration near mGluR is expected to be in the 1 μM range (Kalivas, personal communications), with concentration at P_b in the 5 μM range. For extreme case 1, with no PFC firing, the concentrations should not change much, particularly that near mGluRs since the xc- pumps essentially control that tone in the control case. Similarly, for extreme case 2, without the xc- pumps, Glu release due to firing should fail to provide tone to the mGluRs. A set of transporter

concentrations that satisfy these conditions was obtained iteratively, and reproduced the levels well as shown by the predictions in Table 5. In extreme case 1, the tone on the mGluRs is not affected much in the absence of synaptic release, and it has negligible effect on Glu concentration at the outer boundary 4b. If the xc- pumps are removed, the tone on the mGluRs drops to zero, since the synaptic release is immediately taken up by the transporters precluding a build up of Glu in region 2 and outside.

The model exhibited expected trends for standard variations in parameters. For instance, in the control case, with all other conditions at nominal levels, as the transporter concentration in G_2 increases, Glu concentration in region R_a reduces. The time characteristics of glutamate concentration at the release point (cleft center) is similar to that from analytical solutions in Barbour and Hausser (1997) for three dimensional diffusion of 5000 glutamate molecules taken at cleft center in a 20 nm disc, where Glu concentration rapidly diminished from an initial mM level to approximately 10 μ M, and then decays away asymptotically. The result shows more rapid reduction in synaptic glutamate concentration than for a simulation of release of 5000 molecules at a synapse (Rusakov and Kullmann 1998) for a smaller cleft (100 nm radius) and a diffusion coefficient $D = .3 \mu\text{m}^2/\text{ms}$. This is probably due to the smaller cleft size and no free to porous space transition outside the cleft, causing glutamate to encounter tortuous diffusion more rapidly, slowing down its removal. Glu concentrations in all the regions were also found to decay at nearly the same rate, along similar asymptotes, as noted in Rusakov (2001) for diffusion out of the synapse into a tortuous isotropic medium, with no diffusion obstacles.

Table 5 shows the model predictions of the concentrations of Glu in the perisynaptic

region with column 2 representing the control case with the basal level of the extracellular glutamate concentration of 5 μM (point P_b in region R_B). Columns 2 and 3 show that with the transporter concentrations shown in the table, the xc- pumps and synaptic Glu release have the predictable physiological effects mentioned earlier.

Good estimates for the number of transporter and xc- exchanger molecules in the perisynaptic space are not available in the literature presently. One of the capabilities of the proposed computational framework is that it can provide first order predictions for these concentrations indirectly for specific geometries (Table 4) by integrating known transient and steady state information related to Glu homeostasis in the perisynaptic space. The framework can also be used to study glial configurations in the perisynaptic space, another topic about which little is known presently.

2.3.9. Summary and Future Research

A computational modeling framework is proposed for the characterizing the effect of cocaine on the PFC–NAc glutamatergic pathway. Some components of the model have been developed while others are still under development. Partial validation of the model has been performed using data reported in the literature. An important objective of the chapter is to illustrate the process of developing computational models systematically for the pathway, starting with the basics in section 2.

The single cell PFC model of section 2.3.3 will be incorporated into a network model which will have approximately 20 PFC cells with interneurons networked in a manner similar to that in Durstewitz et al. (2000) to study the effect of background inputs, and noise, which will provide better estimates of cellular firing and synaptic release at the

terminals. The simplified Glu release model of section 2.3.4 will be analyzed further for analytical insights. Such insights may be useful as we refine the detailed models for the same mechanisms as reported in section 2.3.5. We are presently working on refining the models developed, including improved estimates of the parameters in Tables 1 and 2, including for cocaine cases. In the detailed models, we will study the effect of other parameters including the number of synaptic vesicles released, synaptic diameter, coefficient of glutamate release, and glutamate receptor binding sites (Rusakov, 2001).

In addition to parametric studies and quantifying individual contributions of the mechanisms as described next, the models are also being used to study other system characteristics such as bifurcation/bistability, robustness, etc. which provide analytical insights for such systems:

Individual contributions of the neuroplasticity mechanisms: The framework and models developed can be used to quantify the relative contributions of the mechanisms of neuroplasticity in the PFC–NAc Glu transmission pathway. The various neuroplasticity mechanisms (change in AGS3 signaling at the soma and at the terminals, down–regulation of the xc- pump, and change in tone of the mGluR2/3 autoreceptors) work together to change Glu release at the terminals. It will be instructive to quantify the individual contribution of each mechanism, and a reliable computational model will also facilitate such investigations. One of the techniques is to develop a state–space model using all the relevant equations for the particular pathway, linearize the model, and then determine its principal modes. This process (Schmidt and Jacobsen, 2004) would help identify the mechanisms involved and their relative importance.

Stability and robustness analyses. The neuroplasticity mechanisms considered are found to increase the excitability of the PFC cell for the cocaine case compared to natural rewards such as food, with an almost ‘bistable’ type response characteristic. The specifics and importance of the mechanisms contributing to bistability can be studied using analytical techniques such as bifurcation analysis (Gruber et al., 2003). The models differ from those of Gruber et al. (2003) and Kitano et al. (2002) due to the inclusion of the effects of neuroplasticity. We will consider robustness issues (Gruber et al., 2003; Du and Nair, 2002) using known bounds on the parameters.

Once the pre-synaptic model is adequately developed, the post-synaptic mechanisms will be studied and incorporated into a model of the NAc cell, developed along similar lines as the PFC of section 2.3.3, with relevant post-synaptic mechanisms such as long term potentiation/depression (LTP/LTD) due to cocaine. A network of NAc cells can then be developed and linked to the network of PFC cells. This will then complete the development of an overall computational model of the PFC–NAc glutamatergic pathway.

2.3.10. Systems Level Model and Extensions

After the component and overall computational models for PFC, NAc and the PFC–NAc network are developed, we proceed to next higher level, the systems level. The system in our case will be the motivational circuit focusing on the common pathway of reinstatement shown in Figure 12. Kalivas and Volkow (2005) suggest the final common pathway includes the glutamate release in the NAc from PFC terminals (that we are modeling presently) and is preceded by release of dopamine from VTA projections at the PFC. One can model the VTA to PFC pathway and its role in reinstatement, and then extend it to modeling the larger circuit in Figure 12 to study plasticity in this circuit and

its role in cocaine reinstatement.

Once developed, such a modular modeling framework can also be used to *identify as yet unknown relationships* and possible missing components and mechanisms in the Glu transmission pathway, and continuously refined using experimental data and better understanding of the neurobiology that is being constantly generated. For instance, possible plasticity in transporter uptake dynamics in the perisynaptic space can be investigated using the model. Another important utility of the framework will be to *generate testable hypotheses*.

Limitations. A lack of understanding of some of the mechanisms at the present time limit us to using largely linear modeling techniques, e.g., regulation of release probability by mGluR2/3. With a better understanding of the phenomena involved, we will be in a position to consider and include appropriate nonlinear modeling techniques, to improve model fidelity. If the mechanism is partially or fully known, it is possible that all the parameters for that sub-model may not be available. In such cases different values for the parameters have to be tried (within known bounds) to check if the predictions at select important locations in the model are consistent with experimental observations (as has been shown successfully in some cellular modeling applications, e.g., Tyson et al., 2001). Similarly, there would be limitations in ‘filling gaps’ at the present time and those have to be accounted for in the model. The models proposed here are largely deterministic and modeling the realistic stochastic effects may be challenging compared to the neurobiological understanding and computational tools available presently. Unexpected model predictions that may not support observations can also be anticipated in such research, and in such cases, alternative explanations will have to be explored.

2.4. CONCLUSIONS

We report a computational modeling framework for characterizing the changes in the PFC–NAc glutamatergic pathway due to cocaine. The framework consists of ‘modules’ at the molecular and cellular levels, facilitates viewing the overall problem as a set of discrete modules serving particular functions. Such a framework also permits the modules to be updated continuously as new data (e.g., kinetic constants for specific pathways) and information emerge. As noted earlier, some of the modules reported here are themselves not complete, and the focus of the chapter is on the ‘framework’ and methodology for such computational studies.

For the specific problem modeled, it is clear that the projection from the prefrontal cortex to accumbens spiny cells is critical for exhibited learned behaviors to approach or avoid motivationally relevant stimuli that the organism has previously experienced. This system undergoes pathological adaptations following repeated exposure to addictive drugs that produces the addiction behavioral pathology (i.e. intrusive cravings and relapse). The models reported are being built upon experimentally defined physiological and drug–induced changes in electrophysiology and enzyme kinetics that regulate glutamate transmission at the PFC–accumbens synapse. By modeling this system it should be possible to determine how the pathological adaptations affect excitatory transmission, and ultimately to test these predictions. Conversely, modeling the pathological changes that are more readily identified experimentally as aberrations in normal function, we can become informed about the underlying physiological parameters that allow a given pathological change to manifest as the altered function. For example,

knowing that reduced xc- exchange by cocaine increases the release probability of glutamate provides information on how physiological aspects of the terminal are organized in order to permit this to happen (e.g., stimulation of metabotropic glutamate receptors, levels of G protein regulatory proteins, etc). The reported cross-disciplinary research including computational modeling can facilitate discovery of the details of the biological pathways that underlie cocaine addiction.

ACKNOWLEDGMENT

A Mohan and J Gall were supported on a National Science Foundation GK12 Fellows award DGE 440514 (Nair); G. Li was supported on an NSF REU award EEC 0244045 (Nair); A Pendyam was partially supported on a sub-contract from the Medical University of South Carolina, DA015369 (Nair). Support from these sources is gratefully acknowledged.

2.5. REFERENCES

1. Baker DA, McFarland K, Lake RW, Shen H, Tang XC, Toda S, Kalivas PW (2003) Neuroadaptations in cystine-glutamate exchange underlie cocaine relapse. *Nature Neuroscience* 6:743-9.
2. Barbour B, Hausser M (1997) Intersynaptic diffusion of neurotransmitter. *Trends in Neuroscience* 20:377-84.
3. Bhalla US, Iyengar R (1999) Emergent properties of networks of biological signaling pathways, *Science* 283:381-387.
4. Bhalla US, Iyengar R (2001) Functional modules in biological signaling networks. *Novartis. Found Symp.* 239: 4-13.
5. Bhalla US (2002) Biochemical signaling networks decode temporal patterns of synaptic input. *J. Comp. Neurosci.* 13: 49-62.
6. Bhalla US (2004) Models of cell signaling pathways. *Current Opinion in Genetics and Development* 14: 375-381.

7. Billups B, Graham BP, Wong AY, Forsythe ID (2005) Unmasking group III metabotropic glutamate autoreceptor function at excitatory synapses in the rat CNS. *Journal of Physiology* 565:885–96.
8. Blackwell KT (2005) Modeling calcium concentration and biochemical reactions. *Brains, minds and Media*. vol.1.
9. Bower JM, Beeman D (2003) The book of GENESIS: *Exploring realistic neural models with the GEneral NEural SIMulation System*, Internet Edition.
10. Bowers MS, McFarland K, Lake RW, Peterson YK, Lapish CC, Gregory ML, Lanier SM, Kalivas PW (2004) Activator of G protein signaling 3: a gatekeeper of cocaine sensitization and drug seeking. *Neuron* 22:269–81.
11. Brown GP, Blizer RD, Connor JH, Wong T, Shenolikar S, Iyengar R and Landau EM (2000) Long-term potentiation induced by theta frequency stimulation is regulated by a protein phosphatase-1-operated gate, *Journal of Neuroscience* 20:7880–7887.
12. Byrne JH, Roberts JL (2004) From Molecules to Networks—*An introduction to cellular and molecular neuroscience*, Elsevier Academic Press.
13. Capriles N, Rodaros D, Sorge RE, Stewart J (2003) A role for the prefrontal cortex in stress- and cocaine-induced reinstatement of cocaine seeking in rats. *Psychopharmacology* 2003 168:66–74.
14. Carnevale NT, Hines ML (2006) *The NEURON Book*, Cambridge, UK: Cambridge University Press.
15. Castro-Alamancos MA, Connors BW (1997) Distinct forms of short term plasticity at excitatory synapses of hippocampus and neocortex, *Proc. National Academy of Sciences* 94: 4161–4166.
16. Colombo JA (2005) Glutamate uptake by rat brain astroglia incubated in human cerebrospinal fluid. *Medical Science Monitor* 11:BR13–7.
17. Danbolt NC (2001) Glutamate uptake. *Progress in Neurobiology* 65:1–105.
18. Diamond JS (2005) Deriving the glutamate clearance time course from transporter currents in CA1 hippocampal astrocytes: transmitter uptake gets faster during development. *Journal of Neuroscience* 25(11):2906–16.
19. Dietrich D, Kral T, Clusmann H, Friedl M, Schramm J (2002) Presynaptic group II metabotropic glutamate receptors reduce stimulated and spontaneous transmitter release in human dentate gyrus. *Neuropharmacology* 42:297–305.
20. Dong Y, Nasif FJ, Tsui JJ, Ju WY, Cooper DC, Hu XT, Malenka RC, White FJ (2005) Cocaine-induced plasticity of intrinsic membrane properties in prefrontal cortex pyramidal neurons: adaptations in potassium currents. *Journal of Neuroscience* 25:936–40.
21. Du H, Nair S (2002) Robust Adaptive Compensation for a Class of Nonlinear Systems, *ASME Journal of Dynamic Systems, Measurement, and Control* 124:231–234.

22. Dundr M, Hoffmann–Rohrer U, Hu Q, Grummt I, Rothblum LI, Phair RD, Misteli T (2002) A kinetic framework for a mammalian RNA polymerase in vivo, *Science* 298: 1623–1626.
23. Durstewitz D, Seamans JK, Sejnowski TJ (2000) Dopamine–mediated stabilization of delay–period activity in a network model of prefrontal cortex. *Journal of Neurophysiology* 83:1733–50.
24. Eungdamrong NJ, Iyengar R (2004) Modeling cell signaling networks, *Biology of the Cell* 96: 335–362.
25. Ferrell JE (1996) Tripping the switch fantastic: How a protein kinase cascade can convert graded inputs into switch–like outputs, *Trends in Biochemical Sciences* 21:460–466.
26. Ferrell JE (1997) How responses get more switch–like as you move down a protein kinase cascade, *Trends in Biochemical Sciences* 22:288–289.
27. Furuta A, Rothstein JD, Martin LJ (1997) Glutamate transporter protein subtypes are expressed differentially during rat CNS development. *Journal of Neuroscience* 17:8363–75.
28. GENESIS software and tutorials: <http://www.genesis-sim.org/GENESIS/>
29. Grewer C, Rauen T (2005) Electrogenic glutamate transporters in the CNS: molecular mechanism, pre–steady–state kinetics, and their impact on synaptic signaling, *Journal of Membrane Biology* 203:1–20.
30. Gruber AJ, Solla SA, Surmeier DJ, Houk JC (2003) Modulation of striatal single units by expected reward: a spiny neuron model displaying dopamine–induced bistability. *Journal of Neurophysiology* 90:1095–114.
31. Goldstein RZ, Volkow ND (2002) Drug addiction and its underlying neurobiological basis: neuroimaging evidence for the involvement of the frontal cortex. *American Journal of Psychiatry* 159:1642–52.
32. Hartwell LH, Hopfield JJ, Leibler S, Murray AW (1999) From molecular to modular cell biology, *Nature* 402:C47–52.
33. Hodgkin AL, Huxley AF (1952) A quantitative description of membrane current and its application to conduction and excitation in nerve, *Journal of Physiology* 117:500–544.
34. Huang CF, Ferrell JE (1996) Ultrasensitivity in the mitogen–activity protein kinase cascade, *Proceedings of the National Academy of Sciences USA* 93: 10078–10083.
35. Izhikevich EM (2003) Simple model of spiking neurons, *IEEE Transactions on Neural Networks* 14(6):1569–1572.
36. Izhikevich EM (2007) *Dynamical Systems in Neuroscience: The Geometry of Excitability and Bursting*, The MIT press.
37. Kalivas PW, Volkow N (2005) The neural basis of addiction: a pathology of motivation and choice, *American Journal of Psychiatry*, 162:1403–1413.

38. Kalivas PW, Volkow N, Seamans J (2005) Unmanageable motivation in addiction: a pathology in prefrontal–accumbens glutamate transmission, *Neuron* 45:647–50.
39. Keener JP, Sneyd J (1998) *Mathematical Physiology*, Springer–Verlag: New York.
40. Kitano K, Cateau H, Kaneda K, Nambu A, Takada M, Fukai T (2002) Two–state membrane potential transitions of striatal spiny neurons as evidenced by numerical simulations and electrophysiological recordings in awake monkeys. *Journal of Neuroscience* 22:RC230.
41. Kitano H (2002) Computational systems biology, *Nature* 420:206–210.
42. Koch C (1998) *Biophysics of Computation: Information Processing in Single Neurons*, Oxford University Press..
43. Koch C, Crick F (2003) A framework for consciousness, *Nature Neuroscience* 6(2):119–26.
44. Koch C, Segev I (2001) *Methods in Neuronal Modeling– From Ions to Networks*, The MIT Press.
45. Leblois A, Boraud T, Meissner W, Bergman H, Hansel D (2006) Competition between Feedback Loops Underlies Pathological Dynamics in the Basal Ganglia, *Journal of Neuroscience* 26(13):3567–3583.
46. Legewie S, Blüthgen N, Herzog H (2005) Quantitative analysis of ultrasensitive responses. *FEBS Journal* 272: 4071–4079.
47. Lehre KP, Levy LM, Ottersen OP, Storm–Mathisen J, Danbolt NC (1995) Differential expression of two glial glutamate transporters in the rat brain: quantitative and immunocytochemical observations. *Journal of Neuroscience* 15:1835–53.
48. Lehre KP, Danbolt NC (1998) The number of glutamate transporter subtype molecules at glutamatergic synapses: chemical and stereological quantification in young adult rat brain. *Journal of Neuroscience* 18:8751–7.
49. Lehre KP, Rusakov D (2002) Asymmetry of glia near synapse favors presynaptic glutamate escape, *Biophysical Journal* 83(1):125–134.
50. Li G, Nair SS, Lees S and Booth F (2005) Regulation of G₂/M transition in mammalian cells by oxidative stress, *Proceedings of the Dynamics and Control Division, ASME International Mechanical Engineering Congress and Exposition*, Nov 5–11, Orlando, FL.
51. Lorez M, Humbel U, Pflimlin M–C, Kew JNC (2003) Group III mGluR’s as autoreceptors in the cerebral cortex, *British Journal of Pharmacology* 138:614–625.
52. Marder E, Goaillard JM. (2006) Variability, compensation and homeostasis in neuron and network function, *Nature Reviews Neuroscience*, 7(7):563–74.
53. Mauk MD (2000) The potential effectiveness of simulations verses phenomenological models, *Nature Neuroscience* 23:649–711.

54. McFarland K, Davidge SB, Lapish CC, Kalivas PW (2004) Limbic and motor circuitry underlying footshock-induced reinstatement of cocaine-seeking behavior. *Journal of Neuroscience* 24:1551–60.
55. Nasif FJ, Hu XT, White FJ (2005) Repeated cocaine administration increases voltage-sensitive calcium currents in response to membrane depolarization in medial prefrontal cortex pyramidal neurons. *Journal of Neuroscience* 25:3674–9.
56. NEURON software and tutorials: <http://neuron.duke.edu/> (includes links to sites for database libraries, discussion groups, etc.)
57. Neves SR, Iyengar R (2002) Modeling of signaling networks. *BioEssays* 24: 1110–1117.
58. NIH Neuroscience Blueprint (2004), <http://neuroscienceblueprint.nih.gov/>.
59. Pape HC (1996) Queer current and pacemaker: the hyperpolarization activated cation current in neurons, *Annual Reviews in Physiology* 58:299–327.
60. Peters YM, O'Donnell P, Carelli RM (2005) Prefrontal cortical cell firing during maintenance, extinction, and reinstatement of goal-directed behavior for natural reward. *Synapse* 56(2):74–83.
61. Rusakov DA, Kullmann DM (1998) Extrasynaptic glutamate diffusion in the hippocampus: ultrastructural constraints, uptake, and receptor activation. *Journal of Neuroscience* 18:3158–70.
62. Rusakov DA (2001) The role of perisynaptic glial sheaths in glutamate spillover and extracellular Ca²⁺ depletion. *Biophysical Journal* 81:1947–1959.
63. Saez-Rodriguez J, Kremling A, Conzelmann H, Bettenbrock K, Gilles ED (2004) Modular analysis of signal transduction networks, *IEEE Control System Magazine* 24 (4): 35–52.
64. Schmidt H, Jacobsen EW (2004) Identifying feedback mechanisms behind complex cell behavior, *IEEE Control System Magazine* 24 (4): 91–101.
65. Seamans JK, Yang CR (2004) The principal features and mechanisms of dopamine modulation in the prefrontal cortex. *Progress in Neurobiology* 74:1–58.
66. Smolen PD, Baxter DA, Byrne JH (2004) Mathematical modeling and analysis of intracellular signaling pathways, In “*From Molecules to Networks: An Introduction to Cellular and Molecular Neuroscience*” (edited by J. Byrne and J. Roberts). Elsevier Academic Press.
67. Sun W, Rebec GV (2005) The role of prefrontal cortex D1-like and D2-like receptors in cocaine-seeking behavior in rats, *Psychopharmacology* 177:315–23.
68. Terman D, Rubin JE, Yew AC, Wilson CJ (2002) Activity patterns in a model for the subthalamopallidal network of the basal ganglia, *Journal of Neuroscience* 22:2963–76.
69. Trantham-Davidson H, Neely LC, Lavin A, Seamans JK (2004) Mechanisms underlying differential D1 versus D2 dopamine receptor regulation of inhibition in prefrontal cortex, *Journal of Neuroscience* 24:10652–9.

70. Trommershauser J, Schneggenburger R, Zippelius A, Neher E (2003) Heterogeneous Presynaptic release probabilities: functional relevance for short-term plasticity, *Biophysical Journal* 84:1563–1579.
71. Warr O, Takahashi M, Attwell D (1999) Modulation of extracellular glutamate concentration in rat brain slices by cystine–glutamate exchange. *Journal of Physiology* 514:789–93.

2.7. TABLES

Table 1. Parameters for the illustrative RS, IB, CH and FS cell models

Type	Maximal conductance (mS/cm ²)	Leakage potential E _L (mV)	Scaling factor of τ _n
RS	$g_{Na} = 150$ $g_{DR} = 20$ $g_{Ca} = 0.1$ $g_{AHP} = 8$	-55	4
IB	$g_{Na} = 150$ $g_{DR} = 20$ $g_{Ca} = 0.3$ $g_{AHP} = 6$	-55	4
CH	$g_{Na} = 150$ $g_{DR} = 20$ $g_{Ca} = 0.65$ $g_{AHP} = 3.3$	-58	4.5
FS	$g_{Na} = 200$ $g_{DR} = 15$ $g_{Ca} = 0.2$ $g_{AHP} = 3$	-58	4

Table 2. Parameter adjusted in Glu release model of Figure 9 with cocaine (a–Grewer and Rauen 2005; b–Baker et al.,2003)

Variable	Control	Withdrawal
N_glu_release_spike	10mM ^a	10 mM
N_glu_ex	4 μM ^b	2 μM
k_1	1	0.5
k_2	1	0.3
k_3	1	0.5
k_4	1	1

Table 3. Initial estimates of plasticity effects on extrasynaptic neurotransmitter concentrations for model (Baker et al.,2003; McFarland et al.,2003,2004)

Normal	Glu (%)	DA (%)	Chronic	Glu (%)	DA (%)
Basal	100	100	Basal	50	100
Natural Reward	150	200	Natural Reward	50	200
Cocaine Reward	150	300	Cocaine Reward	200	400

Table 4. Reported ranges for some of the parameters used in the synapse model

Parameter	Value
Glia coverage, %	0 %; 50%; 95% (Rusakov, 2001)
Volume fraction, α	0.12 (CA1) (Lehre and Rusakov 2002) 0.21 (Barbour and Hausser 1997) 1.0 (unrestricted diffusion)
Diffusion coefficient D, $\mu\text{m}^2/\text{ms}$	0.1–0.6 (Rusakov, 2001) 0.05–0.75 (Rusakov and Kullmann 1998)
Tortuosity, λ	1.4 (Lehre and Rusakov 2002) 1.0 (unrestricted diffusion) (Barbour and Hausser 1997)
$k_1, \text{M}^{-1}\text{ms}^{-1}$	10^4 (Lehre and Rusakov 2002)
k_{-1}, ms^{-1}	0.2 (GLAST/GLT) 0.02 (EAAT4) (Lehre and Rusakov 2002)
k_{-2}, ms^{-1}	0.1 (Lehre and Rusakov 2002)
$K_d, \mu\text{M}$	300 (low affinity, singly bound receptors) 1 (high affinity) (Rusakov, 2001)
Number of molecules per vesicle	2500–7500 (Lehre and Rusakov 2002)
Glia volume fraction, %	9.71 ± 0.83 (Lehre and Rusakov 2002)
Synaptic diameter, μm	0.2, excitatory hippocampal area CA1 0.4, parallel fiber synapse of cerebellum 0.6 climbing fiber synapses in cerebellum (Rusakov, 2001)
Intersynaptic distance, μm	2–20 (CA-1, Rusakov, 2001) 0.5 (striatum radiatum and gyrus dentatus of hippocampus; Danbolt, 2001)
Concentration of GLAST/GLT, near glia, mM	1.0 (Lehre and Rusakov 2002)
Average probability of release from single vesicle	0.25–0.4 (studies performed on the calyx of Held, Trommerhauser et al., 2003)

Table 5. Model predictions for control and two extreme cases

Parameters	Control Case	Extreme Case 1	Extreme case 2
Freq (Hz)	2	0	2
Trans G _{1a}	2.75 mM	2.75 mM	2.75 mM
Trans G _{1b}	1.25 mM	1.25 mM	1.25 mM
Trans G _{2a}	0.025 mM	0.025 mM	0.025 mM
Trans G _{2b}	0.01875 mM	0.01875 mM	0.01875 mM
Release Probability	0.24	0.24	0.24
xc- vel. (nM/ms)	0.6	0.6	0.6
PREDICTIONS of steady state Glu in μM at location P_i			
Conc P _a (in R _a)	0.08	0.08	0
Conc P _m (MgluR)	0.09	0.087	0
Conc P _{G1} (in G _{1a})	0.5	0.57	0
Conc P _{G2} (in G _{2a})	3.7	3.6	0
Conc P _b (in R _b)	4.91	4.89	0

2.8. FIGURES

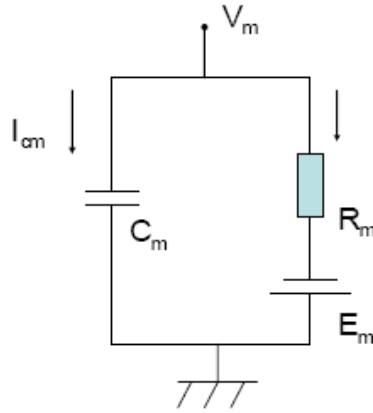


Figure 1. Model of a standard RC circuit.

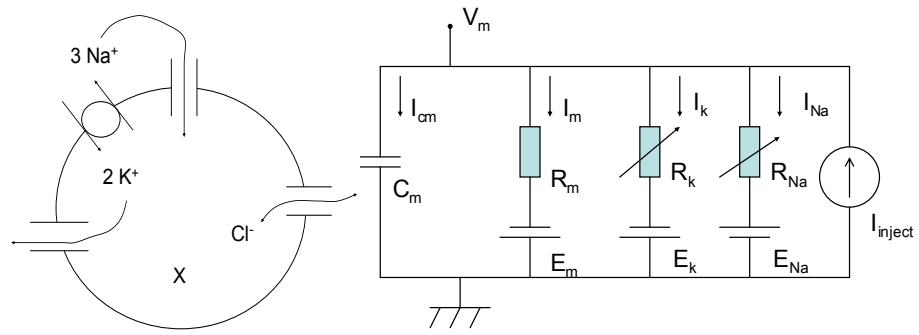


Figure 2. Simplified circuit model of a neuron.

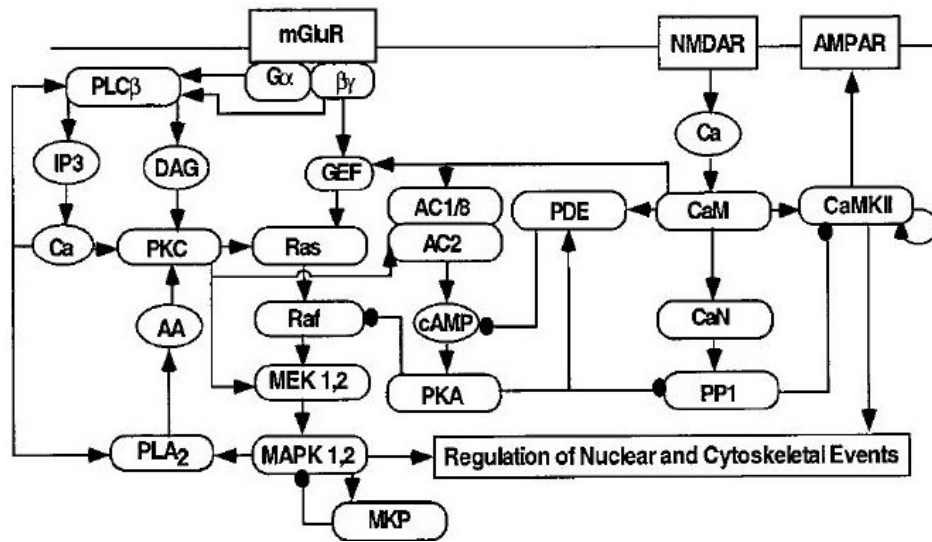


Figure 3. A model for the glutamate-activated signaling network (Bhalla and Iyengar, 1999).

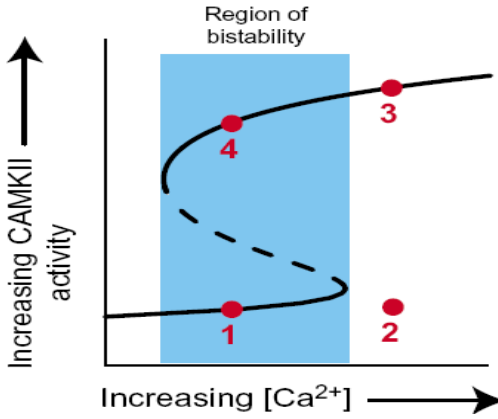


Figure 4. Bifurcation diagram showing how CaMKII activity changes as [Ca²⁺] varies (Smolen et al., 2004).

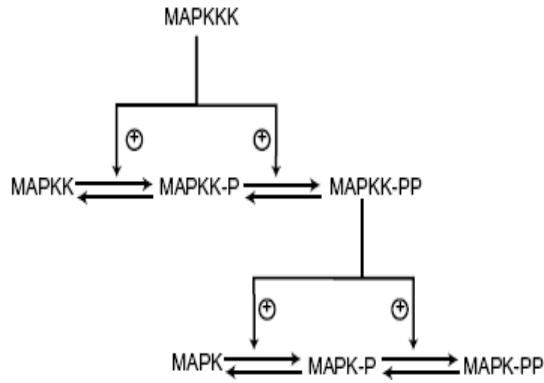


Figure 5. Scheme of the MAPK cascade (Smolen et al., 2004).

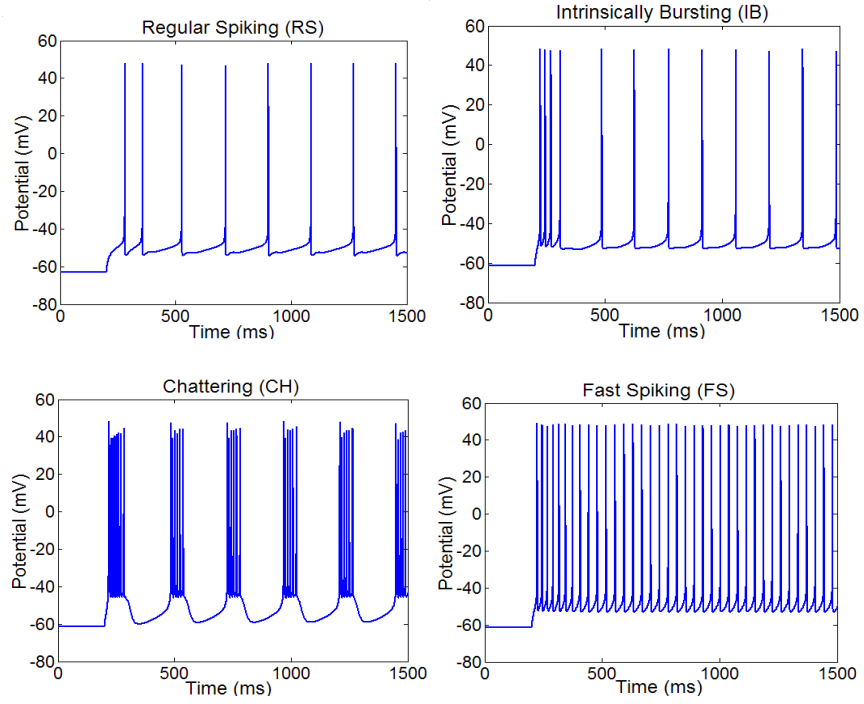


Figure 6. Different firing patterns produced by the two-compartment model.

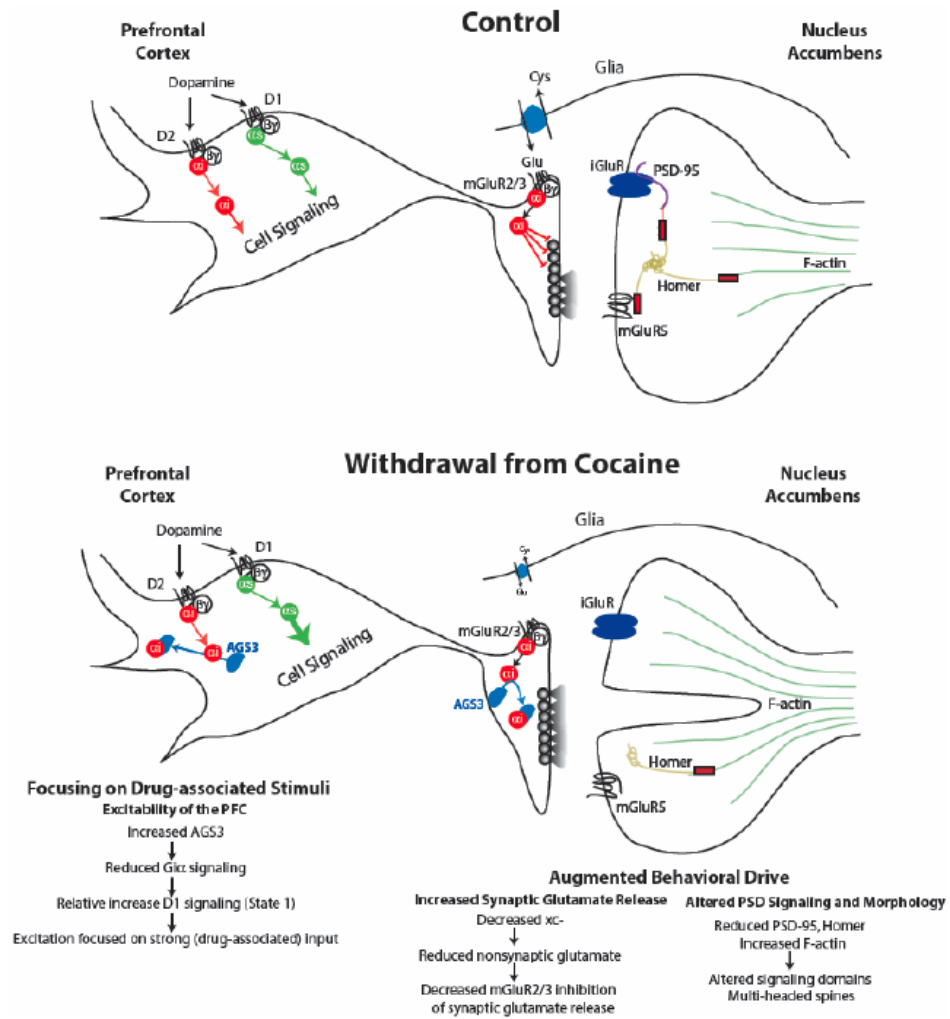


Figure 7. Hypothesized cellular adaptations in the PFC–NAc Glu pathway in cocaine withdrawal (Kalivas et al., 2005).

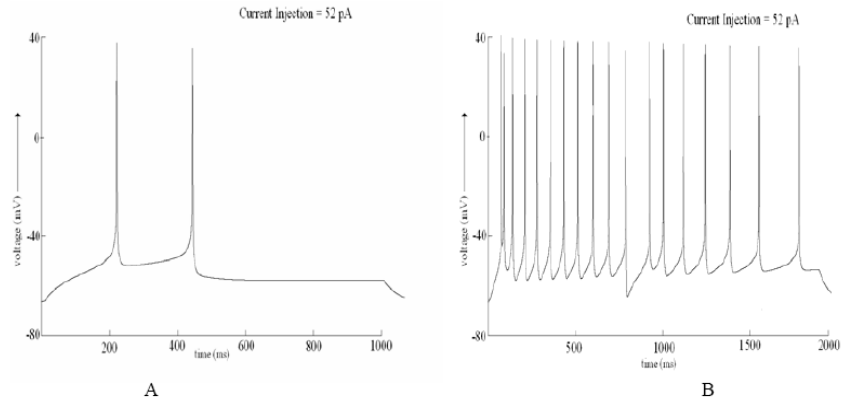


Figure 8. Preliminary action potential predictions for an *in vitro* single PFC cell for control (A) and cocaine (B) cases, using hypothesized changes in Dong et al. (2005) and Nasif et al. (2005).

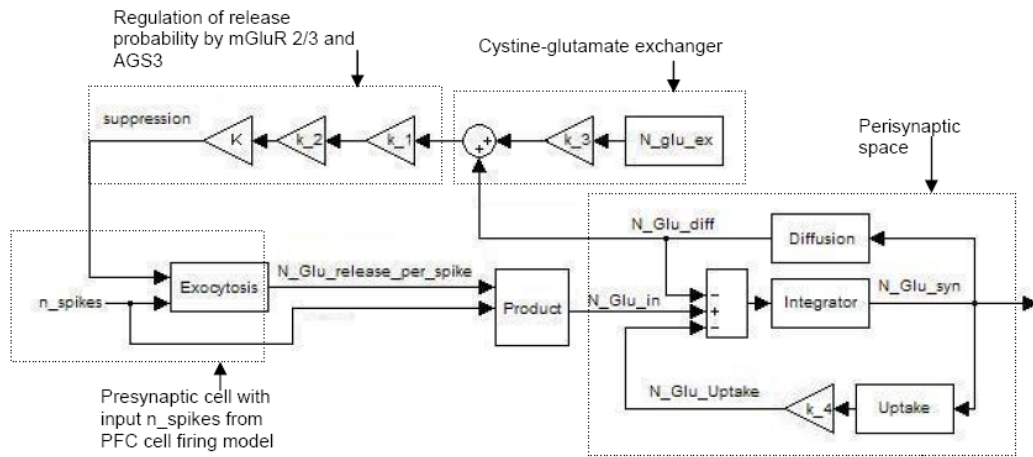


Figure 9. Model for Glu neuroplasticity in pyramidal cell terminals projecting to NAc.

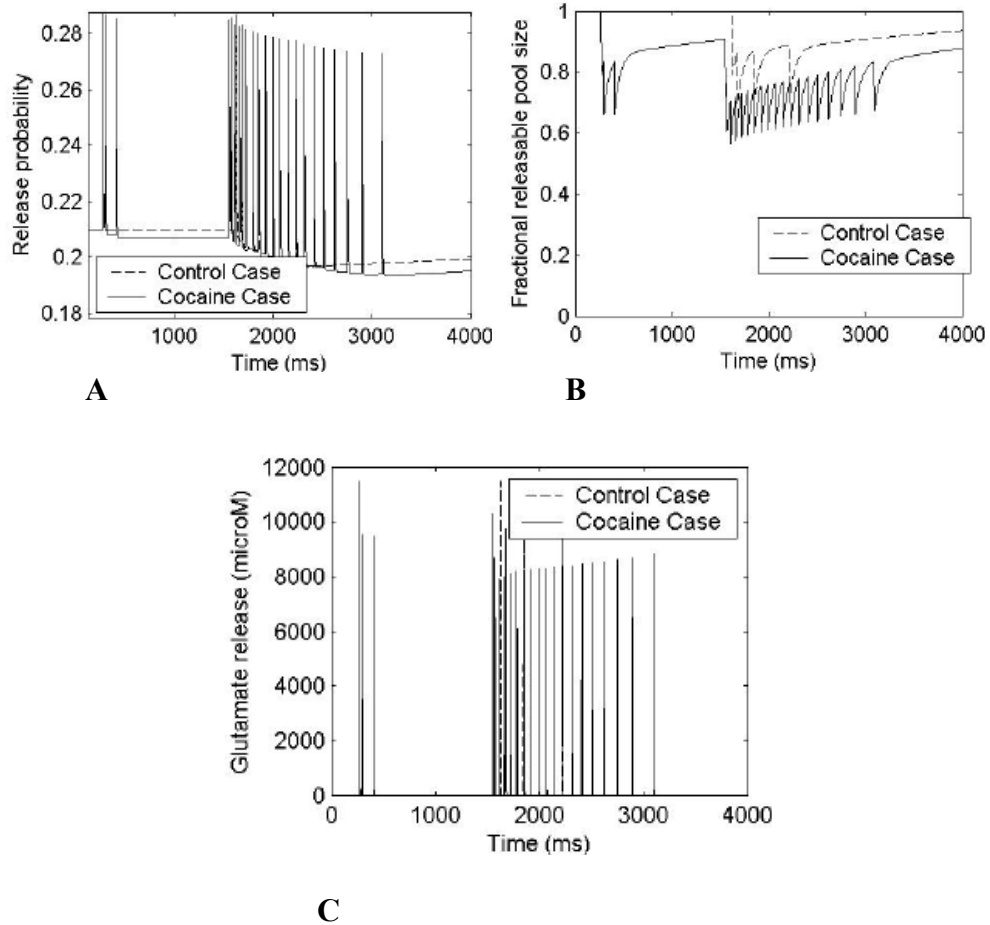


Figure 10. Model predictions of the concentration of synaptic Glu at the PFC–NAc synapse.

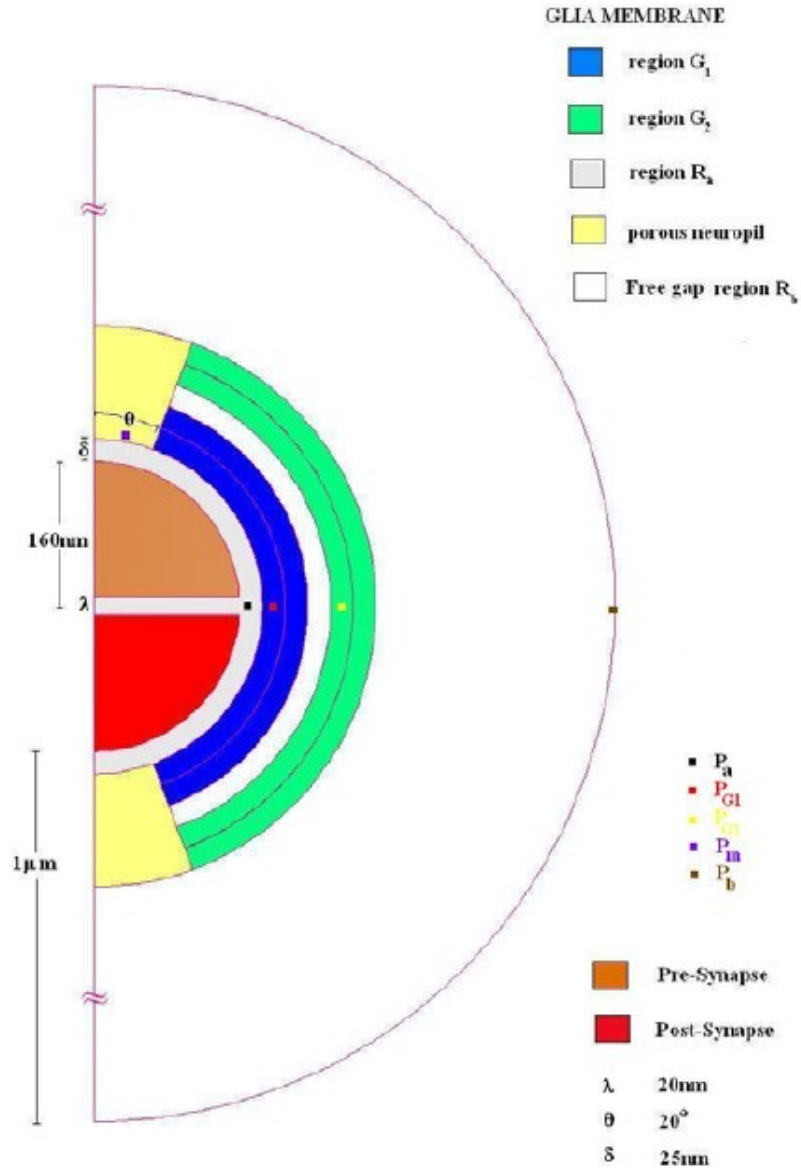


Figure 11. Glial configuration in the perisynaptic space around the PFC–NAc synapse: the synaptic gap is 20 nm, each shell is of thickness $\delta = 25$ nm, divided radially into segments of 20° each; other details of the geometry are provided in the text.

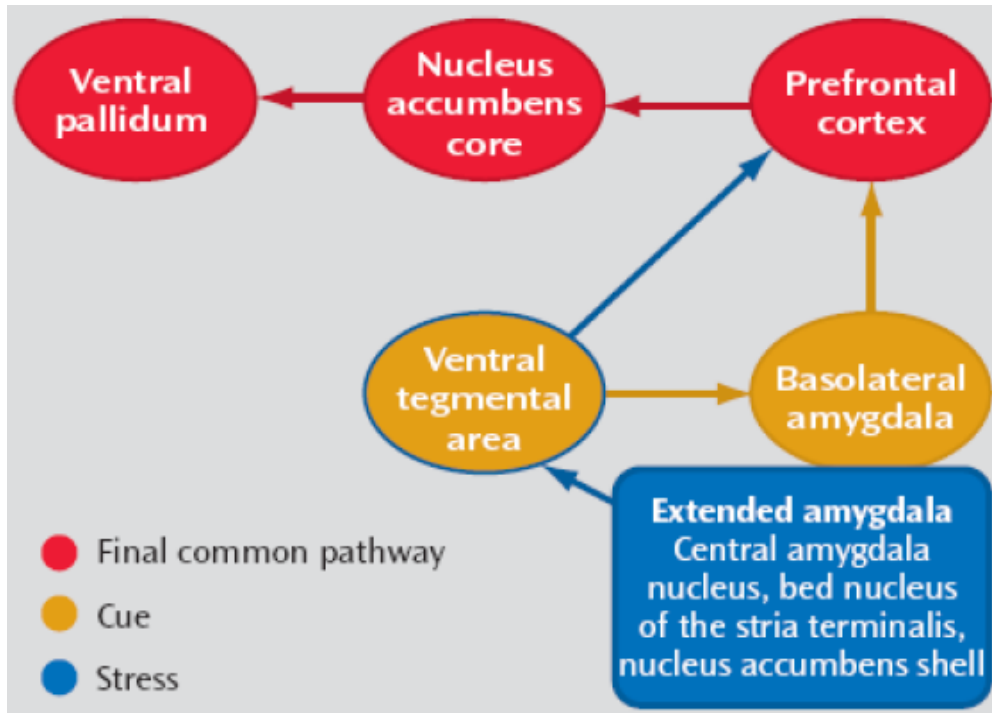


Figure 12. Neural circuitry mediating drug seeking (adapted from Kalivas and Volkow, 2005). The series projection from the prefrontal cortex to the nucleus accumbens core to the ventral pallidum is a final common pathway for drug seeking initiated by stress, a drug-associated cue, or the drug itself (which increases dopamine release in the prefrontal cortex).

CHAPTER 3

Molecular diffusion model of neurotransmitter homeostasis around synapses supporting gradients

3.1. ABSTRACT

Neurotransmitter homeostasis in and around a synapse involves complex random processes such as diffusion, molecular binding and uptake by transporters. A three-dimensional stochastic diffusion model of a synapse was developed to provide molecular level details of neurotransmitter homeostasis not predicted by alternative models based on continuum approaches. The development was illustrated through an example case cortico-accumbens synapse that successfully integrated neuroadaptations observed after chronic cocaine. The stochastic model was used to predict the contributions of non-synaptic sources to extracellular concentration in control, natural reward seeking, and chronic cocaine cases, and to estimate molecular influx rates into the perisynapse. A sensitivity analysis predicted that surface density of glial transporters had the largest effect on glutamate concentrations, among the parameters considered. The stochastic model of the example synapse was further generalized to characterize glial morphology by studying the role of diffusion path length in supporting neurotransmitter gradients and isolating the synapse. For the same set of parameters, diffusion path length was found to be proportional to the gradient supported.

3.2. INTRODUCTION

A typical chemical synaptic environment has substantial morphological specialization that reflects functional requirements in controlling the movement of substances. The glial

environment is a critical regulator of communication and cross talk between synapses (Barbour, 2001; Rusakov, 2001; Franks, Bartol, and Sejnowski, 2002; Savtchenko and Rusakov, 2007; Zheng, Scimemi, and Rusakov, 2008), and probably of the overall extrasynaptic transmission in the central nervous system (Bergles and Jahr, 1997; Danbolt, 2001). Besides the structure of the perisynaptic glial environment, a number of mechanisms participate in the synaptic tuning of circuits in brain tissue, and contribute to synaptic efficacy, plasticity, and neurotransmitter homeostasis in the extracellular space (ECS; Zheng et al., 2008). These mechanisms include vesicular release, neurotransmitter diffusion into the perisynapse, receptor activity (e.g., AMPA and NMDA), inhibition of synaptic vesicular release via activation of negative feedback autoreceptors (e.g., mGluR2/3), binding to transporters and uptake via the glial environment, and non-synaptic production (e.g., via cystine–glutamate exchange located primarily on glia). However, the specifics of how the glial environment and the various mechanisms involved achieve neurotransmitter homeostasis are not completely understood. Further, the presence of multiple interacting parameters makes it difficult to achieve precise experimental control near a single synapse. Therefore, an alternative is to construct a computational model to study the role of glial morphology and associated mechanisms in shaping the neurotransmitter landscape and receptor activity.

Previous modeling studies related to neurotransmitter time courses (e.g., glutamate) have focused on synaptic receptor activation (Clements et al., 1992; Franks et al., 2002) and determined the accessibility of synaptically released neurotransmitter to the ECS, by considering diffusion out of the synapse and elimination by glial transporters (Barbour, 2001; Diamond, 2005). These neurotransmitter diffusion models have relied on simple

geometric representations of ECS, and have included analytical (Holmes, 1995; Kleinle et al., 1996), continuum (Rusakov and Kullmann, 1998; Rusakov, 2001) and stochastic approaches (Clements, 1996; Stiles, Van Helden, Bartol, Salpeter, and Salpeter, 1996; Franks et al., 2002; Tao and Nicholson, 2004; Savtchenko and Rusakov, 2007; Zheng et al., 2008). Pendyam, Mohan, Kalivas, and Nair, (2009) reported a compartmental model of the synaptic environment based on a continuum approach, and by incorporating a non-synaptic source, cystine–glutamate; they were able to show how cocaine–induced neuroadaptations influence glutamate transmission in a cortico-accumbens synapse.

The compartmental model used in Pendyam et al. (2009) is extended in the present study by developing a three–dimensional stochastic diffusion model of a synapse (Figure 1; explained later) to provide molecular level details of neurotransmitter homeostasis that could not be predicted by alternative models based on continuum approaches. The molecular diffusion model considered a realistic morphological representation of glia and ECS and was used to study homeostasis during control, natural reward and cocaine cases. The model was then generalized to quantify the role of diffusion path length (defined as the distance that a molecule travels from the synaptic cleft to the ECS) in supporting neurotransmitter gradients, by considering several candidate glial configurations.

3.3. METHODS

An example case of a prefrontal glutamatergic synapse onto a nucleus accumbens spiny cell (referred to hereafter as cortico-accumbens synapse) was used to illustrate the proposed computational framework. The molecular diffusion model was constrained using biological data, including known parameter ranges (Table 1) as described next.

3.3.1 Model Inputs

Firing frequency and molecules per release. For the glutamatergic cortico-accumbens synapse example case, basal presynaptic firing frequency ranged from 1–3 Hz (Trantham, Szumlinkski, McFarland, Kalivas, and Lavin, 2002), with burst frequencies up to 15 Hz during natural reward seeking behavioral states (Chang, Zhang, Janak, and Woodward, 1997; Sun and Rebec, 2006). Neurotransmitter release from a nerve terminal during exocytosis depends on the size of the synapse, vesicular properties such as volume, neurotransmitter concentration and number available for exocytosis, and geometric parameters such as diameter of the fusion pore (Danbolt, 2001). For general synapses, molecules per release typically varies from 4,000–80,000 (Bruns and Jahn, 1995), and this was the range used in the study (Table 1).

Autoreceptor regulation of release probability. Release probability is regulated following the stimulation of presynaptic autoreceptors (e.g., mGluR2/3–glutamate; Billups, Graham, Wong, and Forsythe, 2005), which are located outside the synaptic cleft (Alagarsamy, Sorensen, and Conn, 2001). The probability that an action potential results in a vesicular release ranges from <0.1 to 1 (Murthy and Sejnowski, 1997). For the example case considered, GTP γ S binding revealed that G protein signaling by stimulating mGluR2/3 increased as a logarithm of agonist dose (Xi, Baker, Shen, Carson, and Kalivas, 2002); hence the relationship between release probability and autoreceptor occupancy was logarithmic. Using this relationship, the mGluR2/3 autoreceptor function was modeled as a change in release probability from 0.14 (basal) to 0.12 (natural reward seeking; Table 1). Each action potential in the model resulted in an instantaneous vesicular release into the cleft. For example, a firing frequency of 2 Hz had a release

probability of 0.14 in the basal case, and, on average, it resulted in a release event every 3.57 seconds.

Ionotropic receptors. Synaptic receptors (AMPA and NMDA) were co-localized in the cleft with an AMPA/NMDA ratio of 0.81 ± 0.33 ($n = 17$; mean \pm sd; unpublished data) based on the maximum peak height of the current obtained during basal conditions in the nucleus accumbens. This was in the range of previous reports that measured AMPA/NMDA ratio in accumbens brain slices (Thomas, Beurrier, Bonci, and Malenka, 2001; Wolf et al., 2005; Kourrich, Rothwell, Klug, and Thomas, 2007; Conrad et al., 2008).

Diffusion. Diffusion of neurotransmitter in the ECS is complicated by several factors such as glial geometry, receptor binding, transporter uptake, viscosity, temperature, change in structure with time (Nicholson, 2001; Franks et al., 2002; Habre, Harbetova, and Segeth, 2004; Sykova, 2004; Diamond, 2005; Saftenku, 2005) and change in local properties with pathology (e.g., volume fraction; Sykova, 1997). Diffusion in the porous neuropil is typically characterized by volume fraction α (void space/total tissue volume) and tortuosity λ (hindrance to diffusion imposed by local boundaries or local viscosity; Nicholson, 2001). Volume fraction α in brain tissue is estimated to be around 0.2 (Nicholson and Sykova, 1998) while tortuosity λ is estimated to be 1.2–2.4 based on diffusion measurements over a distance of 100–300 μm (Nicholson, 2001). However, experimental estimates of diffusion coefficients (D) in the perisynaptic region (i.e., <1 μm from cleft) have not been reported for synapses with tightly packed glia (Rusakov and Kullmann, 1998; Hrabe et al., 2004). Hence, in the proposed model D was iteratively determined in the range, 0.05–0.41 $\mu\text{m}^2/\text{ms}$ (Saftenku, 2005; Table 1) to satisfy

model constraints described later.

Glutamate Transporters. Glial transporters (XAG) modulate glutamate transmission by regulating neurotransmitter access to glutamate receptors and to ECS, thus maintaining appropriate neurotransmitter gradients (Danbolt, 2001; Zheng et al., 2008; Pendyam et al., 2009). XAG present on glial membranes (Danbolt, 2001) have surface densities ranging from 2,500–10,000 molecules/ μm^2 (Bergles and Jahr, 1997; Lehre and Danbolt, 1998). For the present model, equivalent surface density of XAG was determined iteratively within the cited range to satisfy model constraints.

Cystine-glutamate exchanger. *Estimated extracellular concentrations of glutamate can* vary from 25 nM (Herman and Jahr, 2007) to 5 μM (Baker et al., 2003). In vivo extrasynaptic concentrations assessed by microdialysis revealed that the majority of glutamate outside of the synaptic cleft is not of synaptic origin (Timmerman and Westerink, 1997; Melendez, Vuthiganon, and Kalivas, 2005). Also, extracellular glutamate in tissue slices and cell culture experiments was partly of non-synaptic origin (Haydon, 2001; Le Meur, Galante, Anulo, and Audinat, 2007). While a number of sources of non-synaptic extracellular glutamate have been suggested (Danbolt, 2001; Haydon, 2001; Baker et al., 2003; Cavelier, Hamann, Rossi, Mobbs, and Attwell, 2005;), extracellular glutamate measured by microdialysis in the accumbens arises primarily from cystine–glutamate exchange (xc-; Xi et al., 2002; Baker et al., 2003). xc- production rate was iteratively selected in a range 5–50 mM hr^{-1} by varying the surface density of xc- on glia (Table 1).

3.3.2. Cocaine-induced neuroadaptations

Chronic cocaine administration causes instability in extracellular glutamate in the nucleus accumbens that is thought to contribute to the vulnerability to relapse (Kalivas, Volkow, and Seamans, 2005). Rats withdrawn from chronic cocaine administration show dysregulation of extracellular glutamate in the nucleus accumbens due, in part, to reduced xc- and mGluR2/3 signaling (Baker et al., 2003). Microdialysis measurements during drug-seeking have shown a significant overflow of synaptic glutamate (McFarland, Lapish, and Kalivas, 2003; McFarland, Davidge, Lapish, and Kalivas, 2004). Other changes included alterations in the following: glutamate release (McFarland et al., 2003), postsynaptic glutamate signaling (Conrad et al., 2008), group II metabotropic glutamate receptors (mGluR2/3; Xi et al., 2002) and AMPA/NMDA ratio. Further, Pendyam et al. (2009) predicted down regulation of XAG by 40% after chronic cocaine. The stochastic approach was employed to verify this finding also, as described later.

3.3.3. Steady State model constraints for the cortico-accumbens example case

Control condition. The model should typically satisfy the following biological constraints (i) Low synaptic concentrations at steady state to avoid significant receptor excitotoxicity (e.g., ~100 nM for glutamate; Patneau and Mayer, 1990); and (ii) Extracellular steady state glutamate concentrations should not exceed $5.6 \pm 1 \mu\text{M}$ for low (2 Hz; control basal; Baker et al., 2003) and high (12–15 Hz; natural reward seeking; Sun and Rebec, 2006) presynaptic stimulation frequencies.

Cocaine condition. The basal extracellular concentration measured by dialysis after cocaine reinstatement (1 Hz; referred henceforth as cocaine basal) should be in the range of 2.55-3.23 μM (Baker et al., 2003; Szumlinski et al., 2006). However, during drug

seeking (i.e., 15 Hz; referred henceforth as cocaine seeking), extracellular concentration of glutamate should be in the 11.9-14.7 μM range (McFarland et al., 2003, 2004; Szumlinski et al., 2006).

3.3.4. Development of the stochastic model

The stochastic molecular diffusion model was created using the MCell program (Version 3.1.812), a general Monte Carlo simulator designed for cellular microphysiology studies (Stiles et al., 1996; Stiles and Bartol, 2001; Kerr et al., 2008). A three-dimensional spatially realistic model of the cortico-accumbens synapse was constructed using the software Blender (www.blender.org), an open source, modeling and animation package that can export Model Description Language (MDL) files to MCell. To facilitate visual rendering by the OpenDX (www.opendx.org) script, MCell exports mesh objects, molecule, receptor site positions and their states to DReAMM (www.mcell.psc.edu) in a suitable format, with molecule positions recorded at every time step.

The geometry of the example case cortico-accumbens (Figure 1) consisted of a synapse surrounded by assemblies of simplified glial sheaths (G_i) with porous space between them (Rusakov, 2001) as observed in vivo (Rusakov and Kullmann, 1998). The configuration in Figure 1 had an average gap of 40 nm (Thorne and Nicholson, 2006) between glial sheaths, and a glial sheath thickness of 100 nm (Rusakov, 2001) based on the minimum width of glial profiles observed in electron micrograph studies. The structure of an individual sheath was akin to that previously reported but the model had multiple sheaths (G_{1-3}) configured appropriately to satisfy constraints. Molecules were surface populated with ionotropic glutamate receptors (AMPA and NMDA) inside a cleft

of height 30 nm, metabotropic glutamate receptors (mGluR2/3) located at $\varphi = 20^0$ around the presynaptic terminal, and XAG on both sides of the glial sheaths (Figure 1). Based upon studies indicating that the highest densities of XAG are closer to the synapse (Danbolt, 2001; Lehre and Danbolt, 1998), G_1 had the highest surface density of XAG (Table 1). The non-synaptic source of glutamate, xc-, was modeled as being located on the outer surface of the glial sheath G_3 . Beyond G_3 , the porous ECS contained randomly placed glial boulders of varying dimensions without surface populated XAG or xc-. The configurations of the glial sheaths and boulders were iteratively varied to obtain a volume fraction of 0.23 (Sykova, 2004). A no-flux boundary condition was imposed at the outer edge of the model such that no molecules entered or left the outer boundary, to simulate identical neighboring synapses.

The experimentally defined concentrations of extracellular glutamate, $[Glu]_{ex}$, reported by in vivo microdialysis (Baker et al., 2003; McFarland et al., 2003, 2004; Szumlinski et al., 2006) during control and cocaine conditions were modeled as being outside glial region G_3 (ECS of volume $1.418 \mu\text{m}^3$) of the configuration in Figure 1. Concentration within the synaptic cleft (of volume $2.29 \times 10^{-3} \mu\text{m}^3$), $[Glu]_{syn}$, near mGluR2/3 (located at $\varphi = 20^0$ with a volume $1.25 \times 10^{-4} \mu\text{m}^3$), $[Glu]_{mGluR}$, and $[Glu]_{ex}$ were computed using the total number of free glutamate molecules in the respective regions.

3.3.5. Implementation of the kinetics and reaction schemes

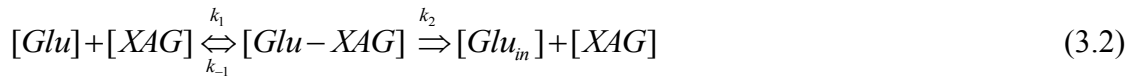
Diffusing glutamate molecules stochastically interacted with the surface populated receptors based on the reaction schemes described next. Details related to the implementation of diffusion–reaction systems on surfaces and in a solution used by

MCell can be found in Kerr et al. (2008). Upon release, glutamate molecules reacted with synaptic and perisynaptic receptors (e.g., AMPA, NMDA, or mGluR2/3) following the scheme in equation. 3.1,



where, $[Glu]$, $[R]$, and $[GluR]$ represented the molecules of glutamate, glutamate receptors (ionotropic/metabotropic), and the glutamate–receptor bound complex, respectively. The kinetics of AMPA and NMDA were set to match those previously published by Lester and Jahr (1992), Jonas, Major, and Sakmann (1993) and Attwell and Gibb (2005) (Table 1). The binding kinetics for mGluR2/3 of $k_1 = 10^8 \text{ M}^{-1}\text{ms}^{-1}$ and $k_{-1} = 18 \text{ ms}^{-1}$ were iteratively determined based on the disassociation constant K_d (0.187 nM; Schoepp and True, 1992) to satisfy nominal values of glutamate concentration near mGluR2/3 and simultaneously produce an occupancy of 50% to establish tone on the autoreceptor (Billups et al., 2005) during control basal conditions.

The surface populated XAG on the glial sheaths G_{1-3} interacted with the glutamate molecules per the reaction scheme in equation. 3.2,



where, $[XAG]$, and $[Glu-XAG]$ represented the molecules of the transporter, and the glutamate transporter complex, respectively, and $k_2*[Glu_m]$ represented the uptake rate of glutamate by XAG. The kinetics for XAG were taken from Rusakov (2001) who based it on experiments by others (Wadiche, Arriza, Amara, and Kavanaugh, 1995; Bergles and Jahr, 1997), $k_1 = 10^4 \text{ M}^{-1}\text{ms}^{-1}$, $k_{-1} = 0.2 \text{ ms}^{-1}$, and $k_2 = 0.1 \text{ ms}^{-1}$. $[GluD]$ represented the

glutamate eliminated from the system, and was given by equation. 3.3, with a rate $k_3 = 0.026 \text{ ms}^{-1}$ (Geiger, Roth, Taskin, and Jonas, 1999).



The non-synaptic source, xc-, located on the outer surface of glial sheath G_3 , was modeled to release glutamate molecules into the ECS of volume $1.418 \mu\text{m}^3$ using the reaction scheme in equation. 3.4,



at the rate $k_4 = 0.092 \text{ ms}^{-1}$ (17 mM hr^{-1} ; Pendyam et al., 2009).

Iterative evaluation. The iterative process began with values in the lower end of the ranges for the parameters reported in Table 1, while monitoring $[Glu]_{\text{syn}}$, $[Glu]_{\text{mGluR}}$, $[Glu]_{\text{ex}}$ and % receptor occupancy at mGluR2/3 (Figure 1). It was iteratively determined that a single quantal vesicular release of 22,000 molecules was required during every action potential to simultaneously satisfy $[Glu]_{\text{syn}}$, $[Glu]_{\text{mGluR}}$ and $[Glu]_{\text{ex}}$ for control and cocaine cases. After satisfying the requirements for the control basal case, the cocaine basal and cocaine seeking cases were simulated by modeling known cocaine-induced changes to xc- (modeled by reducing total number of xc- molecules by 50%) and mGluR2/3 signaling (modeled as a combination of release probability and firing frequency). Through further iterative changes, multiple parameter sets were identified that satisfied some of the model constraints in control and cocaine conditions, but the model values listed in Table 1 constituted the values that satisfied all the constraints simultaneously, i.e., steady state $[Glu]_{\text{syn}}$, $[Glu]_{\text{mGluR}}$ and $[Glu]_{\text{ex}}$ in the control basal,

natural reward seeking, cocaine basal and cocaine seeking cases while maintaining 50% receptor occupancy at mGluR2/3 in the control basal case.

The model used an integration time step of 0.5 μ sec so that the corresponding mean diffusion length computed by MCell allowed the system to be sampled sufficiently at this scale. Conservation of molecules was confirmed at each time step by computing the numbers of free, bound and transported glutamate molecules. To check for numerical accuracy, the integration time step was decreased by a factor of 5 and no significant change ($\sim 3\%$) were found in $[\text{Glu}]_{\text{syn}}$, $[\text{Glu}]_{\text{mGluR}}$ and $[\text{Glu}]_{\text{ex}}$. At initialization of each simulation, the exact number and position of receptors were homogeneously assigned by MCell on specified surfaces (for e.g., XAG on glial sheath G_1 varied from 2737 to 2874 molecules between trials). The surface density of receptor molecules (AMPA, NMDA, mGluR2/3, XAG and xc-) used in the configuration in Figure 1 are listed in Tables 1 and 2. Due to the stochastic nature of the model, multiple trials were conducted to obtain average estimates for $[\text{Glu}]_{\text{syn}}$, $[\text{Glu}]_{\text{mGluR}}$ and $[\text{Glu}]_{\text{ex}}$ such that the estimates were within one standard deviation from the experimentally reported mean (see model constraints). This required 10 trials and so all parameters/results reported in this paper were averaged across 10 trials.

3. 4. RESULTS

Example synapse – control and cocaine cases

Multiple 3-D configurations of glia surrounding the example case cortico-accumbens synapse were studied by varying the number of glial sheaths, coverage, thickness, and glial boulders in the ECS. As cited above, the model parameters were iteratively adjusted

to satisfy model constraints (see section 2.3). By using the iterative process and by providing appropriate resistance to the flow of glutamate molecules, the configuration in Figure 1 established all model constraints simultaneously.

3.4.1. Transient and steady state concentration characteristics

Each model synaptic release resulted in peak cleft concentrations in the mM range that decayed in a biphasic manner with fast and slow time constants of 360 μ s, and 8 ms, respectively.

As cited, the configuration in Figure 1 satisfied steady state constraints on $[\text{Glu}]_{\text{syn}}$, $[\text{Glu}]_{\text{mGluR}}$ and $[\text{Glu}]_{\text{ex}}$. It should be noted that a single glutamate molecule in the synaptic cleft (volume of $2.29 \times 10^{-3} \mu\text{m}^3$) resulted in $[\text{Glu}]_{\text{syn}}$ increasing to 0.7 μM . Since the steady state biological $[\text{Glu}]_{\text{syn}}$ were typically three-four times lower ($\sim 0.2 \mu\text{M}$), we concluded that experimental estimates of low steady state concentrations measured in the synapse may be due to the intermittent presence of a single glutamate molecule. This holds true for the region in the vicinity of mGluR2/3 autoreceptors (volume of $1.25 \times 10^{-4} \mu\text{m}^3$) where $[\text{Glu}]_{\text{mGluR}}$ was monitored. By labeling glutamate molecules, the model further showed that transient characteristics were primarily dominated by synaptic release while steady state concentrations were controlled by non-synaptic sources. The relative contributions (normalized) of synaptic and non-synaptic sources to transient and steady state glutamate concentrations after a release are shown in Figure 2.

Approximately 4,250 glutamate molecules of non-synaptic origin maintained a steady state $[\text{Glu}]_{\text{ex}}$ of 5 μM in the ECS (volume of $1.41 \mu\text{m}^3$). The neurotransmitter molecule numbers in ECS varied from 3,750–4,250 across the control basal trials resulting in average $[\text{Glu}]_{\text{ex}}$ being 4.7 μM , while average $[\text{Glu}]_{\text{ex}}$ during the natural reward seeking

was 5.6 μM corresponding to a molecular variation of 4,500–5,250 across trials. The model reproduced extracellular glutamate concentration levels for cocaine basal, and cocaine seeking as 3.2 μM , and 14.7 μM respectively, only after a 40% reduction in XAG, verifying the prediction based on a continuum model in Pendyam et al. (2009). This corresponded to a variation of 2,500–3250 glutamate molecules in cocaine basal and 11,750–12,500 in cocaine seeking, across trials.

3.4.2. Receptor occupancy during control and cocaine conditions

AMPA/NMDA receptor occupancy was mediated by synaptic and non-synaptic glutamate sources during control basal case. As cited, the AMPA/NMDA ratio was 0.8 ± 0.33 in the control basal case and changed to 1.15 ± 0.41 ($n = 12$; unpublished data; also see Kourrich et al., 2007; Conrad et al., 2008) in the cocaine basal case in the nucleus accumbens. Figure 3 shows the percentage occupancy for AMPA and NMDA receptors during transient and steady state conditions for control and cocaine cases in the presence of synaptic and non-synaptic sources. Percentage occupancy was defined as the ratio of receptors singly bound to glutamate (synaptic and non-synaptic), to the total receptors in the volume considered. Table 2 shows the surface density and the equivalent number of receptor molecules that were homogeneously distributed. As cited above, in between spike events, glutamate molecules (non-synaptic origin) from ECS diffused into the cleft and this resulted in <10% of the high affinity NMDA receptors being bound during the steady state control basal case. Since AMPA occupancy was <1%, the predicted level of NMDA receptor occupancy would not lead to postsynaptic signaling (Parsons, Danysz, and Zieglansberger, 2005).

3.4.3. Parametric studies

A sensitivity analysis was used to rank the following model parameters using the configuration in Figure 1: total transporter molecules, non-synaptic glutamate molecules, number of molecules/release, diffusion coefficient, and volume fraction. Each parameter was varied by +/-10% around the model value in Table 1, to find their relative effect of the outputs of interest, i.e., $[Glu]_{syn}$, and $[Glu]_{ex}$. The differences in the outputs based on this +/-10% change were then normalized by dividing with the largest value across all parameters. The resulting normalized numbers reported in Table 3 were indicative of the relative importance (rank) of the parameters as far as their effect on the output was concerned. The details of the % variation in the parameters of interest compared to the control basal case are reported below.

Total transporters. A +/-10% change in XAG on all sheaths G_{1-3} resulted in a decrease/increase in $[Glu]_{syn}$ by 25%/37%; and in $[Glu]_{ex}$ by 8%/9%. Further, transporters on each glial sheath were varied independently to quantify their role on the outputs of interest. A +/-10% change in transporters on G_1 alone resulted in a decrease/increase in $[Glu]_{syn}$ by 11%/11%. As expected, a +/-10% change in XAG on G_1 alone resulted in no significant variation in $[Glu]_{ex}$. A +/-10% change in XAG for G_2 alone resulted in decrease/increase of $[Glu]_{syn}$ by 6%/4% and less than 1% change in $[Glu]_{ex}$. The same +/-10% change in XAG on G_3 alone resulted in a decrease/increase in $[Glu]_{syn}$ by 12%/12% and in $[Glu]_{ex}$ by 7%/8%.

Non-synaptic sources. A +/-10% change in xc- resulted in an increase/decrease in $[Glu]_{syn}$ by 12%/3%, and in $[Glu]_{ex}$ by 11%/4%.

Molecules per release. A +/-10% change in the number of molecules per release

resulted in no change in $[\text{Glu}]_{\text{syn}}$, and in less than 0.5% change in $[\text{Glu}]_{\text{ex}}$. This showed that synaptically released glutamate was consumed entirely by XAG in the control basal case.

Diffusion coefficient, D . A +/-10% change in diffusion coefficient resulted in an increase/decrease in $[\text{Glu}]_{\text{syn}}$ by 19%/16%, and a decrease/increase in $[\text{Glu}]_{\text{ex}}$ by 3%/3%. Reducing D restricted efflux of molecules to the ECS after a release, and this increased the availability of molecules to the glial rich transporters in the perisynaptic environment. At the same time, a low value of D constrained influx of molecules from the ECS to the perisynapse during steady state.

Volume fraction, α . To study the effect of volume fraction, an extreme case of no glial boulders in the region outside G_3 was considered. This led to a four-fold increase in α from 0.2 to 0.9, which in turn resulted in an increase in $[\text{Glu}]_{\text{syn}}$ by 17%, and in $[\text{Glu}]_{\text{ex}}$ by 10%.

Example case synapse – generalized study

3.4.4. Characterizing isolation for a general synapse based on glial sheath geometry

Certain synapses are tightly ensheathed by glial processes while others are left open (Sykova, 2004; Rollenhagen and Lubke, 2006). The generalized study considered the following question – Given the same parameter set, how do configurations A–F in Figure 4 compare in maintaining a specific neurotransmitter gradient? To characterize diffusion path length and synaptic isolation, the stochastic framework for the example case cortico-accumbens synapse was generalized by considering a lower $[\text{Glu}]_{\text{ex}}$ of 1 μM , and comparing three types of glial configurations akin to those previous proposed (e.g., Barbour, 2001; Rusakov, 2001), namely, porous (no glial sheaths and transporters

distributed uniformly in that region), one, and two glial sheaths (Figure 4). The key difference between the configurations in Figure 4 was their orientation, coverage, placement and number of glial sheaths, and resulted in different diffusion path lengths. The two sheath model with the longest path length (configuration G) was set as the baseline model. So, for this configuration, the diffusion coefficient, number of the transporter and non-synaptic molecules, were iteratively determined to satisfy the following constraints: $[Glu]_{syn}$ of 0.2 μM while maintaining $[Glu]_{ex}$ of 1 μM establish a neurotransmitter gradient ($[Glu]_{ex}-[Glu]_{syn}$) of 0.8 μM . The resulting parameter set for this baseline model (configuration G, Figure 4) was as follows: molecules per release = 2000, total transporter molecules (G_{1-2}) = 2150 and non-synaptic source molecules = 38 with other parameters the same as in Table 1.

Holding all parameter values fixed as in the baseline model, a comparative study determined the relative effectiveness of configurations A–G in maintaining a specified neurotransmitter gradient. Figure 5 shows the variation in $[Glu]_{syn}$, $[Glu]_{ex}$ and mGluR2/3 receptor occupancy across all the glial configurations A-G in Figure 4. The dotted line connects the gradients achieved by each of these configurations. For the porous geometry in configuration A, $[Glu]_{syn}$, and $[Glu]_{ex}$ were the same at 0.52 μM . For the one sheath glial geometries (configuration B and C), $[Glu]_{syn}$ dropped from 0.37 to 0.29 μM while $[Glu]_{ex}$ increased from 0.48 to 0.53 μM . For all the configurations considered, geometries with two glial sheaths (configurations D-G) showed the largest variation in concentrations measured at two locations based on the amount of synaptic isolation they provided. For instance, $[Glu]_{syn}$ dropped from 0.35 to 0.15 μM going from configuration

D to G (Figure 5). As cited, the reference model (configuration G) supported the largest neurotransmitter gradient between the synapse and ECS as seen in Figure 5.

As an additional study, we investigated differences in transporter efficiency between volume populated (Pendyam et al., 2009) and surface populated model (configuration G in Figure 4), using the parameter set as in the baseline model study. XAG molecules were uniformly volume populated upto 50 nm on each side from the center line in the continuum case. The continuum model thus had more space between the glial sheaths for molecular diffusion, i.e., 140 nm compared to 40 nm in the stochastic model. The volume populated continuum model resulted in an approximately 100% increase in $[Glu]_{syn}$ and $[Glu]_{mGluR}$ (i.e., 0.35 μ M and 0.38 μ M, respectively), compared to the stochastic model, where $[Glu]_{ex}$ rose only by 10% to 1.1 μ M. Although, the continuum model maintained a concentration gradient between the synaptic and extracellular space, it did not establish the required model constraints. The cause for this was a 50% decrease in transporter efficiency in the volume populated model.

3.5. DISCUSSION

Neurotransmitter homeostasis was modeled using a three-dimensional stochastic diffusion model of an example cortico-accumbens synapse to provide molecular level insights. Previous stochastic models of synaptic environments have not typically considered non-synaptic sources of glutamate or modeled neurotransmitter gradients, both of which were included in the models considered in the present study. The example case synapse was further generalized to investigate the effect of diffusion path length on synaptic isolation and receptor occupancy using several feasible glial geometries. The insights provided by the models are described next.

Example case synapse – control and cocaine cases

3.5.1. Stochastic molecular model quantifies the role of non-synaptic neurotransmitter sources in control and cocaine conditions

Homeostasis. By combining physiological values from the literature and empirically derived changes due to chronic cocaine, the example case cortico-accumbens model reproduced experimentally observed glutamate concentrations for various cases (see model constraints in section 2.3). The model provided molecular level details not predicted by the continuum-based approach (Pendyam et al., 2009). Specifically, by labeling glutamate from synaptic and non-synaptic sources, the model showed that the non-synaptic source contribution to the homeostatic extracellular concentration varied from 100% (i.e., ~4000 molecules total) in the control basal case to 84% (i.e., ~5000 molecules total) and 24% (i.e., ~12,000 molecules total), respectively, in the natural reward and cocaine seeking cases. This study established that only non-synaptic sources maintained homeostatic concentration levels in the control basal condition for such synapses (Figure 2).

Receptor occupancy. The model also provided molecular insights related to % occupancy of different synaptic receptors (AMPA and NMDA and mGluR2/3). The configuration in Figure 1 showed that there was a constant influx of 5 molecules/ms from the ECS into the glial environment (measured at the G_3 opening, between release events in the control basal case, with an average $[Glu]_{ex}$ of 4.7 μM), and this reduced to 2 molecules/ms resulting in 50% mGluR2/3 occupancy. As shown in Table 2, mGluR2/3 occupancy increased to 100% during steady state cocaine seeking conditions. This can be explained by noting that steady state $[Glu]_{ex}$ was three times higher during cocaine seeking (14 μM) compared to natural reward seeking (5.6 μM), and that transporters were down-

regulated by 40% causing increased influx of glutamate from ECS rendering mGluR2/3 ineffective. This influx of molecules into the cleft also increased occupancy of high affinity synaptic NMDA receptors. Thus, the example case synapse provided molecular level quantification of the contribution of non-synaptic sources to the regulation of homeostasis and receptor occupancy.

3.5.2. Glial glutamate transporters had the largest effect on glutamate concentrations

The signs on the various sensitivity numbers in Table 3 followed expected biological trends. By considering changes in glutamate concentrations from the nominal values at the three locations for the configuration in Figure 1, total transporters were found to be most important parameter in controlling $[\text{Glu}]_{\text{syn}}$ and $[\text{Glu}]_{\text{ex}}$. Counter to intuition, it was found that independently varying transporters by $\pm 10\%$ on glial sheath G_3 (see results) had a greater effect on $[\text{Glu}]_{\text{syn}}$ as compared to a similar change on G_1 . Another observation was that, around the nominal operating point, variation of $\pm 10\%$ in non-synaptic source molecules was ranked second (after transporters) as far as its effect on $[\text{Glu}]_{\text{ex}}$ was concerned (Table 3). Thus, the study helped highlight the role of glial sheaths and XAG in regulating molecular influx rates at steady state that may be critical for perisynaptic receptor activity. These observations, although specific to the example case, should hold for other geometries that isolate the synapse and support neurotransmitter gradients.

Example case synapse – generalized study

3.5.3. Diffusion path length correlates with degree of synaptic isolation and magnitude of neurotransmitter gradient

A generalized study of the example synapse was considered to characterize the role of diffusion path length and glial geometry in supporting gradients, i.e., which of the configurations in Figure 4 (with baseline model being configuration G, and $[\text{Glu}]_{\text{ex}} = 1 \mu\text{M}$) with varying diffusion path lengths yields the largest gradient?

As expected, it was found that the porous geometry of configuration A could not support neurotransmitter gradients and resulted in the largest mGluR2/3 occupancy as shown in Figure 5. For the one sheath geometries (see configurations B and C), a structured glial configuration ensured better utilization of transporters, compared to configuration A. This was reflected by the increased gradient (Figure 5). Configurations D and E represented the two-sheath versions of configurations B and C. As seen in Figure 5, going from configurations D to E, it was observed that while $[\text{Glu}]_{\text{syn}}$ decreased, there was a corresponding increase in $[\text{Glu}]_{\text{ex}}$. By increasing the interaction of the diffusing molecules with transporters, configurations D and E supported higher neurotransmitter gradient as compared to their corresponding one sheath models B and C. The dotted line in Figure 5 summarized the finding in this comparative study, that for the same set of parameters, diffusion path length was proportional to the gradient supported.

A comparative analysis of transporter efficiency revealed that volume populating transporters (continuum approach) was found to be 50% less efficient compared to the surface populated case, for the baseline configuration G. This is because volume population of transporters in space compartments makes them less concentrated and hence less efficient, i.e., uptake rate decreases. The results suggested that by reducing the size of the space compartments, the continuum model would better approximate the

surface populated stochastic model as also noted by others (Stiles and Bartol, 2001; Franks et al., 2002).

3.5.4. Limitations

As cited, glial configurations and diffusion very close to synapses ($\sim 1 \mu\text{m}$) are not well understood, particularly for synapses that support gradients between the cleft and the ECS. Hence, the glial configurations considered should be viewed as being only 'equivalent' in that they provide the same resistance to the flow of neurotransmitter observed in vivo. Secondly, the example case synapse considered only one neurotransmitter and stimulation of several of its receptors. Finally, another modeling assumption was that mGluR2/3 kinetics were based on satisfying two conditions simultaneously namely, maintaining $[\text{Glu}]_{\text{mGluR}} \sim 0.2 \mu\text{M}$ and achieving 50% receptor occupancy during control basal conditions. The biological realism of the kinetic values for these receptors needs to be determined. Refined estimates for parameter values and the kinetics of other reactions would further enhance model predictions. The model can incorporate other neurotransmitters such as dopamine and GABA that might also modulate the homeostatic mechanisms.

3.6. CONCLUSION

A biophysically realistic stochastic modeling framework was proposed to study neurotransmitter homeostasis around a class of synapses that supported neurotransmitter gradients. An example case of a cortico-accumbens synapse in control and cocaine conditions was considered to obtain molecular level insights including how non-synaptic sources affected homeostasis and receptor occupancy. Generalized models of the

example case were then considered and these shed light on the role of glial configurations in maintaining neurotransmitter gradients. While porous approximations of the neuropil can only describe average behaviors of molecules, the configurations considered showed that glial geometries had characteristic diffusion path lengths that were correlated to gradients achievable and to % occupancy of synaptic and perisynaptic receptors. Thus, such models provide guidance about glial morphology around a class of synapses that support neurotransmitter gradients.

ACKNOWLEDGEMENT

We thank Dr. Markus Dittrich, Pittsburg Supercomputing Center for providing assistance with the MCell software and for helpful comments on an earlier draft. This research was supported in part by USPHS grants DA015369, DA03906 (PWK), and subcontract from DA015369 and PSC grant IBN090001P to University of Missouri (SSN).

3.8. REFERENCES

1. Alagarsamy, S., Sorensen, S. D., and Conn, P. J. (2001). Coordinate regulation of metabotropic glutamate receptors. *Cur. Op. Neurobiol.*, 11, 357–362.
2. Attwell, D., and Gibb, A. (2005). Neuroenergetics and the kinetic design of excitatory synapses. *Nat. Rev. Neurosci.*, 6, 841–849.
3. Baker, D. A., McFarland, K., Lake, R. W., Shen, H., Tang, X. C., Toda, S., and Kalivas, P.W. (2003). Neuroadaptations in cystine–glutamate exchange underlie cocaine relapse. *Nat. Neurosci.*, 6, 743–749.
4. Barbour, B. (2001). An evaluation of synapse independence. *J. Neurosci.*, 21(20), 7969–7984.
5. Bergles, D. E., and Jahr, C. E. (1997). Synaptic activation of glutamate transporters in hippocampal astrocytes. *Neuron*, 19, 1297–1308.
6. Billups, B., Graham, B. P., Wong, A. Y., and Forsythe, I. D. (2005). Unmasking group III metabotropic glutamate autoreceptor function at excitatory synapses in the rat CNS. *J. Physiol.*, 565, 885–896.

7. Bruns, D., and Jahn R. (1995). Real-time measurement of transmitter release from single synaptic vesicles. *Nature*, 377, 62–65.
8. Cavelier, P., Hamann, M., Rossi, D., Mobbs, P., and Attwell, D. (2005). Tonic excitation and inhibition of neurons: ambient transmitter sources and computational consequences. *Prog. Biophys. Mol. Biol.*, 87, 3–16.
9. Chang, J. Y., Zhang, L., Janak, P. H., and Woodward, D. J. (1997). Neuronal responses in prefrontal cortex and nucleus accumbens during heroin self-administration in freely moving rats. *Brain Res.*, 754, 12–20.
10. Clements, J. D., Robin, A., Lester, J., Tong, G., Jahr, C. E., and Westbrook G.L. (1992). The time course of glutamate in the synaptic cleft. *Science*, 258, 1498–1501.
11. Clements, J. D. (1996). Transmitter time course in the synaptic cleft: its role in central synaptic function. *Trends in Neuroscience*, 19, 163–171.
12. Conrad, K.L., Tseng, K.Y., Uejima, J.L., Reimers, J.M., Hen, L.J., Shaham, Y., Marinelli, M., and Wolf, M.L. (2008). Formation of accumbens GluR2-lacking AMPA receptors mediates incubation of cocaine seeking. *Nature*, 454(7200), 118–121.
13. Danbolt, N.C. (2001). Glutamate uptake. *Prog. Neurobiol.*, 65, 1–105.
14. Diamond, J.S. (2005). Deriving the glutamate clearance time course from transporter currents in CA1 hippocampal astrocytes: transmitter uptake gets faster during development. *J. Neurosci.*, 25, 2906–2916.
15. Franks, K.M., Bartol, T.M., and Sejnowski, T.J. (2002). A Monte Carlo model reveals independent signaling at central glutamatergic synapses. *Biophys. J.*, 83, 2333–2348.
16. Geiger, J.R.P., Roth, A., Taskin, B., and Jonas, P. (1999). In: P. Jonas and H. Monyer (Eds.), *Handbook of experimental pharmacology* (pp. 363–398). Berlin: Springer.
17. Haydon, P. (2001). Glia: listening and talking to the synapse. *Nat. Neurosci.*, 2, 2185–191.
18. Herman, M.A., and Jahr, C.E. (2007). Extracellular glutamate concentration in hippocampal slice. *J. Neurosci.*, 27, 9736–9741.
19. Holmes, W.R. (1995). Modeling the effect of glutamate diffusion and uptake on NMDA and non-NMDA receptor saturation. *Biophys. J.*, 69, 1734–1747.
20. Hrabe, J., Harbetova, S., and Segeth, K. (2004). A model of effective diffusion and tortuosity in the extracellular space of the brain. *Biophys. J.*, 87, 1606–1617.
21. Jonas, P., Major, G., and Sakmann, B. (1993). Quantal components of unitary EPSCs at the mossy fibre synapse on CA3 pyramidal cells of rat hippocampus. *J. Physiol.*, 472, 615–663.
22. Kalivas, P.W., Volkow, N., and Seamans, J. (2005) Unmanageable motivation in addiction: pathology in prefrontal–accumbens glutamate transmission. *Neuron*, 45, 647–650.
23. Kerr, R.A., Bartol, T.M., Kaminsky, B., Dittrich, M., Chang, J.C., Baden, S.B., Sejnowski, T.J., and Stiles, J.R. (2008). Fast Monte Carlo simulation methods for biological reaction–diffusion systems in solution and on surfaces. *S.I.A.M. J. Sci. Comp.*, 30(6), 3126–3149.

24. Kleinle, J., Vogt, K., Luscher, H. R., Muller, R., Senn, W., Wyler, K., and Streit, J. (1996). Transmitter concentrations profiles in the synaptic cleft: an analytical model of release and diffusion. *Biophys. J.*, *71*, 2413–2426.
25. Kourrich, S., Rothwell, P.E., Klug, J.R., and Thomas, M.J. (2007). Cocaine experience controls bidirectional synaptic plasticity in the nucleus accumbens. *J. Neurosci.*, *27*, 7921–7928.
26. Lehre, K.P., and Danbolt, N.C. (1998). The number of glutamate transporter subtype molecules at glutamatergic synapses: chemical and stereological quantification in young adult rat brain. *J. Neurosci.*, *18*, 8751–8757.
27. Lehre, K.P., and Rusakov, D. (2002). Asymmetry of glia near central synapse favors presynaptically directed glutamate escape. *Biophys. J.*, *83*, 125–134.
28. Lester, R.A., and Jahr, C.E. (1992). NMDA channel behavior depends on agonist affinity. *J. Neurosci.*, *12*, 635–643.
29. Le Meur, K., Galante, M., Anulo, M.C., and Audinat, E. (2007). Tonic activation of NMDA receptors by ambient glutamate of non-synaptic origin in the rat hippocampus. *J. Physiol.*, *580*, 373–383.
30. McFarland, K., Lapish, C.C., and Kalivas, P.W. (2003). Prefrontal glutamate release into the core of the nucleus accumbens mediates cocaine-induced reinstatement of drug-seeking behavior. *J. Neurosci.*, *23*, 3531–3537.
31. McFarland, K., Davidge, S.B., Lapish, C.C., and Kalivas, P.W. (2004). Limbic and motor circuitry underlying footshock-induced reinstatement of cocaine-seeking behavior. *J. Neurosci.*, *24*, 1551–1560.
32. Melendez, R.I., Vuthiganon J., and Kalivas, P.W. (2005). Regulation of extracellular glutamate in the prefrontal cortex: focus on the cystine-glutamate exchanger and group I metabotropic glutamate receptors. *J. Pharmacol. Exp. Ther.*, *314*, 139–147.
33. Murthy, V.N., and Sejnowski, T.J. (1997). Heterogeneous release properties of visualized individual hippocampal synapses. *Neuron*, *18*, 599–612.
34. Nicholson, C. (2001). Diffusion and related transport mechanism in brain tissue. *Reports on progress in physics*, *64*, 815–884.
35. Nicholson, C., and Sykova, E. (1998). ECS structure revealed by diffusion analysis. *Trends in Neuroscience*, *21*(5), 207–215.
36. Parsons, C.G., Danysz, W., and Zieglansberger, W. (2005). Excitatory amino acid neurotransmission. *Handbook Exp. Pharmacol.*, *169*, 249–303.
37. Patneau, D.K., and Mayer, M.L. (1990). Structure–activity relationships for amino acid transmitter candidates acting at N–methyl–D–aspartate and quisqualate receptors. *J. Neurosci.*, *10*, 2385–2399.
38. Pendyam, S., Mohan, A., Kalivas, P.W., and Nair, S.S. (2009). Computational model of extracellular glutamate in the nucleus accumbens incorporates neuroadaptations by chronic cocaine. *Neuroscience*, *158*, 1266–1276.
39. Rollenhagen, A., and Lubke, J.H.R. (2006). The morphology of excitatory central synapses: from structure to function. *Cell Tissue Res.*, *326*, 221–237.
40. Rusakov, D.A. (2001). The role of perisynaptic glial sheaths in glutamate spillover and extracellular Ca²⁺ depletion. *Biophys. J.*, *81*, 1947–1959.
41. Rusakov, D.A., and Kullmann, D.M. (1998). Extrasynaptic glutamate diffusion in

- the hippocampus: ultrastructural constraints, uptake, and receptor activation. *J. Neurosci.*, *18*, 3158–3170.
42. Saftenku, E.E. (2005). Modeling of slow glutamate diffusion and AMPA receptor activation in the cerebellar glomerulus. *J. Theo. Bio.*, *234*, 363–382.
 43. Savtchenko, L.P., and Rusakov, D.A. (2007). The optimal height of the synaptic cleft. *Proc. Natl. Acad. Sci. USA.*, *104*(6), 1823–1828.
 44. Schoepp, D.D., and True, R.A. (1992). 1S, 3R-ACPD-sensitive (metabotropic) [³H] glutamate receptor binding in membranes. *Neurosci. Lett.*, *145*, 100–104.
 45. Stiles, J.R., and Bartol, T.M., (2001). In E. De Schutter (Ed.), *Computational Neuroscience: Realistic Modeling for Experimentalists* (pp. 87–127). Boca Raton: CRC Press.
 46. Stiles, J.R., Van Helden, D., Bartol, T.M. Jr., Salpeter, E.E., and Salpeter, M.M. (1996).
 47. Miniature endplate current rise times <100 μs from improved dual recordings can be modeled with passive acetylcholine diffusion from a synaptic vesicle. *Proc. Natl. Acad. Sci. USA.*, *93*, 5747–5752.
 48. Sun, W., and Rebec, G.V. (2006). Repeated cocaine self-administration alters processing of cocaine-related information in rat prefrontal cortex. *J. Neurosci.*, *26*, 8004–8008.
 49. Sykova, E. (1997). The ECS in the CNS: Its regulation, volume and geometry in normal and pathological neural function. *The Neuroscientist*, *3*, 28–41.
 50. Sykova, E. (2004). Extrasynaptic volume transmission and diffusion parameters of the ECS. *Neuroscience*, *129*, 861–876.
 51. Szumlinski, K.K., Abernathy, K.E., Oleson, E.B., Kullmann, M., Lominac, K.D., He, D.Y., Ron, D., During, M., and Kalivas, P.W. (2006). Homer isoforms differentially regulate cocaine-induced neuroplasticity. *Neuropsychopharmacology*, *4*, 768–777.
 52. Tao, L., and Nicholson, C. (2004). Maximal geometrical hindrance to diffusion in brain ECS surrounding uniformly spaced convex cells. *J. Theo. Bio.*, *229*, 59–68.
 53. Thomas, M.J., Beurrier, C., Bonci, A., and Malenka, R.C., (2001). Long term depression in the nucleus accumbens: a neural correlate of behavioral sensitization to cocaine. *Nat. Neurosci.*, *4*(12), 1217–1223.
 54. Thorne, R.G., and Nicholson, C. (2006). In vivo diffusion analysis with quantum dots and dextrans predicts the width of brain ECS. *Proc. Natl. Acad. Sci. USA.*, *103*(14), 5567–5572.
 55. Timmerman, W., and Westerink, B.H. (1997). Brain microdialysis of GABA and glutamate: what does it signify?, *Synapse*, *27*, 242–261.
 56. Trantham, H., Szumlinski, K., McFarland, K., Kalivas, P.W., and Lavin, A. (2002). Repeated cocaine administration alters the electrophysiological properties of prefrontal cortical neurons. *Neuroscience*, *113*, 749–757.
 57. Volynski, K.E., Rusakov, D.A., and Kullmann, D.M. (2006). Presynaptic fluctuations and release-independent depression. *Nat. Neurosci.*, *9*, 1091–1093.
 58. Wadiche, J.I., Arriza, J.L., Amara, S.G., and Kavanaugh, M.P. (1995). Kinetics of human glutamate transporter. *Neuron.*, *14*, 1019–1027.
 59. Wolf, J.A., Moyer, J.T., Lazarewicz, M.T., Contreras, D., Benoit-Marand, M., O'Donnell, P., and Finkel, L.H. (2005). NMDA/AMPA ratio impacts state

- transitions and entrainment to oscillations in a computational model of nucleus accumbens medium spiny projection neuron. *J. Neurosci.*, 25(40), 9080–9095.
60. Xi, Z.X., Baker, D.A., Shen, H., Carson, D.S., and Kalivas, P.W. (2002). Group II metabotropic glutamate receptors modulate extracellular glutamate in the nucleus accumbens. *J. Pharmacol. Exp. Ther.*, 300, 162–171.
61. Zheng, K., Scimemi, A., and Rusakov, D.A. (2008). Receptor actions of synaptically released glutamate: The role of transporters on the scale from nanometers to microns. *Biophys. J.*, 95, 4584–4596.

3.9. TABLES

Table 1. Ranges for parameter values for configuration in figure 1.

Parameter	Model value ^a	Range of values (citation)
Diffusion coefficient ($\mu\text{m}^2/\text{ms}$)	0.085	0.05–0.75 (Rusakov & Kullmann, 1998; Saftenku, 2005)
xc- (mM hr^{-1})	17 ^b	5–50 (Baker et al., 2003)
AMPA/NMDA dynamics		
AMPA k_1 ($\text{M}^{-1}\text{ms}^{-1}$)/ k_{-1} (ms^{-1})	4 x 10 ⁶ /2	4–10x10 ⁶ /2–3 (Jonas et al., 1993; Attwell & Gibb, 2005)
NMDA k_1 ($\text{M}^{-1}\text{ms}^{-1}$)/ k_{-1} (ms^{-1})	5 x 10 ⁶ /15 x 10 ⁻³	5–7x10 ⁶ /5–16 x 10 ⁻³ (Lester & Jahr, 1992; Attwell & Gibb, 2005)
Transporter dynamics		
XAG (molecules/ μm^2)	see ‘c’ below	2,500–10,000 (Bergles & Jahr, 1997; Lehre & Danbolt, 1998)
k_1 ($\text{M}^{-1}\text{ms}^{-1}$)/ k_{-1} (ms^{-1})/ k_2 (ms^{-1})	10 ⁴ /0.2/0.1	10 ⁴ /0.2/0.1 (Lehre & Rusakov, 2002)
Release parameters		
No. of molecules per release	22,000	4,700–80,000 (Bruns & Jahn, 1995)
K_d value of mGluR2/3 (μM)	0.187	0.1–0.3 (Schoepp & True, 1992)
Maximum release probability	0.4 (max)	0.1–0.5 (Billups et al., 2005; Volynski, Rusakov, & Kullmann, 2006)
Release probability used (tuned to operate near K_d value of mGluR)	0.14 (basal)	(based on log–linear interpolation from values cited in Xi et al., 2002)
Presynaptic firing frequencies		
Firing freq (Hz) (basal)	1–2	1–3 (Trantham et al., 2002)
Firing freq (Hz) (natural reward seeking)	12–15	12–15 (Chang et al., 1997; Sun & Rebec, 2006)
Geometric parameters		
Average extracellular gap (nm)	40	34–68 (Thorne & Nicholson, 2006)
Intersynaptic distance (μm)	2	2–20 (Rusakov, 2001)

^a values used to populate the configuration in Figure 1

^b surface density (molecules/ μm^2) of xc- was distributed on the outer surface of glial sheath G₃ as follows: 111; corresponding molecules of xc—471

^c surface density (molecules/ μm^2) of XAG was distributed as follows: G₁–1700, G₂–400, and G₃–400; corresponding molecules of XAG: G₁–2771, G₂–1490, and G₃–2708

Table 2. Glutamate receptor occupancy (bound receptors/total receptors) during transient and steady state conditions for configuration in figure 1.

Parameter	AMPA	NMDA	mGluR2/3
Total receptors (molecules)	18	30	22
Surface density (molecules/ μm^2)	130	200	900
Occupancy in % during transient/steady state			
Control basal*	21/0	35/6	69/52
Control rewards	18/0	36/8	98/59
Cocaine basal**	7/0	61/10	65/67
Cocaine seeking	21/0	73/46	99/89

* Control basal AMPA/NMDA Ratio: 0.62 ($n = 10$)

** Cocaine basal AMPA/NMDA Ratio: 0.96 (AMPA receptors = 30; NMDA receptors = 29)

AMPA/NMDA occupancy in transient state averaged for ~0–50ms

AMPA/NMDA occupancy in steady state averaged for ~3000ms

Table 3. Normalized sensitivity analysis to rank the parameters for configuration in figure 1.

Parameters	Glutamate concentrations*	
	[Glu]_{syn}	[Glu]_{ex}
Transporters (molecules)	1.00	1.00
Diffusion ($\mu\text{m}^2/\text{ms}$)	-0.54	0.34
^{xc-} (molecules)	-0.23	-0.86
No. of molecules per release (molecules)	0.01	-0.01
mGluR2/3 (molecules)	-0.04	0.03

*The signs indicate direction of change when the parameter varied from -10% to +10% around the model value

3.10. FIGURES

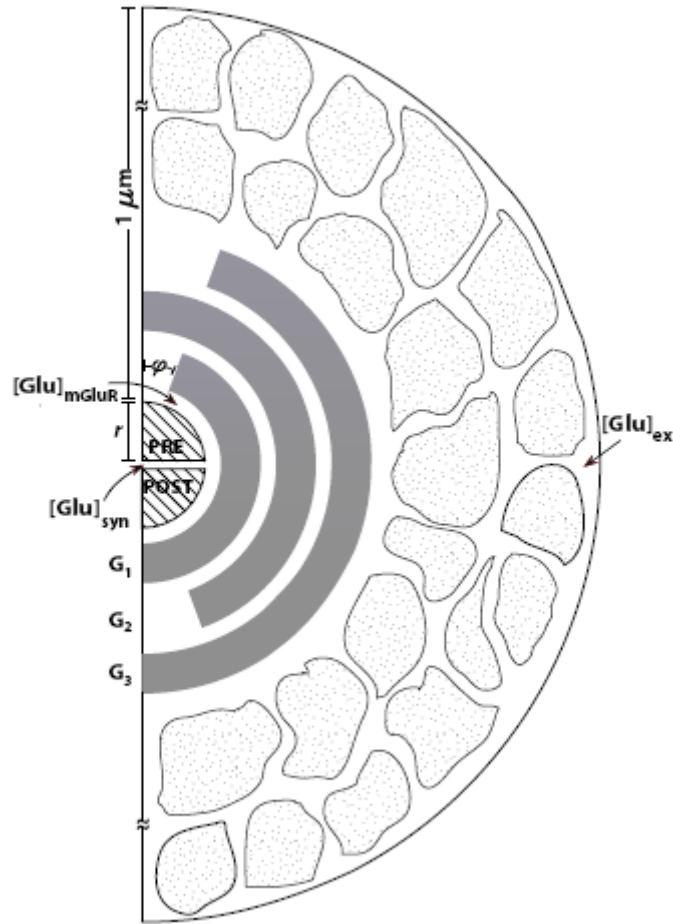


Figure 1. The glial configuration of the example case cortico-accumbens synapse used to study glutamate homeostasis (2-D representation of 3-D synaptic environment). A cleft or radius $r = 160$ nm separated the two hemispheres, and was surrounded by glial sheaths (G_i , $i = 1-3$; $i = 1$ being the closest to the synapse) with the highest density of XAG in G_1 . The cleft was populated with AMPA and NMDA receptors. Each impermeable glial sheath was 100 nm thick and was surface populated with XAG. Binding, uptake and efflux were modeled as stochastic processes. Non-synaptic glutamate source, xc-, was modeled on the outer surface of glial sheath G_3 . The complex structural geometry in the porous ECS consisted of realistic glial boulders randomly placed in the porous neuropil

to yield experimental estimates of volume fraction. $[Glu]_{syn}$, $[Glu]_{mGluR}$ and $[Glu]_{ex}$ represented glutamate concentrations measured within the synaptic cleft, in the perisynaptic region containing mGluR2/3 (located presynaptically at $\varphi = 20^\circ$ from vertical), and extracellular space beyond glial sheath G_3 .

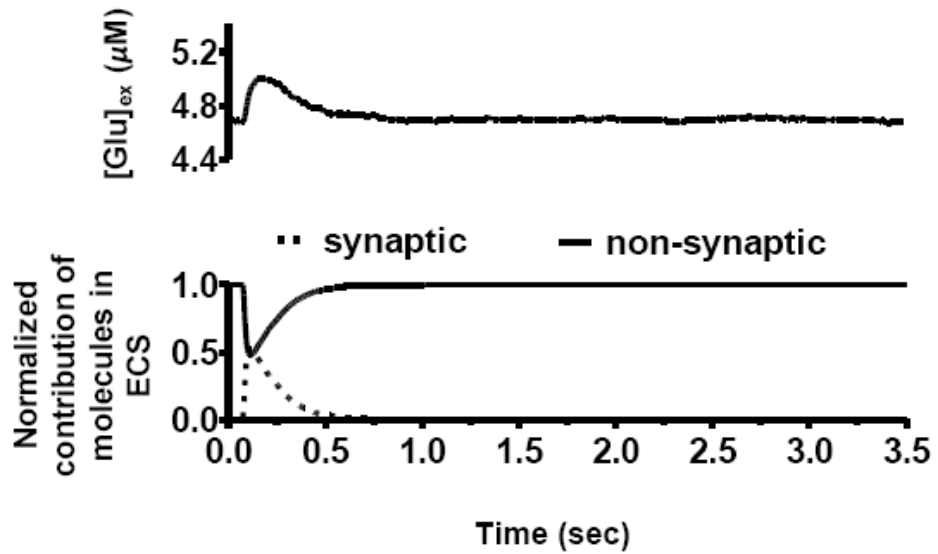


Figure 2. Top panel shows $[Glu]_{ex}$. Bottom panels show the normalized contributions of synaptic and non-synaptic glutamate to transient and steady state control basal concentrations of $[Glu]_{ex}$. Extracellular concentration was primarily due to the xc- at steady state for the control basal case since synaptically released glutamate molecules were entirely consumed by glial transporters.

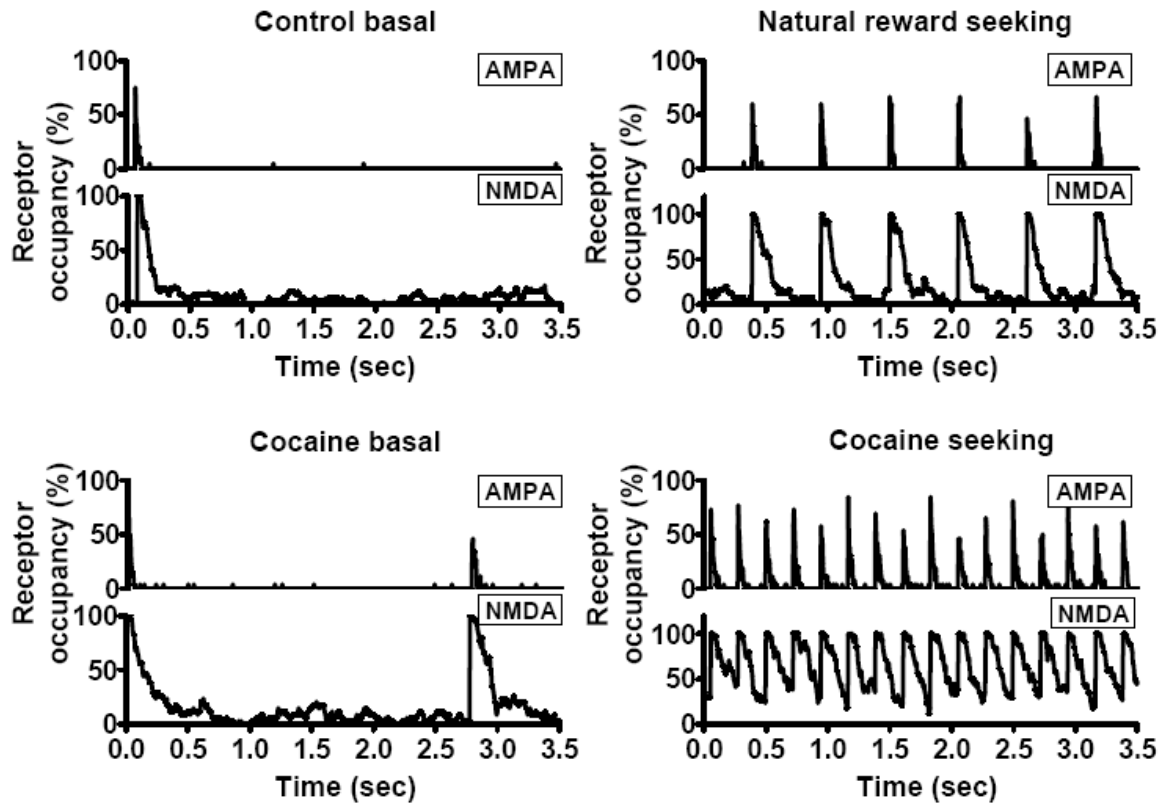


Figure 3. % receptor occupancy characteristics for AMPA and NMDA during the control basal, natural reward seeking, cocaine basal and cocaine seeking cases based on synaptic and non-synaptic sources. At steady state, there was an influx of glutamate molecules of non-synaptic origin into the perisynaptic region to maintain tone on mGluR2/3. This influx of molecules resulted in approximately 10% of the high affinity NMDA receptors being occupied, in the control basal condition, which, in the absence of AMPA mediated depolarization due to less than 1% occupancy of those receptors, did not lead to post synaptic signaling.

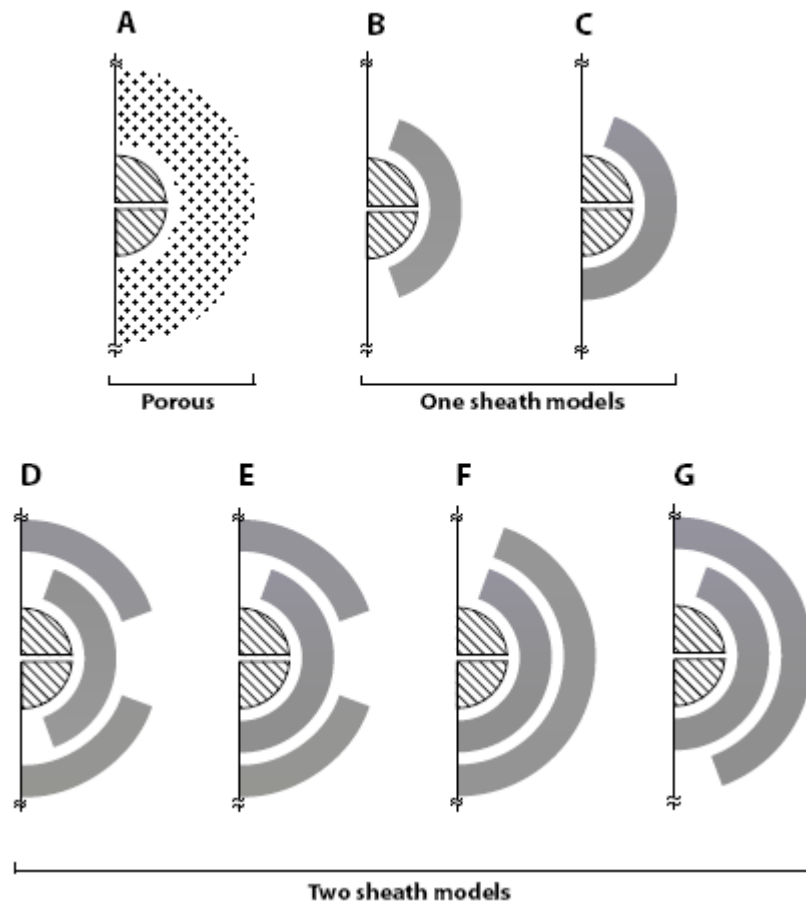


Figure 4. Three distinct types of glial configurations (porous, one, and two sheaths) used to characterize diffusion path length and synaptic isolation for a general synapse with $1 \mu\text{M}$ extracellular concentration, using the same legends as in Figure 1. Glial transporters were homogeneously distributed in the shaded region. Configurations B and C with different orientation of openings on pre and post synaptic regions represent the one sheath cases, and configurations D–G represent two sheath cases. The diffusion path length increased from configurations A to G.

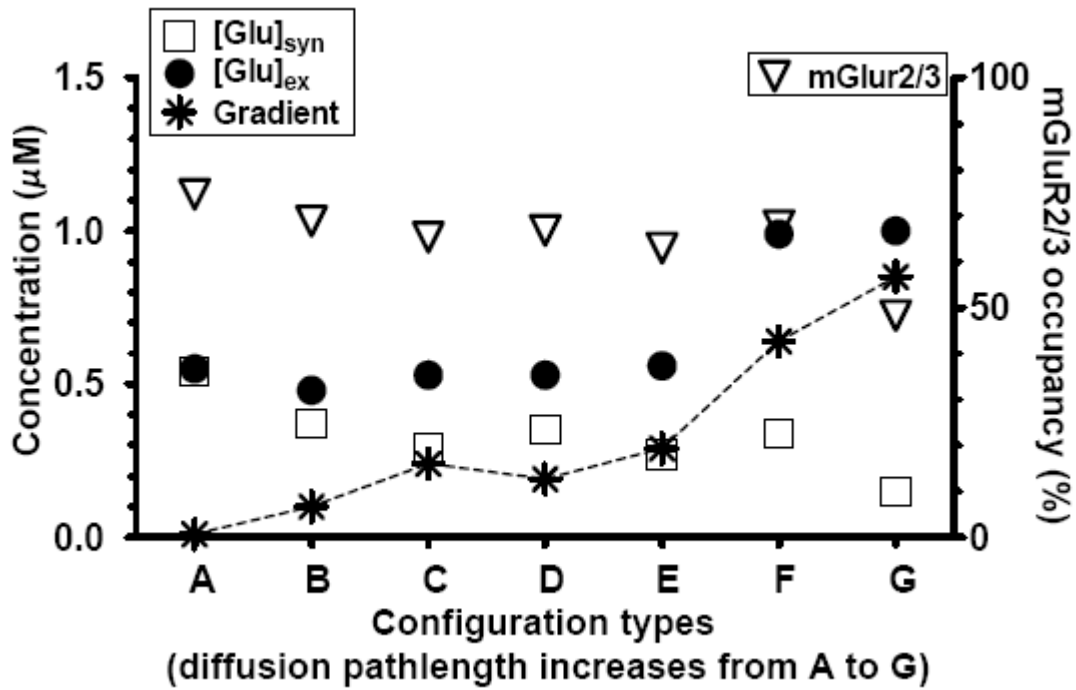


Figure 5. Comparison of $[Glu]_{syn}$ and $[Glu]_{ex}$ under control conditions for various glial configurations shown in Figure 4, for the same set of parameters, with configuration G as the baseline model. The baseline model established 50% mGluR2/3 occupancy. Porous glia (configuration A) with zero diffusion path length supported no neurotransmitter gradient. The dotted line connects the gradient ($[Glu]_{ex} - [Glu]_{syn}$) achieved by each of these configurations. The diffusion path length increased from configuration A to G, and this path length was correlated to the neurotransmitter gradient between the ECS and the cleft.

CHAPTER 4

Computational model predicts formation of distinct groups of neurons in the basal amygdala with fear conditioning

4.1. ABSTRACT

The basolateral amygdala plays an important role in the acquisition and expression of both fear conditioning and fear extinction. To understand how a single structure could encode these “opposite” memories, we developed a biophysical network model of the basal amygdala (BA) neurons during auditory fear conditioning and extinction. Membrane channel properties were selected in order to match waveforms and firing properties of pyramidal cells and interneurons in BA, from published *in vitro* studies. Hebbian plasticity was implemented in excitatory AMPA and inhibitory GABA_A receptor-mediated synapses to model learning. The occurrence of synaptic potentiation vs. depression was determined by intracellular calcium levels, according to the calcium control hypothesis. The model was able to replicate conditioning- and extinction-induced changes in tone responses of BA neurons in behaving rats. Our main finding is that BA activity during both acquisition and extinction can be controlled by a balance between pyramidal cell and interneuron activations. The model provides insights into the role of connectivity and amongst the three types of cells within the BA in conditioning and extinction, the mechanism of spontaneous recovery, and the role of amygdala NMDA receptors in extinction learning.

4.2. INTRODUCTION

It is well established that the amygdaloid complex plays an important role in the acquisition and expression of learned fear associations (Davis, 2006; LeDoux, 2000; Maren and Quirk, 2004). The components of the amygdala that are critical for fear conditioning are the lateral nucleus (LA), the basal nucleus (BA), and the central nucleus (CE) (Maren, 2001). BLA is widely accepted to be a key site of synaptic events that contribute to fear learning (Paré et al., 2004; Sigurdsson et al., 2007). There are two main types of neurons within the LA and the BA: pyramidal-like glutamatergic projection neurons, and local circuit γ -amino butyric acid (GABA)-ergic interneurons (McDonald, 1984).

In auditory fear conditioning, convergence of tone (conditioned stimulus, CS) and foot-shock (unconditioned stimulus, US) inputs in LA lead to potentiation of CS inputs, resulting in larger tone responses in LA (Blair et al., 2001). Increased LA responses are relayed to the CE via the basal nuclei (Pitkanen, 2000), and the intercalated (ITC) cell masses (Paré et al., 2004), eliciting fear responses via successive projections to brain stem and hypothalamic sites (LeDoux, 2000). As a result, rats learn to freeze to tones that predict foot-shock. Once acquired, conditioned fear associations are not always expressed. Repeated presentation of the tone CS in the absence of the US causes conditioned fear responses to diminish rapidly, a phenomenon termed fear extinction (Myers and Davis, 2007; Rescorla, 2002). The neural mechanisms of fear extinction are not well understood, and a neural analysis of extinction and inhibition is still in its infancy (Delamater, 2004; Quirk and Mueller, 2008). Some psychological theories described extinction as an “unlearning” process due to a violation of the CS-US association established in fear acquisition (Rescorla and Wagner, 1972). This unlearning

view has been challenged by the observation that fear recovers spontaneously after extinction. An alternative theory proposes that extinction does not erase the CS-US association, but instead forms a new memory that inhibits conditioned responding (Bouton and King, 1983; Quirk, 2002). Given the central role of the LA in the acquisition and expression of fear memory, it has been proposed that this structure may be a site of inhibition in extinction (Hobin et al., 2003; Myers and Davis, 2002; Sotres-Bayon et al., 2004).

Further, the amygdaloid complex also plays a key role in extinction of those memories (Falls et al., 1992; Herry et al., 2006; Laurent et al., 2008; Sotres-Bayon et al., 2007). A recent article reported that two distinct fear and extinction cell populations within the basal nucleus of the amygdale (BA) are exclusively activated during fear conditioning and fear extinction (Herry et al., 2008). Given that extinction is itself a learning process, an important goal is to understand how a single structure such as the BA can encode both fear acquisition and extinction memories.

The electrophysiological and morphological properties of LA/BA neurons have been characterized in a number of studies (Faber et al., 2001; Faber and Sah, 2002, 2005; Lang and Paré, 1998; Paré et al., 1995; Washburn and Moises, 1992a, b; Womble and Moises, 1993). There are several *in vitro* and *in vivo* recording studies of LA neurons during fear conditioning and extinction (McKernan and Shinnick-Gallagher, 1997; Ono et al., 1995; Paré and Collins 2000; Quirk et al. 1995, 1997; Repa et al., 2001). Further, computational models have long been used to understand emotional learning and memory, and to explain a wide range of behavioral responses (e.g., Grossberg and Schmajuk, 1987). Armony et al. (1995) developed an anatomically constrained neural network

(connectionist) model of fear conditioning based on single-unit recording data. Focusing on areas of convergence of CS and US pathways, tone inputs with a specific frequency (CS) were associated with a mild foot-shock (US). Using simplified computational units, a neural network model of the thalamo-cortico-amygdala circuitry was constructed and trained using a modified Hebbian-type learning rule (Armony et al., 1995). The model was able to reproduce data related to frequency-specific changes of the receptive fields known to exist in the auditory thalamus and amygdala, but extinction and other related phenomena were not simulated. Balkenius and Morén (2001) proposed a neural network model for emotional conditioning. The model focused on the amygdala and the orbitofrontal cortex and their interaction; the amygdala was the locus of acquisition and the orbitofrontal cortex was the site for extinction learning. The model simulated basic phenomena related to emotional conditioning including acquisition, extinction, blocking, and habituation. The main drawback of such connectionist models is that the elementary units for cells are not biophysically realistic, and therefore cannot model the underlying neural processes responsible for learning. What is needed is a model that incorporates recent advances in cellular neurophysiology and synaptic plasticity.

Most recently, a spiking neuron network model (Vlachos et al., 2009) was able to replicate three key experimental findings: (i) Emergence of fear cells during fear conditioning in one context; (ii) Emergence of extinction cells during extinction training in a different context; (iii) Post extinction activation of the same fear cells in the original conditioning context. Contrary to experimental findings (Herry et al., 2008) that reported a distinct functional connectivity of fear and extinction cells to hippocampus and pre-frontal cortex, which suggested a rigid organization of those cells this model showed that

fear and extinction cells can emerge dynamically as a result of the identical learning mechanism being applied to the population as a whole.

To address that BA can encode both fear acquisition and extinction memories we employed a computational modeling approach, incorporating known biophysical and connectivity properties of basal amygdala neurons, to predict learning-induced changes in the responses of single-units to conditioned stimuli. The goal of the computational model was further employed to understand how connectivities and their properties affect the formation of different types of cells in the BA post fear conditioning. The overall goal is to bridge biophysical and network modeling approaches in order to gain insight into how the amygdala solves the “problem” of extinction, and ultimately how it interacts with other structures to regulate fear expression.

Starting with experimentally validated biophysical single cell models, we developed a BA network consisting of twelve pyramidal cells and two GABAergic interneurons, the details of which are discussed next. Hebbian-type plasticity was implemented in the AMPA (alpha-amino-3-hydroxy-5-methyl-4-isoxazolepropionic acid) and the GABA_A receptor synapses involved in fear learning. Using this model, we showed the effect of various connectivity's, synaptic weights and cells on learning both conditioning and extinction.

4.3. METHODS

4.3.1. Single cell models

Compartmental models of three types of pyramidal cells were used to develop Basal amygdala (BA) structure. The BA cells were modeled with two compartments representing apical dendrite and soma akin to Guoshi et al. (2009) as shown in Figure 1.

The choice of compartments required were based on how similar the models could reproduce the somatic voltage recordings seen experimentally. All conductance based equations used are in Hodgkin-Huxley type formulation (Byrnes and Roberts, 2004) as shown in Eqn. 4.1,

$$C_m dV_x/dt = -g_L(V_x - E_L) - g_d(V_x - V_d) - \sum I_x^{\text{int}} - \sum I_x^{\text{syn}} + \sum I_x^c + I_x \quad (4.1)$$

where V_x is the somatic/dendritic membrane potential (mV), I_x^{int} and I_x^{syn} are the intrinsic currents and the synaptic currents in the soma/dendritic compartments, I_x is the electrode current applied to the soma /dendrite, C_m is the membrane capacitance and g_c is the coupling conductance between the soma and the dendrite ($C_m = 1.0 \mu\text{F}/\text{cm}^2$ for all cells).

The ionic channel currents I_x^{syn} , were modeled as,

$$I_x^c = g_c m^p h^q (V - E_i), \quad (4.2)$$

where, g_c was its maximal conductance, m its activation variable (with exponent p), h its inactivation variable (with exponent q), and E_i its reversal potential. The kinetic equation for each of the gating variables x (m or h) takes the form

$$\frac{dx}{dt} = \frac{x_\infty(V, [\text{Ca}^{2+}]_i) - x}{\tau_x(V, [\text{Ca}^{2+}]_i)} \quad (4.3)$$

where, x_∞ is the steady state gating voltage- and/or Ca^{2+} - dependent gating variable and τ_x is the voltage- and/or Ca^{2+} - dependent time constant. The maximal conductance densities for all ionic currents and the expressions of x_∞ and τ_x for each gating variable are listed in Tables 1.

BA Model. As cited, recent studies (Herry et al., 2008) have confirmed that there are three types of nuclei in the BA, namely, fear cells, extinction resistant and extinction cells. Pyramidal cells in the BA exhibit a range of firing properties in response to

prolonged current injection, ranging from full frequency adaptation to firing repetitively (Faber et al., 2001). To represent different firing patterns, two different types of BA pyramidal cells were developed: type A with full adaptation and type B with medium adaptation (see Li et al., 2009 for details), which are major cell types in basolateral amygdala. BA also contains local GABAergic interneurons (Li et al., 2009) which were modeled as fast spiking aspiny cells.

Calcium Dynamics. Intracellular calcium was regulated by a simple first-order differential equation of the form (Warman et al., 1994):

$$\frac{d[Ca^{2+}]_i}{dt} = -f \frac{I_{Ca}}{(V)(F)(A)} + \frac{[Ca^{2+}]_{rest} - [Ca^{2+}]_i}{\tau_{Ca}} \quad (4.4)$$

where f is the fraction of the Ca^{2+} influx ($f = 0.024$), $V = wA$ with w being the shell thickness ($1\mu\text{m}$) and A is the cell surface area, F is the Faraday constant, τ_{Ca} is the Ca^{2+} removal rate. The resting Ca^{2+} concentration is $[Ca^{2+}]_{rest} = 50$ nmol/l, which is the same as the initial concentration (Durstewitz et al., 2000). The unit of the Ca^{2+} concentration is $\mu\text{m/l}$.

4.3.2. Synaptic currents and Hebbian learning

In the network, excitatory transmission was mediated by AMPA/NMDA neurotransmitters, while the inhibitory input was mediated by GABA_A receptors. The AMPA/NMDA and GABA_A synaptic currents were modeled by dual exponential functions (Durstewitz et al., 2000):

$$I_{AMPA} = \bar{A}w(t)g_{AMPA,max} \frac{\tau_1\tau_2}{\tau_2 - \tau_1} [\exp(-t/\tau_2) - \exp(-t/\tau_1)](V - E_{AMPA}) \quad (4.5)$$

$$I_{NMDA} = \bar{A}wg_{NMDA,max}s(V) \frac{\tau_1\tau_2}{\tau_2 - \tau_1} [\exp(-t/\tau_2) - \exp(-t/\tau_1)](V - E_{NMDA}) \quad (4.6)$$

$$I_{GABAA} = \bar{A}wg_{GABAA,max} \frac{\tau_1\tau_2}{\tau_2 - \tau_1} [\exp(-t/\tau_2) - \exp(-t/\tau_1)](V - E_{GABAA}) \quad (4.7)$$

where $w(t)$ is the adjustable synaptic weight for certain AMPA synapses (see below; w was held fixed for all NMDA synapses); \bar{A} is a normalization constant chosen so $g_{AMPA,max}$, $g_{NMDA,max}$ and $g_{GABAA,max}$ assume maximum values of the conductance's; τ_1 and τ_2 are the rise and decay time constants respectively. For AMPA receptor channels, $\tau_1 = 0.55$ ms and $\tau_2 = 2.2$ ms; for NMDA receptor channels, $\tau_1 = 10.7$ ms and $\tau_2 = 125.0$ ms, and for GABA_A receptors, $\tau_1 = 0.25$ ms and $\tau_2 = 3.75$ ms. The voltage-dependent variable $s(V)$ which implements the Mg²⁺ block was defined as: $s(V) = [1 + 0.33 \exp(-0.06 V)]^{-1}$ (Zador et al., 1990). The maximal conductances were chosen as: $g_{AMPA,max} = 1$ nS, $g_{NMDA,max} = 0.5$ nS and $g_{GABAA,max} = 0.6$ nS. Synaptic reversal potentials were set as $E_{AMPA} = E_{NMDA} = 0$ mV and $E_{GABAA} = -75$ mV (Durstewitz et al., 2000).

4.3.3. Hebbian Learning Rule

A biophysical Hebbian rule termed ‘calcium control hypothesis’ was used (Gerstner and Kistler 2002; Shouval et al., 2002a; 2002b) to implement learning by adjusting the synaptic weight w_j in Eqn. 4.8 as,

$$\Delta w_j = \eta([Ca]_j)\Delta t(\lambda_1\Omega([Ca]_j) - \lambda_2 w_j) \quad (4.8)$$

where η is the Ca²⁺-dependent learning rate and Ω is a Ca²⁺-dependent function with two thresholds (θ_d and θ_p ; $\theta_d \leq \theta_p$); λ_1 and λ_2 represent scaling and decay factors respectively; the local calcium level at synapse j is denoted by $[Ca]_j$ and Δt is the simulation time step.

With this learning rule, the synaptic weight decreases when $\theta_d < [Ca]_j < \theta_p$, and increases (with modulation by the decay term $\lambda_2 w_j$) when $[Ca]_j > \theta_p$. One of the key assumptions of this learning rule is that the dominant source of calcium influx in the postsynaptic cell is through NMDA receptors. This calcium influx was calculated as based on Shouval et al. (2002b)

$$I_{Ca}^N = P_0 w^{-1} G_{NMDA} (V - E_{Ca}) \quad (4.9)$$

where G_{NMDA} is the NMDA conductance in equation (the term w^{-1} ensures that it is calculated per synapse). The concentration of the calcium pool at synapse j followed the same dynamics as in Eqn. 4.8, with $f_j = 0.024$ (Warman et al. 1994), $\tau_j = 50$ ms (Shouval et al. 2002b), V is the volume of a spine head with a diameter of 2 μm (Kitajima and Hara 1997). The initial synaptic weights with learning parameters are shown in Table 2.

4.3.4. Network Architecture

The basal amygdala contained consisted of three clusters of pyramidal cells, namely, fear cells (F), extinction cells (E), and extinction-resistant (ER) cells; and two local interneurons. The F, ER and E clusters each had three pyramidal cells each: one type A, one type B and one type C. Fear and extinction cells inhibited each other via local interneuron; Fear cells and ER cells also inhibited each other via local interneuron (as suggested by Herry et al., 2008). Also, Pyramidal cells in each cluster excited each other. Also, fear cells received excitatory input from LA while Extinction cells receive tone but not shock input and the ER cells receive both tone/shock inputs. Synaptic plasticity was implemented in all excitatory and inhibitory synapses.

A total of 12 cells with 9 pyramidal and 3 GABergic interneurons were modeled in the BA network (figure 2A). As cited, the BA network has three groups of neurons, each

consisting of three pyramidal cells and one interneuron.

4.3.5. Training protocol and afferent projections

The schedule of tone and shock inputs in the simulation was based on *in vivo* studies (Burgos-Robles et al., 2009). We scaled down the timing of the auditory fear conditioning protocol by approximately three orders of magnitude, so that it would be suitable for computational study. The simulation included sensitization, conditioning, and extinction phases (fig. 2B). Each tone lasted 10 s and each shock lasted 200 ms, and the interval between two tones was 30 s. During the habituation phase, 5 tones were presented to the network. Following habituation, 5 paired tones and shocks were provided in the conditioning phase, with shock present during the last 100 ms of the tone. In extinction, 20 tones were delivered to the neurons without any shock (pure tones). The gap between conditioning and extinction phases was 200 s. Simulations were performed on a personal computer using the software package NEURON with the implicit Euler method integration method, and a time step of 20 μ s.

LA neuron responses during the fear training were created offline by using previously developed LA network model (Li et al., 2009) using the protocol as cited. The BA cells received conditioning information from LA as shown in Figure 2A. Independent, Poisson-distributed, random excitatory background inputs were delivered to all the cells in the network to achieve reported spontaneous firing rates. The specific tone/shock synaptic inputs were represented by regular spike trains delivered to the AMPA/NMDA channels. The output of the BA circuit was measured from the various types of pyramidal cells and set to match the output observed experimentally (Figure 3, Herry et al., 2006).

4.4. RESULTS

4.4.1. Firing properties of single neurons

The single cell BA modeled using NEURON reproduced the basic spiking behavior of intrinsic bursting prefrontal neurons (Durstewitz et al., 2000) as shown in Figure 4. Voltage responses of the three types of BA pyramidal cell (Type A and B) models in response to three different levels of current injections are shown in Figure 5 (Faber et al. 2001). With 600 ms, 400 pA depolarizing current step, cell A fired only three spikes, cell B fired 9 spikes before it adapted. A slow depolarizing sag was observed in response to a hyperpolarizing current injection (Figure 5), a phenomenon termed “anomalous rectification” due to the activation of the I_H current (Womble and Moises, 1993). The BA interneuron model showed no frequency adaptation and fired at relatively high frequency in response to depolarizing current steps (Figure 5), consistent with experimental observations (Mahanty and Sah, 1998; Washburn and Moises, 1992b).

4.4.2. Activity of the BA model

Due to conditioned Lateral Amygdala input and a potentiated LA-BAf connection, BA fear cells should show conditioned responses, which should extinguish as LA input extinguishes. ER cells should get conditioned since they received direct shock input; the conditioned responses should not extinguish because of persistent potentiation of the cortical tone input (from Te3). This is due to the already potentiated pyramidal-pyramidal synapses in that cell cluster and the relatively constant inhibition from the interneuron. The inhibition should not increase much during extinction since the interneurons do not receive direct tone or shock inputs. Since the extinction cells (E) do not receive direct shock inputs, their responses should not be potentiated by conditioning 126

After the first extinction, the bursting inputs from IL should potentiate the pyramidal-to-pyramidal connection of extinction cells. The tone synapses of extinction cells should also be potentiated as the random activity present at tone synapses coincides with bursting in IL. As a result, the tone response of extinction cells should increase after the long gap. Since both the tone-pyramidal and pyramidal-pyramidal synapses of extinction cells are strengthened by the IL input during the long gap and the IL input was robust during re-extinction, both synaptic strengths should continue to potentiate in re-extinction, resulting in a progressive increase of the tone response of extinction neurons. These are expected results from the framework implemented in the software NEURON.

4.4.3. Model Characteristics

The model assumed that IL has a strong projection to BAe during the long gap (weight of 40 assuming a single synapse (Table 3), i.e., if we assume multiple synapses, this number weight reduced proportionately). This means that it could cause several synapses connected within the three extinction (E) cell cluster to potentiate. These include the pyramidal-pyramidal synapses between the three cells within the E cluster, the tone- pyramidal synapses, the pyramidal-interneuron synapses, and the interneuron-pyramidal synapses.

In Figure 5, we show preliminary results from the network model. These include change in pyramidal cell synaptic weights to tone and tone/shock inputs. The network model development is part of future research, with the expected characteristics detailed above.

4.5. DISCUSSION

We describe a biophysical network model of the basal amygdala (BA) network to

study how distinct populations of cells might form in the BA after an auditory fear conditioning protocol that includes sensitization, conditioning, extinction and extinction recall. Our network represents a first attempt to incorporate cellular neurophysiology and synaptic plasticity mechanisms into a biophysical model to investigate the underlying mechanisms in the BA. The model provides a plausible mechanism as to how different connectivity's might result in the formation of the three distinct groups of fear, extinction, and extinction-resistant neurons.

4.5.1. Limitations

Some of the limitations of the study are as follows: (i) The model parameters in table 1 were selected to match experimental data as closely as possible. Improved understanding of connectivity and learning mechanisms within the BA will help refine these estimates; (ii) The model did not consider possible afferents from the hippocampus (Corcoran and Maren 2004) that might be involved in the process; (iii) The model did not consider any inputs from mPFC as cited in Herry et al.(2008).

4.6. CONCLUSIONS

In conclusion, we have provided a framework with different connectivities in realistic BA neurons, incorporating known conductances, and synaptic plasticity mechanisms, that can lead to the formation of distinct groups of cells. The biophysical realism of the model allows us to study the underlying mechanisms that cause such cells to emerge. Various expected results from the network model are listed above. The ultimate goal of this computational study is to model pathologies associated with the fear circuit (e.g., post traumatic stress disorder) and assist in the development of new treatments.

ACKNOWLEDGEMENT

This work was supported in part by National Institutes of Health grants 1R01MH087755-01 (SN) and MH-058883 (GJQ).

4.7. REFERENCES

1. Bower JM, Beeman D (2003). The Book of GENESIS: Exploring Realistic Neural Models with the GEneral NEural SIMulation System, Internet Edition (<http://www.genesis-sim.org/GENESIS>).
2. Burgos-Robles A, Vidal-Gonzalez I, Quirk GJ (2009). Sustained conditioned responses in prelimbic prefrontal neurons are correlated with fear expression and extinction failure. *J Neurosci.* 29: 8474–8482.
3. Byrne JH, Roberts JL. (2004). From Molecules to Networks – An introduction to cellular and molecular neuroscience. Elsevier Academic Press.
4. Degenetais E, Thierry AM, Glowinski J, Gioanni Y (2002). Electrophysiological properties of pyramidal neurons in the rat prefrontal cortex: an in vivo intracellular recording study. *Cereb Cortex* 12: 1–16.
5. Durstewitz D, Seamans JK, Sejnowski TJ. (2000). Dopamine-mediated stabilization of delay-period activity in a network model of prefrontal cortex. *J Neurophysiol* 83: 1733-1750.
6. Faber ESL, Callister RJ, Sah P. (2001) Morphological and electrophysiological properties of principal neurons in the rat lateral amygdala in vitro. *J Neurophysiol* 85: 714-723.
7. Floresco SB, Tse MT (2007) Dopaminergic regulation of inhibitory and excitatory transmission in the basolateral amygdala-prefrontal cortical pathway. *J Neurosci* 27:2045–2057.
8. Gabbott PL, Warner TA, Busby SJ (2006) Amygdala input monosynaptically innervates parvalbumin immunoreactive local circuit neurons in rat medial prefrontal cortex. *Neuroscience* 139:1039 –1048.
9. Geisler, S., Derst, C., Veh, R.W., Zahm, D.S., (2007). Glutamatergic afferents of the ventral tegmental area in the rat. *J Neurosci.*, 27:5730–43.
10. Gerstner W, Kistler W. (2002). Spiking neuron models: Single neurons, populations, plasticity. Cambridge University Press.
11. Guarraci, F. A. & Kapp, B. S. (1999). An electrophysiological characterization of ventral tegmental area dopaminergic neurons during differential Pavlovian fear conditioning in the awake rabbit. *Behavioral Brain Research*, 99: 169-179.
12. Herry C, Ciocchi S, Senn V, Demmou L, Muller C, Luthi A (2008) Switching on and off fear by distinct neuronal circuits. *Nature.*, 454: 600-606.

13. Vlachos I, Kumar A, Luthi A, Aertsen Ad (2009) Dynamical emergence of fear and extinction cells in the amygdala—a computational model. *BMC Neuroscience*.
14. Hugues S, Garcia R, Le'na I (2007) Time course of extracellular catecholamine and glutamate levels in the rat medial prefrontal cortex during and after extinction of conditioned fear. *Synapse* 61:933–937.
15. Jones, B.F., Groenewegen, H.J., Witter, M.P. (2005). Intrinsic connections of the cingulate cortex in the rat suggest the existence of multiple functionally segregated networks. *Neuroscience*, 133:193–207.
16. Kitajima T, Hara K. (1997). An integrated model for activity-dependent synaptic modifications. *Neural Networks* 10: 413-421.
17. Li, G, Nair, S. S., Quirk G. J., (2009). A biologically realistic network model of acquisition and extinction of conditioned fear associations in lateral amygdala neurons. *J Neurophysiol* 101: 1629–1646.
18. Likhtik E, Pelletier JG, Popescu AT, Paré D. (2006). Prefrontal control of the amygdala. *J Neurosci*. 25: 7429-7437.
19. Mahanty NK, Sah P. (1998). Calcium-permeable AMPA receptors mediate long-term potentiation in interneurons in the amygdala. *Nature* 394: 683-687.
20. Orozco-Cabal, L., Pollandt S., Liu J., Vergara L., Shinnick-Gallagher P., Gallagher J.P. (2006) A novel rat medial prefrontal cortical slice preparation to investigate synaptic transmission from amygdala to layer V prelimbic pyramidal neurons. *J Neurosci Methods* 151:148 –158.
21. Rodriguez-Romaguera J, Sotres-Bayon F, Mueller D, Quirk GJ (2009) Systemic propranolol acts centrally to reduce conditioned fear in rats without impairing extinction. *Biol Psychiatry* 65:887– 892.
22. Shouval HZ, Castellani GC, Blais BS, Yeung LC, Cooper LN. (2002a) Converging evidence for a simplified biophysical model of synaptic plasticity. *Biol Cybern* 87: 383-391.
23. Shouval HZ, Bear MF, Cooper LN. (2002b). A unified model of NMDA receptor-dependent bidirectional synaptic plasticity. *Proc Natl Aca Sci* 99: 10831-10836.
24. Sotres-Bayon, F., Sierra-Mercado, D., Quirk, G.J.(2009) Amygdala input to medial prefrontal cortex is necessary for excitatory drive and conditioned tone responses, but not bursting. *Society for Neuroscience abstract* 880.8.
25. Vertes RP (2004) Differential projections of the infralimbic and prelimbic cortex in the rat. *Synapse* 51:32–58.
26. Washburn MS, Moises HC. (1992). Electrophysiological and morphological properties of rat basolateral amygdaloid neurons in vitro. *J Neurosci* 12: 4066-4079.
27. Womble MD, Moises HC. (1993). Hyperpolarization-activated currents in neurons of the rat basolateral amygdala. *J Neurophysiol* 70: 2056-20605.

4.8. TABLES

Table 1. (a) Gating variables for ion channels used in the network model

Current Type	Gating Variable	α	β	x_∞	τ_x (ms)
I_{Na}	$p=3$	$\frac{-0.2816(V+25)}{\exp(-(V+25)/9.3)-1}$	$\frac{0.2464(V-2)}{\exp((V-2)/6)-1}$	$\alpha/(\alpha+\beta)$	$1/(\alpha+\beta)$
	$q=1$	$0.098 \times \exp(-(V+40.1)/10)$	$\frac{1.4}{\exp(-(V+10.1)/10)+1}$	$\alpha/(\alpha+\beta)$	$1/(\alpha+\beta)$
I_{DR}	$p=4$	$\frac{-0.036(V-13)}{\exp(-(V-13)/25)-1}$	$\frac{0.0108(V-23)}{\exp((V-23)/12)-1}$	$\alpha/(\alpha+\beta)$	$1/(\alpha+\beta)$
I_M	$p=2$	$\frac{0.016}{\exp(-(V+52.7)/23)}$	$\frac{0.016}{\exp((V+52.7)/18.8)}$	$\alpha/(\alpha+\beta)$	$1/(\alpha+\beta)$
I_H	$p=1$	—	—	$\frac{1}{\exp((V+89.2)/9.5)+1}$	$1727 \times \exp(0.019V)$
I_D	$p=1$	—	—	$\frac{1}{\exp(-(V+8.6)/11.1)+1}$	1.5
	$q=1$	—	—	$\frac{1}{\exp((V+21)/9)+1}$	569
I_{Ca}	$p=2$	—	—	$\frac{1}{\exp(-(V+24.6)/11.3)+1}$	$1.25 \times \text{sech}(-0.031(V+24.6))$
	$q=1$	—	—	$\frac{1}{\exp((V+12.6)/18.9)+1}$	420.0
I_C	$p=2$	$\frac{-0.0064V_m - 0.1152}{\exp(-(V_m+18)/12)-1}$ with $V_m = V + 40 \log_{10}([Ca]_{i1})$	$1.7 \times \exp(-(V_m+152)/30)$	$\alpha/(\alpha+\beta)$	$\max(1/(\alpha+\beta), 1.1)$
I_{sAHP}	$p=1$	$\frac{0.0048}{\exp(-5 \log_{10}([Ca]_{i2})+17)}$	$\frac{0.012}{\exp(2 \log_{10}([Ca]_{i2})+20)}$	$\alpha/(\alpha+\beta)$	48

(b) Gating variables for interneuron ion channels used in the network model

Current Type	Gating Variable	α	β	x_∞	τ_x
I_{Na}	$p=3$	$2.1 \times \exp((V+18.5)/11.57)$	$2.1 \times \exp(-(V+18.5)/27)$	$\alpha/(\alpha+\beta)$	$1/(\alpha+\beta)$
	$q=1$	$0.045 \times \exp(-(V+29)/33)$	$0.045 \times \exp((V+29)/12.2)$	$\alpha/(\alpha+\beta)$	$1/(\alpha+\beta)$
I_{DR}	$p=4$	$0.15 \times \exp((V+19)/10.67)$	$0.15 \times \exp(-(V+19)/42.68)$	$\alpha/(\alpha+\beta)$	$1/(\alpha+\beta)$

Table 2. Maximal conductance densities

		I_{Na}	I_{DR}	I_M	I_H	I_D	I_{Ca}	I_C	I_{sAHP}	τ_{Ca}
Pyramid A	Soma	120	12	0.30	–	–	0.1	–	–	–
	Dendrite	40	3	0.30	0.1	1.0	0.2	0.5	0.10	1000
Pyramid B	Soma	120	12	0.20	–	–	0.1	–	–	–
	Dendrite	40	3	0.20	0.1	0.4	0.2	0.5	0.15	500
Pyramid C	Soma	120	12	0.25	–	–	0.1	–	–	–
	Dendrite	40	3	0.25	0.1	0.1	0.2	0.5	0.50	120
Interneuron	Soma	35	8	–	–	–	–	–	–	–
	Dendrite	10	3	–	–	–	–	–	–	–

Table 3. Model parameters for network connections and inputs

Connection	Initial weight	f_{min}	f_{max}	Learning factors		Ca ²⁺ threshold (μmol)	
				scaling	decay	low	high
LA to F (Pyr)	5	0.8	3	7	0.01	0.45	0.55
IL to E (Pyr)	5 (40 during bursting)	–	–	–	–	–	–
Tone to E & ER (Pyr)	5	0.8	3	7	0.01	0.45	0.55
Shock to E & ER (Pyr)	40	–	–	–	–	–	–
Pyr to Pyr	5	0.8	3	7	0.01	0.45	0.55
Pyr to Inter	5	0.8	3	2	0.01	0.45	0.55
Inter to Pyr	5	0.8	3	2	0.01	0.45	0.55
Inter to Inter	2	–	–	–	–	–	–

Table 4. How to develop the Basal Amygdala model?

Experiment	Model Output
Single Cell	<p>Pyramidal Cell</p> <ul style="list-style-type: none"> • Develop two compartment models for the following types of pyramidal cells – Type A, Type B and Type C. • Connect the single soma and single dendrite using axial resistance, g_c. • The three types of pyramidal cells should be populated with I_{Na}, I_{DR}, I_M, I_{Ca}, I_D, I_H, I_{sAHP}, I_C and synaptic currents I_{AMPA}, I_{NMDA} and I_{GABA}. • The pyramidal cell soma should have Ca^{2+} pools such that I_{Ca} and synaptic current I_{GABA} affect it and the Ca^{2+} pool affected by I_{Ca} modulates synaptic weight of I_{GABA}. • The pyramidal cell dendrite should have Ca^{2+} pools such that the I_{Ca} affects the synaptic weights for I_C and I_{sAHP}. <p>Interneuron</p> <ul style="list-style-type: none"> • Develop two compartment models for interneuron. • Connect the single soma and single dendrite using axial resistance, g_c. • The interneuron should be populated with I_{Na}, I_{DR}, and synaptic currents I_{AMPA}, I_{NMDA} and I_{GABA}. • The pyramidal cell dendrite should have Ca^{2+} pools such that it is affected by synaptic current I_{NMDA} and modulates I_{AMPA}.
Single Network Model	<ul style="list-style-type: none"> • The single network model should be developed by connecting the pyramidal soma to the I_{AMPA} and I_{NMDA} of the interneuron dendrite. • An inhibitory connection is made from soma of interneuron to the synaptic current I_{GABA} present in soma of the pyramidal cell
Basal Amygdala Network Model	<ul style="list-style-type: none"> • As shown in Figure 2, three populations of nuclei present in the BA circuit are developed. • The Fear nuclei (F) consists of the one each of three types of pyramidal cells connected as mutually excitatory. • Each of the fear cells excites the two interneurons while receiving inhibitory input from them. • The Fear nuclei (F) receive input from Lateral Amygdala and provide output to the Central Nucleus (CE). • As cited, the interneurons receive excitatory input from fear cells while inhibiting the three types of pyramidal cells that make up the fear nuclei. This type of connectivity exists for Extinction and Extinction resistant cells. • Extinction resistant and Extinction nuclei both consist of the three types of pyramidal cells that are mutually exciting each other. The Extinction resistant nuclei receive excitatory input from tone and shock while Extinction nuclei receive excitatory input only from tone.

Table 5. Expected behavior of components in the BA model

Experiment	Model Output
<p>Only Current Injection (400pA, 300pA and -100pA for 600 ms)</p>	<p>Single Cell Output</p> <ul style="list-style-type: none"> • Voltage response of the pyramidal (BA_F, BA_{ER}, BA_E) and interneuron cells (BA_I) to injection current should match experimental output (Faber et al., 2000).
<p>Sensitization</p>	<p>Network Output</p> <ul style="list-style-type: none"> • Synaptic weights should grow for the LA-BA_F synaptic input. • No change in synaptic weights should be noticed for Tone-BA_{ER} and Tone-BA_E inputs. • Synaptic weights should grow for BA_F-BA_F and BA_{ER}-BA_{ER} but not BA_E-BA_E connections. • Synaptic weights should grow for BA_I-BA_I and BA_{ER}-BA_I connections with no change in weights for BA_E-BA_I connections. • Synaptic weights for BA_I-BA_F and BA_I-BA_{ER} connections should grow during sensitization, while, no change should be observed for BA_I-BA_E connection. • Tone response for BA_F, BA_{ER} and BA_E cells should match baseline experimental data as observed in Herry et al. (2008) as also shown in Figure 3.
<p>Conditioning</p>	<p>Network Output</p> <ul style="list-style-type: none"> • Synaptic weights should continue to grow for the LA-BA_F synaptic input. • Synaptic weights should grow for Tone-BA_{ER} inputs with no change for Tone-BA_E inputs. • Synaptic weights should continue to grow for BA_F-BA_F and BA_{ER}-BA_{ER} but not BA_E-BA_E connections. • Synaptic weights should decay for BA_F-BA_I, and BA_{ER}-BA_I with no change in weights for BA_E-BA_I connections. • Synaptic weights should stabilize for BA_I-BA_F and BA_I-BA_{ER} connections while no change should be observed for BA_I-BA_E cells • Tone response for BA_F and BA_{ER} cells should go up while no change is observed in BA_E cells
<p>Extinction</p>	<p>Network Output</p> <ul style="list-style-type: none"> • Synaptic weights should decrease for the LA-BA_F synaptic input. • Synaptic weights should grow for Tone-BA_{ER} connections with no change for Tone-BA_E connections. • Synaptic weights should gradually decay for the BA_F-BA_F connections and weights grow for BA_{ER}-BA_{ER} connections but not for the weights for BA_E-BA_E connections. • Synaptic weights should gradually decay for BA_F-BA_I connection, and BA_{ER}-BA_I connection with no change in weights for BA_E-BA_I connection. • BA_I-BA_F connection and BA_I-BA_{ER} should increase, while, no change should be observed for BA_I-BA_E connections. • Tone response for BA_F cell decreases, BA_E cell increases, while no change in observed in BA_{ER} cells

4.9. FIGURES

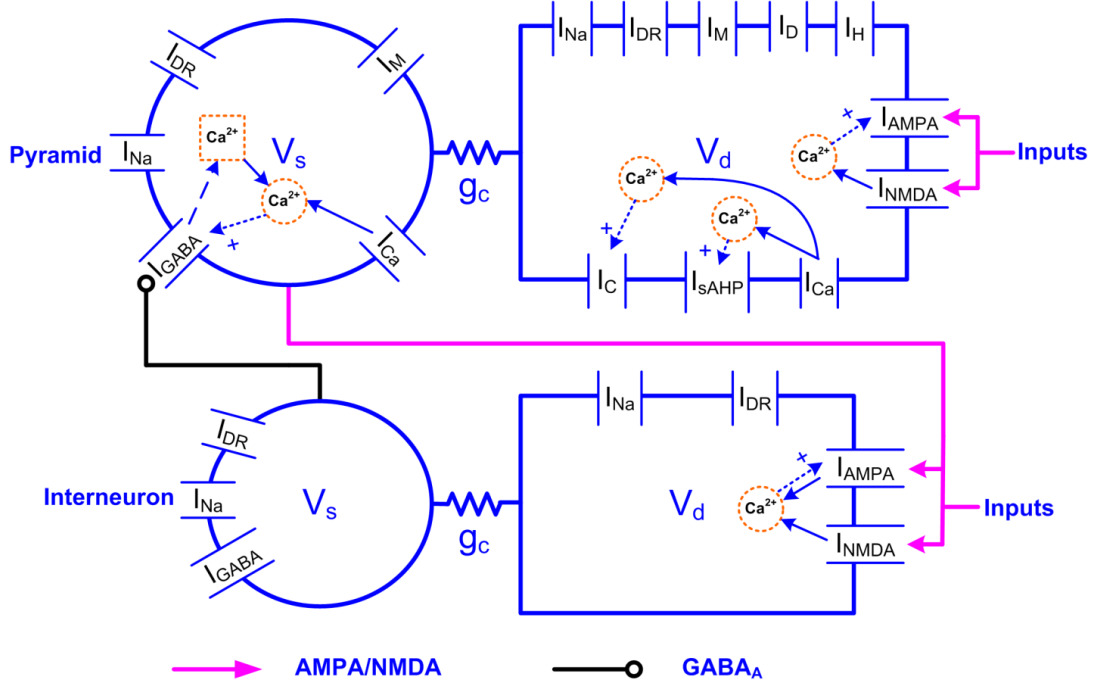


Figure 1. Two-compartment pyramidal cell and interneuron models with ionic and synaptic currents. For the pyramidal cell, two different Ca^{2+} pools mediated by voltage-dependent calcium channels (VDCCs) regulated I_C and I_{sAHP} currents in the dendrite. The plasticity at AMPA receptors was a function of NMDA Ca^{2+} , and plasticity at GABA_A synapses was a function of Ca^{2+} from two sources described in the text. For the interneuron, the Ca^{2+} underlying learning at the AMPA synapse came from both AMPA and NMDA receptors.

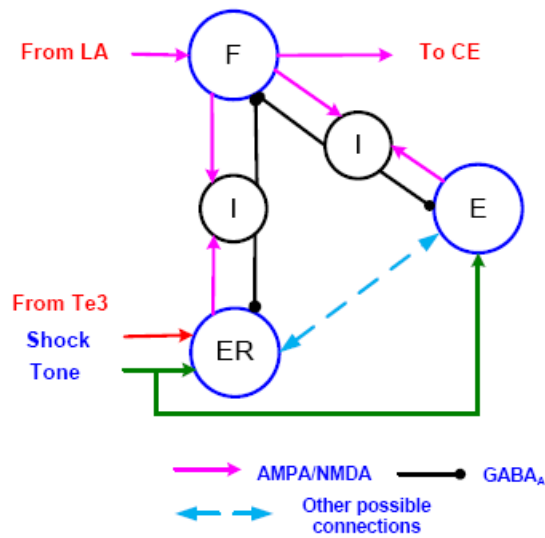


Figure 2. Schematic of BA network model. **A.** Each pyramidal cell cluster (Fear, Extinction, Extinction-resistant) has multiple cells that excite each other (not separately shown), and excite interneurons. Each interneuron is excited by all the pyramidal cells from the connected clusters.

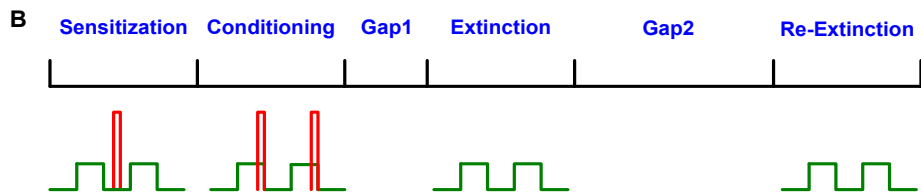


Figure 2B. Simulation schedule showing tone (green) and shock (red) inputs during sensitization, conditioning and the two extinction phases. Green lines show tone and red show shock inputs (see Methods). There was a short gap between conditioning and extinction, and a longer gap before re-extinction.

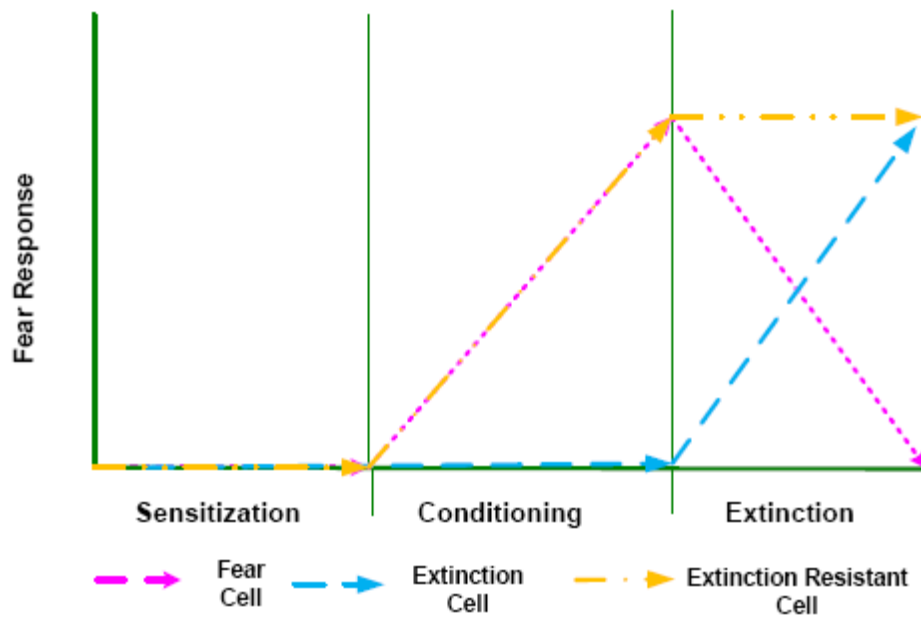
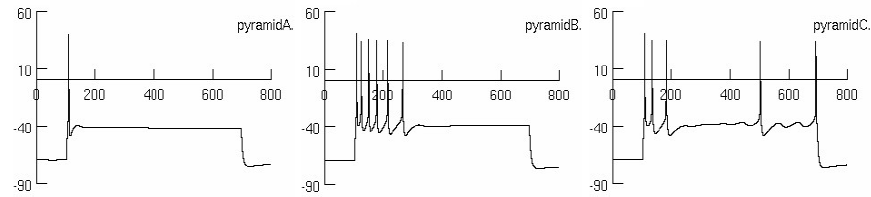


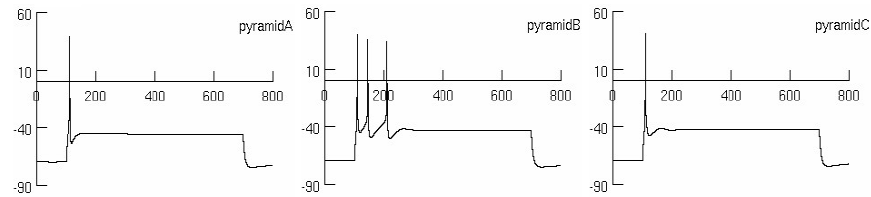
Figure 3. Responses of various cell types in the BA network as observed by Herry et al. (2008), and these are to be reproduced by the model network.

Pyramid Cells

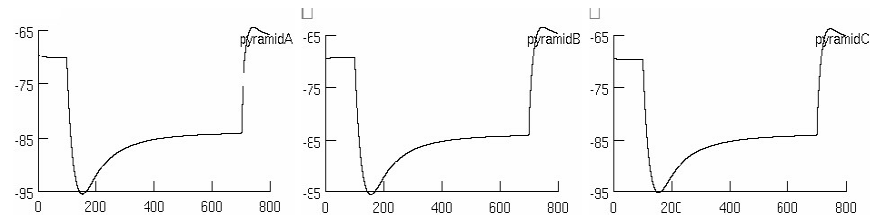
I = 400 nA



I = 300 nA



I = -100 nA



Interneuron

I = 400 nA

I = 300 nA

I = -100 nA

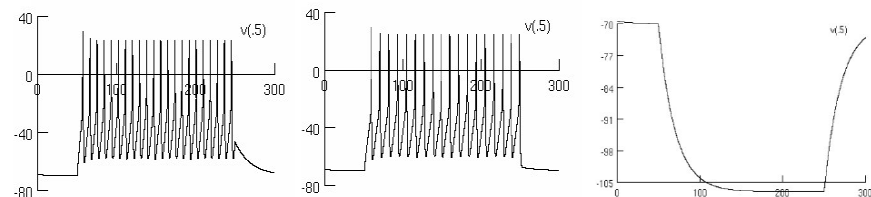


Figure 4. Responses of units to intracellular current pulses. **A:** voltage responses of the three types of LA pyramidal cell models (A, B and C) to three 600 ms current injections starting from 100 ms (top row: 400 pA; middle row: 300 pA; lower row: -100 pA). Compare to Fig. 2 of Faber et al. (2001) (reproduced as supplementary figure 1). **B:** voltage responses of the interneuron model to 200 ms current injections of the same magnitude (top row: 400 pA; middle row: 300 pA; lower row: -100 pA).

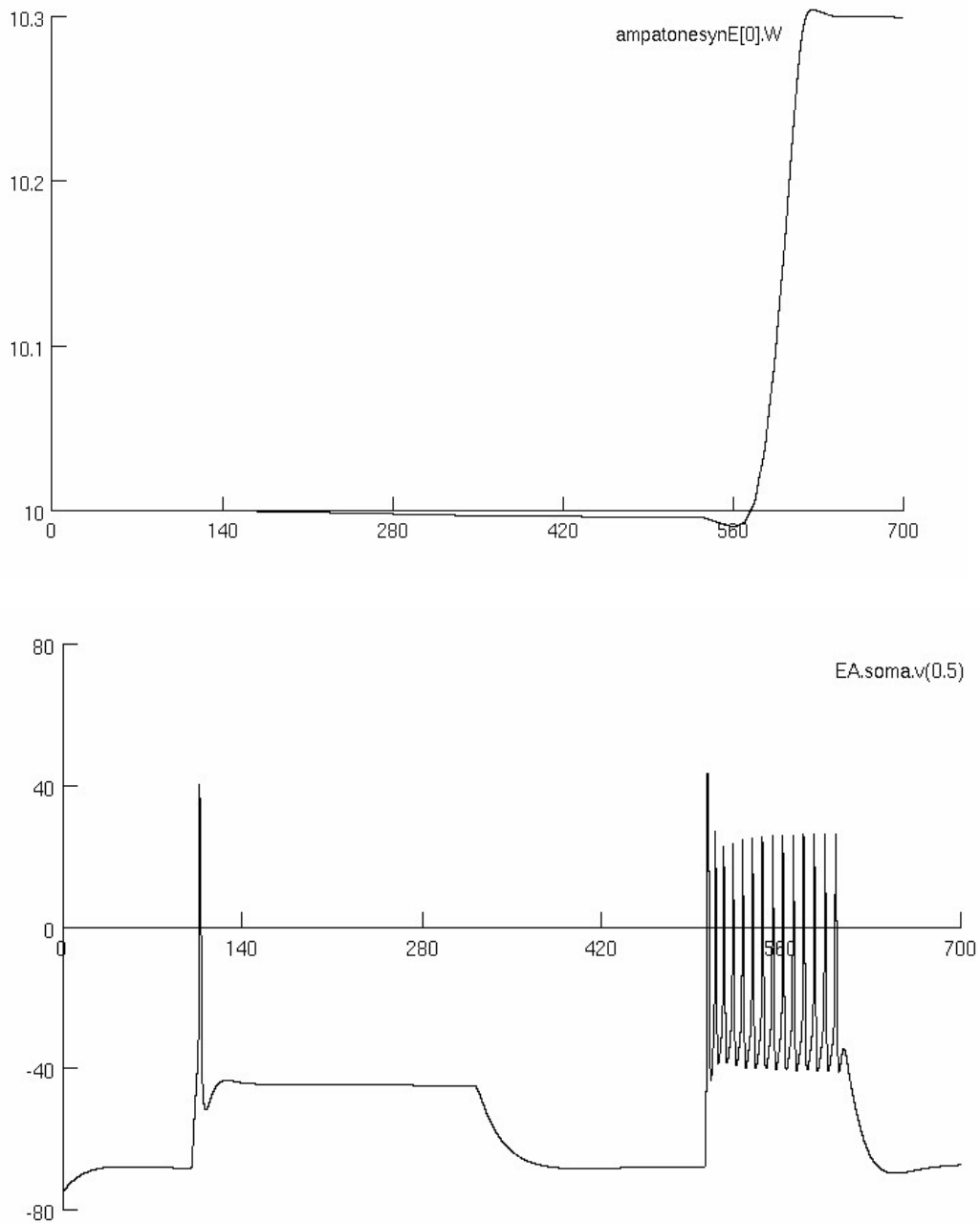


Figure 5A. Preliminary results of network model. Type A Pyramidal Cell during sensitization. Upper panel shows change in synaptic weight to tone input of 200 Hz. Bottom panel shows change in synaptic voltage to tone input of 200 Hz. For the sensitization, the tone starts from 100 ms, ends at 300 ms, the shock starts from 500 ms, ends at 600 ms.

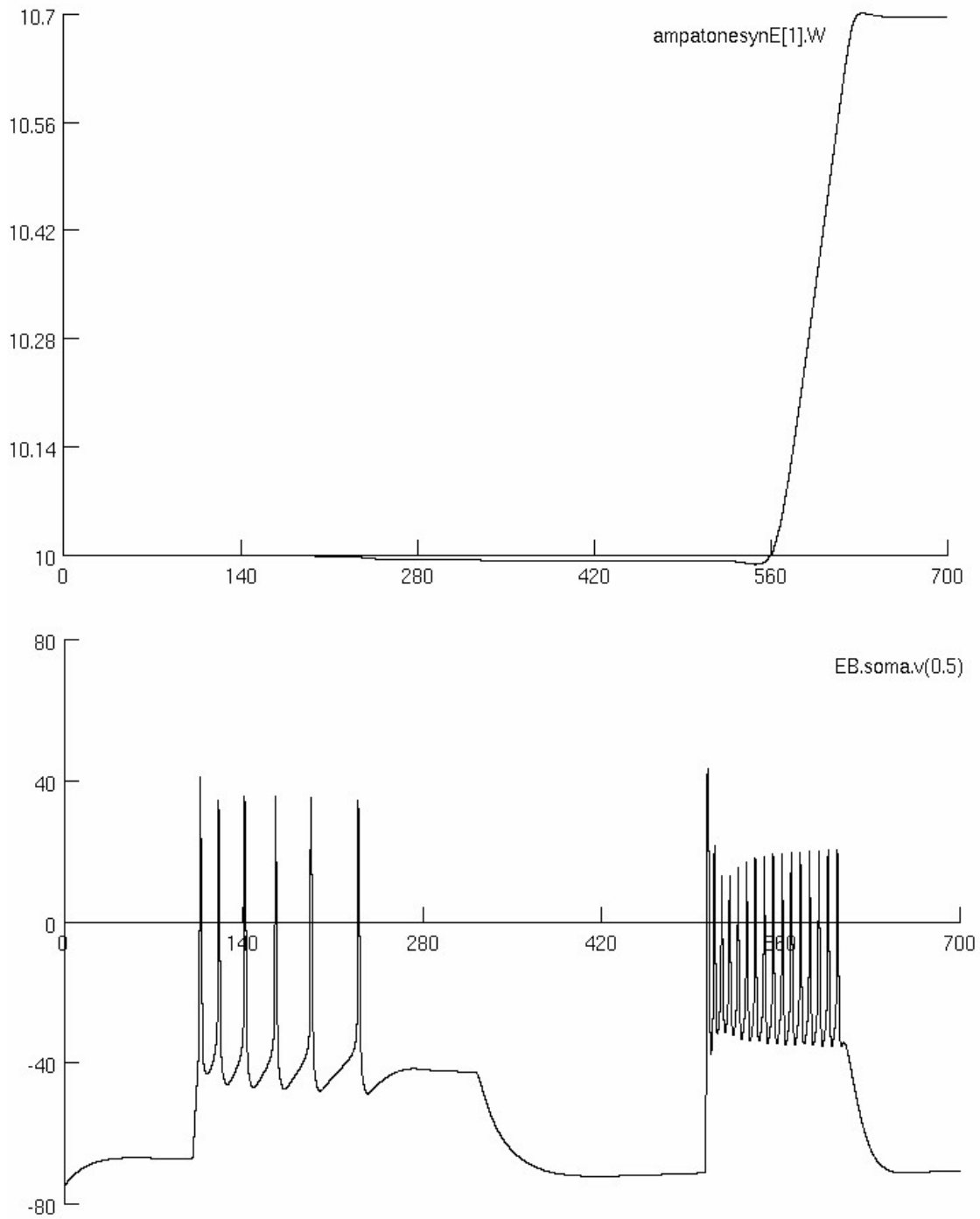


Figure 5B. Preliminary results from Type B Pyramidal Cell during sensitization. Upper panel shows change in synaptic weight to tone input of 200 Hz. Bottom panel shows change in synaptic voltage to tone input of 200 Hz.

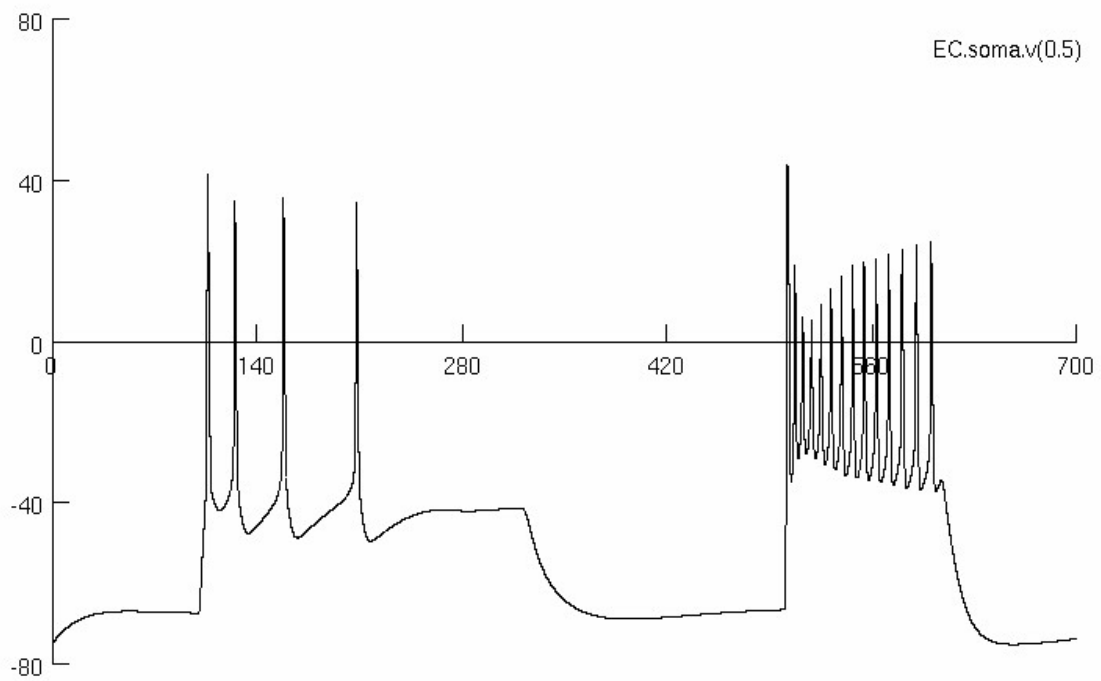
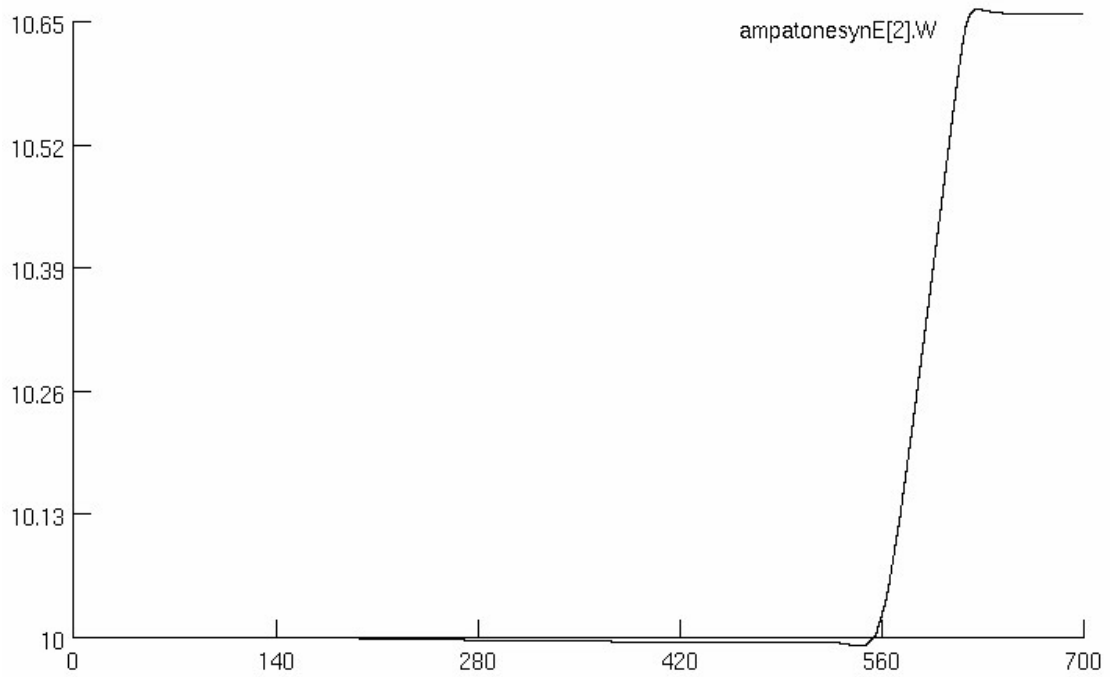


Figure 5C. Preliminary results for Type C Pyramidal Cell during sensitization. Upper panel shows change in synaptic weight to tone input of 200 Hz. Bottom panel shows change in synaptic voltage to tone input of 200 Hz.

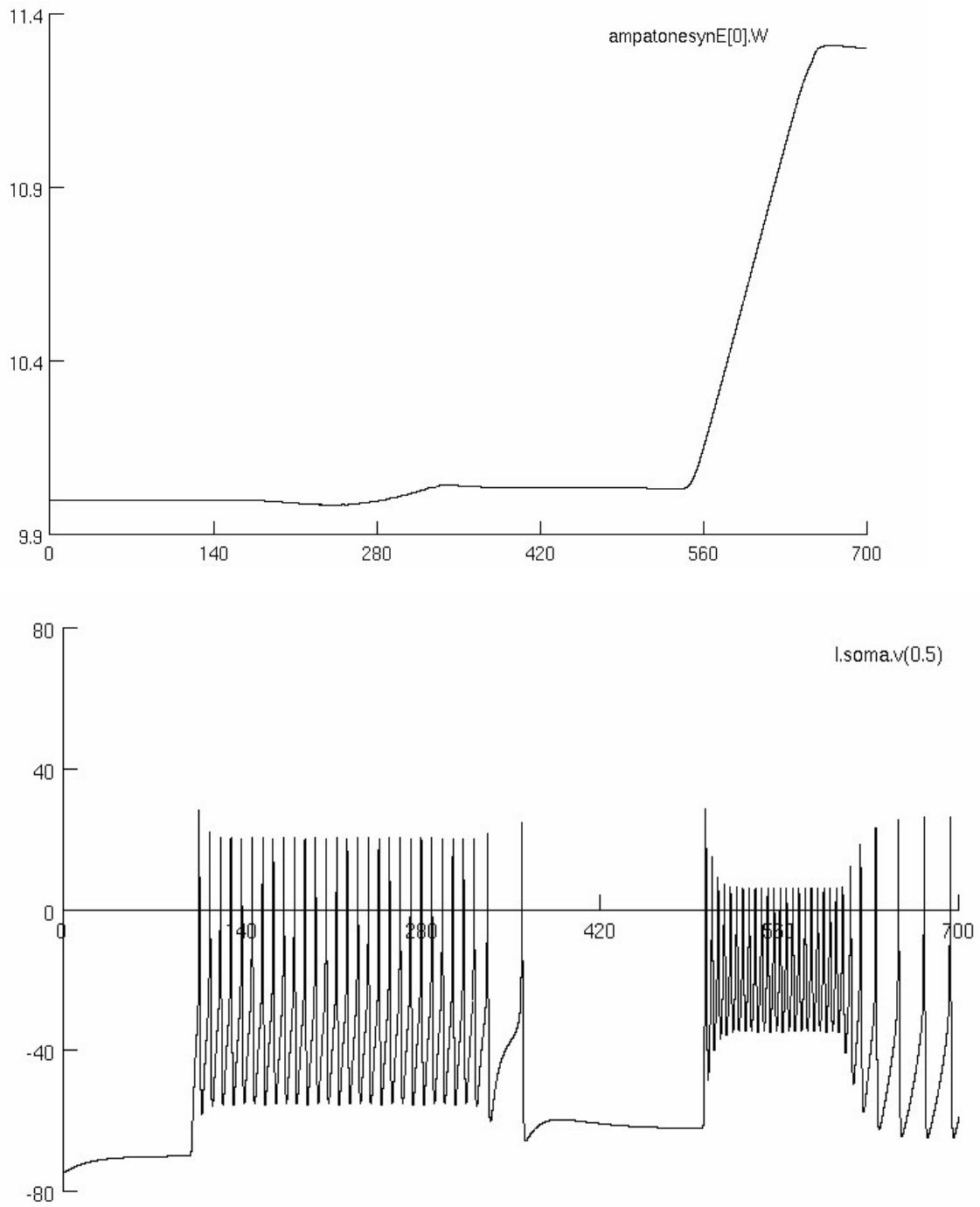


Figure 5D. Preliminary results for Interneuron during sensitization. Upper panel shows change in synaptic weight to tone input of 200 Hz. Bottom panel shows change in synaptic voltage to tone input of 200 Hz.

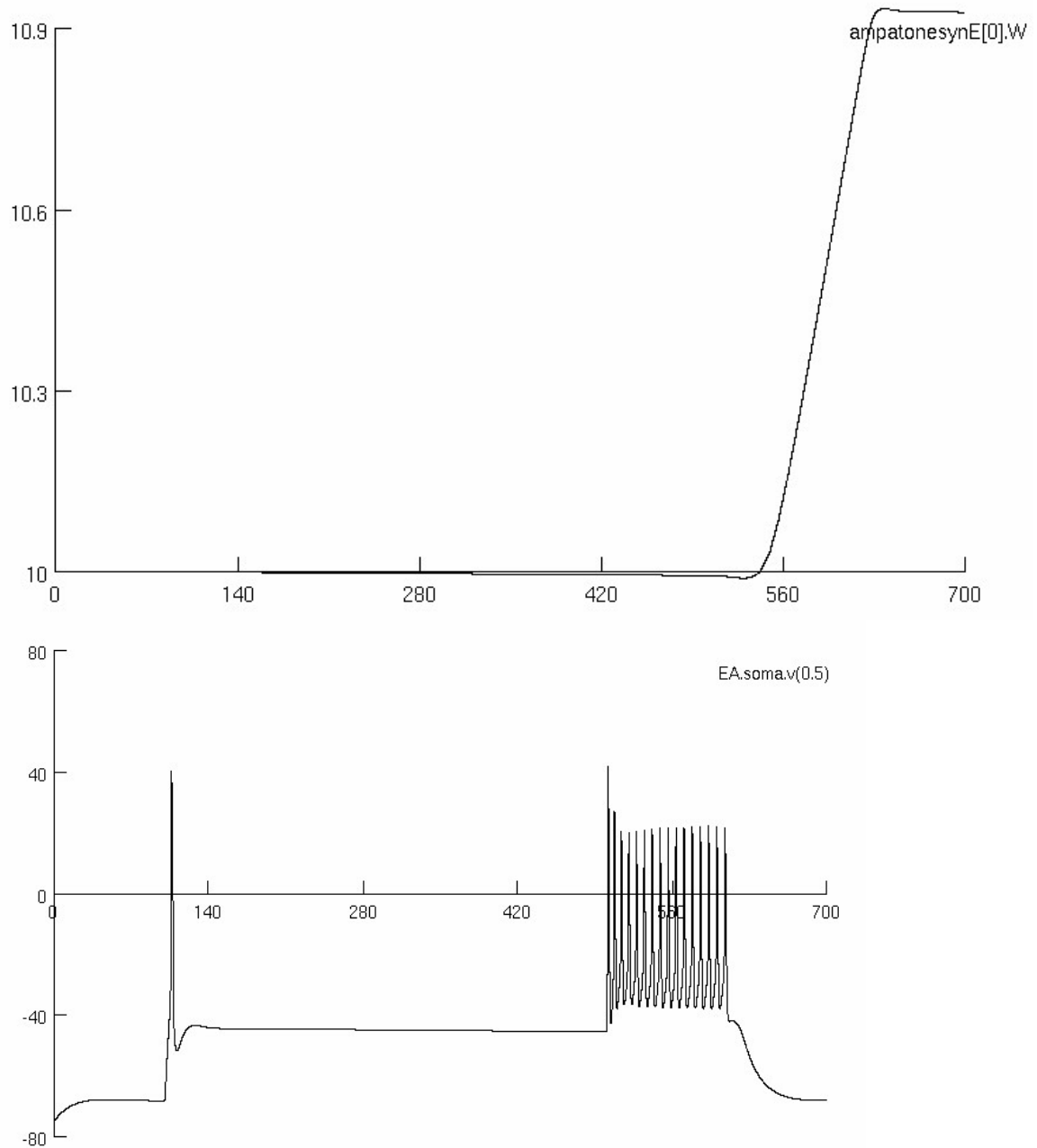


Figure 5E. Preliminary results for Type A Pyramidal Cell during conditioning. Upper panel shows change in synaptic weight to tone input of 200 Hz. Bottom panel shows change in synaptic voltage to tone input of 200 Hz. For the conditioning, the tone starts from 100 ms, ends at 600 ms, the shock starts from 500 ms, ends at 600 ms.

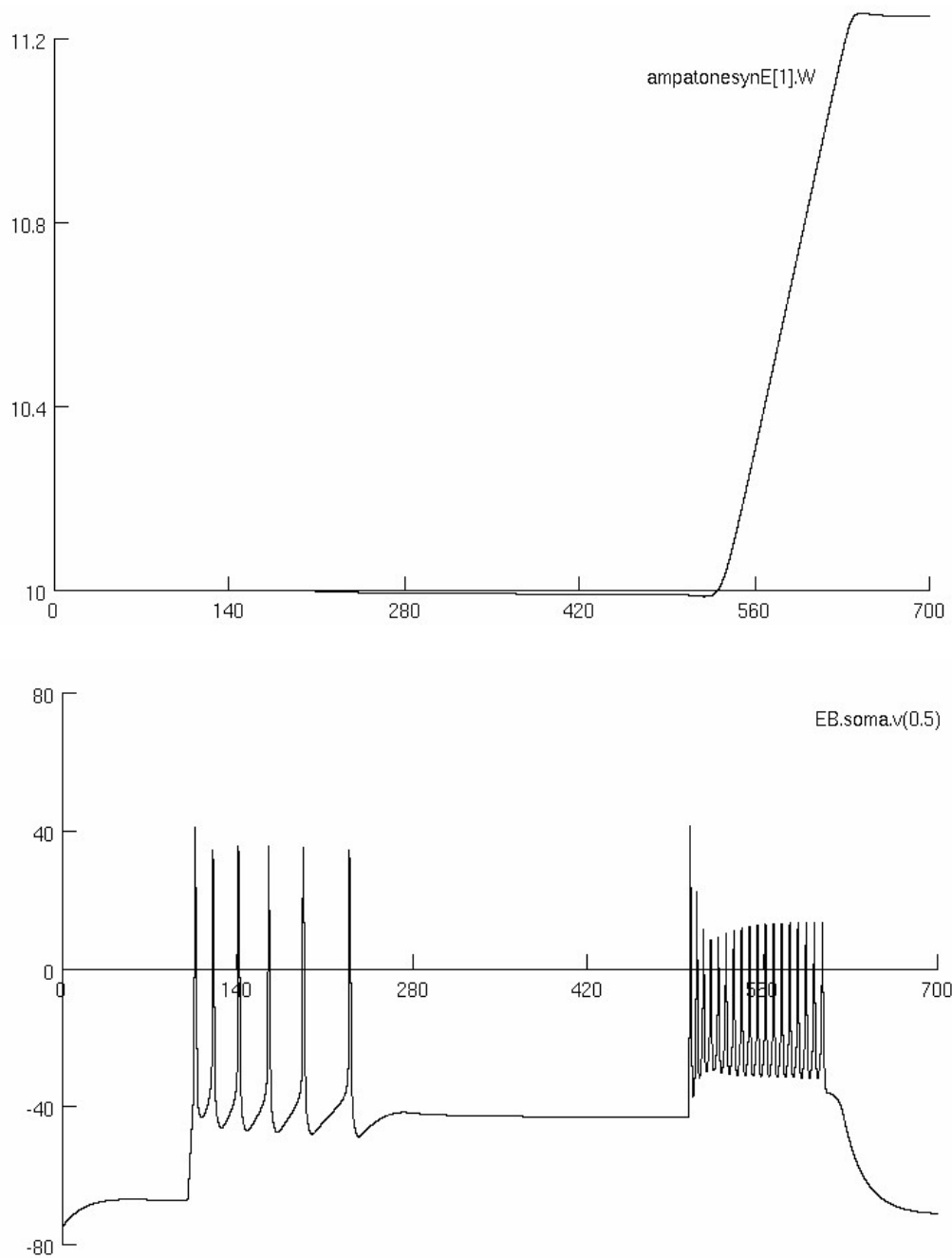


Figure 5F. Preliminary results for Type B Pyramidal Cell during conditioning. Upper panel shows change in synaptic weight to tone input of 200 Hz. Bottom panel shows change in synaptic voltage to tone input of 200 Hz.

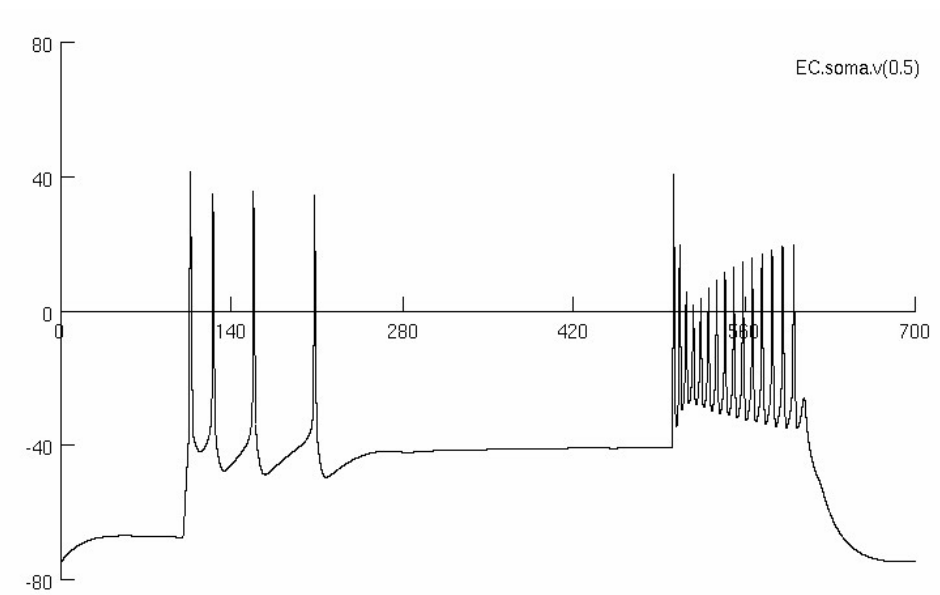
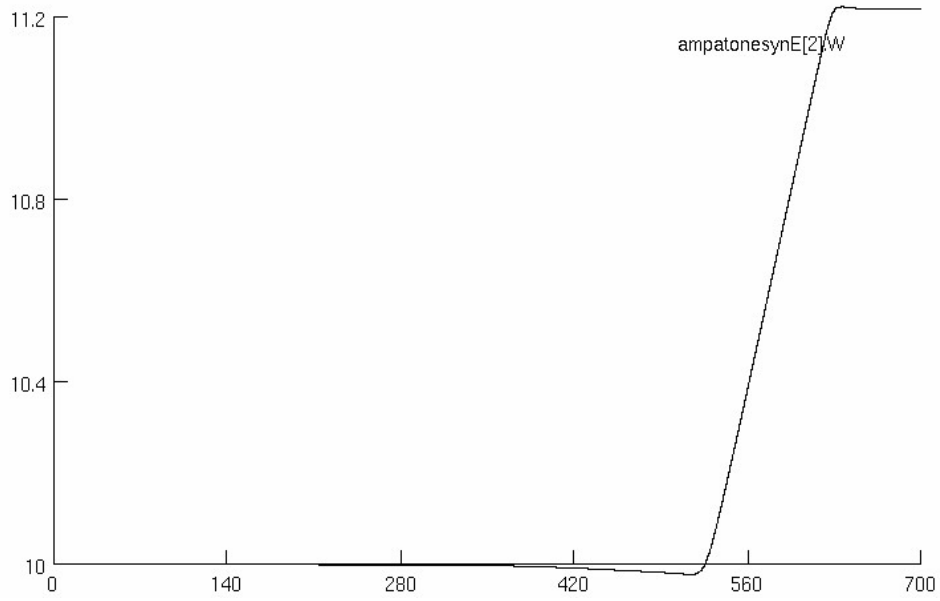


Figure 5G. Preliminary results for Type C Pyramidal Cell during conditioning. Upper panel shows change in synaptic weight to tone input of 200 Hz. Bottom panel shows change in synaptic voltage to tone input of 200 Hz.

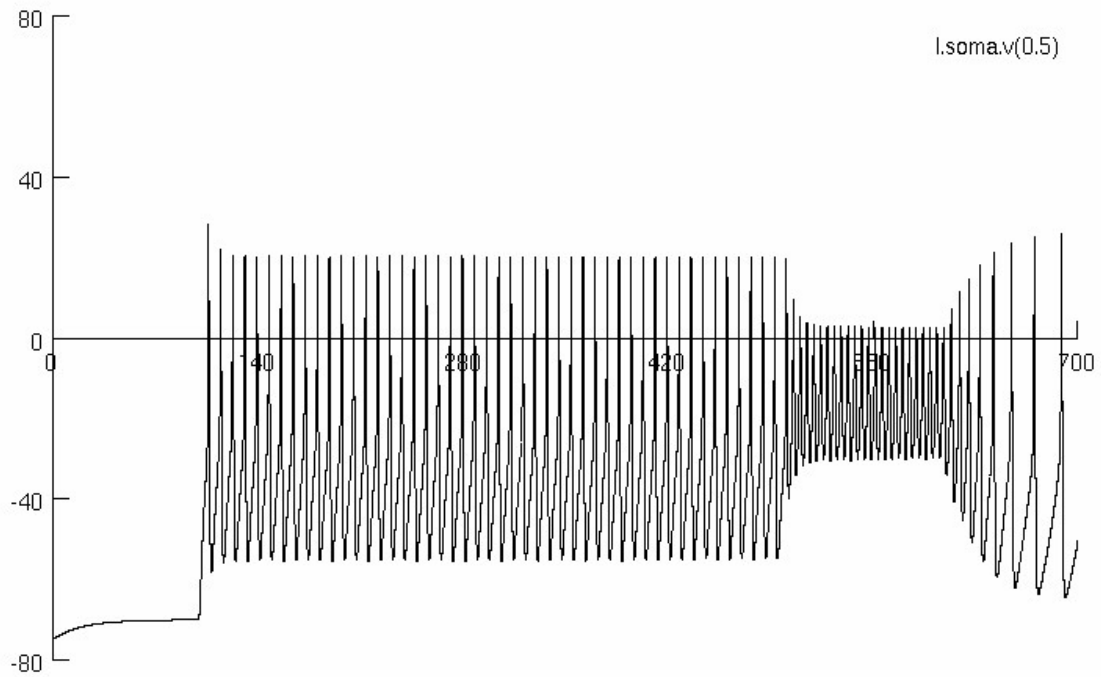
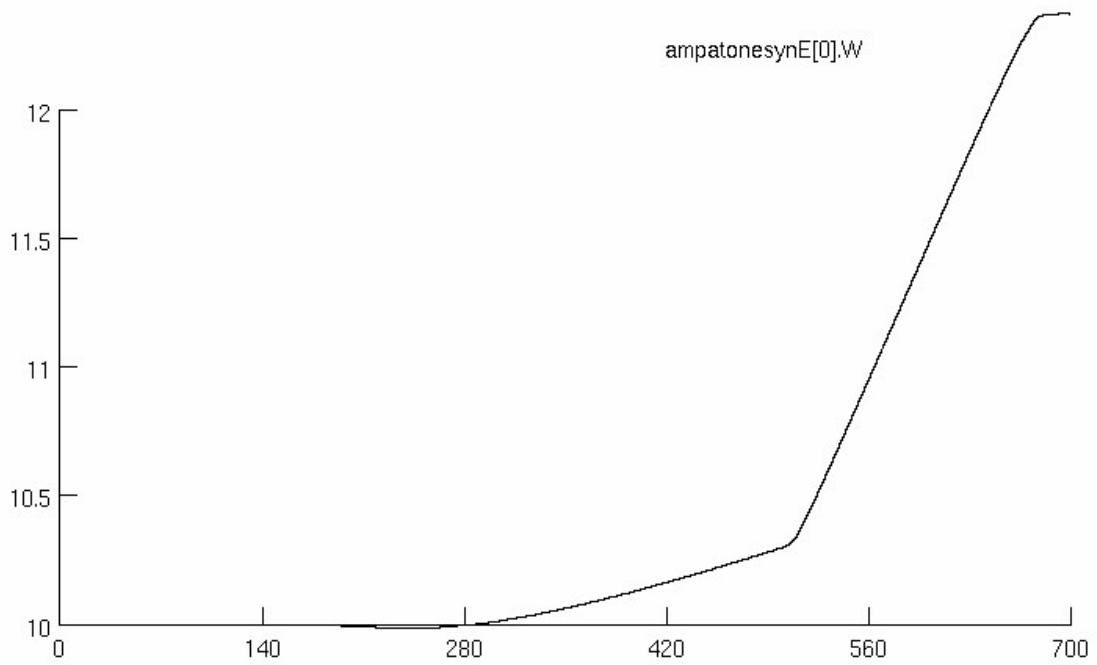


Figure 5H. Preliminary results for Interneuron during conditioning. Upper panel shows change in synaptic weight to tone input of 200 Hz. Bottom panel shows change in synaptic voltage to tone input of 200 Hz.

CHAPTER 5

Computational model of rapid transmission of information in a group-living insect predicts underlying rules for emergent behavior in the antipredator signals

5.1. ABSTRACT

In nature, individual behavioral rules are fine-tuned by natural selection for effective group behavior and antipredator response. Although only some the individuals in a group of the treehopper *Umberia crassicornis* have information about the predator's location, the synchronous signaling behavior of the offspring yields an emergent pattern that provides the defending parent with information about predator presence and location. The presence of multiple interacting individuals makes it difficult to achieve precise experimental control of the stimuli received by any one individual; therefore an alternative to the experimental dissection of behavior is to construct models of individual behavior. A rule based computational model of rapid signaler-receiver interactions was developed to understand the mechanisms underlying their collective antipredator response. This model with unknown parameters is then used to evaluate and to recreate the biological group signal for a family of treehoppers. The model compares the spatial and temporal signal properties obtained from experiments with those predicted by the model to generate an error index. A gradient descent scheme is used to minimize this index and optimize the parameters used in the model. This is done by characterizing signaling probability versus distance from predator, signal length versus number of signalers and the pair wise association of different individuals in a group signal. The model provided additional insights and predictions related to group behavior of the

nymphs as they communicated with their mother during predator attacks.

5.2. INTRODUCTION

Cooperative, reciprocal communication is one of the defining features of social behavior in animals (Wilson, 1975). Group-living individuals often communicate the presence, location and quality of important features of the environment, such as food resources or predation. When groups are large, adaptive responses of the group as a whole often arise from individual actions based only on local information (Buhl et al., 2006; Couzin et al., 2005; DeAngelis and Mooij, 2005; Sumpter, 2006). It is thus these individual behavioral rules are fine-tuned by natural selection for effective group behavior. One of the challenges of identifying the behavioral rules underlying group behavior is that the behavior may be expressed only when the individual is in a large group (Couzin et al., 2005). The presence of multiple interacting individuals makes it difficult to achieve precise experimental control of the stimuli received by any one individual. An alternative to the experimental dissection of behavior is to construct models of individual behavior (e.g., Buhl et al., 2006; Couzin et al., 2005; Gueron et al., 1996; Pratt et al., 2005). Competing hypotheses about behavioral rules (e.g., importance of visual vs. acoustic cues) can be tested for their effect on group behavior, and the results compared to the behavior of natural groups. This approach has been very successful in understanding the simple rules underlying complex, adaptive behavior of groups including fish schools and bird flocks (Camazine et al., 2003). It has also been useful in understanding the rules of communicative interactions in social insect colonies, in which communication among colony members allows the colony to efficiently exploit

food resources in the environment (Couzin and Franks, 2003; Sumpter and Pratt, 2003).

An agent/individual-based modeling approach (Grimm and Railsback, 2005) is used to understand the rules underlying the collective antipredator response of a group-living insect. In the treehopper *Umberia crassicornis* (Hemiptera: Membracidae), females defend their brood against predator attack. Offspring develop in a cylindrical aggregation on a stem of their host plant, as shown in Figure 1 (Cocroft, 1999; Wood, 1975). When a predator approaches, the brood produces a synchronous group signal, transmitted to the female as substrate borne vibrations (Cocroft, 1996; 1999). Recently we have learned that group signals not only alert the female to a predator's presence, but also provide information about the location of the predator attack (Ramaswamy and Cocroft, 2009). This information may be critical to successful defense, because the female has to locate and approach the predator in order to drive it away (Cocroft, 2002). The main weakness of models, despite their natural applicability to insect societies, has been the lack of data to reliably estimate model parameters (Pratt et al., 2005). In this respect, study of social communication in *U. crassicornis* has some decided advantages: individuals are stationary, rather than rapidly moving as in many social insects. Individuals live on the surface of their host plants, rather than being concealed underground and because the signals produced are mechanical waves, they are easily recorded, manipulated and played back. According to Couzin (2007), synchronized group behavior is mediated through sensory modalities such as vision, sound, pressure and odor detection and individuals tend to maintain a personal space by avoiding those too close to themselves; group cohesion results from a longer-range attraction to others; and animals often align their direction of travel with that of nearby neighbors.

Thus, we developed a computational model to understand the behavioral rules that explain how a group of individuals, most of whom have no direct information about the predator attack, and produce spatio-temporal patterns of signaling that reveals the predator's location to the defending female. The model reveals how variation in signaling threshold, response delay, signaling duration, neighborhood distance, internal probability and number of callers influence the production of group displays. Starting with several rules associated with input parameters to evaluate their consequences for group signaling behavior, we developed an initial model. As cited, we compared the simulated group signaling behavior to a suite of patterns measured in biological aggregations to optimize the model. These patterns include the relationship signaling probability versus distance from predator, signal length versus number of signalers and the pair wise association of different individuals in a group signal. This model is thus an effective tool for investigating hypotheses about individual behavior leading to group phenomena.

5.3. METHODS

5.3.1. Study System

Juveniles (nymphs) of *Umbonia crassicornis* develop in a cylindrical aggregation along a stem of their host plant (Cocroft, 1999; Wood 1975), with their mother sitting below the aggregation. The aggregation often extends up to 10 body lengths or more of the mother's away from her location. Nymphs are subject to intense predation in their exposed locations on plant stems (Cocroft, 1996; 2002). Flying predators, and probably walking predators, almost always attack the ends of the aggregation (Cocroft, 2002). In response to a predator attack, nymphs produce synchronized vibrational signals that elicit

maternal protection (Cocroft, 1996). Each individual nymph signal lasts for about 30-40 ms and is accompanied by a distinct rocking movement of the body (Cocroft, 1999) that lasts for a much longer duration. The rocking behavior was used as an assay for vibrational signals produced by nymphs. Signaling by the 2-3 individuals closest to the predator elicits signaling from neighbors, leading to a composite group signal that spreads from the source and typically lasts for 300-600 ms (Cocroft, 1999) but could extend up to 1400 ms in some cases. When disturbed, aggregations produce a group signal every 2-3 s (Cocroft, 1999). Note that each nymph signals only once during a given group signal (Cocroft, 1999). Maternal response to offspring signals includes approaching the predator, wing-buzzing and kicking at the predator (Brach, 1975; Cocroft, 2002). The defending mother also produces her own signals, particularly after the predator departs.

5.3.2. Experimental Design

Umbonia crassicornis individuals (late-instar nymphs or teneral adults) were collected in and around Miami in FL, USA and used to establish a greenhouse population on potted host plants (Mimosaceae: *Albizia julibrissin*) at the University of Missouri-Columbia in Missouri, USA. The treehoppers were maintained at 20-30⁰C on a 12:12 (L:D) cycle.

Potted plants with single-family aggregations were brought to the laboratory before the experiments began. Predation was simulated at both ends of the aggregation. Previous results have suggested differential spatial patterns of signaling associated with the predator attacking one end of the aggregation versus the other (Ramaswamy and Cocroft, 2009). We refer to the end closer to the base of the branch and below which the mother is

found, as the 'bottom end' of the aggregation, and the opposite end as the 'top end' of the aggregation. *Umbonia crassicornis* nymphs signal when attacked by a predator and when they receive vibrational signals from other nymphs. In this experiment, we played back the recorded signals of nine nymphs from one end of the aggregation at a time. Each of the stimuli of nine signals lasted for duration of 350 ms and was played back to the aggregation every 2.5 seconds. The experiment was done in a manner so as to not provide visual cues associated with predation. The signals were played back from a Macintosh G5 computer through an electromagnet after amplification. The amplitude of the played back signals was standardized. The signals were also calibrated on the same plant to account for the differential frequency filtering of the individual stem. This was done by playing back white noise through the stem and recording it with an accelerometer. A filter that compensates for changes in frequency was made using MATLAB and applied to the stimulus before the stimulus was played back. The end from which the stimulus was played back was alternated for each family. The behavior of the nymphs and the defending mother was recorded using a digital video camera recorder (*SonyDCRTRV830*). The video sequences were digitized using a Macintosh G4 computer and analyzed with *Final Cut Pro 2* (Apple Inc., Cupertino, CA, USA). A Knowles BU 1771 accelerometer (Knowles Acoustics, Itasca, IL, USA), was used to record vibrational signals. This accelerometer was attached adjacent to the electromagnet used for playing back the signals using wax. The accelerometer was connected to the digital video camera recorder through a custom-made amplifier. During video analysis, each nymph was given a unique number and the number of times it signaled in response to the playback was counted. The recorded signals were used to confirm nymph signaling.

We determined whether a nymph responded or not to a single playback stimulus. We also determined the position of each nymph. We obtained the distance of each nymph from the base of the aggregation as well as from the left margin of the cylindrical stem. These measurements were obtained from still images captured at the start of each treatment and standardized using measurements of total aggregation length. Both these data (distance measures and whether a nymph signaled or not) were acquired for the two treatments (playback from the top and bottom ends of the aggregation) separately.

Data used for this study were chosen from 10 different families. Only one side of the cylindrical aggregation could be captured by the video and only these nymphs were used for the analysis. When *U. crassicornis* aggregations were symmetrical around the stem, we did not bias the side of the aggregation visible to the camera; hence this is unlikely to affect the results. When *U. crassicornis* aggregations were not entirely symmetrical around the stem, we positioned the plant such that most nymphs were visible to the camera. The number of unseen nymphs was also noted so that their influence on the group signal could be estimated in the model. The recorded signals were analyzed using a MATLAB program. The recordings were cleaned by de-amplifying stray individual nymph signals, the signals produced by the defending mother and the sounds associated with her wing buzzing and walking. For each recording, we obtained an average playback signal that was calculated using only the signals that did not elicit nymphal response. All signals in the recording were reduced from the averaged signal to obtain signals of only the nymphs that signaled within the aggregation. We measured the parameters of each group signal within a treatment (length of signal, number of signalers). This allowed us to identify relationships between the number of nymphs that produced the signals (obtained

from the video recordings) and the group signal parameters for each treatment.

5.3.3. Computational Model

The plant stem was modeled as a cylinder populated with nymphs whose locations were determined after analyzing the video data. Each nymph had a unique 3-D location on the cylinder (x and θ ; Figure 1), and was modeled facing left or right based on spatial data. The spatial locations for the unseen nymphs (i.e., not captured by the video camera) were estimated by randomly picking the observed nymphs and assigning them equivalent spatial locations on the unseen side of the branch. Each nymph was modeled as a distinct agent whose behavior was governed by a set of rules. As in the experimental treatment, for the 10 families considered, predator attacks were either simulated at the top or the bottom end of the aggregation by having a cluster nymphs initiate antipredator signals. The other nymphs in the aggregation then used local cues and decided to signal based on the proposed rule base, described later. The signaling behavior thus propagated through the aggregation.

Model parameters. The agent based model considered several unknown properties for each individual based on biological observation. These included: R = time delay between perception of neighbor's signal and initiation of its own signal; N = neighborhood, defined as the radius within which an individual can detect that another individual has signaled; T = threshold, defined as the number of signaling neighbors required to elicit signal in a nymph; D = duration of the individual nymph rocking signal, p = probability of signaling, given that the threshold had been reached, and I = number of nymphs used to initiate firing from a predetermined set of nymphs at the beginning of the simulation

(top or bottom end). The group signal G generated as a result could thus be written as a function of the input parameter vector P as shown in Eqn. 5.1.

$$G = f(\vec{P}); \quad \text{where } P = (R, N, T, D, p, I) \quad (5.1)$$

For each Umbonia family, the ranges for the following input parameters, Delay (R), Neighborhood (N), Threshold (T), Initiators (I) and Duration (D) were hypothesized based on biological observation (Table 1). For each aggregation, a total of three to eight nymphs were predetermined to form the pool of initiators. The initiator nymphs were located at the vertical edge of the aggregation and assumed to be most prone to predator attacks. If two or more nymphs were located within a 1 cm bin along the y axis at a particular x position, it was assumed that the first nymph shielded the other nymphs. With the Initiator array defined, a random nymph was selected and the closest neighbors in the counterclockwise direction were picked based on I . This process thus considered a cluster of nymphs that typically signal during a predator attack in the field.

The computational model was used to address questions regarding the influence nymphs in the aggregation on an individual's signaling behavior. The present model considered the bimodal signaling property of nymph by incorporating (a) A sigmoid function that took into account the number of nymphs that signaled previously on a individual likely hood of signaling in a group signal and (b) A sine function that considered the sensitization/conditioning phase which resulted in a change in signaling probability across all nymphs in the aggregation temporally. This was then used to effectively characterize how nymphs that typically signal using local cues are influenced by global information. The cases considered questioned if the model best replicated

biologically observed spatio-temporal properties, when a. Only local information was considered; b. If local and global information was considered; c. If only global information was considered.

Each nymph was modeled to produce two types of signaling behaviors namely, vibration and rocking. The vibrational signals propagated through the substrate and were assumed to be perceived by all the other nymphs in the aggregation, irrespective of spatial location. Experiments have shown that this kind of global information typically lasted for 59.5 ms for every nymph call and this value was considered in the model. Alternatively, the rocking behavior was hypothesized to be a signal influencing the nymphs in a localized neighborhood and typically lasting for over 100 ms based on video analysis. This value of rocking behavior duration was iteratively determined.

The signaling probability (sp) for the nymphs was modeled as a sine function ($0-\pi/2$) to incorporate conditioning and sensitization (positive feedback) behavioral phases observed in such populations. A sine function helped incorporate the variability in the number of signalers observed temporally. For a particular group signal, the model assigned a constant signaling probability (i.e., 0.2-0.8) for all the nymphs in the aggregation except for the initiators of each group signal and was computed as follows:

$$sp = 0.65 * \sin\left(\pi / 2 * \frac{current\ signal}{total\ signals + 1}\right) + 0.15 \quad (5.2)$$

where, a total of twenty group signals were typically simulated. This function assumed that the agent signaling was predominantly based on local cues and implicitly considered rocking behavior as the primary output of the agent.

As cited, the model also considered the vibrational influence (via substrate) of number of nymphs that had signaled previously in the aggregation for a group signal and its influence on the likelihood of nymph signaling. This was assumed to be the global information and modeled as a sigmoid function to capture the substrate vibrations generated from uncorrelated sound sources. This was computed as follows:

$$\sigma(i) = 0.2 * \left(\frac{1}{1 + \alpha * e^{-m}} \right) \quad (5.3)$$

where, m is the total number of nymphs in that particular family i , α is the normalizing constant specific to each family to preserve the shape of the sigmoid typically varying from 0.125 to 0.6. Different families, depending on their genotype and the environmental conditions under which they were raised, had variation in group signal parameters. This function was added to generate variability in calling within a group signal and to better represent the nymphs in the wild who may have varying internal thresholds to elicit signaling behavior.

Rule based model. Once a predator attack is simulated by the initiators, a nymph would participate in a group signal only if the following conditions were satisfied:

- (i) If the nymph under consideration has not fired previously in that group signal
- (ii) If the pair-wise distance between nymph under consideration and other nymphs that signaled previously was less than the neighborhood (N) measured as the vector distance between two adjacent nymphs
- (iii) If the number of signaling neighbors required to elicit an individual's signal for the nymph under consideration defined as threshold (T) was met which implied

that number of signaling neighbors continued to produce a signal due to the rocking behavior (D) after a delay (R)

- (iv) If the above mentioned conditions were satisfied and if the random generated probability (p) for the nymph under consideration was less than $sp+\sigma(i)$.

Once the decision to signal had been made, each nymph in the aggregation signaled after a delay (R) for the duration of rocking behavior (D). Thus, every other agent (nymph) in the aggregation determined its state of signaling during each time step based on local cues. Also, the number of nymphs and the time step they decided to signal was recorded. As cited, the rule based model was used to simulate twenty biological group signals (G) for 10 experimentally-studied family groups of treehoppers, for two types of treatments (top and bottom end). Figure 2 shows the schematic of the model.

Spatial and Temporal Parameters. The following spatio-temporal parameters were characterized to compare model output with biological data, namely, (a) The relationship between signaling probability of nymphs and distance to predator (referred to hereafter as Signaling probability, SP). The signaling probability (SP) per bin was calculated based on the proportion of nymphs that signaled in bins of 1.5 cm to the total number of nymphs present in a particular bin and dividing it by the total group signals. This was based on seen nymphs. Mathematically, signaling probability per bin was given by

$$SP = \frac{\left(\frac{\text{no. of nymphs signaled}}{\text{total no. of nymphs}} \right)}{\text{total group signals}} \quad (5.4)$$

- (b) The relationship between inter-individual distance and the likelihood of making the same signaling decisions (referred to hereafter as Association Index, AI) described by

the simple ratio index (SRI) and computed per distance bins were given by equation 5.5.

$$AI(i, j) = \sum_{n=1}^n \left(\frac{Flag(i, n) AND Flag(j, n)}{Flag(i, n) XOR Flag(j, n)} \right) \quad (5.5)$$

where, $Flag(i, n)$ was the firing condition (1 or 0) for nymph i during signal n and $d(i, j)$ is the vector distance from nymph i to nymph j , given by:

$$d(i, j) = \sqrt{(x_i - x_j)^2 + (y_i - y_j)^2} \quad (5.6)$$

where, (x_i, y_i) gave the (x, y) position of the i nymph. The AI (i, j) was then sorted out in bins of 0.5 cm length and averaged across all group signals per family. This was based on seen nymphs. (c) The relationship between the number of signalers and group signal duration (referred to hereafter as Signal Length, SL). Signal Length was estimated based on adding the time delay (R) and vibrational duration of 59.5 ms after the point the last nymph decided to signal. Since, biological experiments recorded group signals from all the nymphs in the aggregation, we estimated the total number signalers for the biological data which could then be compared to the model output. Figure 3 shows representative plots used to compare biological data and model output for signal length, signaling probability and association index.

5.3.4. Error Computation

The model was constrained to the above mentioned spatial and temporal properties obtained from twenty biological experiments across 10 families to generate an error index. Figure 3 also shows schematic of the various relationships used to compute error between model output and biological data.

Signaling Probability Error (E_{SP}): The signaling probability error (E_{SP}) was computed as the difference between the ratios for biological and model values. Mathematically,

$$SP_E = \left(\frac{Area_{top} - Area_{bottom}}{Max(Area_{top}, Area_{bottom})} \right)_{Biological} - \left(\frac{Area_{top} - Area_{bottom}}{Max(Area_{top}, Area_{bottom})} \right)_{Synthetic} \quad (5.7)$$

$$E_{SP} = (0.33(SP_E)^2)$$

Association Index Error (E_{AI}): The association error index (E_{AI}) comprised of two components weighted equally. E_{AI} was computed by comparing the maximum of the association index (AI_{max}) averaged between biological and model results and by comparing the point (X_{max}) where AI_{max} begins to drop off in relation to the nymph to nymph distance.

$$E_{AI} = (0.165(\Delta AI_{max})^2 + 0.165(\Delta X_{max})^2) \quad (5.8)$$

Signal Length Error (E_{SL}): The error index for signal length (E_{SL}) comprised of two components weighted equally. E_{SL} was computed by comparing the slopes of linear curves (SL_{slope}) used to fit biological and model results for individual families and comparing the intercept for signal length ($SL_{intercept}$) based on 10 signalers.

$$E_{SL} = (0.165(\Delta SL_{slope})^2 + 0.165(\Delta SL_{intercept})^2) \quad (5.9)$$

5.3.5. Optimization using Gradient scheme

To ensure proper generalization capabilities, a cross-validation procedure was applied by splitting the data into two groups. The training set consisted of 14 treatments from 7 families that were randomly chosen from the original biological data set. The remaining 6 treatments from 3 families were used as the testing set. The gradient descent method thus used a 70:30 cross validation scheme to optimize the parameter vector P such that the

weighted root mean squared of the errors was minimized for all the nymph families (n). The model reported thus minimized the difference in the error indices across each spatio-temporal component for each family by calculating the root mean square error given by

$$E_{RMS}(n) = \sqrt{(E_{AI} + E_{SP} + E_{SL})} \quad (5.10)$$

and the total error (E_T) was computed by considering the average E_{RMS} across all families and given by

$$E_T(\bar{P}) = \frac{\sum E_{RMS}(n)}{n} \quad (5.11)$$

As cited, the iterative process was used to adjust \bar{P} , based on the lowest value for E_T , using a gradient descent method with a learning rate η , as shown in Eqns.5.12 and 5.13.

$$\Delta \bar{P}_i = -\eta * grad[E_T(\bar{P})] \quad (5.12)$$

$$\bar{P}_{new} = \bar{P}_{old} + \Delta \bar{P} \ni \Delta E_T < 0 \quad (5.13)$$

The objective was to ensure the appropriate update of the parameter vectors such that each iteration reduced E_T . As cited, the parameters were adjusted within the ranges outlined in Table 1, using the gradient procedure cited above. Through further iterative changes, we identified multiple parameter sets that produced group signals with desired properties. The computational model was developed using MATLAB version 7.1 (Math works Inc., Natick, US). An integration time-step of 1 ms was used.

5.4. RESULTS

5.4.1. Model Training and Validation

We employed a weighted root mean square method as described in Eqns. 5.7—5.11

in conjunction with gradient descent technique (Eqns. 5.12, 5.13) to reduce the total error component (E_T) across all families and obtain an optimal parameter set (Table 2). The error component for each family (E_{SL} , E_{AL} , E_{SP} and E_T) was normalized based on the largest error value across all families. As cited, the model was constrained to biological data based on the following spatio-temporal properties (a) the relationship between distance to predator and individual signaling probability; (b) the relationship between the number of signalers and group signal duration; and (c) the relationship between inter-individual distance and the likelihood of making the same signaling decisions. Such a spatio-temporal composite estimate considered the behavior of all the nymphs in the aggregation.

Several extreme cases were conducted to validate the model and are briefly discussed next. Setting duration (D) to 0 ms resulted in no others nymph signals. Setting threshold (T) to 0 nymphs resulted in no other nymph to signal but initiators. Setting neighborhood (N) to 0 cm resulted in no other nymph to signal but initiators. As an alternative, we set the neighborhood (N) to the size of the aggregation. In this case, as expected it was noticed that signaling probability across bins was pretty much a constant. This is because all the nymphs equally perceive any other nymph calling in the aggregation and thus, the probability of calling is high across the aggregation and does not drop as seen in the biological case. Further, the neighborhood no longer acted as a gating variable compared to a case where neighborhood was set to 1.5 cm (Figure 4), thus, signal length remained a constant despite the number of signalers increasing. This process further validated the agent based modeling approach that used unknown parameters and rules to reproduce spatio-temporal signaling patterns observed in biological data.

The choice of optimal parameters was based on the lowest E_T as determined by the gradient scheme. Table 2 shows the initial conditions (trial 1) and the list of parameters that resulted in the lowest training error across families when each parameter was varied by a unit change. Figure 5 shows the behavior of error components (E_{SP} , E_{AI} , E_{SL}) across training and testing trials.

Further, as an alternative, training and testing families were combined which resulted in E_T being similar to the case where 70% of the biological families were considered (data not shown). A different starting point was considered in the model to examine the convergence of parameters. Figure 6 shows the E_T across training and testing families for the parameters in Table 2. Figure 7 shows the convergence of parameters for two sets of initial conditions using the 70:30 training to testing ratio respectively.

The gradient method thus helped identify the parametric set for which training and testing data reported the lowest composite error, E_T , while ensuring the system was not over trained. After being trained and tested in this manner, the model could provide useful predictions. Since, experimental biologists have no direct means of measuring duration of rocking behavior, latency/delay, neighborhood required to sustain group signal length, the proposed model could be used to estimate some of these agent properties.

5.4.2. Effect of local (sensitization) versus global information

As cited, the computational model used a combination of local and global cues to match spatio-temporal trends observed in experiments. In order to systematically characterize the impact of using local vs. global cues in the model a series of experiments were performed. The sine function (L) represented the sensitization/condition phase in

the model and also implicitly considered using local cues for propagation of antipredator signaling. As cited, this function increased the probability of signaling for the nymphs across the aggregation temporally. The sigmoid function (G) considered was incorporated to generate variability within a single group signal and considered the impact of the nymphs that had signaled previously on an individual's likelihood of signaling. The cases considered include, a. Only sensitization, i.e., all local information with no sigmoid (L:0.2-1, G:0); b. Sine modeled from 0.2-0.8 with sigmoid from 0-0.2 (L:0.2-0.8, G:0-0.2); c. Sine modeled from 0.2-0.5 with sigmoid 0-0.5 (L:0.2-0.5, G:0-0.5); d. Sine going from 0-0.2 with sigmoid from 0.2-0.8; e. No sine with sigmoid going from 0.2-1.0 (L:0, G: 0.2-1). Each of these cases were then qualitatively compared to the biological case to examine the influence of local vs. global cues.

Figure 8 depicts the variation in the spatio-temporal parameters compared to the biological data as a result of varying the contribution of global information. The study revealed that the case that considered equal contribution of global (G:0-0.5) and local (L:0.2-0.5) information on the likelihood of nymph signaling resulted in the best match to the biological data while comparing the spatial properties. This

5.4.3. Parametric studies

A sensitivity analysis was performed to rank the parameters. This was done due to the absence of any precise guidelines for standard deviation of the parameters considered. We chose parameter values that deviated from the optimal values by a unit in both directions. The sensitivity analysis was used to rank the following model parameters: Neighborhood, Threshold, Delay and Duration. Each parameter in Table 1 was varied by +/- unit change about the optimal parameter set (trial 12; Table 2) to find their relative

effect of the outputs of interest E_{SP} , E_{SL} , E_{AI} and E_T . The differences in the outputs based on this +/- unit change in parameters were then normalized by dividing with the value of the optimal parameter. This was then divided by the relative change in the parameter of interest. The absolute value was then normalized based on the highest across the output for interest. The resulting normalized numbers reported in Table 3 are indicative of the relative importance (rank) of the parameters as far as their effect on the output was concerned.

Signaling Probability Error (E_{SP}). As cited, the signaling probability error (E_{SP}) was determined by calculating the difference between the probability density ratios for biological and model results for each biological family. As shown in Table 3, E_{SP} was most sensitive to the changes in parameter Neighborhood (N). Signaling probability results were governed by the density of nymphs which varied depending on the family type. Threshold was the second most important parameter to influence signaling probability of agent nymphs. As expected, Duration of signaling had no influence on the signaling probability error.

Association Index Error (E_{AI}). The Association Index error (E_{AI}) provided an insight into how far a nymph could influence signaling in the aggregation. E_{AI} was most sensitive to the changes in parameter Neighborhood (N). About the optimal point, varying Delay (R) had a stronger influence on E_{AI} compared to Threshold (T).

Signal Length Error (E_{SL}). The signaling length error (E_{SL}) was determined by calculating two components, namely, comparing the slopes between the biological and model results and by comparing the intercept (signal length) between the model and biological data for x number of signalers. Despite these components being weighted

equally towards the calculation of E_{SL} , the model showed that E_{SL} was most sensitive to the changes in the parameter Threshold, T . Neighborhood was the parameter least influencing E_{SL} . As this study was done around the optimal set, the lack of influence of change in duration on E_{SL} indicates that this parameter may be optimal.

Total Error (E_T). As cited, to ensure proper cross-validation, the families were randomly split into training and testing categories. About the optimal set, variation in delay followed by neighborhood had the largest impact on error.

5.5. DISCUSSION

We report a computational framework to study emergent signaler-receiver interactions in the *U. crassicornis* group-living insects. This agent based model was used to test the emergence of informative global patterns by providing interacting juvenile nymphs with limited local cues. For natural selection to act on and shape rules followed by individuals that lead to group-level phenomena, there had to be variation in the group signals. The biological families considered had nymphs varying from 18 to 95. The total number of nymphs that signaled to produce group signals and signal length varied amongst the families. Despite the size of the aggregation, the trends seem consistent.

5.5.1. Agent based model predicts the underlying rules and parameters used by nymphs to produce antipredator signals

The proposed agent based model incorporated a rule based system and considered several unknown parameters to recreate group signal behavior as observed experimentally. The hypothetical parameters led to group signals that matched observed patterns in group signals measured experimentally. Most significantly, based on two

distinct initial conditions, and by employing a gradient scheme, the model predicted agent parameters that will most likely influence signaling behavior during a predator attack. The model predicted the following agent properties, Neighborhood of 1.5 cm, Threshold of 2 nymphs, Delay of 130 ms and Duration of 200 ms with 3 nymphs initiating group signals when the predator attacked at the top end of the aggregation while the cluster of nymphs was 2 initiated signaling for cases where predator attack was at the bottom end of the aggregation. This prediction was further validated by the alternate study that considered a different initial condition. Counter to intuition, the model predicted that for the nymph under consideration to signal, at least two nymphs has to be signaling within a neighborhood of 1.5 cm to elicit an individual's signal. The model also predicted the order in which nymphs signal based which could eventually be verified by biologists using a high speed camera. In addition, this model could be used to address at what point (duration of signal) does the agent perceive the antipredator signal.

5.5.2. Effect of local versus global information

The model was to systematically consider the influence of incorporating global information and evaluate its impact on the spatio-temporal parameters while simultaneously comparing it with the biological output. Contrary to previous belief, the model revealed that individual nymph signaling is also perceived globally and in conjunction with other local cues influences the nymph likelihood of calling to produce antipredator signals. This study further indicated that such models could be used to further explore other scenarios to better estimate the contribution of global behavior and its influence on antipredator signals in the colony of treehoppers.

5.5.3. Model predicts relationships between agent properties and spatio-temporal characteristics

A sensitivity analysis of the agent based model provided insights into the relationships between the agent parameters and the spatio-temporal properties. Specifically, it was found that spatial property errors, E_{AI} and E_{SP} were strongly dependent on Neighborhood (N), while counter to intuition; E_{SL} was dependent on Threshold (T) about the optimal point. However, the model estimated Delay (R) as the most significant parameter affecting Total Error (E_T) followed by Neighborhood (N) and Threshold (T). Biological observations of the signal behavior reveal that the Delay needs to be large enough to extend the short individual nymph signals into a relatively long group signal.

The model provides for an ideal platform to study how the variation in parameters can result in a change in the number of signalers. An aspect of artificiality in the model arises from the behavior of the mother not being incorporated into the model. Recent studies have suggested that the presence of the defending mother alters the threshold of nymph signaling (Ramaswamy and Cocroft, 2009). The next generation of models will incorporate feedback from the mother and refine the input parameters.

5.5.4. Limitations and Future work

The present model does not use other properties that could be estimated by processing biological group signals to yield time to peak, peak amplitude and total energy. Alternatively, other parameters maybe necessary to better capture agent decisions to participate in group signaling behavior. For example, the parameter Delay, considers three phases hypothesized to be involved in influencing a nymph's decision to signal.

These include the nymphs perception that other nymphs in the neighborhood are signaling, the time taken for it to decide to signal and the neural processing that induces a delay in exhibiting rocking behavior. Further, the availability of spatial data for the entire aggregation may help fine tune model properties. Ongoing studies with high speed camera could be used to investigate the range of tactile sensing (i.e., nymphs signals even if no one in its neighborhood signals), order of nymph calling, duration of rocking and predicted by the model and result in the identification of key individuals responsible for rapid transmission of information.

5.6. CONCLUSION

The paper proposed a novel framework to determine the effect of various parameters in emergent signaling behavior in a colony of nymphs. Contrary to previous belief, the model showed that a combination of local and global cues is responsible for group interaction in such colonies where only a few nymphs are aware of a predator attack. The model incorporated agent properties and signaling rules to generate group behavior based on locally available information. This computational model developed consistently reproduced the spatio-temporal characteristics as observed by experimentalists and was used to predict local cues and agent parameters used to produce antipredator signals.

5.7. REFERENCES

1. Brach.V. (1975). A case of active brood defense in the thornbug, *Umbonia crassicornis* (Homoptera: Membracidae). *Bull South California Academy of Sciences*, 74, 163–164.
2. Buhl, J., Sumpter, D.J.T., Couzin, I.D., Hale, J.J., Despland,E., Miller, E.R., and Simpson, S.J. (2006). From disorder to order in marching locusts. *Science*, 312, 1402–1406.

3. Camazine, S., Deneubourg, J.L., Franks, N.R., Sneyd, J., Theraulaz, G. and Bonabeau, E. (2003). *Self-Organization in Biological Systems*. Princeton University Press, Princeton, NJ.
4. Cocroft, R.B. (1996). Insect vibrational defense signals. *Nature*, 382, 679–680.
5. Cocroft, R.B. (1999). Offspring-parent communication in a subsocial treehopper (Hemiptera: Membracidae: *Umbonia crassicornis*). *Behavior* 136, 1–21
6. Cocroft, R.B. (2002). Antipredator defense as a limited resource: unequal predation risk in broods of an insect with maternal care. *Behavioral Ecology*, 13 (1), 125–133.
7. Couzin, I.D., and Franks, N. R. (2003). Self-organized lane formation and optimized traffic flow in army ants. *Proceedings of the Royal Society of London*, 270, 139–146.
8. Couzin, I.D, Krause, J., Franks, N.R., Levin, S.A. (2005). Effective leadership and decision-making in animal groups on the move. *Nature*, 513–516.
9. Couzin, I. D. (2007). Collective minds. *Nature*, 445(7129), 715-715.
10. DeAngelis, D.L. and Mooij, W.M. (2005). Individual-based modeling of ecological and evolutionary processes. *Annual Review of Ecology, Evolution and Systematics*, 36, 147- 68.
11. Grimm, V., and Railsback, S. F. (2005). *Individual-based Modeling and Ecology*. Princeton University Press, Princeton, NJ.
12. Gueron, S., Levin, S.A., Rubenstein, D.I. (1996). The dynamics of herds: from individuals to aggregations. *Journal of Theoretical Biology*, 182, 85–98.
13. Pratt, S.C, Sumpter, D.J.T., Mallon, E.B., and Franks, N.R. (2005). An agent-based model of collective nest choice by the ant *Temnothorax albipennis*. *Animal Behavior*, 70, 1023– 1036.
14. Ramaswamy, K., and Cocroft, R.B. (2009). Offspring parent communication: collective signals in treehopper broods indicate predator location. *Animal Behaviour*. (in press)
15. Sumpter, D.J.T. (2006). The principles of collective animal behavior. *Philosophical Transactions of the Royal Society of London B*, 361, 5–22.
16. Sumpter, D.J.T., and Pratt, S. C. (2003). A modeling framework for understanding social insect foraging behavior. *Behavioral Ecology and Sociobiology*, 53, 131–144.
17. Wilson, E.O. (1975). *Sociobiology: The new synthesis*. Harvard University Press, Cambridge, MA.
18. Wood, T.K. (1975). “Defense in two pre-social membracids (Homoptera: Membracidae)”. *Canadian Entomology*, 107, 1227–1231.

5.8. TABLES

Table 1. Input parameters and ranges

Parameter	Units	Ranges
Delay (R)	ms	50 – 200
Duration (D)	ms	40 – 200
Neighborhood (N)	cm	0.5 – 2.5
Threshold (T)	Nymphs	1 – 3
Initiators (Top or Bottom)	Nymphs	1 – 3

Table 2. Input parametric set and error

Trial	PARAMETERS						Training Error	Testing Error
	N (cm)	Initiators B (nymphs)	Initiators T (nymphs)	T (nymphs)	Delay (ms)	Duration (ms)		
1	1	3	3	3	140	180	0.65	0.51
2	1	3	3	2	140	180	0.51	0.50
3	1.5	3	3	2	140	180	0.44	0.45
4	1.5	2	3	2	140	180	0.44	0.45
5	1.5	2	3	2	130	180	0.43	0.45
6	1.5	2	3	2	130	200	0.43	0.45
7	1.5	2	3	2	130	180	0.43	0.45
8	1.5	2	3	2	130	200	0.43	0.45
9	1.5	2	3	2	130	180	0.43	0.45
10	1.5	2	3	2	130	200	0.43	0.45
11	1.5	2	3	2	130	180	0.43	0.45
12	1.5	2	3	2	130	200	0.43	0.45

Table 3. Normalized values showing change in error per unit change in input parameters

Parameter	E_{AI}	E_{SL}	E_{SP}	E_T
Neighborhood	1.00	0.73	1.00	0.48
Threshold	0.10	1.00	0.83	0.39
Delay	0.81	0.32	0.14	1
Duration	0	0	0	0

5.9. FIGURES

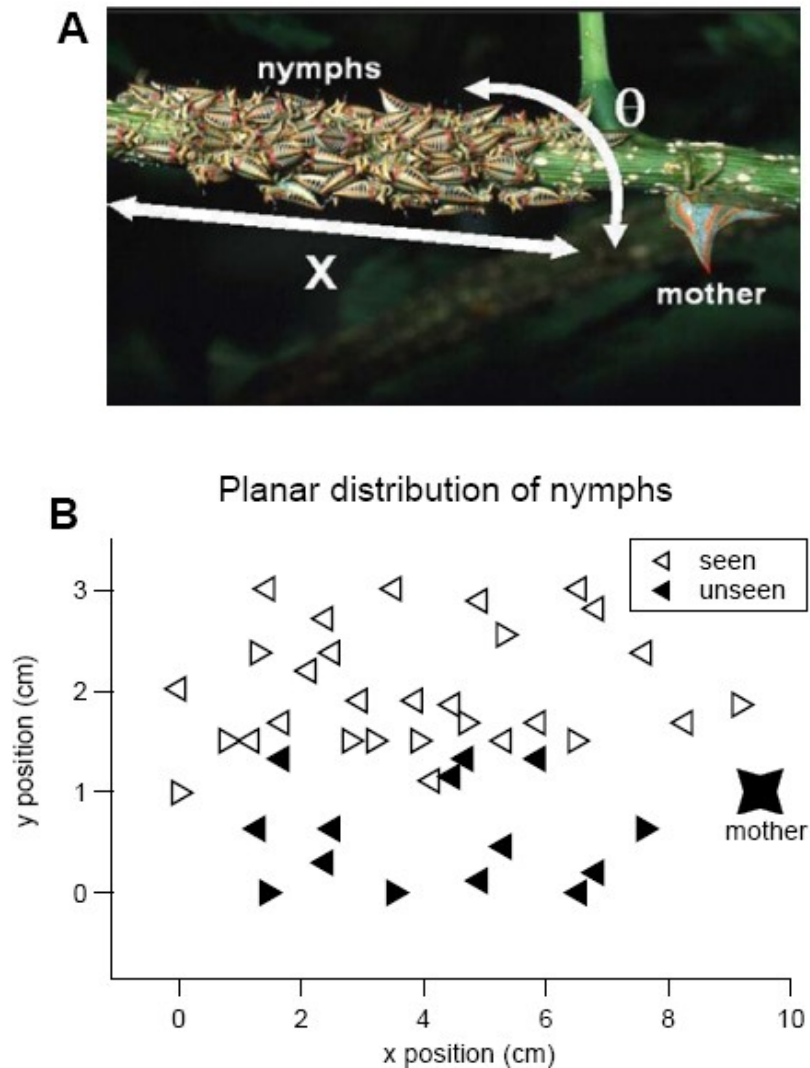


Figure 1. **A.** Nymph location on stem with mother at the far end of the aggregation. . Spatial data is provided for nymphs seen by the camera which is resolved into polar coordinates to populate the nymphs in the model. The cylindrical stem is resolved as a flat sheet. **B.** Model shows nymphs captured by camera and estimates unseen ones. The model is used to reproduce the unseen nymphs by randomly assigning them values on the opposite side of the seen branch. Calling is initiated by five nymphs located on the right and propagates through the aggregation based on the rules.

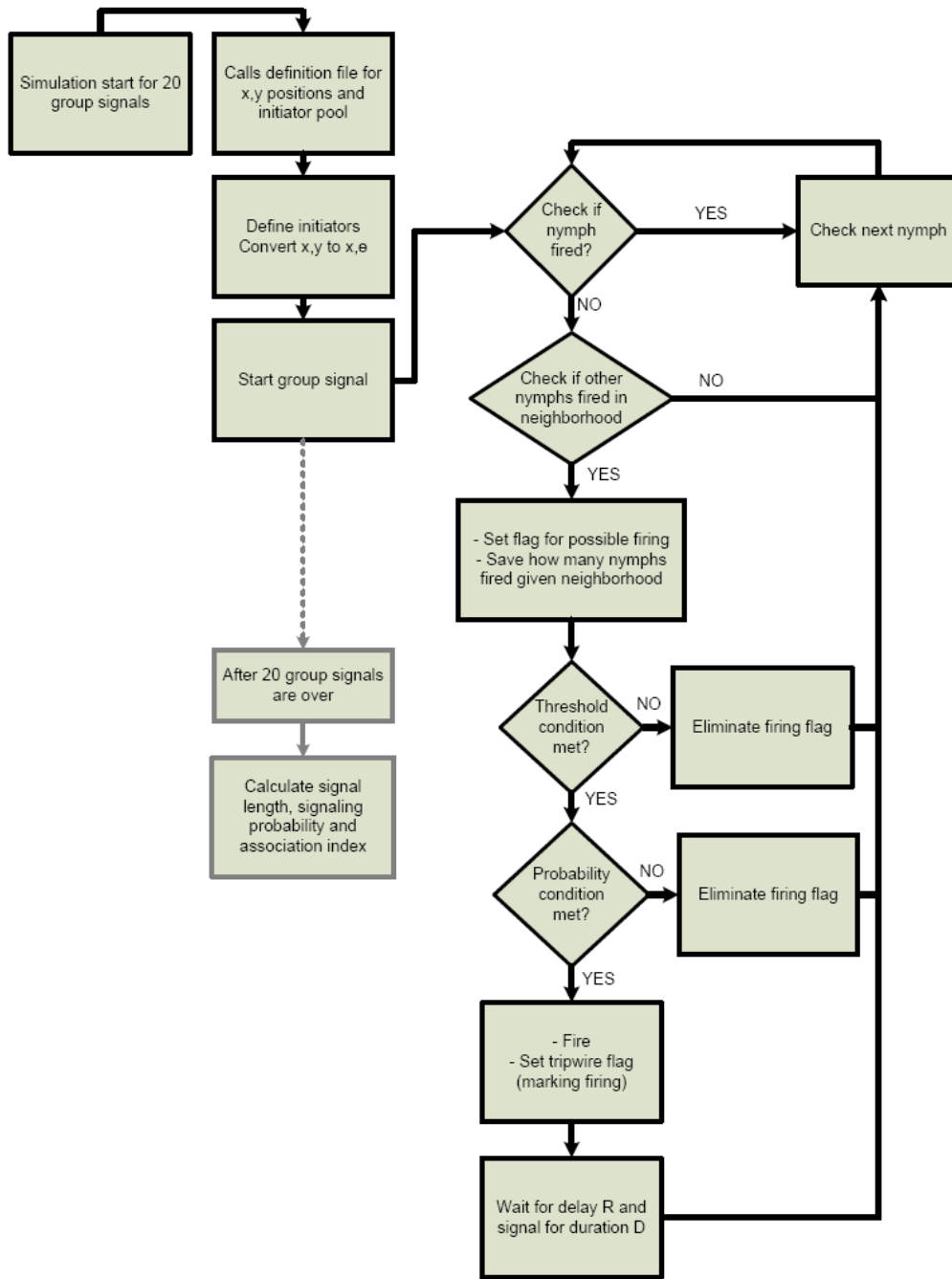


Figure 2. Flowchart depicts schematic of the model

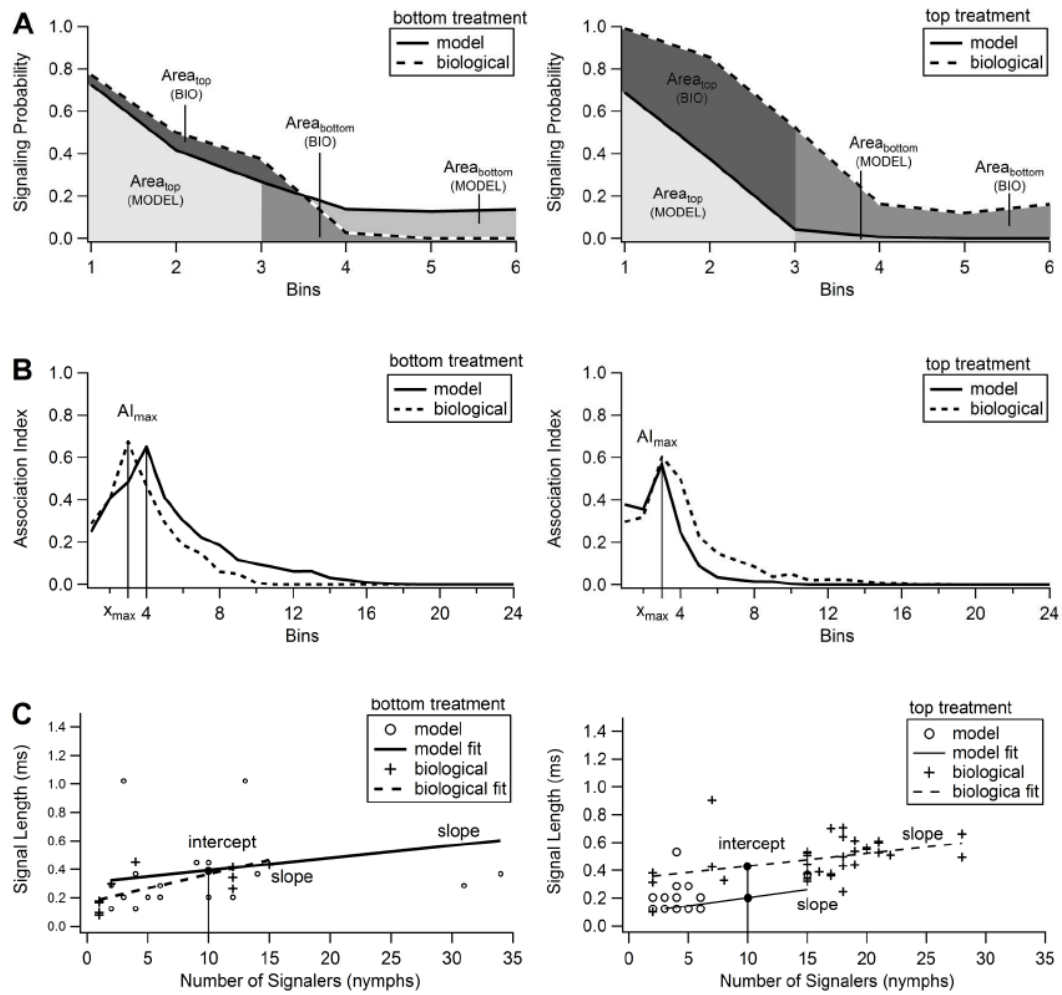


Figure 3. Comparison of biological and model results for a particular family/treatment used to compute error. **A.** Association index. **B.** Scatter plot for Signal length. **C.** Signaling probability.

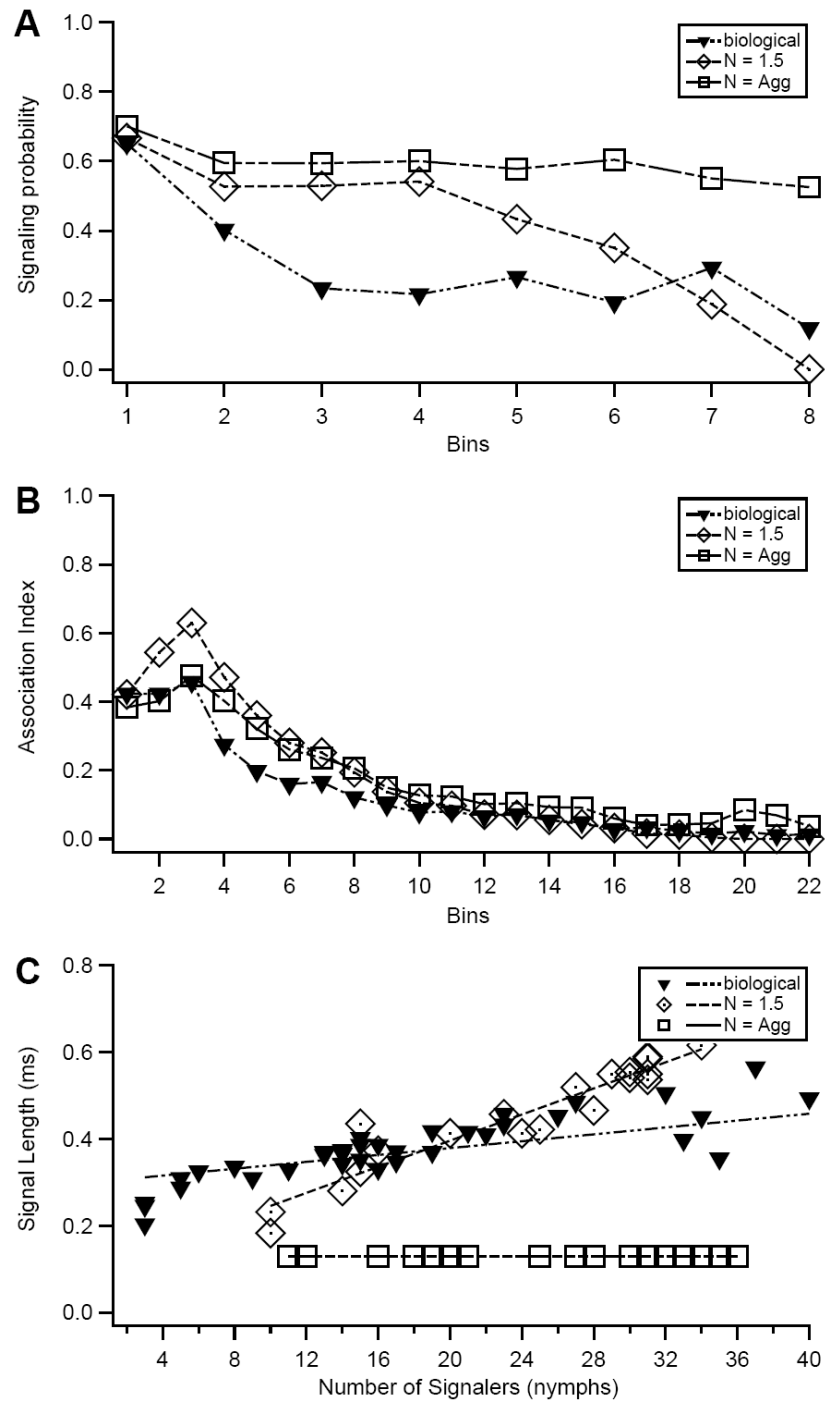


Figure 4. Validation case that considered neighborhood the size of the aggregation. The study revealed that when neighborhood is the size of the aggregation, signaling probability is higher across the aggregation as neighborhood no longer acts as a gating variable as shown in the case where $N=1.5$ cm.

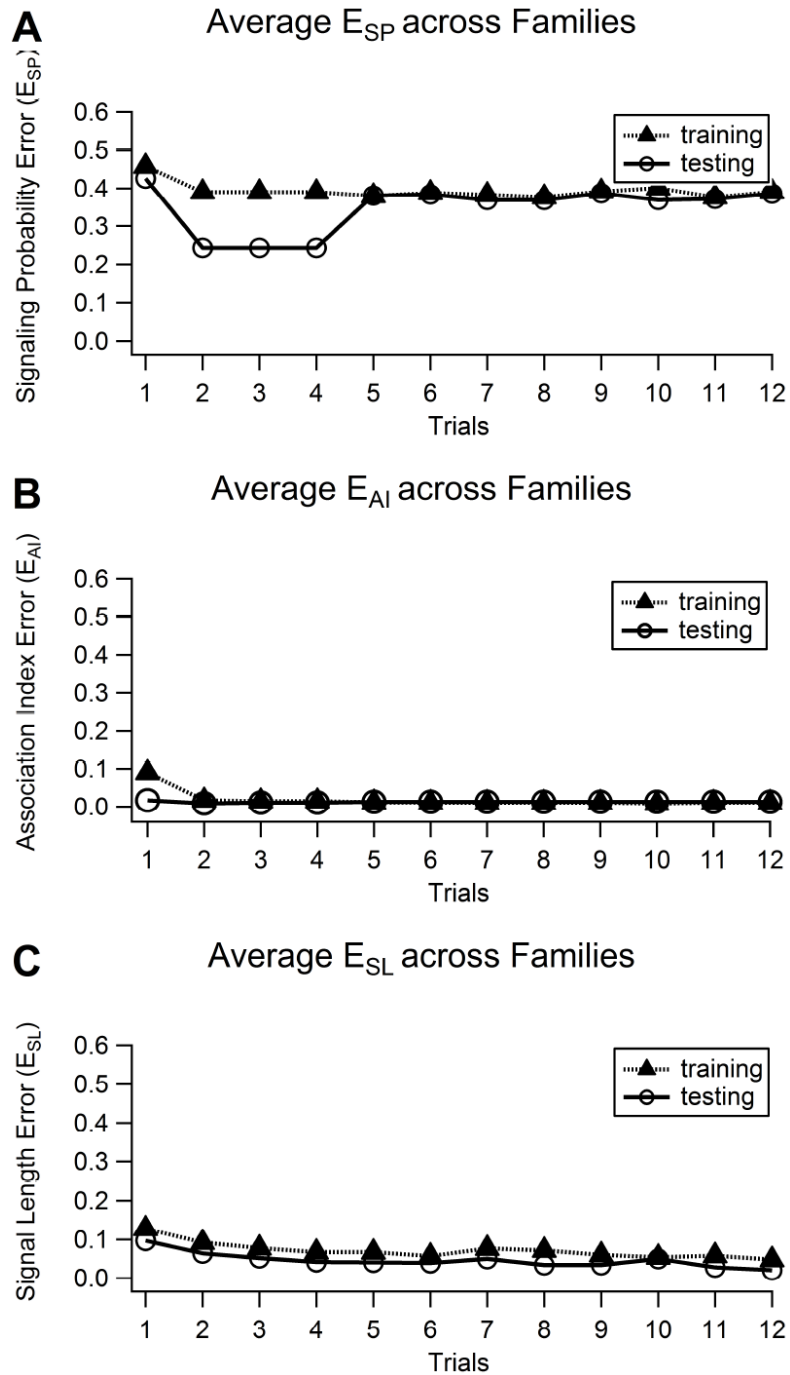


Figure 5. Variation in training and testing for individual error components across trials for parameters in Table 2. **A.** Association Index Error (E_{AI}). **B.** Signaling Probability Error (E_{SP}). **C.** Signal Length Error (E_{SL}).

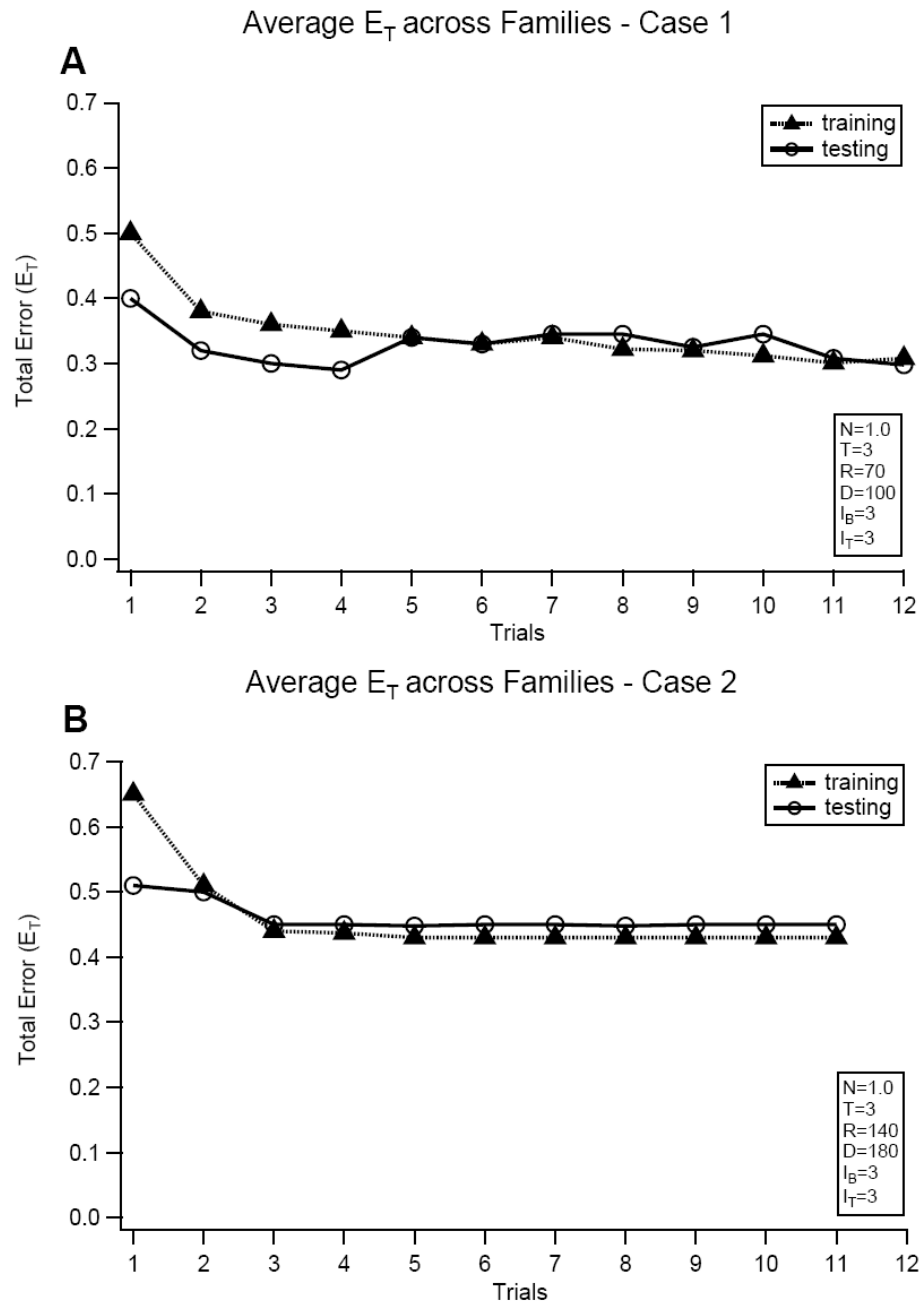


Figure 6. Comparison of Total Error (E_T) for training vs. testing data based on the two initial conditions (Table 2) computed using the gradient scheme.

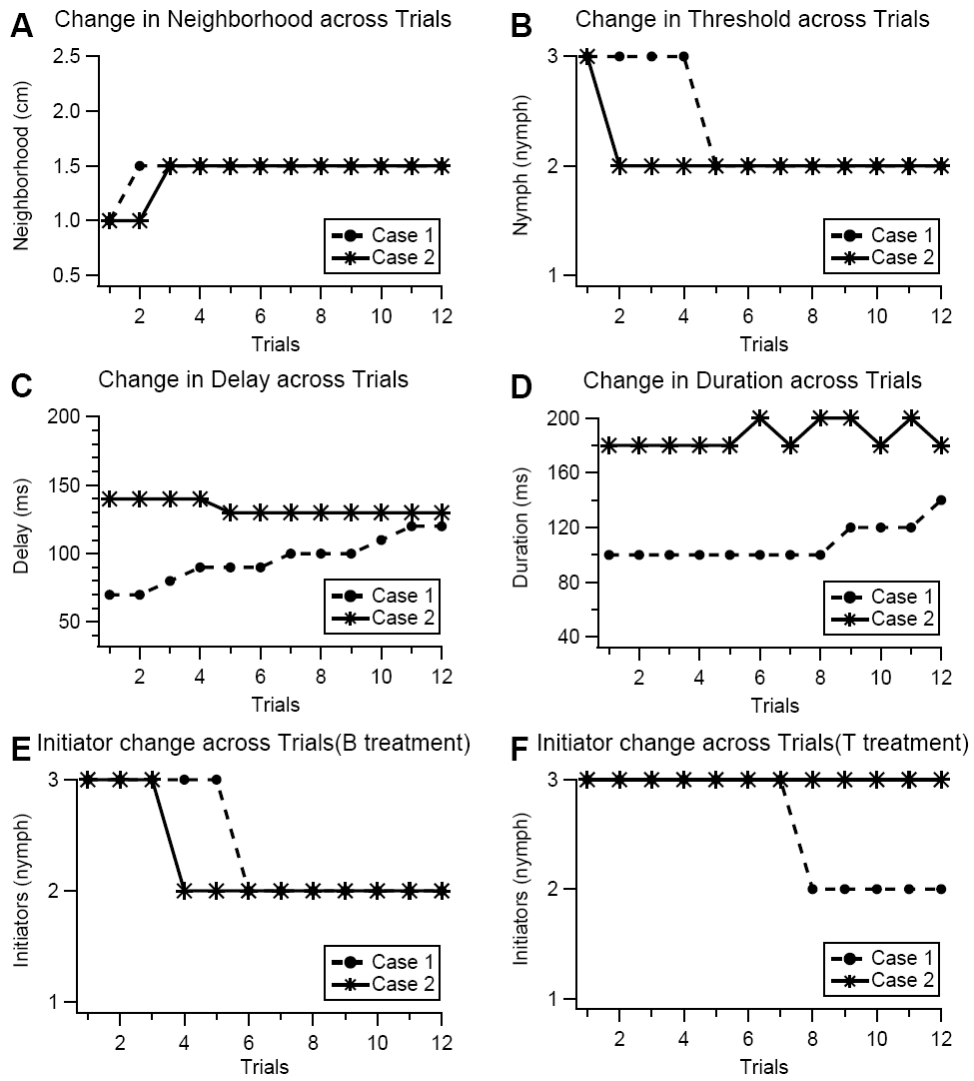


Figure 7. Convergence of parameters across trials. **A.** Neighborhood. **B.** Threshold **C.** Delay. **D.** Duration. **E.** Initiator for bottom treatment. **F.** Initiator for top treatment.

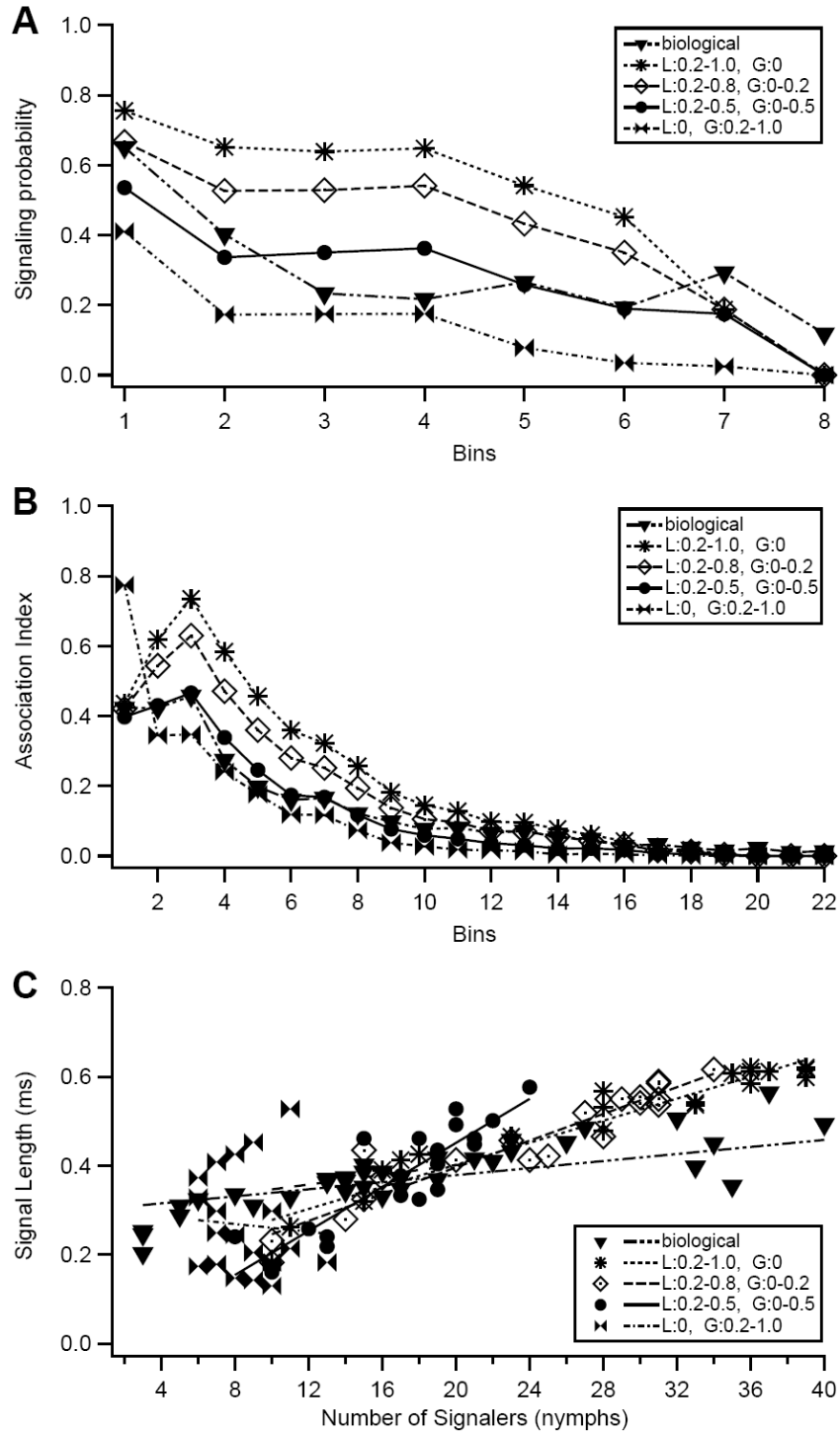


Figure 8. Comparing the influence of varying the importance of global information on **A.** Signaling Probability. **B.** Association Index. **C.** Signal Length.

CHAPTER 6

Conclusions and Future Research

Biophysical computational models were developed at the molecular, cellular and behavioral levels for three neuroscience topics. Biological models at a molecular level were developed to elucidate the mechanisms of cue-primed cocaine reinstatement in rats. At the network level, a model of a basal amygdala circuit was developed to understand how three different classes of cells are formed in that structure after auditory fear conditioning in rats. At the behavior level, an agent based model was developed to understand the emergence of antipredator signals in a colony of treehopper insects (*Umberia crassicornis*) protected by a mother. The contributions of the dissertation are summarized below, together with brief descriptions of future research extensions.

6.1. SUMMARY

Molecular Level Modeling

A biologically realistic molecular diffusion model of the PFC-NAc synapse verified that a 30-40% down-regulation of transporters was necessary to obtain experimentally observed increases in glutamate concentrations in rats during cocaine-seeking. This model further quantified the contribution of cystine glutamate exchangers in control and cocaine seeking cases, and provided molecular insights into receptor activity at steady state conditions. The framework also helped characterize diffusion path lengths and the contribution of glial geometry on synaptic isolation.

Future research pertaining to this topic include the following: (i) inclusion of other neurotransmitters such as dopamine in the model, and also considering multiple synapses to see how neuroplasticity due to cocaine might affect the firing of the post-synaptic cell; and (ii) development of molecular level models to quantify LTP and LTD in both pre- and post-synaptic terminals in the PFC-NAc synapse.

Network Level Modeling

Working closely with neuroscientists we modeled the Basal Amygdala nucleus of the fear circuit to determine how different connectivity between cells could give rise to clusters of fear, extinction, extinction-resistant and extinction cells, after classical auditory fear conditioning.

Future research pertaining to this topic includes the following: (i) studying the role of BA oscillations in enabling learning; and (ii) studying the modulation of the fear and extinction cells by contextual factors by including a model of the hippocampus.

Behavior Level Modeling

An agent-based computational model was used to understand how complex, adaptive behavior emerge from simple behavioral rules, in a colony of group dwelling insects, *Umbonia*. The model predicted the underlying rules and parameters used by nymphs to produce antipredator signals. It also predicted relationship between agent parameters and spatio-temporal characteristics, and helped establish and quantify the role of global information in antipredator signaling, something that was previously assumed to be solely based on local cues.

Future research pertaining to this topic includes: (i) Experimentally verifying the model prediction that global cues affect nymph signaling; (ii) Using the model to estimate the time when the nymph decides to signal by further decomposing the parameter Delay in Perception, Decision and Neuronal Delay; and (iii) using high speed camera analysis to verify the order of nymph signaling.

Appendix A.1

Computational model of extracellular glutamate in the nucleus accumbens incorporates neuroadaptations by chronic cocaine

A.1.1. ABSTRACT

Chronic cocaine administration causes instability in extracellular glutamate in the nucleus accumbens that is thought to contribute to the vulnerability to relapse. A computational framework was developed to model glutamate in the extracellular space, including synaptic and nonsynaptic glutamate release, glutamate elimination by glutamate transporters and diffusion, and negative feedback on synaptic release via metabotropic glutamate receptors (mGluR2/3). This framework was used to optimize the geometry of the glial sheath surrounding excitatory synapses, and by inserting physiological values, accounted for known stable extracellular, extrasynaptic concentrations of glutamate measured by microdialysis and glutamatergic tone on mGluR2/3. By using experimental values for cocaine-induced reductions in cystine-glutamate exchange and mGluR2/3 signaling, and by predicting the down regulation of glutamate transporters, the computational model successfully represented the experimentally observed increase in glutamate that is seen in rats during cocaine-seeking. This model provides a mathematical framework for describing how pharmacological or pathological conditions influence glutamate transmission measured by microdialysis.

A.1.2. INTRODUCTION

Repeated cocaine administration causes enduring changes in glutamate transmission in the nucleus accumbens that may contribute to relapse vulnerability (Kalivas et al.,

2005). These changes include alterations in glutamate release (McFarland et al., 2003), postsynaptic glutamate signaling (Conrad et al., 2008), dendritic spine morphology (Robinson and Kolb, 2004), and group II metabotropic glutamate receptors (mGluR2/3; Xi et al., 2002). The diversity of neuroadaptations has proven difficult to synthesize into a portrait of cocaine-induced pathology. While obtaining experimental measurements of glutamate transmission is critical, an alternate approach is to mathematically model an ‘archetypal’ synapse by extracting common features of the synaptic environment from a large number of synapses (Clements et al., 1992; Kleinle et al., 1996; Rusakov and Kullmann, 1998; Rusakov, 2001; Barbour, 2001; Diamond, 2005; Saftenku, 2005). These models have focused on synaptic glutamate release, diffusion out of the synapse and elimination by glutamate transporters (XAG) in an effort to understand the accessibility of synaptically released glutamate to the extracellular environment.

The mathematical models cited are based upon *in vitro* electrophysiological research and are appropriate for assessing concentrations of glutamate in the synaptic cleft and the near adjacent perisynaptic environment. However, *in vivo* extrasynaptic concentrations assessed by microdialysis reveal that the majority of glutamate outside of the synaptic cleft is not of synaptic origin (Miele et al., 1996; Timmerman and Westerink, 1997; Melendez et al., 2005). Also, extracellular glutamate in tissue slices and cell culture experiments is partly of nonsynaptic origin (Jabaudon et al., 1999; Haydon, 2001; Le Meur et al., 2007). While a number of sources of nonsynaptic extracellular glutamate have been suggested (Danbolt, 2001; Haydon, 2001; Cavelier et al., 2005), extracellular glutamate measured by microdialysis in the accumbens arises primarily from cystine-glutamate exchange (xc-; Baker et al., 2002; Xi et al., 2002). Cystine-glutamate exchange

is the rate-limiting step in glutathione synthesis (McBean, 2002), and glutamate derived from xc- stimulates perisynaptic mGluR2/3, and thereby inhibits synaptic glutamate release (Xi et al., 2002; Moran et al., 2005).

These data indicate that mathematical modeling of glutamate transmission should include nonsynaptic sources of glutamate. Moreover, rats withdrawn from chronic cocaine administration show dysregulation of extracellular glutamate in the nucleus accumbens due, in part, to reduced xc- and mGluR2/3 signaling (Baker et al., 2003; Madayag et al., 2007). Therefore, including extrasynaptic glutamate is required to model relevant cocaine-induced neuroplasticity. Also, while mathematical models considering only synaptically released glutamate predict that each glutamate synapse functions in relative isolation from other synapses (Kleinle et al., 1996; Barbour, 2001; Lehre and Rusakov, 2002; Sykova, 2004), microdialysis during cocaine-seeking measures significant overflow of synaptic glutamate (McFarland et al., 2003, 2004).

In order to reproduce cocaine-induced adaptations in extracellular glutamate, we modeled synaptic glutamate transmission, different glial geometries populated with XAG and xc-, and the regulation of glutamate release by mGluR2/3. Combining physiological values from the literature and empirically derived changes produced by chronic cocaine, the proposed mathematical framework was able to accurately portray both basal and cocaine altered extracellular glutamate levels as measured by microdialysis.

A.1.3. METHODS

A.1.3.1. Model inputs and baseline diffusion, binding and transport parameters

Baseline physiological parameters for glutamate transmission were employed, primarily as described in previous models of glutamate transmission (table 1). The principal mechanisms involved in transient glutamate dynamics in the perisynaptic region are glutamate diffusion out of the synapse after release, binding to transporters and uptake into glia (Danbolt, 2001), production of glutamate by the xc- located in glia (Pow, 2001; Sato et al., 2002), and activation of mGluR2/3 autoreceptors reducing synaptic release probability (Dietrich et al., 2002; Losonczy et al., 2003; Billups et al., 2005).

Synaptic release and regulation by mGluR2/3 autoreceptors. *In vivo* estimates of basal firing frequency in prefrontal cortical (PFC) neurons projecting to the nucleus accumbens range from 1 to 3 Hz with the capacity for periods of burst firing up to 15 Hz (Chang et al, 1997; Peters et al., 2005; Sun and Rebec, 2006). Although the probability that an action potential will release a synaptic vesicle can range from <0.1 to 1 depending upon the experimental preparation (Allen and Stevens, 1994; Murthy and Sejnowski, 1997), the average synaptic release probability more typically ranges from 0.1 to 0.5, with estimates for cortex being at ~0.4 (Trommershauser et al., 2003; Billups et al., 2005; Volynski et al., 2006). Release probability at glutamatergic synapses is reduced by up to 50% following stimulation of presynaptic mGluR2/3 autoreceptors (Dietrich et al., 2002; Losonczy et al., 2003; Billups et al., 2005), which are located outside of the synaptic cleft (Alagarsamy et al., 2001). Using *in vivo* microdialysis it has been shown that blocking mGluR2/3 elevates extracellular concentrations of glutamate (Xi et al., 2002) and electrophysiological studies in tissue slices reveal that the glutamate providing this tone is

derived primarily from nonsynaptic sources (Bandrowski et al., 2003; Moran et al., 2005). Given these studies indicating that partial tone exists on mGluR2/3 regulating glutamate release, the basal levels of glutamate in the vicinity of perisynaptic mGluR2/3 were adjusted in the present model to produce ~50% occupancy, based upon the range of K_d and K_i values reported at this receptor (0.1 to 0.3 μM glutamate; Schoepp and True, 1992). In the proposed model, presynaptic tone on mGluR2/3 was computed as release probability. mGluR2/3 is a Gi-coupled metabotropic receptor, and analysis of GTP γ S binding reveals that G protein signaling by stimulating mGluR2/3 is increased as a logarithm of agonist dose (Xi et al., 2002; Bowers et al., 2004). Thus, the relationship between release probability and mGluR2/3 occupation was modeled as the logarithm of glutamate concentration, with a $K_d = 0.187 \mu\text{M}$ glutamate (Schoepp and True, 1992) and maximum release probability with no mGluR2/3 stimulation set at 0.4 (see above). Each action potential provoking glutamate release (a function of firing frequency and release probability) resulted in an instantaneous vesicular release of a fixed number of molecules into the cleft. This fixed number was selected iteratively from the range 4700-80,000 reported by Bruns and Jahn (1995) and set at 10,000 (table 1).

Diffusion. In a complex medium, several factors can impose constraints on diffusion, including geometry, binding, uptake, viscosity, temperature, or change in structure with time (Nicholson, 2001, Sykova, 2004, Diamond, 2005, Saftenku, 2005). Diffusion in the extracellular space is typically characterized by volume fraction α (void space/total tissue volume) and tortuosity λ (hindrance to diffusion imposed by local boundaries or local viscosity) (Nicholson, 2001). Volume fraction α in brain tissue is estimated to be around 0.2 (Nicholson and Sykova, 1998). Tortuosity λ varies due to

constriction, wiggle and topological factors (Nicholson, 2001) and is estimated to be ~1.2-2.4 based on diffusion measurements over a range of 100-300 μm (Nicholson, 2001). Rice and Nicholson (1991) reported values for α and λ as 0.21 and 1.54, respectively, for the rat striatum. To account for the complex factors cited, diffusion coefficient values have been reported in the range from 0.05-0.41 $\mu\text{m}^2/\text{ms}$ (Saftenu, 2005), based on typical tortuosity estimates. Further, different cellular elements including spines, small axonal boutons, protein, glia, and microfilaments may result in additional tortuosity in the microenvironment of a synapse (Saftenu, 2005). Experimental estimates of diffusion coefficients in the perisynaptic region have not been reported for synapses with tightly packed glia. In the proposed model, with high density glia close to the synapse, we iteratively determined the diffusion coefficients to satisfy steady state and transient constraints on glutamate concentrations at three locations (P_{syn} , P_{mGluR} , and P_{ex} in figure 1). This iterative process is described in more detail below.

Glutamate transporters (XAG). Glutamate transport into glia is the primary mechanism for eliminating extracellular glutamate (Danbolt, 2001). XAG uptake rates depend on local glutamate concentration and the kinetics of transporter binding (see eqn. 3 below). The glutamatergic axon terminals from the PFC to the accumbens were assumed to be covered by a glial sheath (Lehre et al., 1995). The density of XAG is non-uniform, and glial membranes that face neuropil have a higher expression of transporters than membrane surfaces facing other glia (Cholet et al., 2002). XAG are expressed with a high density in the hippocampus, with surface density ranging from 2500-10,800 molecules/ μm^2 (Bergles and Jahr, 1997; Lehre and Danbolt, 1998). Based upon glutamate uptake assays (Colombo, 2005) and transporter binding studies (Danbolt, 2001) it was

estimated that surface density values for XAG in the nucleus accumbens is 22-35% (550-3780 molecules/ μm^2) of the value in the hippocampus and cortex. Thus, for the present model (where XAG is volume populated as described later), the equivalent surface density of XAG was determined iteratively by varying it within the range of 550-3780 molecules/ μm^2 (table 1).

Cystine-glutamate exchangers (xc-). Wyatt et al. (1996) estimated the maximum uptake rate for cystine to be 450 $\mu\text{M hr}^{-1}$ based on cerebellar slices. The density of xc- in the cortex is higher by a factor of 2.4 compared to the cerebellar molecular layer (1 mM hr^{-1} ; Warr et al. 1999). Based on microdialysis studies, Baker et al. (2003) reported basal extracellular glutamate concentrations to be 1.1 and 5.6 μM in the prefrontal cortex and nucleus accumbens, respectively. Iterations to satisfy model constraints resulted in the consideration of a range from 5 – 50 mM hr^{-1} for the density of xc- in the nucleus accumbens and a final value of 41 mM hr^{-1} under basal conditions (table 1).

A.1.3.2. Model inputs and cocaine-induced neuroadaptations

The parameters adjusted in the model to estimate neuroadaptive changes produced by withdrawal from chronic cocaine are outlined in table 2. Withdrawal from daily cocaine administration elicits a 50% reduction in K_m for [^{35}S] cystine uptake into accumbens tissue slices (Baker et al., 2003), and recently a 40% reduction in cystine uptake was reported after withdrawal from cocaine self-administration (Madayag et al., 2007). Also, a 40% reduction in the concentration of glial transporter (GLT-1) has been reported in membrane homogenates from the nucleus accumbens of rats withdrawn from cocaine self-administration (Knackstedt et al., 2007). Based upon these data the concentration of

xc- was reduced by 50% (table 2). Previous studies using [³⁵S]GTP γ S binding in accumbens homogenates revealed that G protein coupling to mGluR2/3 is reduced by approximately 70% after cocaine (Xi et al., 2002). Assuming a logarithmic relationship between [³⁵S]GTP γ S binding and vesicle release probability (see above), the cocaine-induced reduction in mGluR2/3 function was modeled as a change in release probability from 0.14 (control) to 0.34 (cocaine treated condition). Thus, a release event occurred every 2.9 action potentials in the cocaine case, instead of every 7.1 action potentials under basal conditions. Finally, cocaine-seeking behavior is associated with an increase in firing frequency of accumbens neurons, driven in part by inputs from the prefrontal cortex (Hollander and Carelli, 2007). Basal firing frequency in prefrontal pyramidal neurons can range from 1 to 15 Hz, and the neurons can burst fire at a rate of >1 burst/sec and a single burst event can include >50 spikes (Sun and Rebec, 2006). The *in vivo* basal firing of prefrontal pyramidal cells is reduced after withdrawal from self-administered cocaine (Trantham et al., 2002; Sun and Rebec, 2006), but the firing rate during burst events is significantly elevated in response to a cocaine injection in rats trained to self-administer cocaine (Sun and Rebec, 2006). The apparent hyperexcitability of prefrontal neurons after chronic cocaine may be associated with the increased excitability observed in dissociated prefrontal pyramidal cells after chronic cocaine (Dong et al., 2005). Given this complex profile of changes in pyramidal cell firing after chronic cocaine, in the present model the behavioral transition to cocaine-seeking was modeled simply as an increase in overall firing frequency from 1 (basal) to 15 Hz (cocaine-seeking).

A.1.3.3. Modeling the synapse and glial geometry

Upon release at the center of the synapse, glutamate molecules diffuse through the porous cleft into the perisynaptic space (Barbour and Hausser, 1997), where XAG dense astrocytes reduce glutamate spillover to near zero (Diamond and Jahr, 2000; Danbolt 2001). The configuration of the glial sheath (G_i in figure 1) is akin to that previously reported (Rusakov, 2001), but distinct in that in the present model we include xc-. Also, as an approximation of glial folds, the glial membranes were modeled in the form of multiple impermeable sheaths (the dark line at the center of each sheath in figure 1 represents an impermeable surface, i.e., flux=0 across this surface) with porous space in between them. XAG was volume populated on both sides of each glial sheath G_i (permeable to glutamate up to 25 nm thickness on each side of the impermeable center surface of the 50 nm thick G_i). Glutamate concentration at mGluR2/3 receptors was monitored in the model at the presynaptic location P_{mGluR} in figure 1 (compartment $i, j = 1, 2$, starting at $\theta=20^0$).

The extracellular space is thus modeled as a porous medium with four glial sheaths whose centerlines were 75 nm apart (close to the range of 38-64 nm reported in the extracellular space of the rat neocortex *in vivo* by Thorne and Nicholson, 2006). Of this 75 nm, 50 nm is volume populated with XAG and/or xc-, as described above. This permits the glutamate molecules to move up to 75 nm between the impermeable surfaces of each sheath. Based upon studies indicating that the highest densities of XAG are closer to the synapse (Lehre and Danbolt, 1998; Danbolt, 2001; Cholet et al., 2002), G_1 had the highest density of XAG and the density decreased radially outwards to G_4 . Cystine-glutamate exchangers were modeled as being located on the outer surface of the glial

membranes of regions G₄ (table 1). Beyond the last glial sheath (G₄), the extracellular space contained only glutamate without XAG or xc-. The experimentally defined concentrations of extracellular glutamate reported by *in vivo* microdialysis (table 2) were modeled as being at point P_{ex} in figure 1, outside glial region G₄.

Mathematical details. In the configuration of figure 1, the two synaptic hemispheres were assumed rigid permitting no diffusion (i.e., flux = 0 along the periphery), with synaptic radius $r = 160$ nm from the center, and a separation of $\delta = 20$ nm (synaptic cleft) (Rusakov and Kullmann, 1998; Rusakov, 2001; Diamond, 2005). Around this synapse are 40 concentric 25 nm thick shell compartments ($i_1 - i_{40}$) resulting in the outer boundary of the perisynaptic region modeled being at a distance of 1 μ m from the edge of the synapse. Each of these shells was divided into 9 compartments (20° angle increments, $j_1 - j_9$) circumferentially, permitting XAG and xc- concentrations to be assigned individually to each compartment of any shell.

The synaptic cleft volume was discretized into $m = (1 \dots N_m)$ cylindrical segments where R_m was the outer radius ($R_m = m * dR_m$) of each of the cylindrical segment with dR_m being the thickness. The width of each cylinders is δ , such that the volume of each concentric cylinder is $\pi(R_m^2 - R_{m-1}^2) * \delta$, with the contact surface between adjacent elements being $S_m = 2\pi R_m * \delta$. The extracellular space were discretized into $i = (1 \dots N_i)$ concentric spherical elements each of thickness σ , and each spherical element was divided into $j = (1 \dots N_j)$ annular sections where N_j was determined by θ . In the model for the cleft, $m=4$, and $dR_m = 40$ nm, and for the spherical shells, $\sigma=25$ nm and $\theta = \pi/9$ rad.

The specific mathematical equations used are described next. These standard conservation and flux equations (see Rusakov, 2001 for a comprehensive description

including derivations) were used to analyze the effect of the proposed glial geometry. A mass balance for extracellular glutamate in each $(i,j)^{th}$ compartment (with XAG and/or xc-, as appropriate) yields eqn.A.1 (Rusakov, 2001),

$$Glu(i, j, t) = Glu(i, j, t - dt) + (J_R \Sigma(i, j, t) S_R + J_T \Sigma(i, j, t) S_T) \frac{dt}{V(i, j)} + (v_+ - v_-) dt$$

(A.1)

where dt was the time step, $S_R(i, j) = 2\pi R_i^2 (\cos \theta_j - \cos \theta_{j-1})$ was the surface area between adjacent volume elements in the radial direction, and $S_T(i, j) = 2\pi R_i \sin \theta_j^*(\sigma)$ was the surface area shared by adjacent volume elements in the tangential direction, with $R_i = r + \sigma^*i$. The radial and tangential fluxes into the compartment were denoted by J_R and J_T , respectively. Each compartment had a volume of $V(i, j) = 0.5(S_R(i, j) + S_R(i-1, j)) * (\sigma)$. The term v_+ accounted for the production of glutamate by xc- and unbinding of glutamate from the transporters ($v_+ = cg(i, j) + k_I^*[Glu-XAG]$, where $cg(i, j)$ is the constant production rate of glutamate by xc- for compartment (i, j) , while the term ($v_- = k_I^*[Glu]*[XAG]$) accounted for the reduction in glutamate due to transporter binding. For compartments that are not populated with XAG or xc-, the corresponding terms in eqn. A.1 are omitted. Also, eqn.A.1 is appropriately modified for the compartments in the synaptic cleft, to exclude XAG, xc-, and the tangential flux, and include synaptic release.

The glutamate flux J_{AB} between any two adjacent volume compartments A and B was computed by eqn. A.2,

$$J_{AB}(t) = -D \nabla(Glu) = -\frac{D}{ds} (Glu_A(t - dt) - Glu_B(t - dt))$$

(A.2)

where ds was the spatial distance between compartment centroids and D the diffusion coefficient. For each compartment, this flux was calculated considering two others

connected to it radially, and two connected in the tangential direction. Within any glial compartment, binding of glutamate with transporters is governed by eqn. A.3, (Rusakov and Kullmann, 1998),



where $[Glu]$, $[XAG]$, and $[Glu-XAG]$ represent the compartmental concentrations of glutamate, transporter, and the bound complex, respectively, and $k_2*[Glu_{in}]$ represents uptake rate of glutamate by XAG.

The discrete form of the differential equation for this kinetic equation is given by eqn. set A.4 (Rusakov, 2001):

$$\begin{aligned} [Glu]_t &= [Glu]_{t-dt} + (-k_1[Glu]_{t-dt}[XAG]_{t-dt} + k_{-1}[Glu - XAG]_{t-dt})dt \\ [Glu - XAG]_t &= [Glu - XAG]_{t-dt} + \{-(k_{-1} + k_2)[Glu - XAG]_{t-dt} + k_1[Glu]_{t-dt}[XAG]_{t-dt}\}dt \\ [Glu - XAG]_t + [XAG]_t &= [Glu - XAG]_{t-dt} + [XAG]_{t-dt} = [XAG_{total}] \\ [Glu_{in}]_t &= [Glu_{in}]_{t-dt} + k_2 * [Glu - XAG]_{t-dt} * dt \end{aligned} \quad (\text{A.4})$$

The kinetics for XAG were taken from Rusakov (2001) and Lehre and Rusakov (2002) who based it on experiments reported in the literature (Wadiche et al., 1995; Bergles and Jahr, 1998), $k_1 = 10^4 \text{ M}^{-1}\text{ms}^{-1}$, $k_{-1} = 0.2 \text{ ms}^{-1}$, and $k_2 = 0.1 \text{ ms}^{-1}$. For the outermost shell, e.g., $i = 40$, the boundary condition of flux = 0 was imposed at the outer edge of all compartments, to simulate identical neighboring synapses. That is, no flux enters or leaves the outer boundary of this shell.

Iterative evaluation. The computational model was developed using C++ software (Microsoft Visual Studio, 2005), and an integration time step of 0.5 μs was used. The concentration of glutamate was considered uniform in each compartment and this concentration was updated (eqns. 1-4) at each integration interval based on diffusion,

uptake by XAG, and production rates for glutamate, as appropriate. Conservation of molecules was confirmed at each time step by computing the numbers of free, bound and transported glutamate molecules. To check for numerical accuracy, we decreased the integration time step by a factor of 10 and found no significant change in concentration estimates. Similarly, insignificant changes in the same estimates were found with variation of spatial resolution of compartments by 50%.

To implement a volume fraction of $\alpha = 0.2$ (Nicholson and Sykova, 1998) in the model shown in figure 1 (which was also iteratively derived; details not shown), we approximated shells $i=20-40$ to be representing cellular obstacles (i.e., space that glutamate cannot flow into), with an effective extracellular space from $i=1-20$ for glutamate overflow. This implies that P_{ex} is now measured in shell 20. The model showed that in the space outside the glial sheaths (i.e., outside shell 12) the steady state concentration of glutamate was uniform for any number of total outside shells, and differed by less than $0.01 \mu\text{M}$ for all cases considered. This observation justifies selection of P_{ex} anywhere in the space outside G_4 for measurement purposes.

As cited earlier, diffusion coefficients close to the synapse have not been reported for synapses with tight glial coverage. With the porous glial geometry in figure 1, we considered three apparent diffusion coefficients, one in the synapse (D_{syn} near P_{syn}), one in the sheath region (D_{sh} in the region that has P_{mGluR}) and one outside the glial sheath region (D_{ex} in the region that has P_{ex}). We noticed that the flow dynamics was governed solely by D_{sh} , with insignificant effects due to variations in D_{syn} and D_{ex} within the range of 0.05 to $0.41 \mu\text{m}^2/\text{ms}$ (data not shown). Accordingly, we used a uniform value of D (from the same range cited above) for all the regions in the model, without loss of

accuracy. It should be noted that the glial sheaths added geometric tortuosity in the model.

The model was adjusted by changing the following parameters within the ranges outlined in table 1: number of molecules/release, xc- concentration, diffusion coefficient and XAG concentration. The iterative process began with values in the lower end of the ranges for these parameters, while monitoring the concentrations of glutamate at P_{syn} , P_{mGluR} , and P_{ex} (figure 1), for the basal control case (2 Hz). When the densities of XAG were iteratively changed in glial sheaths G_i , their relative proportions were maintained, i.e., density (G_1) > density (G_2) and so on. Through this iterative process, numerous solutions were found that satisfied empirically determined concentrations at P_{syn} , P_{mGluR} , and P_{ex} for the control case at 2 Hz (table 2).

After satisfying the requirements for the basal control case, we simulated the basal cocaine and drug-seeking situation by modeling known cocaine-induced changes to xc- and mGluR2/3 signaling (modeled as release probability, see above). Through further iterative changes we identified multiple parameter sets that satisfied some of the constraints in table 2, and the model values listed in table 1 constitute values that satisfied all the constraints simultaneously.

A.1.4. RESULTS

A.1.4.1. Geometry of the glial sheath

Multiple 3-D spherical configurations were studied for glia surrounding the synapse by varying glial coverage, thickness and openings (similar to those in Rusakov, 2001; Barbour, 2001; data not shown). Table 1 shows the range of diffusion coefficients,

number of molecules per release, as well as XAG and xc- concentrations in the various glial sheaths. These were varied iteratively to determine the configuration that brought glutamate concentration at P_{ex} (extracellular compartment sampled by microdialysis) into the range outlined in table 2 at both low and high firing frequencies. At the same time, concentrations at P_{syn} and P_{mGluR} were constrained to be <200 nM. This process involved simultaneous variations of the parameters (see Methods). Following this iterative process, the configuration in figure 1 proved most robust at sustaining glutamate concentrations within the acceptable ranges. Of note, the basal control concentration at P_{ex} did not exceed the range measured by microdialysis at firing frequencies of 15 Hz (table 3, figure 2A). Also, by providing resistance to the flow of glutamate, this configuration established the necessary gradient to support levels of extracellular glutamate at P_{syn} approaching those estimated from *in vitro* slice physiology (Herman and Jahr, 2007) and at P_{mGluR} that are consistent with *in vivo* tone being present on mGluR2/3 (Xi et al., 2002). Thus, at both low and high frequency stimulation, P_{mGluR} remained between 0.1 and 0.3 μ M, which approximates the K_d for glutamate binding to mGluR2/3 (0.19 μ M; Schoepp and True, 1992).

Figure 2B shows how the increase in P_{mGluR} associated with increased firing frequency negatively regulated release probability, i.e., as P_{mGluR} increased with increasing synaptic release, the release probability decreased from 0.14 to 0.12. Thus, as firing frequency ranged from 1 to 15 Hz, the peak concentration at P_{syn} reached as high as 10 mM, which, when averaged over 100 μ s around this peak, resulted in a maximum value of 0.5 mM (figure 2C). As well, transient glutamate concentrations in the synapse (at P_{syn}) were biphasic and within ranges reported by Clements (1996) and Bergles et al.

(1999). The resting concentration at P_{syn} between release events ranged from 0.16 to 0.19 μM (table 3). These levels are somewhat higher than recent published estimates which range from 25 to 100 nM using tonic activity at NMDA receptors in tissue culture (Herman and Jahr, 2007; Le Meur et al., 2007), and could reflect a lack of neuronal glutamate uptake in the present model. Figure 2C also shows the effect of seeking natural rewards (e.g., food that was modeled as an increase in firing frequency to 15 Hz). In this control situation, the level of extracellular glutamate at P_{ex} agreed with measurements and was not significantly different from basal (i.e., remained in the range of 4.6-6.6 μM ; McFarland et al., 2003).

A.1.4.2. Effect of withdrawal from chronic cocaine

Table 2 illustrates the alterations made in parameters by incorporating experimentally determined values for reduced xc- and mGluR2/3 desensitization after chronic cocaine (Xi et al., 2002; Baker et al., 2003). In addition, concentrations at P_{ex} approximated the basal values determined by microdialysis in the accumbens after withdrawal from chronic cocaine, as well as peak values elicited after inducing cocaine-seeking.

The model constraints for the basal extracellular concentration measured by dialysis in P_{ex} after cocaine was in the range of 2.55-3.23 μM (Baker et al., 2003; Szumlinski et al., 2006), and figure 3 shows that when the chronic cocaine-induced changes in xc-, mGluR2/3 and basal firing frequency were introduced, the model accurately depicted the reduced basal levels. However, when cocaine-seeking was introduced into the model (i.e., 15 Hz firing frequency) the extracellular concentration of glutamate (P_{ex}) was expected to be in the range of 11.9-14.7 μM (McFarland et al., 2003, 2004; Szumlinski et al., 2006), and levels attained only 6.3 μM (see figure 3, 0% reduction in XAG).

A.1.4.3. Down regulation of XAG predicts chronic cocaine concentrations

Since the computational model based upon established cocaine-induced neuroadaptations failed to reproduce observed extracellular glutamate concentrations elicited during cocaine-induced drug seeking, other parameters were considered, such as XAG, molecules per release event, volume fraction, ECS width, and apparent diffusion coefficient. Multiple iterations of changes in these parameters revealed that down-regulating XAG produced changes in extracellular glutamate that mimicked those elicited in vivo, while changing the other parameters had lesser or no impact. Figure 3 shows the iterative analysis of changing XAG, and that when XAG was reduced by 40%, increasing firing frequency to 15 Hz produced extracellular glutamate levels in the range observed by microdialysis during cocaine seeking (11.9-14.7 μM).

Figure 4 illustrate the outcome for concentrations at P_{syn} , P_{mgluR} and P_{ex} after introducing the cocaine-altered parameters for xc- and mGluR2/3 (modeled as release probability, see Methods), a 40% reduction in XAG based upon the data in figure 3, and stimulating synaptic transmission at 1 to 15 Hz. Over a firing frequency of 1 to 15 Hz, the change in concentration at P_{mGluR} was similar to that at P_{syn} (table 3). Note that release probability did not change appreciably even though P_{mGluR} increased as a function of increased firing frequency due to the fact that mGluR2/3 signaling is reduced by 70% after chronic cocaine (Xi et al., 2002). By including a 40% reduction in XAG along with the cocaine-induced reductions in xc- and mGluR2/3 signaling, P_{ex} values were in the expected range under both basal (1 Hz) and cocaine seeking (15 Hz) conditions.

A.1.5. DISCUSSION

A computational modeling framework for studying glutamate homeostasis in prefrontal glutamatergic synapses onto nucleus accumbens spiny cells is reported that reproduced extracellular glutamate concentrations as measured by *in vivo* microdialysis. The parameters used include those previously employed in computational models of excitatory neurotransmission, such as synaptic release, diffusion from the synaptic cleft and glutamate uptake, as well as parameters not typically modeled, including xc- and negative feedback on synaptic release by perisynaptic mGluR2/3. These latter parameters were included to model changes in extracellular glutamate concentrations produced by chronic cocaine administration that are hypothesized to result at least in part from cocaine-induced reductions in xc- and mGluR2/3 signaling (Xi et al., 2002; Baker et al., 2003; Moran et al., 2005). The computational model successfully reproduced extracellular concentrations at different firing frequencies in control accumbens. Although incorporating cocaine-induced reductions in xc- and mGluR2/3 signaling reproduced the reduction in concentrations at P_{ex} at low firing frequencies, it was necessary to incorporate a reduction in XAG to predict the large increase at P_{ex} that occurs at the higher firing frequencies achieved during cocaine-seeking. Importantly, recent reports indicate that XAG is reduced in the accumbens after withdrawal from self-administered cocaine, including lower levels of the primary glial transporter, GLT-1, and a decrease in $^3[H]$ -glutamate uptake (Knackstedt et al., 2007).

A.1.5.1. Effect of chronic cocaine on glutamatergic transmission

Withdrawal from repeated cocaine administration results in two changes in extracellular glutamate measured by microdialysis: 1) reduced basal concentrations, and

2) increased levels of glutamate after an acute injection of cocaine that induces cocaine-seeking or sensitized motor activity (Pierce et al., 1996; Reid and Berger, 1996; Hotsenpiller et al., 2001; Baker et al., 2003; McFarland et al., 2003; Madayag et al., 2007). Under basal conditions, glutamate measured by microdialysis is almost entirely of nonsynaptic origin (Miele et al., 1996; Timmerman and Westerink, 1997; Melendez et al., 2005), while the increase following a cocaine injection in chronic cocaine treated animals is of synaptic origin (i.e., blocked by tetrodotoxin or inhibiting prefrontal glutamatergic inputs to the accumbens; Pierce et al., 1996; McFarland et al., 2003). Importantly, an increase in extracellular glutamate (either synaptic or nonsynaptic) does not accompany an acute injection of cocaine or operant responding in animals trained to seek natural rewards such as food (Pierce et al., 1996; Hotsenpiller et al., 2001; McFarland et al., 2003). Thus, in the accumbens of animals chronically pretreated with cocaine, synaptic glutamate transmission appears to escape from the immediate synaptic environment and is measured in significant amounts outside of the synaptic region. The overflow of synaptic glutamate in animals withdrawn from cocaine is in contrast to the lack of diffusion by significant amounts of synaptic glutamate to adjacent synapses predicted under physiological conditions by previous mathematical models (Barbour, 2001; Lehre and Rusakov, 2002; Sykova, 2004) or empirically derived using *in vivo* microdialysis (Miele et al., 1996; Timmerman and Westerink, 1997; Melendez et al., 2005). Thus, it is possible that the cocaine-induced glutamate overflow may be a critical event in addiction. However, stress induces overflow of glutamate in the striatum or prefrontal cortex that is inhibited by TTX (Moghaddam, 2002), indicating that at least

some biological stimuli can also induce release of synaptic glutamate measurable by dialysis.

The concentrations of glutamate estimated by the model at P_{mGluR} and at P_{syn} are presumably capable of stimulating perisynaptic and synaptic glutamate receptors in adjacent synapses, since at 15 Hz firing frequency (e.g., during drug-seeking), the model predicted that the concentration of glutamate at P_{syn} and at P_{mGluR} are 1.1 and 1.2 μM , respectively, and the estimated K_d values for mGluR2 and NMDA receptors are in the range of 200 nM and 2 μM , respectively (Patneau and Mayer, 1990; Schoepp and True, 1992). Moreover, this concentration of glutamate would be expected to partially desensitize NMDA receptors (Cavelier et al., 2005), and could contribute to the increase in AMPA/NMDA current ratio (Kourrich et al., 2007) and AMPA receptor membrane insertion seen after chronic cocaine (Conrad et al., 2008).

A.1.5.2. Limitations of the proposed mathematical model

Two general limitations exist in the proposed model. The first limitation is the simplicity of the model relative to the known physiology and cocaine-induced changes in glutamate transmission. Notably, only occupancy of mGluR2/3 is considered, but occupancy of mGluR1 or mGluR5 can be expected to change glutamate release and synaptic scaling (Malenka and Bear, 2004; Kreitzer and Malenka, 2005), and mGluR1/5 content and/or function is altered by chronic cocaine administration (Swanson et al., 2001; Szumlinski et al., 2006). In addition to xc-, there are other sources of nonsynaptic glutamate release that may tonically stimulate glutamate receptors, such as calcium-dependent release from astroglia and release from junction hemi-channels (Danbolt, 2001; Cavelier et al., 2005). Also, multiple parameter variation studies (e.g.,

simultaneous variations in volume fraction and down-regulation of XAG) should be performed to investigate if they reliably predict the observed changes in extracellular glutamate concentration. Finally, while the glial geometry used in the framework is a reflection of endogenous tortuosity, it oversimplifies the more varied *in vivo* structural geometry. Thus, future models need to consider additional dynamic cellular processes that accompany alterations in firing frequency, as well as more complicated morphological geometries. In addition, it will be important to examine the model in situations known to inhibit drug-seeking *in vivo*, such as by activating cystine-glutamate exchange using N-acetylcystine (Baker et al., 2003; Madayag et al., 2007).

A second important consideration is that in contrast to the standard mathematical models using postsynaptic currents to empirically validate synaptic concentrations of extracellular glutamate, the present model employed *in vivo* microdialysis measures. Although the strengths of microdialysis are that estimates are made *in vivo* and nonsynaptic release is readily determined, microdialysis induces damage artifacts that are distinct from the damage artifacts produced by dissecting tissue for *in vitro* measurements. Two distinctions between estimates of extracellular glutamate made *in vitro* versus with *in vivo* microdialysis are particularly relevant. The first is that previous microdialysis estimates of extraction fraction (i.e. the slope of the line in the no net flux experiment; Bungay et al., 2003) that is used to determine the elimination rate of glutamate in brain tissue by passing different concentrations of glutamate through the probe, found no apparent change in uptake (Baker et al., 2003). In contrast, both [³H]-glutamate uptake and membrane protein content of GLT-1 are reduced ~40% in the accumbens (Knackstedt et al., 2007). Recent modeling of microdialysis concludes that

the extraction fraction may not be a reliable estimate of transmitter uptake (Bungay et al., 2003; Chen, 2006). The reasons for this are two-fold. 1) The presence of a tissue trauma layer changes the tissue resistance and volume in the vicinity of the dialysis probe. While this markedly affects the estimates of extraction fraction, it does not impact the net flux estimate of basal transmitter concentration. 2) The distribution of XAG within the present model is based upon data indicating that uptake sites are concentrated in the vicinity of the synaptic cleft (Lehre and Danbolt, 1998; Danbolt, 2001), while nonsynaptic glutamate release via xc- was inversely distributed with the highest concentration of xc- being found away from the synapse (Sato et al., 2002). This distribution of XAG and xc- can contribute to both the lack of TTX sensitivity in basal glutamate levels and the relatively poor capacity to detect uptake-dependent changes in the extraction fraction (Bungay et al., 2003).

The second distinction raised by modeling glutamate transmission based upon microdialysis measurements relative to in vitro measures is revealed by estimates of extracellular glutamate using NMDA currents in tissue slices being 1-3 orders of magnitude less than dialysis measurements (Cavelier et al., 2005; Herman and Jahr, 2007). However, this fact is largely incorporated into the proposed model that contains a steep gradient of glutamate concentrations between the synapse ($P_{\text{mGluR}} < 0.2 \mu\text{M}$ where the electrophysiological measures are obtained) and the site where the dialysis measurements occur ($P_{\text{ex}} = 5.04 \mu\text{M}$).

A.1.6. CONCLUSIONS

A computational framework of glutamate transmission is presented that incorporates both synaptic and nonsynaptic glutamate release and homeostatic regulation of synaptic release via stimulation of mGluR2/3 autoreceptors. This model accurately reproduced the basal levels of extracellular glutamate measured by microdialysis, as well as the levels of glutamate in the vicinity of mGluR2/3 that provide inhibitory tone on synaptic release. However, in order to achieve changes in extracellular glutamate observed during cocaine seeking, the model required a 40% down-regulation of XAG. Thus, this model provides a general mathematical framework for describing how pharmacological or pathological conditions influence glutamate transmission, and for predicting potential cocaine-induced neuroadaptations (e.g. reduced XAG) that may be important to experimentally evaluate.

A.1.7. ACKNOWLEDGEMENTS

This research was supported in part by USPHS grants DA015369, DA03906 (PWK), and subcontract from DA015369 to University of Missouri (SSN).

A.1.8. NORMANCLATURE

mGluR2/3, Metabotropic glutamate receptors;

xc-, Cystine-glutamate exchange;

XAG, Glutamate transporters;

PFC, Prefrontal cortex;

P_{syn} , P_{mGluR} , and P_{ex} , Glutamate concentrations at synapse, mGluR and extracellular space;

G_i , Glial sheath;

D_{syn} , D_{sh} and D_{ex} , Diffusion coefficient in the synapse, between the sheath and extracellular space;

TTX, Tetrodotoxin;

AMPA, Alpha-amino-3-hydroxy-5-methyl-4-isoxazolepropionic acid;

NMDA, N-methyl-D-aspartic acid;

GLT-1, Glutamate transporter protein

A.1.9. REFERENCES

1. Alagarsamy S, Sorensen SD, Conn PJ (2001) Coordinate regulation of metabotropic glutamate receptors. *Cur Op Neurobiol* 11:357–362.
2. Allen C, Stevens CF (1994) An evaluation of causes for unreliability of synaptic transmission. *Proc Natl Acad Sci USA* 91: 10380-10383.
3. Baker DA, Xi ZX, Shen H, Swanson CJ, Kalivas PW (2002) The origin and neuronal function of in vivo nonsynaptic glutamate. *J Neurosci* 22: 9134-9141.
4. Baker DA, McFarland K, Lake RW, Shen H, Tang XC, Toda S, Kalivas PW (2003) Neuroadaptations in cystine-glutamate exchange underlie cocaine relapse. *Nat Neurosci* 6:743-749.
5. Bandrowski AE, Huguenard JR, Prince DA (2003) Baseline glutamate levels affect group I and II mGluRs in layer V pyramidal neurons of rat sensorimotor cortex. *J Neurophysiol* 89:1308-1316.
6. Barbour B (2001) An evaluation of synapse independence. *J Neurosci* 21: 7969-7984.
7. Barbour B, Hausser M (1997) Intersynaptic diffusion of neurotransmitter. *Tr Neurosci* 20:377-384.
8. Bergles DE, Jahr CE (1997) Synaptic activation of glutamate transporters in hippocampal astrocytes. *Neuron* 19:1297–1308.
9. Bergles DE, Jahr CE (1998) Glial contribution to glutamate uptake at schaffer collateral-commissural synapses in hippocampus. *J Neurosci* 18:7709-7716.
10. Bergles DE, Diamond JS, Jahr CE (1999) Clearance of glutamate inside the synapse and beyond. *Curr Op Neurobiol* 9:293–298.
11. Bowers MS, McFarland K, Lake RW, Peterson YK, Laphis CC, Gregory ML, Lanier SM, Kalivas PW (2004) Activator of G-protein signaling 3: a gatekeeper of cocaine sensitization and drug-seeking. *Neuron* 42: 269-281.
12. Billups B, Graham BP, Wong AY, Forsythe ID (2005) Unmasking group III metabotropic glutamate autoreceptor function at excitatory synapses in the rat CNS. *J Physiol (Lond)* 565:885-896.

13. Bruns D, Jahn R (1995) Real-time measurement of transmitter release from single synaptic vesicles. *Nature* 377: 62-65.
14. Bungay PM, Newton-Vinson P, Isele W, Garris PA, Justice Jr. JB (2003). Microdialysis of dopamine interpreted with quantitative model incorporating probe implantation trauma. *J Neurochem* 86: 932–946.
15. Cavelier P, Hamann M, Rossi D, Mobbs P, Attwell D (2005) Tonic excitation and inhibition of neurons: ambient transmitter sources and computational consequences. *Prog Biophys Mol Biol* 87: 3-16.
16. Chang JY, Zhang L, Janak PH, Woodward DJ (1997) Neuronal responses in prefrontal cortex and nucleus accumbens during heroin self-administration in freely moving rats. *Brain Res* 754: 12–20.
17. Chen KC (2006) Effects of tissue trauma on the characteristics of microdialysis zero-net-flux method sampling neurotransmitters. *J Theor Biol* 238: 863–881.
18. Cholet N, Pellerin L, Magistretti PJ, Hamel E (2002) Similar perisynaptic glial localization for Na⁺, K⁺-ATPase alpha 2 subunit and the glutamate transporters GLAST and GLT-1 in the somatosensory cortex. *Cereb Cortex* 12:515-525.
19. Clements JD, Robin A, Lester J, Tong G, Jahr CE, Westbrook GL (1992) The time course of glutamate in the synaptic cleft. *Science* 258:1498-1501.
20. Clements JD (1996) Transmitter time course in synaptic cleft: its role in central synaptic function. *Tr Neurosci* 19: 163-171.
21. Colombo JA (2005) Glutamate uptake by rat brain astroglia incubated in human cerebrospinal fluid. *Med Sci Monitor* 11:BR13-7.
22. Conrad KL, Tseng KY, Uejima JL, Reimers JM, Hen LJ, Shaham Y, Marinelli M, Wolf ML (2008) Formation of accumbens GluR2-lacking AMPA receptors mediates incubation of cocaine seeking. *Nature*, in press.
23. Danbolt NC (2001) Glutamate uptake. *Prog Neurobiol* 65:1-105.
24. Diamond JS (2005) Deriving the glutamate clearance time course from transporter currents in CA1 hippocampal astrocytes: transmitter uptake gets faster during development. *J Neurosci* 25:2906-2016.
25. Diamond JS, Jahr CE (2000) Synaptically released glutamate does not overwhelm transporters on hippocampal astrocytes during high-frequency stimulation. *J Neurophysiol* 83: 2835-2843.
26. Dietrich D, Kral T, Clusmann H, Friedl M, Schramm J (2002) Presynaptic group II metabotropic glutamate receptors reduce stimulated and spontaneous transmitter release in human dentate gyrus. *Neuropharmacol* 42:297-305.
27. Dong Y, Nasif FJ, Tsui JJ, Ju WY, Cooper DC, Hu XT, Malenka RC, White FJ (2005) Cocaine-induced plasticity of intrinsic membrane properties in prefrontal cortex pyramidal neurons: adaptations in potassium currents. *J Neurosci* 25:936-940.
28. Haydon P (2001) Glia: listening and talking to the synapse. *Nat Neurosci* 2:185-191.
29. Herman MA, Jahr CE (2007) Extracellular glutamate concentration in hippocampal slice. *J Neurosci* 27: 9736-9741.

30. Hollander JA, Carelli RM (2006) Cocaine-associated stimuli increase cocaine seeking and activate accumbens core neurons after abstinence. *J Neurosci* 27: 3535-3539.
31. Hotsenpiller G, Giorgetti M, Wolf ME (2001) Alterations in behaviour and glutamate transmission following presentation of stimuli previously associated with cocaine exposure. *Eur J Neurosci* 14:1843-1855.
32. Jabaudon D, Shimamoto K, Yasuda-Kamatani Y, Scanziani M, Gahwiler BH, Gerber U (1999) Inhibition of uptake unmasks rapid extracellular turnover of glutamate of nonvesicular origin. *Proc Natl Acad Sci USA* 96:8733-8738.
33. Kalivas PW, Volkow N, Seamans J (2005) Unmanageable motivation in addiction: pathology in prefrontal-accumbens glutamate transmission. *Neuron* 45:647-650.
34. Kleinle J, Vogt K, Luscher H -R., Muller R, Senn W, Wyler K, Streit J (1996) Transmitter concentrations profiles in the synaptic cleft: an analytical model of release and diffusion. *Biophys J* 71:2413-2426.
35. Knackstedt LA, Melendez R, Kalivas PW (2007) Cocaine self-administration alters the expression of proteins associated with glutamatergic transmission and homeostasis at cortico-accumbens synapses. Society for Neuroscience Annual Meeting, San Diego, CA: Abstract 815.8.
36. Kourrich S, Rothwell PE, Klug JR, Thomas MJ (2007) Cocaine experience controls bidirectional synaptic plasticity in the nucleus accumbens. *J Neurosci* 27:7921-7928.
37. Kreitzer AC, Malenka RC (2005) Dopamine modulation of state-dependent endocannabinoid release and long-term depression in the striatum. *J Neurosci* 25: 10537-10545.
38. Lehre KP, Levy LM, Ottersen OP, Storm-Mathisen J, Danbolt NC (1995) Differential expression of two glial glutamate transporters in the rat brain: quantitative and immunocytochemical observations. *J Neurosci* 15:1835-1853.
39. Lehre KP, Danbolt NC (1998) The number of glutamate transporter subtype molecules at glutamatergic synapses: chemical and stereological quantification in young adult rat brain. *J Neurosci* 18:8751-8757.
40. Lehre KP, Rusakov D (2002) Asymmetry of glia near synapse favors presynaptic glutamate escape. *Biophys J* 83(1):125-134.
41. Le Meur K, Galante M, Anulo MC, Audinat E (2007) Tonic activation of NMDA receptors by ambient glutamate of non-synaptic origin in the rat hippocampus. *J Physiol* 580.2: 373-383.
42. Losonczy A, Somogyi P, Nusser Z (2003) Reduction of excitatory postsynaptic responses by persistently active metabotropic glutamate receptors in the hippocampus. *J Neurophysiol* 89:1910-1919.
43. Madayag A, Lobner D, Kau KS, Mantsch JR, Abdulhameed O, Hearing M, Grier MD, Baker DA (2007) Repeated N-acetylcysteine administration alters plasticity-dependent effects of cocaine. *J Neurosci* 27: 13968-13976.
44. Malenka RC, Bear MF (2004) LTP and LTD: an embarrassment of riches. *Neuron* 44: 5-21.

45. McBean GJ (2002) Cerebral cystine uptake: a tale of two transporters. *Tr Pharmacol Sci* 23:299-302.
46. McFarland K, Lapish CC, Kalivas PW (2003) Prefrontal glutamate release into the core of the nucleus accumbens mediates cocaine-induced reinstatement of drug-seeking behavior. *J Neurosci* 23:3531-3537.
47. McFarland K, Davidge SB, Lapish CC, Kalivas PW (2004) Limbic and motor circuitry underlying footshock-induced reinstatement of cocaine-seeking behavior. *J Neurosci* 24:1551-1560.
48. Melendez RI, Vuthiganon J, Kalivas PW (2005) Regulation of extracellular glutamate in the prefrontal cortex: focus on the cystine glutamate exchanger and group I metabotropic glutamate receptors. *J Pharmacol Exp Ther* 314:139-147.
49. Miele M, Boutelle MG, Fillenz M (1996) The source of physiologically stimulated glutamate efflux from the striatum of conscious rats. *J Physiol (Lond)* 497:745-751.
50. Moghaddam B (2002) Stress activation of glutamate neurotransmission in the prefrontal cortex: implications for dopamine-associated psychiatric disorders. *Biol Psychiat* 51: 775-787.
51. Moran MM, McFarland K, Melendez RI, Kalivas PW, Seamans JK (2005) Cystine/Glutamate exchange regulates metabotropic glutamate receptor presynaptic inhibition of excitatory transmission and vulnerability to cocaine seeking. *J Neurosci* 25:6389-6393.
52. Murthy VN, Sejnowski TJ (1997) Heterogeneous release properties of visualized individual hippocampal synapses. *Neuron* 18:599-612.
53. Nicholson C (2001) Diffusion and related transport mechanism in brain tissue. *Rep Prog Physics* 64:815-884.
54. Nicholson C, Sykova E (1998) Extracellular space structure revealed by diffusion analysis. *Trends Neurosci* 21:207-215.
55. Patneau DK, Mayer ML (1990) Structure-activity relationships for amino acid transmitter candidates acting at N-methyl-D-aspartate and quisqualate receptors. *J Neurosci* 10:2385-2399.
56. Peters YM, O'Donnell P, Carelli RM (2005) Prefrontal cortical cell firing during maintenance, extinction, and reinstatement of goal-directed behavior for natural reward. *Synapse* 56(2):74-83.
57. Pierce RC, Bell K, Duffy P, Kalivas PW (1996) Repeated cocaine augments excitatory amino acid transmission in the nucleus accumbens only in rats having developed behavioral sensitization. *J Neurosci* 16(4):1550-1560.
58. Pow DV (2001) Visualizing the activity of the cystine-glutamate antiporter in glial cells using antibodies to amino adipic acid, a selectively transported substrate. *Glia* 34:27-38.
59. Reid MS, Berger SP (1996) Evidence for sensitization of cocaine-induced nucleus accumbens glutamate release. *Neurosci Lett* 7:1325-1329.
60. Rice ME, Nicholson C (1991) Diffusion characteristics and extracellular volume fraction during normoxia and hypoxia in slices of rat neostriatum. *J Neurophysiol* 65(2):264-272.
61. Robinson TE, Kolb B (2004) Structural plasticity associated with exposure to drugs of abuse. *Neuropharmacol* 47: 33-46.

62. Rusakov DA, Kullmann DM (1998) Extrasynaptic glutamate diffusion in the hippocampus: ultrastructural constraints, uptake, and receptor activation. *J Neurosci* 18:3158-3170.
63. Rusakov DA (2001) The role of perisynaptic glial sheaths in glutamate spillover and extracellular Ca²⁺ depletion. *Biophys J* 81:1947-1959.
64. Saftenku EE (2005) Modeling of slow glutamate diffusion and AMPA receptor activation in the cerebellar glomerulus. *J Theo Bio* 234: 363-382.
65. Sato K, Keino-Masu K, Masu M, Bannai S (2002) Distribution of cystine/glutamate exchange transporter, system xc-, in the mouse brain. *J Neurosci* 22:8028-8033.
66. Schoepp DD, True RA (1992) 1S-3R-ACPD-sensitive (metabotropic) [³H] glutamate receptor binding in membranes. *Neurosci Lett* 145:100-104.
67. Sun W, Rebec GV (2006) Repeated cocaine self-administration alters processing of cocaine-related information in rat prefrontal cortex. *J Neurosci* 26:8004-8008.
68. Swanson CJ, Baker DA, Carson D, Worley PF, Kalivas PW (2001) Repeated cocaine administration attenuates group I metabotropic glutamate receptor-mediated glutamate release and behavioral activation: A potential role for Homer1b/c. *J Neurosci* 21: 9043-9052.
69. Sykova E (2004) Extrasynaptic volume transmission and diffusion parameters of the extracellular space. *Neuroscience* 129:861-876.
70. Szumlinski KK, Abernathy KE, Oleson EB, Kullmann M, Lominac KD, He DY, Ron D, During M, Kalivas PW (2006) Homer isoforms differentially regulate cocaine-induced neuroplasticity. *Neuropsychopharmacol* 4:768-77.
71. Thorne RG, Nicholson C (2006) In vivo diffusion analysis with quantum dots and dextrans predicts the width of brain extracellular space. *Proc Natl Acad Sci USA* 103: 5567-5572.
72. Timmerman W, Westerink BH (1997) Brain microdialysis of GABA and glutamate: what does it signify. *Synapse* 27:242-261.
73. Trantham H, Szumlinski K, McFarland K, Kalivas PW, Lavin A (2002) Repeated cocaine administration alters the electrophysiological properties of prefrontal cortical neurons. *Neurosci* 113:749-757.
74. Trommershauser J, Schneggenburger R, Zippelius A, Neher E (2003) Heterogeneous Presynaptic release probabilities: functional relevance for short-term plasticity. *Biophys J* 84:1563-69.
75. Volynski KE, Rusakov DA and Kullmann DM (2006) Presynaptic fluctuations and release-independent depression. *Nat Neurosci* 9:1091-1093.
76. Wadiche JI, Arriza JL, Amara SG, Kavanaugh MP (1995) Kinetics of a human glutamate transporter. *Neuron* 14: 1019-1027.
77. Warr O, Takahashi M, Attwell D (1999) Modulation of extracellular glutamate concentration in rat brain slices by cystine-glutamate exchange. *J Physiol* 514:789-793.
78. Wyatt I, Gyte A, Simpson MG, Widdowson PS, Lock EA (1996) The role of glutathione in L-2-chloropropionic acid induced cerebellar granule cell necrosis in the rat. *Arch Tox* 70(11):724-735.

79. Xi ZX, Baker DA, Shen H, Carson DS, Kalivas PW (2002) Group II Metabotropic glutamate receptors modulate extracellular glutamate in the nucleus accumbens. *J Pharmacol Exp Ther* 300:162–171.

A.1.10. TABLE

Table 1. Ranges for parameter values used in model.

Parameter	Range of Values (citation)	Model Value ^a
Diffusion coefficient ($\mu\text{m}^2/\text{ms}$)	0.05 – 0.41 (Rusakov and Kullmann, 1998, Saftenku, 2005)	0.05
k_1 ($\text{M}^{-1}\text{ms}^{-1}$)	10^4 (Lehre and Rusakov, 2002)	10^4
k_{-1} (ms^{-1})	0.2 (GLAST/GLT; Lehre and Rusakov, 2002)	0.2
k_2 (ms^{-1})	0.1 (Lehre and Rusakov, 2002)	0.1
No. of molecules per release	4,700 - 80,000 (Bruns and Jahn, 1995)	10,000
Intersynaptic distance (μm)	2-20 (Rusakov, 2001)	2
K_d for mGluR2/3 (μM)	0.1-0.3 (Schoepp and True, 1992)	0.187
Maximum release probability	0.1-0.5 (Trommershauser et al., 2003; Billups et al., 2005; Volynski et al., 2006)	0.4
XAG conc. (molecules/ μm^2) ^b	550-3780 (Bergles and Jahr, 1997; Lehre and Danbolt, 1998; Colombo, 2005)	see ‘b’ below
xc- (mM hr^{-1}) ^c	5 – 50 (basal values from Warr et al., 1999; Baker et al., 2003)	41

^a Values used to populate model in figure 1 to generate the data shown in figure 2

^b surface density (molecules/ μm^2) of XAG was distributed as follows: G1a-1575, G1b-970, G2a-790, G2b-560, G3a-260, G3b-150, G4a-0, G4b-0; corresponding volume density ($\times 10^{-21}$ moles) of XAG: G1a-1.089, G1b-1.085, G2a-1.082, G2b-1.08, G3a-0.602, G3b-0.463, G4a-0, G4b-0

^c xc- was distributed uniformly in seven compartments of G4b: ($i=12, j = 2-8$)

Table 2. Parameters altered by chronic cocaine administration.

Parameter	Control	Cocaine	Reference
Glutamate concentration at P _{ex} (μM; basal)	5.6 ± 1.0	2.89 ± .34	Baker et al., 2003; Szumlinski et al., 2006
Peak glutamate in P _{ex} (μM; during food seeking/cocaine-seeking)	5.6 ± 1.0	13.3 ± 1.4	McFarland et al., 2003, 2004
xc- (mM hr ⁻¹)	41	^a 20.5	Baker et al., 2003; figure 5C
Release probability	0.14 (basal)	^b 0.34 (basal)	Xi et al., 2002
Firing freq (Hz) (basal)	2	1	Sun and Rebec, 2006; Trantham et al., 2002
Firing freq (Hz) (drug-seeking)	N/A	3-15	Chang et al., 1997; Sun and Rebec, 2006

^a Based upon increase in K_m for cystine from 2.1±0.2 to 4.2±0.2 μM; 28.3±7.9% reduction in catalytic subunit of xc- (xCT)

^b Based upon 70% reduction in mGluR2/3 induced GTPγS binding

Table 3. Model estimates at varying firing frequencies using control and chronic cocaine parameters.

Parameter	Control basal	Control biological reward seeking	Cocaine basal ^a	Cocaine drug seeking ^a
Firing freq (Hz)	2	15	1	15
Release probability	0.14	0.12	0.34	0.30
XAG (moles)	5.4×10^{-21}	5.4×10^{-21}	3.24×10^{-21}	3.24×10^{-21}
xc- (mM hr ⁻¹)	41	41	20.5	20.5
Estimates of steady state Glu concentrations at three locations				
P _{syn} (μM)	0.16	0.19	0.24	1.05
P _{mGluR} (μM)	0.195	0.28	0.27	1.19
P _{ex} (μM)	5.04	6.58	3.03	12.4

^a Cocaine-induced reduction in XAG (40%), xc- (50%) and mGluR2/3 signaling (70%; modeled as release probability)

A.1.11. FIGURES

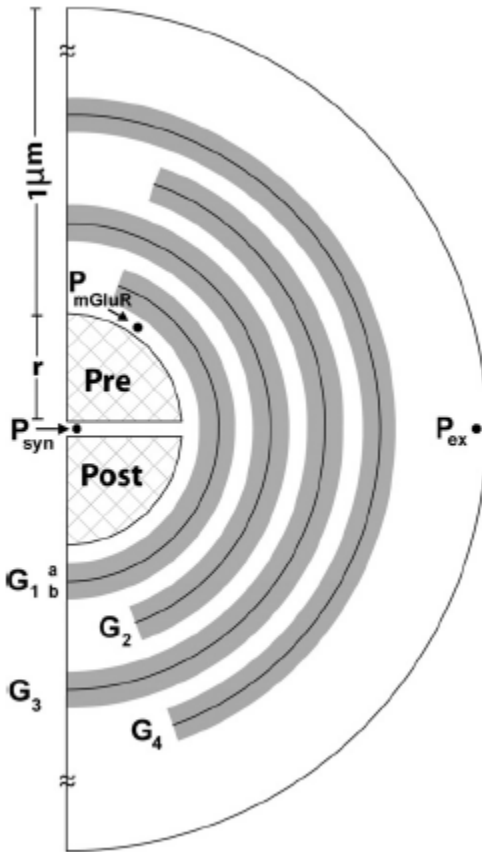


Figure 1. The glial configuration used to study glutamate homeostasis in the perisynaptic space around the PFC-accumbens synapse. The model depicts glutamate transporters (XAG) and cystine-glutamate exchangers (xc-) in glial regions (shaded) in varying concentrations. The cleft ($\delta=20$ nm) separates the two hemispheres of radius ($r = 160$ nm) surrounded by glial sheaths (G_i , $i=1-4$; $i=1$ being the closest to the synapse) with the highest density of XAG in G_1 and decreasing in radially outward sheaths. Each sheath is 50 nm thick with an impermeable surface in the middle, and with XAG volume-populated in the 25 nm thick space on either side, permitting interaction with glutamate molecules in those regions. The perisynaptic space is partitioned in radial (step $\sigma =25$ nm) and tangential (step $\theta =20^\circ$) directions as in Rusakov (2001). Binding, uptake and

efflux are computed for each compartment. Glutamate concentrations were measured at three sites, within the synaptic cleft (at P_{syn}), in the perisynaptic region containing presynaptic mGluR2/3 (at P_{mGluR}), and at the site where dialysis probe measures extracellular glutamate (at P_{ex}).

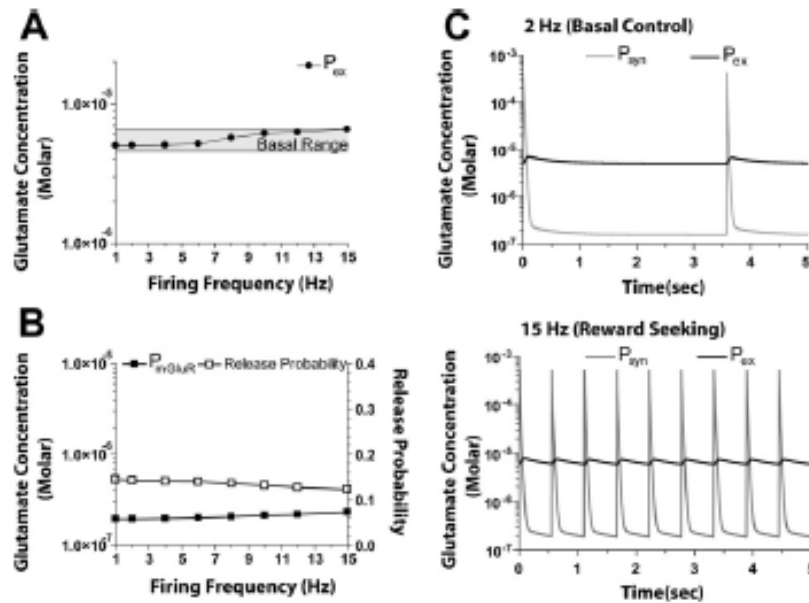


Figure 2. Concentrations of glutamate at different spatial locations under control conditions. **A.** The increase in glutamate at P_{ex} remained within the basal range over the entire 1-15 Hz range of firing. **B.** As firing frequency increases, the concentration of glutamate in the vicinity of perisynaptic mGluR2/3 autoreceptors (at P_{mGluR}) increases producing a concomitant decrease in release probability. **C.** Model output at 2 and 15 Hz over 5 sec, illustrating the dynamic changes in synaptic (at P_{syn}), and extracellular glutamate (at P_{ex}).

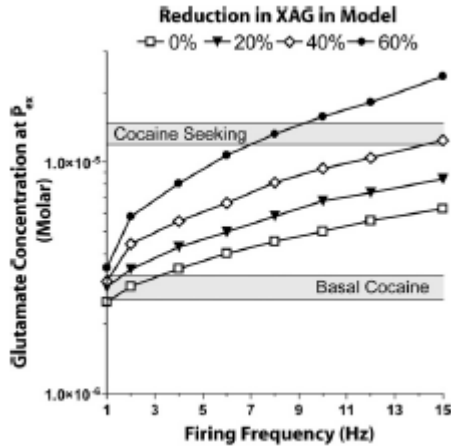


Figure 3. Effect of reducing XAG on the concentration of extracellular glutamate at P_{ex} , in cocaine treated rats. To model the cocaine condition, the function of xc- and mGluR2/3 were reduced by 50% and 70%, respectively. Iterations of the model were then run at different percent decreases in the concentration of XAG over a firing frequency range of 1-15 Hz.

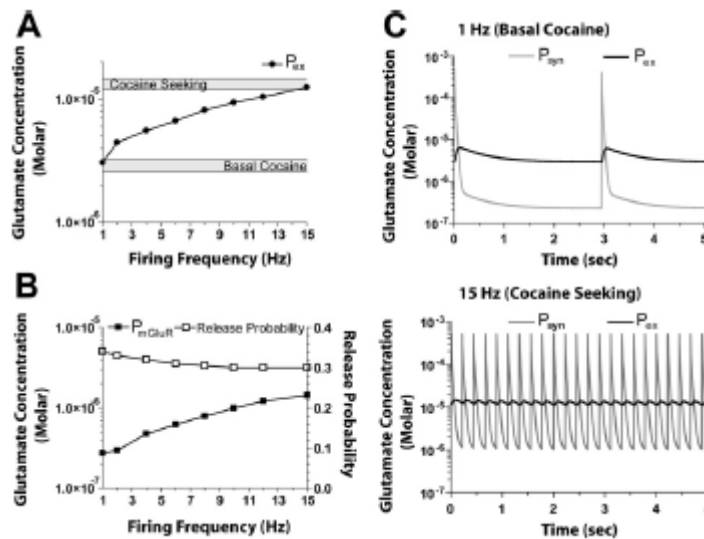


Figure 4. Concentrations of glutamate at three spatial locations under cocaine conditions (i.e., xc- reduced 50%, mGluR2/3 signaling reduced 70%, XAG reduced 40%). **A.** The increase in glutamate at P_{ex} was within the basal range at 1 Hz and increases to the cocaine-seeking range at 15 Hz firing frequency. **B.** As firing frequency increased, the

concentration of glutamate in the vicinity of perisynaptic mGluR2/3 autoreceptors (at P_{mGluR}) increased with a concomitant decrease in release probability. C. Model output at 1 and 15 Hz over 5 sec, illustrating the dynamic changes in synaptic (at P_{syn}), and extracellular concentration (at P_{ex}).

Appendix A.2

Role of perisynaptic parameters in neurotransmitter homeostasis - computational study of a general synapse

A.2.1. ABSTRACT

Extracellular neurotransmitter concentrations vary over a wide range depending on the type of neurotransmitter and location in the brain. Neurotransmitter homeostasis near a synapse is achieved by a balance of several mechanisms including vesicular release from the presynapse, diffusion, uptake by transporters, nonsynaptic production, and regulation of release by autoreceptors. These mechanisms are also affected by the glia surrounding the synapse. However, the role of glial configuration and the parameters involved in achieving this homeostasis is not well understood. A biophysical modeling framework was proposed to reverse engineer glial configurations and parameters related to homeostasis for synapses that support a range of neurotransmitter gradients. The model provided key insights on how effective synaptic isolation occurs during homeostasis through interplay of glial geometry, the placement of transporters, and diffusion, for synapses with extracellular concentrations in the μM range. The framework was then used to identify designs of glial configurations that supported three ranges of extracellular neurotransmitter concentrations for an example case synapse.

A.2.2. INTRODUCTION

Maintenance of accurate levels of *in vivo* extracellular neurotransmitter concentration is critical for several neurological processes such as migration and differentiation of brain cells during development (LoTurco et al. 1995; Nguyen et al. 2001; Manent and Represa 2007) and for synaptic plasticity (Featherstone and Shippy

2008). For monoamine-, acetylcholine- and purine- type neurotransmitters, extracellular concentrations are maintained by synaptic release and are usually at low levels (< 100 nM; van der Zeyden et al. 2008). On the other hand, amino acid-type neurotransmitters, such as glutamate and GABA, have synaptic and nonsynaptic sources (van der Zeyden et al. 2008) to maintain extracellular concentrations in the μ M ranges. In the case of glutamate, estimated extracellular concentrations can vary from 25 nM (Herman and Jahr 2007) to 5 μ M (Bouvier et al. 1992, Baker et al. 2003; Nyitrai et al. 2006, Day et al. 2006). Reports also suggest that extracellular concentrations of glutamate in the range of 2-5 μ M could, in some cases, lead to excitotoxicity (Meldrum and Garthwaite 1990, Herman and Jahr 2007), while higher ambient values can result in pathological conditions such as seizures, ischemia, and epilepsy (Kanai and Endou 2001; Rainesalo et al. 2004; Nyitrai et al. 2006). Several mechanisms, including neurotransmitter diffusion into the perisynaptic space (defined as the cleft and near the synapse) after release, binding/uptake by transporters present on glial sheaths, nonsynaptic production of neurotransmitters and activation of autoreceptors that regulate release, are responsible for maintaining homeostasis in the perisynaptic and extracellular regions. The existence of numerous mechanisms and a lack of consensus on the ambient extracellular glutamate concentration make the characterization of homeostasis difficult for such synapses. This motivated the development of a computational model to provide insights and predictions related to homeostatic conditions for synapses which supported gradients in neurotransmitter concentrations between the synaptic cleft and the extracellular space (referred to hereafter as 'neurotransmitter gradients').

Previous modeling studies related to glutamate have focused on neurotransmitter time courses in the synapse based on receptor (AMPA/NMDA) activation (Clements

et al. 1992; Diamond and Jahr 1997) and on determining the accessibility of synaptically released glutamate to the extracellular space by considering diffusion out of the synapse and elimination by glutamate transporters (Rusakov and Kullmann 1998; Rusakov 2001; Barbour 2001; Franks et al. 2002; Diamond 2005). While these models established guidelines for neurotransmitter profiles and time courses, they did not focus on possible glial configurations and parameters that controlled perisynaptic and extracellular neurotransmitter levels under homeostatic conditions.

Pendyam et al. (2009) reported a computational model of glutamate homeostasis incorporating the mechanisms cited. The model provided a specific glial configuration that supported gradients in glutamate concentration observed after chronic cocaine. The present paper utilized the computational framework to develop other possible glial configurations for a general class of synapses. We considered a cortico-accumbens glutamatergic example case synapse, and asked - What glial configuration and transporter placement/densities would support neurotransmitter gradients in the μM range during normal synaptic functioning? How do perisynaptic parameters such as diffusion, transporter density and distribution, molecules per release, volume fraction, and nonsynaptic production rate, affect homeostasis around a synapse? The insights gained from such a reverse engineering approach can then be used to predict glial configurations for a general class of synapses that support neurotransmitter gradients.

A.2.3. METHODS

A.2.3.1. Model inputs and baseline parameters

Baseline physiological parameters were obtained from other models and parameter estimates reported in the literature.

Molecules per release and firing frequency. Neurotransmitter release from a nerve terminal during exocytosis depends on the size of the synapse, vesicular properties such as volume, neurotransmitter concentration and number available for exocytosis, and geometric parameters such as diameter of the fusion pore (Danbolt 2001). For the glutamatergic cortico-accumbens synapse considered, basal presynaptic firing frequency ranges from 1-3 Hz (Trantham et al. 2002), with burst frequencies up to 15 Hz during reward seeking behavioral states (Chang et al. 1997; Peters et al. 2005; Sun and Rebec 2006). Each action potential (resulting from the firing frequency and release probability) in the model resulted in an instantaneous vesicular release into the cleft. The molecules per release for general synapses typically vary from 4,000-80,000 (Bruns and Jahn 1995), and this was the range used in the study (table 1).

Presynaptic regulation of release probability. Release probability is regulated following the stimulation of presynaptic autoreceptors (e.g., mGluR2/3- glutamate; GABA_B- GABA; and D₂- dopamine; Squire et al. 2002; Dietrich et al. 2002; Losonczy et al. 2003; Billups et al. 2005), which are located outside the synaptic cleft (Alagarsamy et al. 2001). The probability that an action potential results in a vesicular release ranges from <0.1 to 1 (Murthy and Sejnowski 1997). For the example case considered, GTP γ S binding revealed that G protein signaling by stimulating mGluR2/3 increased as a logarithm of agonist dose (Xi et al. 2002); hence the relationship between release probability and autoreceptor occupancy was modeled as a logarithmic function. Using this, the autoreceptor function for mGluR2/3 was modeled as a change in release probability from 0.14 (basal) to 0.12 (natural reward seeking; table 1). The basal level of glutamate in the vicinity of perisynaptic mGluR2/3 was adjusted in the present model to produce ~50% occupancy (Billups et al. 2005), based upon the range of dissociation constant (k_d) values reported for the

receptor (k_d of 0.1 to 0.3 μM ; Schoepp and True 1992).

Diffusion. Diffusion is non-homogenous and anisotropic in the extracellular space. The size and irregular geometry of the diffusion channels differ substantially around individual cells and this directs the movement of several neuroactive substances in the extracellular space (Sykova 2004). Further, different cellular elements including spines, small axonal boutons, protein, glia, and microfilaments may result in additional tortuosity in the microenvironment of a synapse (Saftenku 2005). Diffusion in the extracellular space is typically characterized by volume fraction α (void space/total tissue volume) and tortuosity λ (hindrance to diffusion imposed by local boundaries or local viscosity) (Nicholson, 2001). Volume fraction α in brain tissue is estimated to be around 0.2 (Nicholson and Sykova, 1998). Tortuosity λ is estimated to be 1.2-2.4 based on diffusion measurements over a range of 100–300 μm (Nicholson, 2001). Experimental estimates of diffusion coefficients (D) in the perisynaptic region (i.e., $< 1 \mu\text{m}$ from cleft) have not been reported for synapses with tightly packed glia. In the proposed model, with high density glia close to the synapse, we iteratively determined the diffusion coefficients from the range 0.05-0.41 $\mu\text{m}^2/\text{ms}$ (Saftenku, 2005; table 1) to satisfy steady state and transient constraints, as described later.

Transporters. Neurotransmitter concentration in the perisynaptic region is controlled by high density transporters present on the glia (e.g., for glutamate and GABA) or on the presynapse (e.g., for dopamine, norepinephrine, and serotonin; Squire et al. 2002). These transporters eliminate excess neurotransmitter diffusing out of the cleft and maintain appropriate concentrations (Tanaka et al. 1997, Danbolt 2001), preventing excitotoxicity. The glial membranes that are closest to the synapse have a higher expression of transporters (Cholet et al. 2002) with larger numbers on the postsynaptic side (Lehre and Rusakov 2002). Glutamate transporters (EAATs -

GLAST and GLT; collectively termed XAG) are present on glial membranes (Danbolt 2001) with surface densities ranging from 2,500-10,000 molecules/ μm^2 (Bergles and Jahr 1997; Lehre and Danbolt 1998). For the example case, the equivalent surface density of XAG was determined iteratively by varying it within the range of 550-3,780 molecules/ μm^2 (table 1) as described in the next section.

Nonsynaptic sources. As noted earlier, the extracellular composition of glutamate is derived from both synaptic and nonsynaptic sources (van der Zeyden et al. 2008). Different types of nonsynaptic sources of glutamate (e.g., cystine glutamate exchanger, xc-; Baker et al. 2003) contribute to the extracellular concentration. Wyatt et al. (1996) estimated the exchange rate for xc- to be $450 \mu\text{mol l}^{-1}\text{hr}^{-1}$ based on cerebellar slices (density of xc- is higher in the cortex by a factor of 2.4; Warr et al. 1999). Calculating the xc- exchange rate for configuration 1 resulted in a value of 30 mM hr^{-1} . Iterations to satisfy model constraints resulted in the consideration of production rates for xc- between $10\text{-}55 \text{ mM hr}^{-1}$ (table 1).

A.2.3.2. Framework for modeling a class of synapses

The proposed model is shown in figure 1. The two hemispheres of the synapse were assumed rigid, with radius $r = 160 \text{ nm}$, and a separation of $\delta = 20 \text{ nm}$ (synaptic cleft; Rusakov and Kullmann 1998; Rusakov 2001; Diamond 2005). Around this synapse were 40 concentric 25 nm thick shell compartments ($i_1\text{-}i_{40}$) resulting in the outer boundary of the perisynaptic region modeled being at a distance of $1 \mu\text{m}$ from the edge of the synapse. Each shell was divided into 9 compartments (20° angle increments, $j_1\text{-}j_9$) circumferentially, permitting XAG and xc- concentrations to be assigned individually to each compartment of any shell. For the outermost shell, e.g., $i = 40$, the boundary condition of flux = 0 was imposed at the outer edge of all compartments, to simulate identical neighboring synapses. That is, no flux entered or

left the outer boundary of this shell. XAG and xc- were volume populated on glial sheaths. The individual glial sheath (G_i in fig 1) structure was akin to that previously reported (Rusakov 2001; Pendyam et al. 2009), but the configuration itself was different (fig 1) in its orientation, placement and number of glial folds.

The mathematical equations were the standard conservation and flux equations described in Pendyam et al. (2009) (see Rusakov (2001) for a comprehensive description including derivations). The final set of lumped parameter equations for each compartment, is given by Eqn. A.2.1,

$$\begin{aligned}
 [Glu]_t &= [Glu]_{t-dt} + (-k_1[Glu]_{t-dt}[XAG]_{t-dt} + k_{-1}[Glu - XAG]_{t-dt})dt \\
 [Glu - XAG]_t &= [Glu - XAG]_{t-dt} + (-(k_{-1} + k_2)[Glu - XAG]_{t-dt} + k_1[Glu]_{t-dt}[XAG]_{t-dt})dt \\
 [Glu - XAG]_t + [XAG]_t &= [Glu - XAG]_{t-dt} + [XAG]_{t-dt} = [XAG_{total}] \\
 [Glu_{in}]_t &= [Glu_{in}]_{t-dt} + k_2 * [Glu - XAG]_{t-dt} * dt
 \end{aligned}
 \tag{A.2.1}$$

where $[Glu]$, $[XAG]$, and $[Glu-XAG]$ represent the compartmental concentrations of glutamate, transporter, and the bound complex, respectively, and $[Glu_{in}]$ represents the uptake by XAG. The kinetics for XAG $k_1 = 10^4 \text{ M}^{-1}\text{ms}^{-1}$, $k_{-1} = 0.2 \text{ ms}^{-1}$, and $k_2 = 0.1 \text{ ms}^{-1}$ were taken from Rusakov (2001) and Lehre and Rusakov (2002) who based it on experiments reported in the literature (Bergles and Jahr 1998; Wadiche et al. 1995).

Model constraints. The model should typically satisfy (i) Transient synaptic conditions conforming to reported transmitter decay time course (e.g., for glutamate as in Clements et al. 1992; Tong and Jahr 1994; Clements 1996; Diamond and Jahr 1997); (ii) Steady state synaptic concentrations which need to be low to avoid significant receptor excitotoxicity (e.g., $\sim 100 \text{ nM}$ for glutamate; Patneau and Mayer 1990); and (iii) Steady state extracellular concentrations should not exceed reported basal steady state values (e.g., glutamate basal concentrations are in the range 5.6 ± 1

μM for the cortico-accumbens example; Baker et al. 2003; Sun and Rebec 2006) for low (2 Hz; basal) and high (12-15 Hz; reward seeking) presynaptic stimulation frequencies. The experimentally defined basal and reward seeking concentrations of extracellular glutamate were modeled as being at the point P_{ex} in figure 1, outside glial region G_3 .

Iterative evaluation. The iterative process for each configuration began with values in the lower end of the ranges for the parameters shown in table 1, while monitoring the concentrations of glutamate at P_{syn} , P_{mGluR} , and P_{ex} (fig 1). As cited the densities of XAG were varied in glial sheaths G_i , such that their relative proportions were maintained, i.e., density (G_1) > density (G_2) and so on (see table 1). Through this process, numerous solutions were found that satisfied empirically determined concentrations at P_{syn} , P_{mGluR} , and P_{ex} . These solutions had specific covariations among the parameters, a finding that is discussed in more detail later. The computational model was developed using C++ software (Microsoft Visual Studio 2005, WA, USA), and used an integration time step of 0.5 μs .

A.2.4. RESULTS

As cited, an iterative process was employed to develop the model using the constraints above. We then used the model to obtain insights into the role of geometric and physiological parameters, such as the structure and number of glial sheaths, number of molecules per release, xc- production rate, diffusion coefficient, and XAG density, in establishing homeostasis in neurotransmitter concentrations. The methodology illustrated using the cortico-accumbens synapse is applicable to a general synapse that supports neurotransmitter gradients.

A.2.4.1. Steady state and transient characteristics

Using the iteratively determined model values listed in table 1, configuration 1 satisfied the model constraints, i.e., the steady state extracellular (at P_{ex}) and synaptic (at P_{syn}) glutamate concentrations at basal (2 Hz) and natural reward seeking (15 Hz) presynaptic firing frequencies. The decay time course for glutamate in the cleft is typically biphasic with initial peak amplitude of 1-4 mM, and with 100 μ s and 1-2 ms for the fast and slow time constants, respectively (Clements et al. 1992; Tong and Jahr 1994; Clements 1996). The model proposed in configuration 1 resulted in a peak synaptic concentration of 4 mM, with a biphasic profile and time constants of 120 μ s and 2.1 ms. Transient characteristics were more sensitive to changes in diffusion in the cleft (D_{cleft}) than in the glia. However, the steady state concentrations were not affected by variations in D_{cleft} .

A.2.4.2. Variation in glial geometry

To study the effect of different glial geometries, we started with porous glia (similar to the model in Barbour (2001); not sheaths) and varied XAG numbers to study the effect of transporter placement. Such permeable configurations were not capable of supporting gradients and resulted in uniform concentration profiles throughout the perisynaptic space. To further probe the role of glia (orientation, placement and number of folds) using impermeable sheaths, a number of other geometries were considered (data not shown) of which only three are reported (figs 1-2). Configuration 2 was similar to that described by Rusakov (2001) and configuration 3 was a variation of configuration 2 with interleaved glial sheaths adding to the diffusion path length (defined as the distance that a molecule travels from the synaptic cleft to the extracellular space). When the same set of parameters in the porous glial case above was considered for configurations 2 and 3, we observed

that the concentration profiles around the synapse (at P_{syn} and P_{mGluR}) and extracellular space (at P_{ex}) were all dissimilar, highlighting the role of transporter placement and glial structure.

Configurations 2 and 3 failed to satisfy model constraints using physiological ranges of parameters cited in Table 1. For instance, with extracellular concentrations in the 4-5 μM range, the minimum synaptic concentration achievable for configuration 2 was seven-fold higher than the constraint (i.e., 700 nM). Configuration 3 satisfied all constraints, but the number of transporter exceeded physiological ranges by a factor of two. As cited, configuration 1 simultaneously maintained extracellular and synaptic concentrations in the 4-5 μM and ~ 100 nM ranges, respectively. Thus, configuration 2 was not effective in maintaining synaptic concentration within physiological ranges for μM range concentrations at P_{ex} , as compared to configurations 1 and 3. All this highlights the key role played by glial configurations in creating a diffusion path length, and providing ‘isolation’ (absent in configuration 2), for the class of synapses that support neurotransmitter gradients.

Volume fraction (α). Varying α from 0.2 to 1 in configuration 1 resulted in no variation in steady state extracellular concentration for the basal or reward seeking firing cases, due to high density of XAG and xc- in the perisynapse. This was found to be the case even when XAG density and xc- production are decreased by 50% from their model values. Hence, volume fraction does not appear to have any significant affect on steady state concentration at P_{ex} for the example case.

A.2.4.3. Parameter sensitivity

For configuration 1, each parameter was varied in the range ± 10 -50% of their model values (table 1) to study the relative influence of the parameters on the concentrations at P_{syn} , P_{mGluR} and P_{ex} .

Transporter parameters

Total XAG molecules. Increasing the total XAG molecules in the range of 3,000 to 9,000 resulted in an exponential decrease in the extracellular and synaptic concentrations (fig 3a). For configuration 1, a 50% decrease/increase in total transporters caused a 33%/20% increase/decrease in concentration at P_{ex} . Synaptic steady state concentration reduced at a faster rate reaching half its maximum value with only a 15% increase in total transporters. This showed that variation in XAG had a much larger effect on the concentration at P_{syn} compared to that at P_{ex} . Increase in transporter concentration increased uptake, as expected, decreasing concentrations at P_{ex} and P_{syn} .

XAG binding coefficients. The dissociation constant k_d (defined as k_{-1}/k_1) for transporters varies depending on the brain region (Lehre and Rusakov 2002), and so the model was used to study the effect of varying XAG binding constants. Although variation in XAG binding coefficients provided expected trends, the analysis quantified the effects. Increasing k_1 and k_2 independently by 50% resulted in the concentration at P_{ex} decreasing by 20% and 15%, respectively. With a 50% increase in k_{-1} , the concentration at P_{ex} increased by 16%. Further, with a 50% decrease in k_1 , k_2 and k_{-1} , the concentration at P_{ex} decreased by 30, 27, and -24 % (increase) respectively. These trends may be useful in evaluating the effects of these constants on synapses in other brain regions.

Nonsynaptic neurotransmitter production. As cited, we considered the xc- production rate in the range 10-55 mM hr^{-1} . This resulted in a linear increase in both extracellular and synaptic concentrations, i.e., increase/decrease in xc- production by 50% from the operating point increased/decreased concentration at P_{ex} by 48% and 47%, respectively (fig 4a).

Diffusion coefficient. Increasing the diffusion coefficient in the range 0.025-0.075 $\mu\text{m}^2/\text{ms}$ resulted in an exponential decrease in extracellular concentration while the synaptic concentration increased linearly (fig 4b). A 50% increase/decrease in the diffusion coefficient from its operating point value decreased/increased concentration at P_{ex} by 18%/28% and increased/decreased concentration at P_{syn} by 30%/33%. Since diffusion controls the rate at which the molecules interact with XAG, concentration at P_{ex} increased as the extracellular molecules had difficulty entering the glial sheaths. Increasing the diffusion coefficient two-fold increased synaptic concentration by a factor of seven. Lowering diffusion values helped buffer molecules in the glial structures, facilitating their uptake and leading to a decreased concentration at the synapse.

Molecules per release and presynaptic firing frequency. No significant change in extracellular concentration was observed when presynaptic firing frequencies and number of molecules per release were varied $\pm 50\%$ around the model values. As cited, firing frequencies in cortico-accumbens synapses vary from 1-15 Hz (Sun and Rebec 2006). Varying the number of molecules per release in the range 2000-20000 resulted in a two-fold increase in the concentration at P_{syn} , for all frequencies, indicating rapid clearance by the transporters. At lower frequencies (< 8 Hz), varying the number of molecules per release had no significant impact on the concentration at P_{ex} . At higher frequencies (12 -15 Hz), an increase of about 10% was observed (fig 4c).

In summary, the findings from the parametric studies were that the glial configuration had the greatest impact on neurotransmitter homeostasis, followed by, in order, nonsynaptic sources, transporter densities/binding constants, and diffusion

coefficient. These insights have been used to provide guidelines for reverse engineering general synapses, as described later.

A.2.5. DISCUSSION

The computational models provided several predictions for general synapses that support gradients in neurotransmitter concentrations between the cleft and the extracellular space. Although configuration 1 was utilized for several of the studies, the trends are expected to be similar for other configurations also.

A.2.5.1. Models predict that effective synaptic isolation for $> 1 \mu\text{M}$ extracellular concentrations requires specific glial configurations

It was seen that a configuration with permeable glia could not support neurotransmitter gradients and resulted in a uniform concentration profile throughout the perisynaptic space. As also observed, permeable glia and configurations 2 and 3, resulted in very different neurotransmitter concentration values with the same set of parameters, highlighting the role of glial configuration. Further, we observed that configurations 2 and 3 had lesser uptake rates compared to the permeable glial configuration, showing the importance of transporter placement on glial folds, which, in turn, modulates interactions of transporters with neurotransmitter molecules. Also, an appropriate diffusion coefficient constrained the influx of the neurotransmitter molecules from the extracellular space through the glial sheaths. All this collectively helped achieve synaptic isolation for a range of $>1\mu\text{M}$ extracellular concentrations.

The model is thus an effective tool to characterize/quantify the interplay between glial configuration, transporter placement and tortuosity, in generating the required diffusion path length for synaptic isolation and sustenance of neurotransmitter gradients. As an example, figure 5 illustrates how three parameters, transporter

density, xc- production rate, and diffusion coefficient, are correlated and provide multiple solutions (all satisfying synaptic constraints; figs 3,4) to maintain a specific concentration at P_{ex} , for the cortico-accumbens synapse in configuration 1. This characterization further implies that glial configurations for synapses with $< 1 \mu\text{M}$ extracellular concentrations have simpler geometric structures and would require comparatively less transporter molecules, and lower nonsynaptic production rates.

A.2.5.2. Nonsynaptic sources are required to maintain μM level extracellular concentrations

To study the contribution of synaptic and nonsynaptic sources in maintaining extracellular glutamate concentration, we varied the number of molecules per release in physiological ranges from 2,000-20,000 with no nonsynaptic production sources, for configuration 1. The transporter uptake around the synapse ensured rapid elimination of neurotransmitter even with large number of molecules per release, showing that it has little impact on extracellular concentration. Thus, neurotransmitter release primarily activates postsynaptic receptors and does not contribute significantly to the extracellular concentration for such synapses.

This, in turn, implies that nonsynaptic glutamate sources help maintain extracellular concentrations, as expected; the model showed this when we eliminated synaptic release. Further, an increase/decrease in nonsynaptic production rate resulted in a proportional increase/decrease in the extracellular concentration. This shows that in the proposed model, nonsynaptic sources along with glial sheaths help establish and maintain gradients. Our model results are in agreement with recent microdialysis studies (Melendez et al. 2005), and cell culture/tissue slice experiments (Jabaudon et al. 1999; Haydon 2001) which report that glutamate outside of the cleft is not of synaptic origin.

A.2.5.3. Transporter and nonsynaptic source densities can co-vary to provide tone on presynaptic autoreceptors

The model predicted that under homeostatic conditions, the tone on the presynaptic autoreceptors (mGluR2/3; measured as concentration at P_{mGluR}) was provided by extracellular neurotransmitter, i.e., there was an influx of molecules that established a baseline tone (50%) on the autoreceptor in configuration 1. This prediction was in agreement with experimental reports (Xi et al. 2002 and Moran et al. 2005) that show tone on mGluR2/3 (at P_{mGluR} in fig 1) being derived primarily from nonsynaptic sources.

The model also revealed the ratio of xc- production rate to XAG density had to be constant to maintain the same baseline tone. For pathological conditions (e.g., chronic cocaine or ischemia), the model predicted that this tone will be disturbed, with consequent effects on presynaptic firing rates.

A.2.5.4. Synaptic glial configuration can be predicted for a given extracellular concentration

We used the example case synapse to illustrate how the reverse engineering insights related to glial structures, transporter placement and diffusion coefficient values can be used to provide predictions of possible synaptic glial configurations, for a specified extracellular concentration. It should be noted that other glial geometries that provide the same resistance to flow would also be feasible candidates.

Prediction of configurations for concentrations $< 1 \mu\text{M}$ at P_{ex} . For synapses with extracellular concentration values (at P_{ex}) less than $1 \mu\text{M}$, all three proposed configurations (see figs 1 and 2) were feasible. That is, they satisfied the transmitter decay profile, steady state synaptic concentration to avoid receptor excitotoxicity ($< 100 \text{ nM}$), and supported extracellular concentrations within the $1 \mu\text{M}$ range for high

frequencies. Configurations 1 and 3 achieved concentration levels less than 1 μM with lower transporter densities ($< 2,500$ molecules/ μm^2 ; other predicted parameters in table 2) compared to configuration 2 which required transporter densities in a range of 2,500-5,000 molecules/ μm^2 .

Prediction of configurations for concentrations of 1 μM -5 μM at P_{ex} .

Configurations 1 and 3 achieved extracellular concentrations in the range of 1-5 μM and simultaneously satisfied synaptic constraints, but with more than two-fold increases in transporter density (4,500-7,500 molecules/ μm^2) and xc- production rates (40-65 mM hr^{-1} ; other predicted parameters in table 2), compared to the < 1 μM case. The fact that these two parameters co-vary was noted earlier. As cited, configuration 2 could not maintain extracellular concentrations > 1 μM with P_{syn} in the 100-200 nM range, and with parameters within physiological ranges.

Prediction of configurations for concentrations of > 5 μM at P_{ex} . For extracellular concentrations greater than 5 μM , configuration 1 with three glial sheaths and orientation satisfied the decay time course, the steady state synaptic concentration, and high frequency conditions (fig 4a). This required a further two-fold increase in both the number of transporter molecules (7,500-10,500 molecules/ μm^2) compared for the 1 μM -5 μM case, and an increase in xc- production rate to 50-75 mM hr^{-1} (other predicted parameters in table 2). So, for such synapses, the glial coverage is predicted to be very tight.

In summary, the proposed model provides guidelines for the selection of glial configurations and parameter values (e.g., transporters, nonsynaptic sources, and diffusion coefficient, as in fig. 5) for general synapses supporting gradients.

A.2.5.5. Limitations and future work

Glial configurations very close to synapses are not well understood, particularly for synapses that support gradients between the cleft and the extracellular space. Accordingly, the configurations proposed should be viewed as being only ‘equivalent’ in that they provide the same resistance to the flow of neurotransmitter as other possible realistic configurations. Refined experimental estimates for the ranges of many of the parameters (table 1) would enhance model predictions. In particular, diffusion coefficients close to the synapse have not been reported and the model predictions show that they have to be somewhat low for homeostasis under the conditions considered. On-going studies are focused on gaining additional insights using Monte Carlo approaches with stochastic molecular dynamics and boulder-like glial structures.

A.2.6. CONCLUSIONS

A computational framework was proposed to reverse engineer glial configuration and parameters for a class of synapses that support neurotransmitter gradients between the cleft and the extracellular space. The models provided several insights and predictions pertaining to the the role of glial configuration in isolating the synapse, and to the relative importance of parameters such as glial configuration, diffusion coefficient, transporter density and distribution, molecules per release, volume fraction, and nonsynaptic production, on neurotransmitter homeostasis. Consistent with experimental reports, the model predicted that nonsynaptic sources are necessary for both neurotransmitter homeostasis, and for maintaining tone on the presynaptic autoreceptors, for the example case. The proposed computational models, and the trends it predicted are applicable to general synapses that support gradients.

A.2.7. ACKNOWLEDGEMENTS

This research was supported in part by USPHS grants DA015369, DA03906 (PWK), and subcontract from DA015369 to University of Missouri (SSN).

A.2.8. REFERENCES

1. Alagarsamy, S., Sorensen, S. D., & Conn, P. J. (2001). Coordinate regulation of metabotropic glutamate receptors. *Current Opinion in Neurobiology*, 11, 357-362.
2. Anderson, K. J., Monaghan, D. T., Bridges, R. J., Tavoularis, A. L. & Cotman, C. W. (1990). Autoradiographic characterization of putative excitatory amino acid transport sites. *Neuroscience*, 38, 311-322.
3. Baker, D. A., McFarland, K., Lake, R. W., Shen, H., Tang, X. C., et al. (2003). Neuroadaptations in cystine-glutamate exchange underlie cocaine relapse. *Nature Neuroscience*, 6, 743-749.
4. Barbour, B. (2001). An evaluation of synapse independence. *Journal of Neuroscience*, 21, 7969-7984.
5. Bergles, D. E., & Jahr, C. E. (1997). Synaptic activation of glutamate transporters in hippocampal astrocytes. *Neuron*, 19, 1297-1308.
6. Bergles, D. E., & Jahr, C. E. (1998). Glial contribution to glutamate uptake at schaffer collateral-commissural synapses in hippocampus. *Journal of Neuroscience*, 18, 7709-7716.
7. Billups, B., Graham, B. P., Wong, A. Y., & Forsythe, I. D. (2005). Unmasking group III metabotropic glutamate autoreceptor function at excitatory synapses in the rat CNS. *Journal of Physiology*, 565, 885-896.
8. Bouvier, M., Szatkowski, M., Amato, A., & Attwell, D. (1992). The glial cell glutamate uptake carrier countertransports pH-changing anions. *Nature*, 360, 471-474.
9. Bruns, D., & Jahn R. (1995). Real-time measurement of transmitter release from single synaptic vesicles. *Nature*, 377, 62-65.
10. Chang, J. Y., Zhang, L., Janak, P. H., & Woodward, D. J. (1997). Neuronal responses in prefrontal cortex and nucleus accumbens during heroin self-administration in freely moving rats. *Brain Research*, 754, 12-20.
11. Cholet, N., Pellerin L., Magistretti, P. J., & Hamel, E. (2002). Similar perisynaptic glial localization for Na⁺, K⁺-ATPase alpha 2 subunit and the glutamate transporters GLAST and GLT-1 in the somatosensory cortex. *Cerebral Cortex*, 12, 515-525.
12. Clements, J. D. (1996). Transmitter time course in the synaptic cleft: its role in central synaptic function. *Trends in Neuroscience*, 19, 163-171.
13. Clements, J. D., Robin, A., Lester, J., Tong, G., Jahr, C. E., et al. (1992). The time course of glutamate in the synaptic cleft. *Science*, 258, 1498-1501.
14. Danbolt, N. C. (2001). Glutamate uptake. *Progress in Neurobiology*, 65, 1-105.
15. Day, B. K., Pomerleau, F., Burmeister, J. J., Huettl, P., & Gerhardt, G. A. (2006). Microelectrode array studies of basal and Potassium-evoked release of

- L-glutamate in the anesthetized rat brain. *Journal of Neurochemistry*, 96, 1626-1635.
16. Diamond, J. S. (2005). Deriving the glutamate clearance time course from transporter currents in CA1 hippocampal astrocytes: transmitter uptake gets faster during development. *Journal of Neuroscience*, 25, 2906-2916.
 17. Diamond, J. S., & Jahr, C. E. (1997). Transporters buffer synaptically released glutamate on a sub millisecond time scale. *Journal of Neuroscience*, 17, 4672-4687.
 18. Dietrich, D., Kral, T., Clusmann, H., Friedl, M., & Schramm, J. (2002). Presynaptic group II metabotropic glutamate receptors reduce stimulated and spontaneous transmitter release in human dentate gyrus. *Neuropharmacology*, 42, 297-305.
 19. Featherstone, D. E., & Shippy, S. A. (2008). Regulation of synaptic transmission by ambient extracellular glutamate. *The Neuroscientist*, 14, 171-181.
 20. Franks, K. M., Bartol T. M., & Sejnowski, T. J. (2002). A Monte Carlo model reveals independent signaling at central glutamatergic synapses. *Biophysical Journal*, 83, 2333-2348.
 21. Haydon, P. (2001). Glia: listening and talking to the synapse. *Nature Neuroscience*, 2, 185-191.
 22. Herman, M. A., & Jahr, C. E. (2007). Extracellular glutamate concentration in hippocampal slice. *Journal of Neuroscience*, 27, 9736-9741.
 23. Jabaudon, D., Shimamoto, K., Yasuda-Kamatani, Y., Scanziani, M., Gahwiler, B. H., et al. (1999). Inhibition of uptake unmasks rapid extracellular turnover of glutamate of nonvesicular origin. *Proceedings of the National Academy of Sciences*, 96, 8733-8738.
 24. Kanai, Y., & Endou, H. (2001). Heterodimeric amino acid transporters: molecular biology and pathological and pharmacological relevance. *Current Drug Metabolism*, 2, 339-354.
 25. Lehre, K. P., & Danbolt, N. C. (1998). The number of glutamate transporter subtype molecules at glutamatergic synapses: chemical and stereological quantification in young adult rat brain. *Journal of Neuroscience*, 18, 8751-8757.
 26. Lehre, K. P., & Rusakov, D. (2002). Asymmetry of glia near synapse favors presynaptic glutamate escape. *Biophysical Journal*, 83, 125-134.
 27. Losonczy, A., Somogyi, P., & Nusser, Z. (2003). Reduction of excitatory postsynaptic responses by persistently active metabotropic glutamate receptors in the hippocampus. *Journal of Neurophysiology*, 89, 1910-1919.
 28. LoTurco, J. J., Owens, D. F., Heath, M. J., Davis, M. B., & Kriegstein, A. R. (1995). GABA and glutamate depolarize cortical progenitor cells and inhibit DNA synthesis. *Neuron*, 15, 1287-1298.
 29. Manent, J. B., & Represa, A. (2007). Neurotransmitters and brain maturation: early paracrine actions of GABA and glutamate modulate neuronal migration. *The Neuroscientist*, 13, 268-279.
 30. McFarland, K., Lapish, C. C., & Kalivas, P. W. (2003). Prefrontal glutamate release into the core of the nucleus accumbens mediates cocaine-induced reinstatement of drug-seeking behavior. *Journal of Neuroscience*, 23, 3531-3537.
 31. Meldrum, B., & Garthwaite, J. (1990). Excitatory amino acid neurotoxicity

- and neurodegenerative disease. *Trends in Pharmacological Sciences*, 11, 379-387.
32. Melendez, R. I., Vuthiganon, J., & Kalivas, P. W. (2005). Regulation of extracellular glutamate in the prefrontal cortex: focus on the cystine glutamate exchanger and group I metabotropic glutamate receptors. *Journal of Pharmacology and Experimental Therapeutics*, 314, 139-147.
 33. Moran, M. M., McFarland, K., Melendez, R. I., Kalivas, P. W., & Seamans, J. K. (2005). Cystine/glutamate exchange regulates metabotropic glutamate receptor presynaptic inhibition of excitatory transmission and vulnerability to cocaine seeking. *Journal of Neuroscience*, 25, 6389-6393.
 34. Murthy, V. N., & Sejnowski, T. J. (1997). Heterogeneous release properties of visualized individual hippocampal synapses. *Neuron*, 18, 599-612.
 35. Nicholson, C., & Sykova, E. (1998). Extracellular space structure revealed by diffusion analysis. *Trends in Neuroscience*, 21, 207-215.
 36. Nicholson, C. (2001). Diffusion and related transport mechanism in brain tissue. *Reports on Progress in Physics*, 64, 815-884.
 37. Nguyen, L., Rigo, J. M., Rocher, V., Belachew, S., Malgrange, B., et al. (2001). Neurotransmitters as early signals for central nervous system development. *Cell and Tissue Research*, 305, 187-202.
 38. Nyitrai, G., Kekesi, K. A., & Juhasz, G. (2006). Extracellular level of GABA and Glu: in vivo microdialysis-HPLC measurements. *Current Topics in Medicinal Chemistry*, 6, 935-940.
 39. Patneau, D.K., & Mayer M. L. (1990). Structure-activity relationships for amino acid transmitter candidates acting at N-methyl-D-aspartate and quisqualate receptors. *Journal of Neuroscience*, 10, 2385-2399.
 40. Pendyam, S., Mohan, A., Kalivas, P. W., & Nair, S. S. (2009). Computational model of extracellular glutamate in the nucleus accumbens incorporates the impact by chronic cocaine. *Neuroscience*, 158, 1266-1276.
 41. Peters, Y. M., O'Donnell, P., & Carelli, R. M. (2005). Prefrontal cortical cell firing during maintenance, extinction, and reinstatement of goal-directed behavior for natural reward. *Synapse*, 56, 74-83.
 42. Rainesalo, S., Keranen, T., Palmio, J., Peltola, J., Oja, S. S., et al. (2004). Plasma and cerebrospinal fluid amino acids in epileptic patients. *Neurochemical Research*, 29, 319-324.
 43. Rusakov, D. A. (2001). The role of perisynaptic glial sheaths in glutamate spillover and extracellular Ca²⁺ depletion. *Biophysical Journal*, 81, 1947-1959.
 44. Rusakov, D. A., & Kullmann, D. M. (1998). Extrasynaptic glutamate diffusion in the hippocampus: ultrastructural constraints, uptake, and receptor activation. *Journal of Neuroscience*, 18, 3158-3170.
 45. Saftenku, E. E. (2005). Modeling of slow glutamate diffusion and AMPA receptor activation in the cerebellar glomerulus. *Journal of Theoretical Biology*, 234, 363-382.
 46. Schoepp, D. D., & True, R. A. (1992). 1S-3R-ACPD-sensitive (metabotropic) [3H] glutamate receptor binding in membranes. *Neuroscience Letters*, 145, 100-104.
 47. Squire, L. R., Roberts, J. L., Spitzer, N. C., & Zigmond, M. J. (2002). *Fundamental Neuroscience*, Third Edition. Elsevier Science & Technology Books.

48. Sun, W., & Rebec, G. V. (2006). Repeated cocaine self-administration alters processing of cocaine-related information in rat prefrontal cortex. *Journal of Neuroscience*, 26, 8004-8008.
49. Sykova, E. (2004). Extrasynaptic volume transmission and diffusion parameters of the extracellular space. *Neuroscience*, 129, 861-876.
50. Tanaka, K., Watase, K., Manabe, T., Yamada, K., Watanabe, M., et al. (1997). Epilepsy and exacerbation of brain injury in mice lacking the glutamate transporter GLT-1. *Science*, 276, 1699 -1702.
51. Thorne, R. G., & Nicholson, C. (2006). In vivo diffusion analysis with quantum dots and dextrans predicts the width of brain extracellular space. *Proceedings of the National Academy of Sciences*, 103, 5567-72.
52. Tong, G., & Jahr, C. E. (1994). Block of glutamate transporters potentiates postsynaptic excitation. *Neuron*, 13, 1195-1203.
53. Trantham, H., Szumlinski, K., McFarland, K., Kalivas, P. W., & Lavin, A. (2002). Repeated cocaine administration alters the electrophysiological properties of prefrontal cortical neurons. *Neuroscience*, 113, 749-757.
54. Trommershauser, J., Schneggenburger, R., Zippelius, A., & Neher, E. (2003). Heterogeneous presynaptic release probabilities: functional relevance for short-term plasticity. *Biophysical Journal*, 84, 1563-69.
55. Van der Zeyden, M., Oldenziel, W. H., Rea, K., Cremers, T. I., & Westerink, B. H. (2008). Microdialysis of GABA and glutamate: Analysis, interpretation and comparison with microsensors. *Pharmacology Biochemistry and Behavior*, 90, 135-147.
56. Volynski, K. E., Rusakov, D. A., & Kullmann, D. M. (2006). Presynaptic fluctuations and release-independent depression. *Nature Neuroscience*, 9, 1091-1093.
57. Wadiche, J. I., Arriza, J. L., Amara, S. G., & Kavanaugh, M. P. (1995). Kinetics of a human glutamate transporter. *Neuron*, 14, 1019-1027.
58. Warr, O., Takahashi M., & Attwell, D. (1999). Modulation of extracellular glutamate concentration in rat brain slices by cystine-glutamate exchange. *Journal of Physiology*, 514, 789-793.
59. Wyatt, I., Gyte, A., Simpson, M. G., Widdowson, P. S., & Lock, E. A. (1996). The role of glutathione in L-2-chloropropionic acid induced cerebellar granule cell necrosis in the rat. *Archives of Toxicology*, 70, 724-735.
60. Xi, Z.X., Baker, D.A., Shen, H., Carson, D.S., & Kalivas, P.W. (2002). Group II metabotropic glutamate receptors modulate extracellular glutamate in the nucleus accumbens. *Journal of Pharmacology and Experimental Therapeutics*, 300, 162-171.

A.2.9. TABLES

Table 1. Physiological ranges of parameters and model values for configuration 1.

Parameter	Model value	Range of values (citation)
Diffusion coefficient ($\mu\text{m}^2/\text{ms}$)	0.05	0.05 - 0.75 (Rusakov and Kullmann 1998)
xc- prod rate (mM hr^{-1}) ^a	30	10 - 55 (Warr et al. 1999)
Transporter Dynamics		
Total XAG (molecules) ^b	5,800	2,500 - 10,000 (Bergles and Jahr 1997; Lehre and Danbolt 1998)
k_1 ($\text{M}^{-1} \text{ms}^{-1}$)	10^4	10^4 (Lehre and Rusakov 2002)
k_{-1} (ms^{-1})	0.2	0.2 (Lehre and Rusakov 2002)
k_2 (ms^{-1})	0.1	0.1 (Lehre and Rusakov 2002)
Release Parameters		
No. of molecules per release	5,000	4,700 - 80,000 (Bruns and Jahn 1995)
k_d value of mGluR 2/3 (μM)	0.187	0.1 - 0.3 (Schoepp and True 1992)
Maximum release probability	0.4 (max)	0.1 - 0.5 (Trommerhauser et al. 2003; Billups et al. 2005; Volynski et al. 2006)
Release probability used (tuned to operate near k_d value of mGluR)	0.14 (basal)	0.12 - 0.15 (Xi et al. 2002)
Presynaptic firing frequencies		
Firing freq (Hz) (basal)	1	1 - 3 (Sun and Rebec 2006; Trantham et al. 2002)
Firing freq (Hz) (reward seeking)	15	12 - 15 (Chang et al. 1997; Sun and Rebec 2006)
Geometric parameters		
Average extracellular gap (nm)	50	34 - 68 (Thorne and Nicholson 2006)
Intersynaptic distance (μm)	2	2 - 20 (Rusakov 2001)

^a xc- was volume populated on G_{3b} .

^b XAG was volume populated on glial sheaths G_1 , G_2 , and G_3 with surface density of 1,400, 1,000, and 500 molecules/ μm^2 for configuration 1. Same surface density was for sheaths G_1 , and G_2 in configuration 2 and 3.

Table 2. Prediction of glial configurations and parameters that support specified extracellular concentrations.

Configuration 1			
P_{ex} (extracellular concentration)	< 3 μM	3 - 7 μM	7 -12 μM
Diffusion coefficient (μm ² /ms)	0.13 - 0.25	0.1 - 0.15	0.05 - 0.1
xc- prod rate (mM hr ⁻¹)	15 - 25	30 - 50	>50
Transporter density (x10 ³ molecules/μm ²) ^a	2.5 - 4.5	4.5 - 7	7 - 10
Configuration 2			
P_{ex} (extracellular concentration)	< 1 μM	1 - 3 μM	3 - 5 μM
Diffusion coefficient (μm ² /ms)	0.2 - 0.4	-	-
xc- prod rate (mM hr ⁻¹)	5 - 15	-	-
Transporter density (x10 ³ molecules/μm ²) ^a	2.5 - 5	-	-
Configuration 3			
P_{ex} (extracellular concentration)	< 1 μM	1 - 3 μM	3 - 5 μM
Diffusion coefficient (μm ² /ms)	0.1 - 0.15	0.05 - 0.1	0.053
xc- prod rate (mM hr ⁻¹)	20 - 30	35 - 50	50 - 75
Transporter density (x10 ³ molecules/μm ²) ^a	2.5 - 4.5	4.5 - 7	7 - 10

^a Specifies the range of transporter densities required for glial sheaths G₁, G₂, and/or G₃ to achieve cited extracellular concentration ranges.

A.2.10. FIGURES

Configuration 1

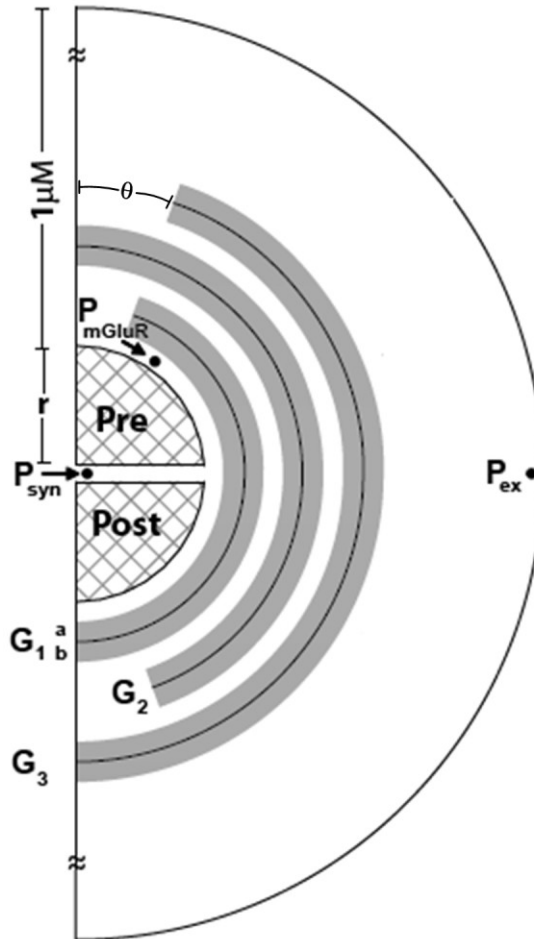


Figure 1. Schematic of configuration 1, with transporters and nonsynaptic sources in glial regions (*shaded*). The cleft ($\delta=20$ nm) separates the two hemispheres of radii $r = 160$ nm, surrounded by glial sheaths (G_i , $i=1-3$; $i=1$ being the closest to the synapse) with the highest density of transporters in G_1 and decreasing in radially outward sheaths. Each sheath was 50 nm thick with an impermeable surface in the middle, and with transporters volume populated in the 25 nm thick space on either side, permitting interaction with neurotransmitter molecules. xc- was volume populated only on sheath G_{3b} . The perisynaptic space was partitioned in radial (step $\sigma = 25$ nm) and tangential (step $\theta = 20^\circ$) directions as in Rusakov (2001) with the dimension of the

opening being 20° from the vertical. Binding, uptake and efflux are computed for each compartment. Neurotransmitter concentrations were measured at three sites, within the synaptic cleft (at P_{syn}), in the perisynaptic region containing presynaptic mGluR (at P_{mGluR}), and at the site of a dialysis probe (at P_{ex}).

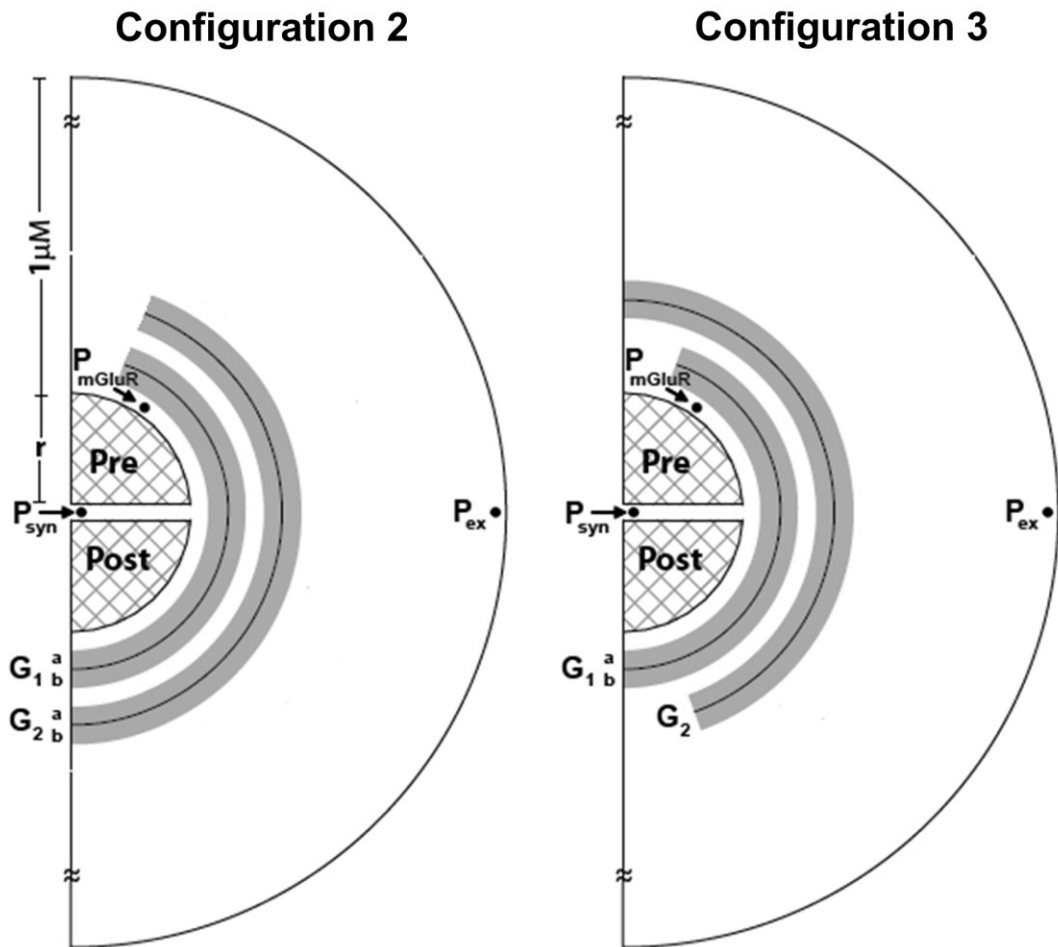


Figure 2. Two additional glial configurations used to study neurotransmitter homeostasis in the perisynaptic space (see fig 1 for locations where measurements are made). **A – configuration 2:** The presynaptic opening reduces the diffusion path length. **B – configuration 3:** Intermediate configuration that adds more diffusion path length compared to configuration 2, but not as much as in configuration 1.

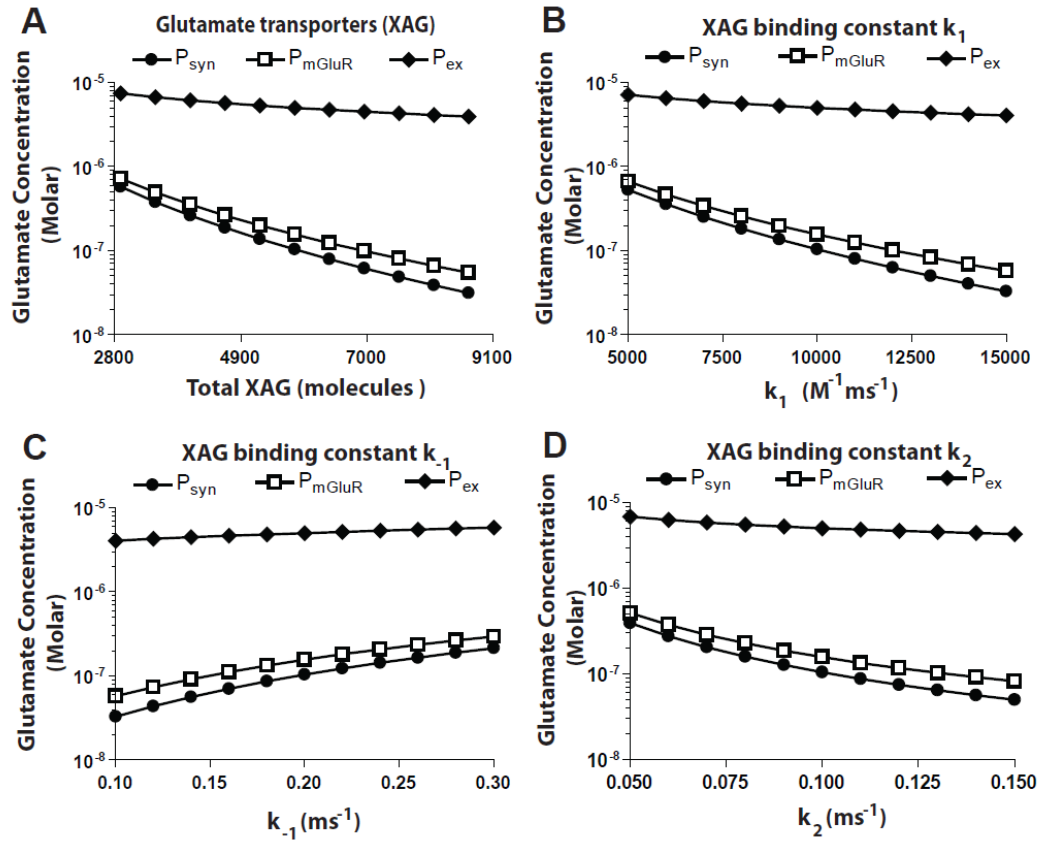


Figure 3. Effect of varying transporter parameters (others model values from table 1) on glutamate concentrations at three spatial locations under basal conditions, for configuration 1. **A.** An increase in transporters resulted in a significant drop in concentrations at P_{syn} and P_{mGluR} , but only a minor drop at P_{ex} . **B.** As the forward binding constant (k_1) was increased, the concentration of glutamate decreased at P_{syn} and P_{mGluR} , with little change at P_{ex} . **C.** As the reverse binding constant (k_{-1}) was increased, concentrations at P_{syn} and P_{mGluR} increased, while concentration at P_{ex} remained constant. **D.** As the binding constant (k_2) was increased, concentration at P_{syn} and P_{mGluR} decreased while it was constant at P_{ex} (see fig 1 for locations where measurements are made).

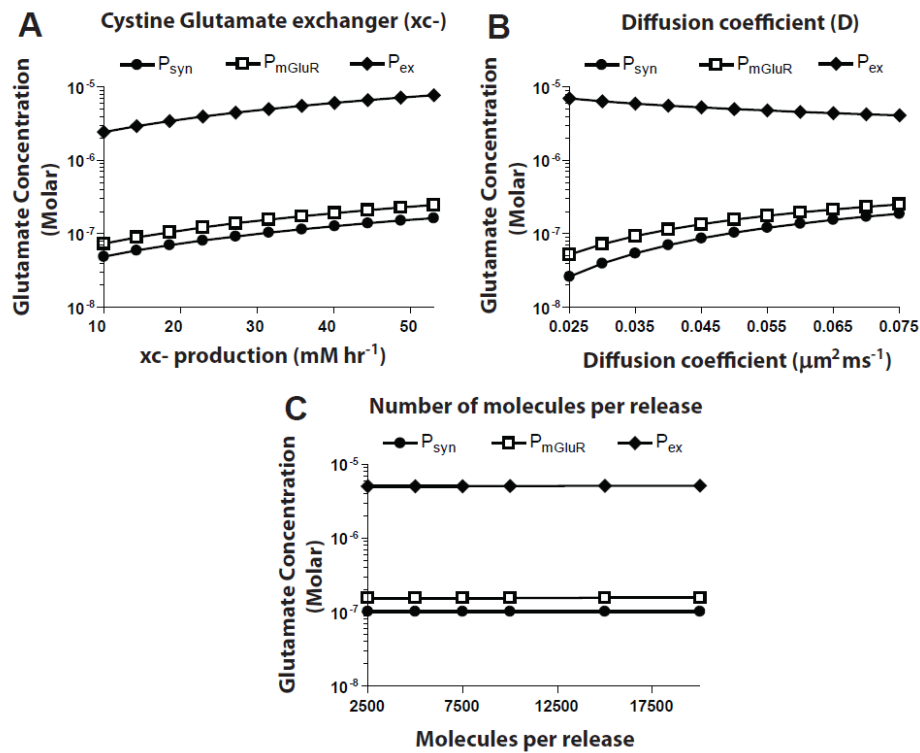


Figure 4. Effect of varying other parameters (rest of the model values from table 1) on glutamate concentrations at three spatial locations under basal conditions, for configuration 1. **A.** An increase in xc- production rate resulted in increased concentrations at P_{syn}, P_{mGluR} and P_{ex}. **B.** Increasing diffusion coefficient values resulted in increased glutamate concentrations at P_{syn} and P_{mGluR}, but decreased values at P_{ex}. **C.** Altering the molecules per release resulted in no change in the concentrations at any location (see fig 1 for locations where measurements are made).

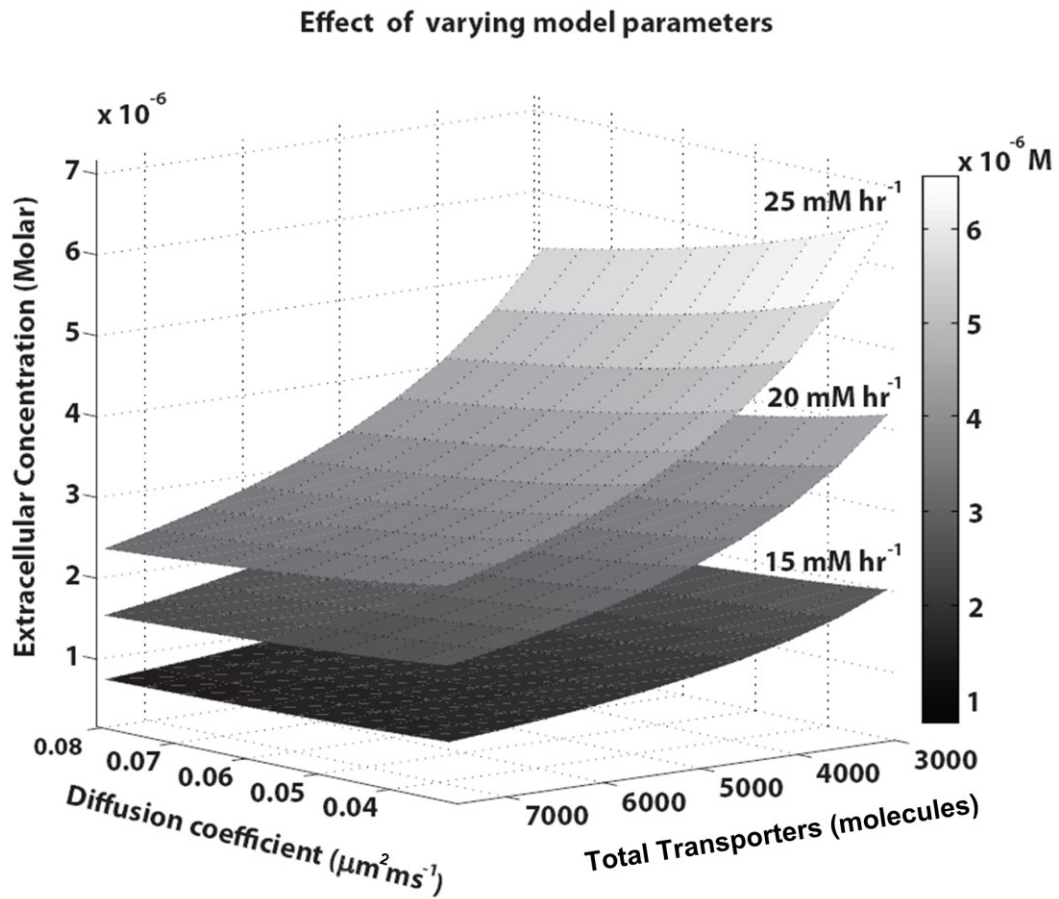


Figure 5. Multiple parameter sets for extracellular concentrations in the range of 1-5 μM were found by concurrently varying total transporters, xc- production rate, and diffusion, in the ranges shown in table 1 (the three surfaces represent three values for xc- prod rate). The other parameters were held constant at model values.

Appendix B.1

Professional Skills in the Engineering Curriculum

B.1.1. ABSTRACT

Faculty from the Department of Electrical and Computer Engineering and the College of Education at the University of Missouri (MU) developed a novel course for engineering graduate students, emphasizing pedagogy and professional skills. The two-semester course sequence, titled “Preparing Engineering Faculty and Professionals,” includes readings from books that cover several different areas: *How People Learn* with focus on the latest findings from cognitive science and their applicability to teaching, *The 7 Habits of Highly Effective People* for discussion of other professional skills, and *The World is Flat* for discussion of global trends and its effects on professionals. Other components of the course include lectures by guest speakers on topics ranging from how universities work and how to run successful research centers, to leadership traits for engineers. A pilot survey of students at the end of the two-course sequence revealed that students had acquired little knowledge about pedagogy and professional skills from other courses in their undergraduate and graduate engineering curriculum; this course addresses such deficits by raising awareness and knowledge of these skills.

B.1.2. INTRODUCTION

Scientists and engineers with advanced degrees have always been expected to possess strong technical skills, whether they work in industry or academia. However, some of the key technical skills they learn in school, including analytic and problem-solving abilities,

might be ineffectual unless accompanied by the professional skills necessary to bring them into play [1], [2]. As an example, Baca [3] reports that engineers pressed into the role of project managers in industry tend to focus on technical issues giving professional/management skills less credence, and consequently fall short of relating their game plans to the overarching strategy of the organization. The need for professional skills is supported by a decade-long survey of engineers in industry and government which revealed that engineers spend 9.7% of their time in informal discussions (receiving and communicating/sending), 21.1% in input/receiving, and 27.3% in information output/sending, with electrical engineers spending about 55% of their time communicating [4]. Such professional skills include listening, message construction, working in groups, decision making, problem solving, leadership, multidisciplinary perspective, negotiation, conflict resolution, goal setting, and understanding diversity and globalization, and these have been identified as vitally important for successful careers [5]-[8]. Engineers presently learn these skills on the job, which has been described as the learning of ‘soft skills the hard way’ [9]. While industry and government play a predominant role in determining the professional engineering environment, educational institutions should not lose sight of their responsibility to address the needs of academic, humanitarian, and national interests [10].

Also, pedagogy (the art of teaching), and grant proposal writing are related professional skills that are also growing in relevance in industry and academia [6]. Pedagogy, including research findings from cognitive science, is explicitly addressed in the preparation of students in the colleges of education, but not in engineering departments. Emphasizing this, the National Academy of Engineering [11] recommends

that “the engineering education establishment, for example the Engineering Deans Council, endorse research in engineering education as a valued and rewarding activity for engineering faculty as a means to enhance and personalize the connection to undergraduate students, to understand how they learn, and to appreciate the pedagogical approaches that excite them”. Thus, formal education of engineers should acknowledge these deficiencies in professional skills and prepare them to be competent in multiple domains [4].

B.1.2.1. The Challenge for Educators

The Accreditation Board for Engineering and Technology, Inc. (ABET) encourages universities to emphasize six “professional” skills, besides “hard” skills, in the undergraduate curriculum: communication, team work, understanding ethics and professionalism, engineering within global and societal context, lifelong learning, and knowledge of contemporary issues [12], [13]. While the engineering community has undertaken several measures to improve all facets of professional skills particularly targeted at undergraduates [13]-[16] with varying degree of success [17], [18], such requirements do not seem to exist or have been enforced in the graduate curriculum, as noted by the Boyer Commission [19] and Austin [20]. The lack of such requirements, together with time constraints due to research, precludes graduate students from reinforcing these essential survival skills. A follow-up to the Boyer Commission report [21] emphasized that as the range of employment for scientists and engineers expands, especially in the non-academic world, it is vital to develop these soft skills before leaving the university setting.

In response to the increased demands to develop professional skills as described

above, and to address the discrepancy between the preparation of graduate students and the realities of both academic work and the labor market, an interdisciplinary team at the University of Missouri developed a two-semester course sequence for engineering graduate students to emphasize the role of professional skills in advanced engineering careers.

B.1.3. ECE 8110/20 PREPARING ENGINEERING FACULTY AND PROFESSIONALS I/II

Titled "Preparing Engineering Faculty and Professionals" (PEFP), the two-semester course sequence (Table I) includes readings from three books that address multiple domains: *How People Learn* [22] (herein "HPL"), examining the latest findings from cognitive science and its applicability to teaching, *The 7 Habits of Highly Effective People* [23] (herein "7 Habits"), discussing professional skills and personal habits on how to be successful, and *The World is Flat* [24], describing global trends impacting professionals in all walks of life. The book reading sessions are interspersed with lectures by guest speakers on a variety of related topics including how universities work, how to run successful research centers, leadership traits for engineer managers, and a faculty panel reflecting on personal experiences/preparation as students. The course sequence (Table I) was designed to broaden students' depth of understanding of professional skills by promoting active learning via small-group and class discussions, debates, and student presentations. Students are also required, in groups, to develop and make presentations on topics that included lesson plan ideas emphasizing pedagogical principles, chapters from book readings, and proposal development. Pedagogical knowledge and interpersonal

communication skills, Team building and personal skills, Proposal development skills, and Globalization and gaining international experience are targeted as four key themes.

The following sections discuss the rationale and some specifics of what is emphasized in each of these four topic categories.

Pedagogy and Interpersonal Communication Skills (Book Reading: HPL). As stated, pedagogy and research findings from cognitive science are explicitly addressed in the preparation of students in the College of Education. However, engineering students and faculty are not exposed to these findings in a formal manner. Teaching skills are becoming more important for finding engineering jobs in academia and industry [1]. Increasingly, the successful “teacher” (or team leader/manager) is a coach more than a lecturer, and should be able to vary styles depending on the learning patterns of students, or of the team/staff [25]. If teaching is primarily the imparting of facts, mentoring is imparting procedures: ways of thinking, performing research, and approaching new problems. A good mentor relationship is personal: a mentee should have opportunities to discuss issues of ethical, ideological, and philosophical concern, as well as more practical matters. Exposure to these research findings will prepare a researcher or a scientist for a role as a manager to mentor junior colleagues.

According to *How People Learn* [22, pp.14-18], findings from cognitive science relevant to both teaching and mentoring (also applicable in industry) include: 1. Preconceptions among students about how the world works. If the students’ initial understanding is not engaged, they may fail to grasp new concepts and information that are taught, or they may only learn them for the purposes of a test and then revert to their preconceptions outside the classroom; 2. Students must: (a) have a deep foundation of

factual knowledge, (b) understand facts and ideas in the context of a conceptual framework, and (c) organize knowledge in ways that facilitate retrieval and application; and 3. Instruction should emphasize a metacognitive approach so that students are aware of their own learning, which enables them to define learning goals and to monitor their progress in achieving them.

Bransford et al. [22, pp.19-21] suggest the following implications for pedagogy: 1. Teachers (or team leaders/managers) must draw out and work with the pre-existing understanding that students bring with them. This contrasts with the model of the learner as an empty vessel, and instead requires the teacher to create tasks and conditions to understand the preconceptions students have, and to address those adequately prior to instruction in the specific topic. It also encourages the usage of formative assessment tools to monitor learning continuously with understanding. Such instruction is characterized as “learner-centered;” 2. Teachers must teach the subject matter in depth, providing many examples that illustrate the same concept at work to provide a firm foundation of factual knowledge. In-depth coverage of fewer topics in an area is thus more beneficial than superficial coverage of many; 3. Teachers must integrate metacognitive skills into the curriculum to strengthen student ability to monitor their own thinking.

This framework for learning applies to both adults, and to children in K-12 education [26]. Learning and mastery of professional skills relevant to the engineering workplace involves an appreciation of these advances in cognitive science, and usage of the corresponding methods proposed to improve “teaching” skills. As an example, awareness of cognitive science findings related to “how people learn” can provide the basis, in many

instances, for realizing why colleagues react as they do in individual and group settings, with both technical and personal biases. The knowledge and understanding of these cognitive findings can also enhance expertise in the other three topic areas.

Team Building and Personal Skills (Book Reading: 7 Habits). Companies use teams as an integral part of their product development, process improvement and manufacturing activities. Further, management techniques such as concurrent engineering, total quality management and business process reengineering are founded upon the concept of people working effectively in teams [13]. Similarly, research is becoming a collective enterprise in industry and academia, implying that graduate students in science and engineering are more likely to work as members of management or research teams. Engineering courses are increasingly being designed to give students the opportunity to experience teamwork first hand, so as to impart the skills necessary to work effectively in teams [13], [27]. As an application of the findings from cognitive science mentioned above (from HPL), consider an example of a team beginning work on an engineering design project. In such a case, team members might bring preconceptions (including misconceptions) to the design meetings; if not adequately discussed and addressed, such preconceptions will considerably diminish the effectiveness of the team in accomplishing project goals. Awareness of possible misconceptions can enable the team leader to give these adequate importance, and to devise techniques to elicit them from members (which includes mentoring), and importantly, to budget sufficient time to discuss the matter. Similarly, the team leader needs to ascertain the depth of technical knowledge that members possess, and accordingly encourage/mentor some to pursue opportunities to strengthen this knowledge where necessary. Finally, team members can be trained in metacognitive

skills to monitor their own contributions to team work, and to their own overall growth. External speakers also address the importance of networking and working in teams as part of a seminar on leadership.

Personal and time management skills are also covered well in the second book reading ‘7 Habits’. This reading partially satisfies the need for instruction in such professional skills, and, importantly, signals to the student that engineering faculty and administrators place importance upon the acquisition of such skills.

Proposal Development Skills – Written Communication. Buckley [28] notes “We listen to a book a day, we speak a book a week, read the equivalent of a book a month, and write the equivalent of a book a year.” Engineers are routinely required to write project reports and proposals. This requires the ability to organize thoughts and communicate them effectively [1], [4]. To enhance these skills, several class periods in the course (2nd semester, see Table I) are devoted to proposal writing, starting with a formal presentation by a professional grant writer from the university. The students are then asked to select a proposal of their choice from a “sample proposals” database (that includes reviewer comments) available at the University for faculty. Students then have to study/research that proposal and understand the critiques prior to the next class. The students are then divided into groups of two or three to discuss their findings related to the proposal selected, including reviewer comments. The entire class then shares their thoughts and ideas related to both the writing and reviewing of proposals. Students are then assigned homework to write a two-page “project summary” for a proposal topic of their choice and submit it on-line to the instructors. The submissions are then stripped of names and identifiers and assigned to two anonymous students for review during the first

half of the following class session. Students then discuss the rationale for their reviews. To close the loop, each student is then provided with the anonymous written critiques (including those from instructors), and then required to revise and resubmit their project summaries.

Globalization and Gaining International Experience (Book Reading - The World is Flat). The course integrates global issues such as understanding of the global supply chain, diversity, the flexible work force, and economics via the book reading from *The World is Flat* by Thomas Friedman [24], and with audio visual sessions of related lectures by several experts including Joseph Steiglitz, Steve Jobs, Bill Gates and Warren Buffett. The students work in groups to present each section of the book reading to the class, Table I, with extensive discussion, including the potential effect of such socio-economic changes on their own careers.

It is noted that throughout the course, students are required to make presentations related to the book readings, including discussion of the issues cited above in small groups. To initiate discussion in groups, key questions are provided by the students presenting that day, and groups are permitted ten minutes to discuss among themselves, before the issue is considered by the entire class.

B.1.4. EXPERIENCE WITH OFFERING THE COURSE

The two-semester PEFP course was first offered during 2005-06 with enrolments of 17/10 (Fall/Winter) that increased the following year to 23/16 (Fall/Winter). The course continues to be offered regularly, attracting enthusiastic students from several departments such as Electrical and Computer Engineering, Biological Engineering, Civil

Engineering, Mechanical and Aerospace Engineering, and Nuclear Engineering. To measure the participants' perceptions of change, a retrospective pre-test (here referred to as "retro-pre") was administered at the end of the course. The retro-pre survey overcomes the possibility of a response shift from pre and post-tests, and is appropriate if the goal of program evaluation is to measure participants' perception of change. However, if program effectiveness is the intent of the evaluation, then a true pre-post-test may be the best approach [29]. Thus, to assess student learning, a retro-pre survey instrument was designed (Table II) to determine the coverage of the relevant topics in the engineering undergraduate and graduate curricula, and student perceptions of how much they had learned from the PEFP course.

This survey was administered at the end of the second semester of the 2006-07 school year. The survey evaluated student attitudes about the engineering undergraduate curriculum, and other aspects of their education, including self-assessed abilities and competencies. Such surveys are less expensive to develop, administer and analyze than other types of assessment methodologies and by limiting the response choices, data collection can be repeated over time [16]. The questionnaires were designed to measure competencies in four areas: Pedagogy and inter-personal communication skills, Team building and personal skills, Proposal development skills, and Globalization and gaining international experience.

The composition of engineering graduate students during the two semesters of 2006-07 was as follows: First semester – a total of 23 students, with 11 US citizens and 12 international students; Second semester – a total of 16 students, with ten US citizens, and six international students. Ten students took both PEFP courses, of which seven

participated in the NSF GK-12 Fellows program (referred henceforth as Fellows). Three of the Fellows were in the second year of the NSF program. The program required the Fellows to attend an intensive two-week summer institute that focused instruction on pedagogy and lesson-planning skills, prior to participation in K-12 classrooms under the supervision of middle-school teachers who were themselves participants in the NSF GK-12 Fellows project [8]. Of the non-GK-12 students enrolled in the PEFP courses, three enrolled in both semesters of the course, and six enrolled in only the second semester.

To compare the gains among the different students enrolled, the survey participants were divided into four different groups, based on status and semesters enrolled in PEFP: *Group 1*: students with four semesters of involvement (due to NSF grant requirements) in the GK-12 Fellows program and PEFP course (n=3); *Group 2*: Fellows with two semesters of the PEFP course (n=4); *Group 3*: regular graduate students (non-Fellows) with two semesters of PEFP classes (n=3); and *Group 4*: non-Fellows enrolled for only one semester of PEFP classes (n=6). Since the retro-pre survey was administered at the end of the second semester in the one-year sequence, students in Group 4 did not respond to the topics covered in the course the prior semester (topic categories 1 and 2 in Table III).

B.1.4.1. Findings from the Pilot Survey and Discussion

Table III lists the results from the survey that covered four topics, each with six items, for an overall total of 24 items. The means were calculated within each group (Groups 1-4, as described earlier) for each item, both about what they learned from their undergraduate and graduate curricula and from the PEFP course. The weighted differences in means were then computed to obtain more accurate comparisons of student

perception of learning in the various topic categories. The weighted difference in means for a particular item, T_g , across all groups, is defined as $T_g = \sum(T_i * n_i) / \sum(n_i)$ where T_i is the difference in means for each group on an item, and n_i is the membership of group i . The average of weighted differences in means across all the topics (i.e., average of T_g across all items in Table III) was found to be 1.22, and so, in the discussion below, only those items for which the weighted differences in means were greater than 1.20 were considered.

Comparison of gains in various topic categories. Averaged across all items in a topic category, the largest perceived gains from the PEFP course compared to what students had learned from their undergraduate or graduate curricula, were in Proposal development (1.92) followed by Pedagogy and inter-personal communication skills (1.67), Globalization and gaining international experience (1.13) and Team building and personal skills (0.18). Each of the topic categories is considered in more detail below.

Pedagogy and inter-personal communication skills. All four groups that participated in the survey showed weighted difference in means T_g greater than 1.20 in five of the six items in the Pedagogy and inter-personal communication skills topic category. The highest gains were in general pedagogical skills (2.30) and how people learn (2.30). These gains possibly occurred because all the groups were involved in intensive discussions and reflections when these topics were covered.

Team building and personal skills. Although exposed to working in groups throughout the course, and to leadership development seminars, students enrolled in the PEFP course showed no significant perceived gain in the area of team building skills. Three of six items in this topic category showed negative weighted means. However,

sensitivity to inter-cultural differences and personal goal setting showed positive changes. The negative numbers could indicate that the students already had exposure to these skills prior to the PEFP course. This might be due to their work in research groups, and/or exposure to teamwork in courses with laboratory projects, such as senior/capstone design. However, it is possible that student perception of the questions in this category, for example on how to lead a team and assess its progress, might be different from the requirements in the real world workplace.

Proposal development skills. Comparing the weighted means for all groups in the listed categories, the largest gains were made, interestingly, in the broad area of proposal development skills. This indicates an active need to address the topic category formally in the engineering curriculum to better prepare graduate professionals. Five of the six items discussed in this topic category showed gains (T_g) over 1.20, with the highest gains in “common mistakes made during grant proposal process” (2.38) and “proposal review process” (2.19).

Globalization and gaining international experience. As stated earlier, this topic category focused on the book *The World is Flat* [24], with discussion of trends, cultural issues, economics, business practices, diversity, and the role of collaboration in the global workplace. Groups debated how globalization might be perceived as a boon or a bane by different peoples around the world. The highest gains for this topic category were in the following two areas: impact of globalization on the way companies do business (1.50), and the role of collaboration in the global market place (1.25).

B.1.4.2. Learning among the Various Groups

The differences in means between the four groups of students were explored further

using each topic category to determine meaningful trends, albeit with low numbers of cases in each group.

Pedagogy and inter-personal communication skills. Among the four groups, Group 1 reported the largest gains in five of the six items within this topic, followed by Group 2, with Group 3 reporting the lowest on five of the six items. This may be an indication that sustained instruction in the area is beneficial since Group 1 students also completed a focused Summer Institute devoted to these topics, followed by year-long interactions with both K-12 teachers and students in classroom settings. Interestingly, Group 1 also consistently rated the learning from their undergrad or graduate curricula the lowest for all items in this category. This could possibly be explained by a lack of knowledge of the nuances of these topics on the part of students in the other groups. That is, there may be a tendency among engineers to rate themselves highly on teaching based solely on their technical knowledge; however, it takes actual teaching experience and, importantly, feedback from students and peers (all provided to Group 1 students), to realize that they may not yet be good teachers.

Team building and personal skills. As mentioned earlier, students enrolled in the PEFP course reported the least overall gain in the area of team building skills, due possibly to the fact that the topic was discussed only in a general sense in the course, without any focused instruction/activities. Even though significant overall gains were not noticed in this category after the PEFP course, Group 1 students reported higher gains, while Group 2 reported the lowest. Group 1 students had taken two years of PEFP courses (due to NSF grant requirements), and had field experience in K-12 classrooms,

probably highlighting the importance of team building skills first-hand to them, compared to the other groups.

Proposal development skills. The intensive focus of this segment seems to have helped students of Group 3 the most. A member of that group mentioned that he had learned a lot because of his personal interest in the topic due to its importance in engineering careers. Group 4 reported the least gains in general in all the items in this category, possibly indicating the need for sustained instruction.

Globalization and gaining international experience. Group 1 reported the largest gains in five of the six items in this category, followed by Group 3, with Group 2 reporting the lowest gains on most items.

B.1.4.3. Information Gained from Undergraduate and Graduate Curriculum

For this analysis, the weighted means for each of the items across all the groups in *Part i* of the survey (“*From undergrad and grad engineering curriculum*”, see Table II) was considered. This resulted in the following numbers representing the perception of the entire class about their knowledge gained from undergraduate and graduate curricula: 2.26 for Pedagogy and inter-personal communication skills, 2.83 for Team building and personal skills, 1.78 for Proposal development skills, and 2.46 for Globalization and gaining international experience. Thus, when viewing information gained from prior curriculum, the class rated Team building skills slightly higher than the others, followed by Globalization and its impact. Interestingly, all groups did feel that they lacked information on Pedagogy and communication skills, with Proposal development skills rated the lowest.

Considering each group separately, Group 1 consistently scored themselves low when

averaged across each of the four topic categories, when compared to the other groups, with an average score of 1.74. Group 4 students, who had attended only one semester of the course, on the other hand, had the highest score of 2.59 when averaged across the 24 items. This interesting trend could also possibly be explained by the extended exposure that Group 1 students had to the topics, and due to their experience in K-12 classrooms. The additional exposure in K-12 classrooms may have clarified the meaning and depth of the recent findings in cognitive science to Group 1 students, highlighting their lack of understanding of the details related to topics such as pedagogy. Conversely, not having the benefit of this experience, Group 4 students were probably lacking depth of knowledge in these topics and therefore could not rate themselves accurately. All this highlights the need for formal instruction in pedagogy and professional skills in the engineering curriculum.

In summary, the pilot data revealed the following trends: 1. When considering the perception of knowledge gained solely from undergraduate and graduate curricula, the average of the weighted means for all topics was ~ 50% of the maximum of 5.0, indicating a perception of lack of such skills. Group 1 consistently scored low in all topic categories compared to the other groups, on knowledge gained from undergraduate and graduate curricula; 2. The largest gains in student perception from the PEPF course sequence occurred in the topic category of Proposal development skills implying a need to address this formally in the graduate curriculum; 3. Group 1 reported the largest gains in knowledge in three of the four topic categories after the course, revealing several interesting trends discussed earlier; 4. When considering the perception of knowledge gained from the course, the average of the weighted means for all the items across all the

topic categories was ~ 70% of the maximum of 5.0, indicating, interestingly, that all students still felt the need to learn more about these topics. This highlights that formal and sustained instruction in the topics addressed may be required to reveal deficiencies to the students themselves. In turn, this should encourage students to pursue opportunities to reinforce the skills by either taking relevant courses or joining appropriate college/campus organizations, while still in school.

It should be noted that the findings from the survey were based on pilot data, and more extensive studies should be performed to validate the reported trends. One of the challenges for graduate students was scheduling the course into the curriculum, and so the two courses were designed to be independent albeit complementary. Mentoring, formative assessment and scaffolding are important topics that could be emphasized in greater depth in future offerings of the course. Since the topics discussed have relevance to undergraduates [12], the course has recently been made open to selected senior undergraduates in engineering.

B.1.5. CONCLUSIONS

A novel course was designed to introduce engineering students formally to professional skills through four topic categories: Pedagogy and interpersonal communication skills, Team building and personal skills, Proposal development skills, and Globalization and gaining international experience. The retro-pre pilot survey revealed that sustained instruction (including metacognition) in these topic categories did increase awareness and understanding of the importance of professional skills. The students were very appreciative of the opportunity to interact with peers who had varied

interests, and to discuss and reflect on such issues. A key component of the course is a discussion of the latest findings from cognitive science, which are summarized in the book *How People Learn* [22]. The cognitive science findings indicate that some of the professional skills may, in fact, be “hard” skills when the neuroanatomical brain organization is considered, and this may further motivate students in appreciating why an understanding of such findings may be important for their professional careers.

B.1.6. ACKNOWLEDGMENT

This research was supported in part by a National Science Foundation GK-12 Fellows grant DGE-0440524 to University of Missouri-Columbia.

B.1.7. REFERENCES

1. Committee on Science, Engineering and Public Policy (COSEP), *Careers in Science and Engineering*. Washington D.C.: National Academy Press, 1996. Available: http://books.nap.edu/catalog.php?record_id=5129
2. T. W. Hissey, “Education and Careers 2000: Enhanced skills for engineers,”
3. *Proc. IEEE*, vol. 88, no. 8, pp. 1367-1370, Aug. 2000.
4. C.M. Baca, “Project manager! Who? Me?,” *Machine Design*, vol. 79, no. 20, pp. 64-66, Oct. 2007.
5. C. Tenopir and D.W. King, *Communication patterns of engineers*. New York: IEEE/Wiley InterScience, 2004.
6. D. Chubin, K. Donaldson, B. Olds, and L. Fleming, “Education Generation Net – Can U.S. Engineering Woo and Win the competition for talent?,” *ASEE Journal of Engineering Education*, vol. 97, no. 3, pp. 245-257, July 2008.
7. J. S. Lamancusa, J. L. Zayas, A.L. Soyster, L. Morell, J. Jorgensen, “The learning factory: Industry-partnered active learning,” *ASEE Journal of Engineering Education*, vol. 97, no. 1, pp. 1-15, Jan. 2008.
8. J.H. McMasters, “Influencing student learning: An industry perspective,” *International Journal of Engineering Education*, vol. 23, no. 3, pp. 447-459, June 2006.
9. *NSF Graduate Teaching Fellows in K-12 Education (GK-12)*, National Science Foundation Publication., Washington DC, Rep. NSF 06-556, 2006. Available: <http://www.nsf.gov/pubs/2006/nsf06556/nsf06556.htm>
10. S. Kumar and J.K. Hsiao, “Engineers Learn Soft Skills the Hard Way: Planting a

- Seed of Leadership in Engineering Classes,” *Leadership and Management in Engineering*, vol.7, pp. 23-28, Jan. 2007.
11. F. C. Berry, P. S. Dipiazza, and S. L. Sauer, “The future of electrical and computer engineering education,” *IEEE Trans.Ed.*, vol. 46, no. 4, pp. 467-476, Nov. 2003.
 12. National Academy of Engineers (NAE), *Educating the Engineer of 2020: Adapting Engineering Education to the New Century*, Washington, D.C., 2005.
 13. Accreditation Board for Engineering and Technology, Inc. (ABET), *Engineering Criteria 2000*, ABET, Baltimore, MD, 1998.
 14. L. J. Shuman, M. Besterfield-Sacre, and J. McGourty, “The ABET ‘Professional Skills’ – Can they be taught? Can they be assessed?,” *ASEE Journal of Engineering Education*, vol. 94, no. 1, pp. 41-55, Jan. 2005.
 15. K.A. Smith, S.D. Sheppard, D.W. Johnson, and R.T. Johnson, “Pedagogies of engagement: classroom-based practices,” *ASEE Journal of Engineering Education*, vol. 94, no. 1, pp. 87-101, Jan. 2005.
 16. D. J. Moore, and D. R. Voltmer, “Curriculum for an engineering renaissance,” *IEEE Trans. Ed.*, vol. 46, no. 4, pp. 452-455, Nov. 2003.
 17. J. McGourty, L. Shuman, M. Besterfield-Sacre, C. Atman, R. Miller, B. Olds, G. Rogers, and H. Wolfe, “Preparing for ABET EC 2000: Research-based assessment methods and processes,” *International Journal of Engineering Education*, vol. 18, no. 2, pp. 157-167, Apr 2002.
 18. J. Kadlowec, K. Bhatia, T.R. Chandrupatla, J.C. Chen, E. Constans, H. Hartman, A.J. Marchese, P. von Lockette, H. Zhang, “Design integrated in mechanical engineering curriculum: Assessment of engineering clinics,” *Journal of Mechanical Design*, vol. 129, pp.682-691, July 2007.
 19. J. W. Pardos, G. D. Peterson, L. R. Lattuca, “Quality assurance of engineering education through accreditation: the impact of Engineering Criteria 2000 and its global influence,” *ASEE Journal of Engineering Education*, vol. 94, no 1, pp. 165-184, Jan. 2005.
 20. Boyer Commission, *Reinventing Undergraduate Education: A Blueprint for America’s Research Universities*. Menlo Park, CA: Carnegie Foundation for the Advancement of Teaching, 1998.
 21. A. E. Austin, “Preparing the next generation of faculty,” *The Journal of Higher Education*, vol. 73, no. 1, pp. 94-122, Jan. 2002.
 22. Boyer Commission, *Three Years after the Boyer Report*. Menlo Park, CA: Carnegie Foundation for the Advancement of Teaching, 2001.
 23. J.D. Bransford, A. L. Brown and R. R. Cocking, Editors, *How People Learn: Brain, mind, experience, and school*, Washington D.C.: National Academy Press, 2001.
 24. S.R. Covey, *The 7 Habits of Highly Effective People*, Free Press, 1990.
 25. T.L. Friedman, *The World is Flat – A Brief History of the Twenty-First Century*, Farrar, Straus and Giroux, NY, 2005.
 26. W.J. McKeachie and M. Svinicki, *McKeachie's teaching tips: Strategies, research, and theory for college and university teachers. College teaching series*, 12th edition. Boston, MA: Houghton Mifflin Company, 2006.

27. D. Bergin, S.K. Khanna, J. Lynch and S.S. Nair, "Infusing design into the G6-9 Curriculum – Two example cases," *International Journal of Engineering Education*, vol. 23, no.1, pp.43-49, 2007.
28. E. Seat and S. M. Lord, "Enabling effective engineering teams: A program for teaching interaction skills," *ASEE Journal of Engineering Education*, vol. 88, no.4, pp. 385-390, 1999.
29. M.H. Buckley, "Focus on Research: We listen a book a day; speak a book a week: Learning from Walter Loban," *Language Arts*, vol. 69, pp.622-626, Dec. 1992.
30. L.G. Hill and D.L. Betz, "Revisiting the Retrospective Pretest," *American Journal of Evaluation*, vol. 26, no.4, pp. 501-517, 2005.

B.1.8 TABLES

Table 1. Course Description and Schedule for the Two-Semester Course ECE 8110/8120
“Preparing Engineering Faculty and Professionals I/II”

Course descriptions:

Part I: This two-semester course (Part II to be taught in Winter semester) will consist of a weekly series of one-hour seminars pertaining to a variety of topics: pedagogy – latest from cognitive science and learning theory, based on material from ‘How People Learn’ (The National Academy Press, 1999 – first book reading); how to be an effective teacher; how does a university function?; engineering teaching and research at leading universities; how do leading industries perform research?; etc., and the importance of professional skills (2nd book reading – ‘The 7 Habits of Highly Effective People’ by Stephen Covey).

Part II: The second course in the two-semester sequence (both independent of each other) continues the format in Part I with a combination of group discussions using book readings and seminars by experts. A major focus in Part II of the course will be on “How to write an effective proposal,” which will span about 4 weeks. As part of that segment, students will review model proposals, model reviews, and the segment will culminate with a ‘hands-on’ proposal writing session. This will be followed by the book reading focusing “globalization and how it affects professionals,” using the book “The World is Flat” by Thomas Friedman.

The requirements for the courses are attendance, participation in class discussions, and submission of materials developed for student presentations.

Instructors: Dr. Satish Nair, Professor of Electrical and Computer Engineering, and Dr. John Lannin, Associate Professor of Learning, Teaching and Curriculum, College of Education.

Typical schedule for ECE 8110 Preparing Engineering Faculty and Professionals - I (Fall semester)

- Week 1: Introduction and overview of course – Profs. Nair and Lannin. Assignment of chapters from book, and formation of student groups to lead the book reading sessions. What is lesson planning and how can one “lead” discussions using the lesson plan format?
- Week 2: Discussion of chapters 1 and 2 of How People Learn (HPL) – group 1 to “lead”.
- Week 3: Discussion of chapters 3 and 4 of How People Learn (HPL) – group 2 to “lead”.
- Week 4: Formal lecture on “Lesson Planning” including demos. Students informed that they are to prepare and present simple lessons in groups during Week 6.
- Week 5: External speaker – e.g., “Leadership Skills” Office of Leadership Development, University of Missouri. (“hands on” seminar)
- Week 6: Lesson plan presentations (emphasizing pedagogy) by student groups.
- Week 7: Discussion of chapters 5 and 6 of How People Learn (HPL) - group 3 to “lead”.

- Week 8: External speaker: Vice President for Academic Affairs or VP for Research, University of Missouri System – How Universities Work? (including admin. structure, promotion and tenure, etc.)
- Week 9: Discussion of chapters 7 and 8 of How People Learn (HPL) - group 4 to “lead”.
- Week 10: “Summary” discussion related to How People Learn – Instructors.
- Week 11: Discussion of “The 7 Habits of Highly Effective People” – Habits 1 and 2
- Week 12: Discussion of “The 7 Habits of Highly Effective People” – Habits 3 and 4
- Week 13: External speaker – e.g., the importance of evaluating performance of projects and how it is done
- Week 14: Discussion of “The 7 Habits of Highly Effective People” – Habits 5, 6 and 7
- Week 15: External speaker – e.g., “Personality Tests – what do they reveal” + strategies for team building
- Week 16: Wrap up of the course and preview of Course II – Faculty organizers. Surveys administered. Students turn in their slides/discussion notes that they used for their presentations.

Typical schedule for ECE 8120 Preparing Engineering Faculty and Professionals – II (Winter semester)

- Week 1: Introduction and overview of course – Profs. Nair and Lannin. Pedagogy and professional skills in engineering. Revisit lesson planning – how can one “lead” discussions using a lesson plan format.
- Week 2: How to write an effective proposal – An Introduction: Grant writer from the college of engineering. A variety of related articles and material distributed. Students are asked to select a model proposal (including reviewer comments) from a univ. database available for faculty, print and read it for discussion in the next class.
- Week 3: Discussion on model proposals that students have printed and brought to class. Students to come up with an idea for a proposal of their own prior to the next class. Prof. Lannin.
- Week 4: How to write an effective proposal – hands-on session focusing on writing the “project summary”, i.e., clearly defining the project idea.
- Week 5: Proposal writing – budget development.
- Week 6: Discussion of chapters 1 and 2 (#1-4) of The World is Flat – led by class group 1.
- Week 7: Discussion of chapters 2 (#5-10) and 3 of The World is Flat – led by class group 2.
- Week 8: Audio video sessions by Bill Gates and Warren Buffet “Go back to school” – PBS video + video of Steve Jobs talk interacting with students.
- Week 9: Discussion of chapters 4 to 7 of The World is Flat – led by class group 3.
- Week 10: No Class – Spring Break.
- Week 11: Discussion of chapters 8 to 10 of The World is Flat – led by class group 4.
- Week 12: Services offered for students – Career Services + Library Services.
- Week 13: Discussion of chapters 11 to 14 of The World is Flat – led by class group 5.
- Week 14: MU Faculty Panel on ‘Careers in academia v/s career in industry’
- a Q/A session with students.

Week 15: Discussion of chapters 15 to 17 of The World is Flat – led by class group 6.
Week16: Wrap up session – faculty organizers. Surveys administered.

Table 2. Graduate Student Survey

<p><i>Your status (circle one):</i> GK-12 Fellow – 1 year 2 years One semester of PEFP class Two semesters of PEFP classes</p>

Rate the importance, in your opinion, of:

- (i) The extent to which the following skills/knowledge was addressed in your undergraduate or graduate engineering curriculum**
- (ii) Your current knowledge of the following skills/knowledge as a result of the PEFP course(s)**

RATE BY CIRCLING ON A SCALE OF 1-5: 1 being ‘very little’ and 5 being ‘a lot’

	Part i					Part ii				
	From undergrad and grad engineering curriculum					From PEFP course(s)				
	1	2	3	4	5	1	2	3	4	5
1 How people learn	1	2	3	4	5	1	2	3	4	5
2 Deep understanding of content	1	2	3	4	5	1	2	3	4	5
3 How to engage students in active learning	1	2	3	4	5	1	2	3	4	5
4 Use various assessment strategies	1	2	3	4	5	1	2	3	4	5
5 General pedagogical skills (e.g., lesson planning)	1	2	3	4	5	1	2	3	4	5
6 Interpersonal communication skills	1	2	3	4	5	1	2	3	4	5
7 Personal time management skills	1	2	3	4	5	1	2	3	4	5
8 How to mentor others	1	2	3	4	5	1	2	3	4	5
9 How to lead a team	1	2	3	4	5	1	2	3	4	5
10 How to assess a team’s progress	1	2	3	4	5	1	2	3	4	5
11 Sensitivity to intercultural differences	1	2	3	4	5	1	2	3	4	5
12 Personal goal setting	1	2	3	4	5	1	2	3	4	5

Rate the importance, in your opinion, of:

(i) The extent to which the following skills/knowledge was available from your undergraduate or graduate engineering curriculum

(ii) Your current knowledge of the following skills/knowledge as a result of the course

RATE BY CIRCLING ON A SCALE OF 1-5: 1 being 'very little' and 5 being 'a lot'

	Part i					Part ii				
	From undergrad and grad engineering curriculum					From PEFP course(s)				
13 Proposal development process	1	2	3	4	5	1	2	3	4	5
14 Various sections of a typical proposal	1	2	3	4	5	1	2	3	4	5
15 How to design a budget	1	2	3	4	5	1	2	3	4	5
16 Agencies who fund research	1	2	3	4	5	1	2	3	4	5
17 Common mistakes made during the grant proposal Process	1	2	3	4	5	1	2	3	4	5
18 Proposal review process	1	2	3	4	5	1	2	3	4	5
19 Global trends in engineering careers	1	2	3	4	5	1	2	3	4	5
20 How global trends impact your career field	1	2	3	4	5	1	2	3	4	5
21 Your preparedness for the global marketplace	1	2	3	4	5	1	2	3	4	5
22 Cultural issues and their impact on globalization	1	2	3	4	5	1	2	3	4	5
23 Impact of globalization on the way companies do Business	1	2	3	4	5	1	2	3	4	5
24 Role of collaboration in the global marketplace	1	2	3	4	5	1	2	3	4	5

Table 3. Results from Graduate Student Survey

Topic category	Number	Item	Means for Part i				Means for Part ii				Difference in Means				Weighted difference in means
			From undergrad and grad engineering curriculum				From PEPF course(s)				Means Part ii - Means Part i				
			Group 1	Group 2	Group 3	Group 4	Group 1	Group 2	Group 3	Group 4	Group 1	Group 2	Group 3	Group 4	T _g
Pedagogy and inter-personal communication skills	1	How people learn	1.00	1.50	1.66	2.33	4.00	3.50	3.66	a	3.00	2.00	2.00	a	2.30
	2	Deep understanding of content	1.66	2.25	3.33	3.00	3.66	3.25	4.00	a	2.00	1.00	0.67	a	1.20
	3	How to engage students in active learning	1.33	2.00	2.66	2.33	4.33	3.50	3.66	a	3.00	1.50	1.00	a	1.80
	4	Use various assessment strategies	1.33	1.75	3.33	2.66	4.00	4.00	3.66	a	2.67	2.25	0.33	a	1.80
	5	General pedagogical skills (e.g., lesson planning)	1.00	1.50	1.33	2.50	3.33	4.00	3.33	a	2.33	2.50	2.00	a	2.30
	6	Interpersonal communication skills	2.66	3.25	2.66	3.33	3.66	3.00	4.00	a	1.00	-0.25	1.33	a	0.60
Team building skills and personal skills	7	Personal time management skills	3.00	3.50	2.33	2.83	3.00	3.00	3.33	a	0	-0.50	1.00	a	0.10
	8	How to mentor others	2.00	3.00	3.00	2.66	2.66	2.75	2.33	a	0.67	-0.25	-0.67	a	-0.10
	9	How to lead a team	2.33	3.25	3.00	3.00	2.33	2.50	2.67	a	0	-0.75	-0.33	a	-0.40
	10	How to assess a team's progress	2.33	2.75	3.33	3.16	2.33	3.00	2.66	a	0	0.25	-0.67	a	-0.10
	11	Sensitivity to intercultural differences	1.33	3.25	2.66	2.50	3.00	4.00	3.33	a	1.67	0.75	0.67	a	1.00
	12	Personal goal setting	2.33	3.50	3.33	2.83	3.66	3.25	4.33	a	1.33	-0.25	1.00	a	0.60

<i>Proposal development – written communication skills</i>	13	Proposal development process	1.33	1.50	1.66	2.33	3.33	3.50	4.33	4.26	2.00	2.00	2.67	1.83	2.06
	14	Various sections of a typical proposal	1.66	1.50	1.33	2.16	3.33	4.00	3.66	4.00	1.67	2.50	2.33	1.83	2.06
	15	How to design a budget	1.33	1.50	2.00	2.16	1.66	2.50	4.00	3.33	0.33	1.00	2.00	1.17	1.13
	16	Agencies who fund research	2.33	1.75	1.33	2.50	3.33	3.50	4.00	4.00	1.00	1.75	2.67	1.50	1.69
	17	Common mistakes made during the grant proposal process	1.33	1.50	1.66	2.00	3.66	4.00	4.66	4.00	2.33	2.50	3.00	2.00	2.38
	18	Proposal review process	1.33	1.50	1.66	1.83	4.00	3.75	4.33	3.50	2.67	2.25	2.67	1.67	2.19
<i>Globalization and gaining international experience</i>	19	Global trends in engineering careers	1.66	2.50	3.00	2.66	4.00	2.75	3.33	3.33	2.33	0.25	0.33	0.67	0.81
	20	How global trends impact your career field	2.00	2.75	2.66	2.66	3.66	3.5	3.33	3.83	1.67	0.75	0.67	1.17	1.06
	21	Your preparedness for the global marketplace	1.66	3.00	2.33	2.5	3.00	3.00	3.00	4.00	1.33	0	0.67	1.50	0.94
	22	Cultural issues and their impact on globalization	1.66	3.00	2.00	2.83	3.00	3.50	4.00	4.00	1.33	0.50	2.00	1.17	1.19
	23	Impact of globalization on the way companies do business	1.30	2.50	2.00	2.83	3.66	3.25	4.00	4.16	2.33	0.75	2.00	1.33	1.50
	24	Role of collaboration in the global marketplace	2.00	3.00	2.33	2.50	3.66	3.75	3.66	3.83	1.67	0.75	1.33	1.33	1.25

^a Group 4 students were not enrolled in the particular semester when Items 1-12 were introduced.

Appendix C.1

Are we like robots?

Subject Area(s) Life Science, Biology, Science and Technology

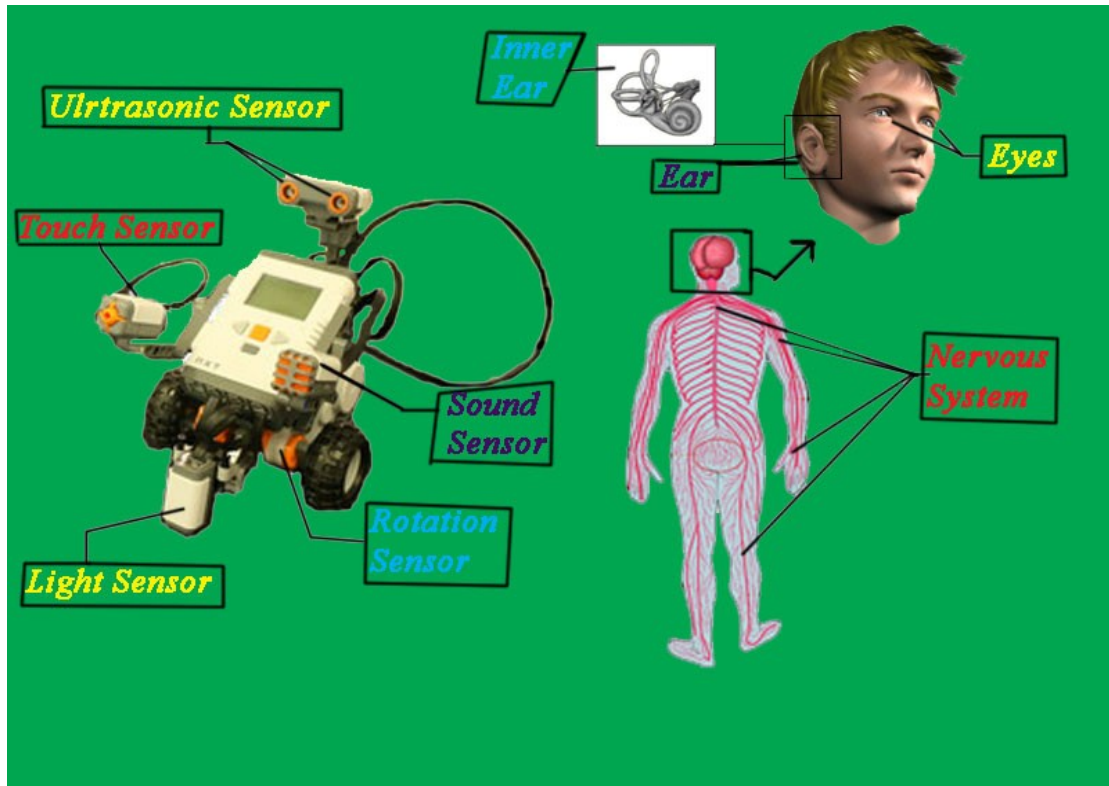


Image 1

ADA Description: Picture of NXT LEGO Robot with electronic sensors with a drawing of the human nervous system

Caption: none

Image file name: electronic_sensors_lego_nxt_nervous_system.jpg

Source/Rights: None

Grade Level: 5 (4-7)

Time Required: 20 min

Summary This lesson displays the similarities that exist between a functioning robot and the human body. This allows children to see the human body as a working system, and from the perspective of an engineer. To reinforce the engineering principles that can be seen in the human body, the lesson contains two examples of robots as comparisons to

humans. The first example, a LEGO NXT Taskbot, serves mainly to compare the five senses with the sensors of a robot. The second example is a computer, in which more specific parts of the body including parts of the brain, nervous system, and various organs in the body are compared to hardware found in computers.

Engineering Connection A major component of biological engineering and neuroscience is the ability to see the human body as a functioning, controlled system, similar to a robot. More and more findings are showing that mathematical principles similar to those used in robotics are extremely useful or even necessary for a complete understanding of the human body. With such fields as biological engineering, systems neurobiology, and biological engineering, engineers are becoming more and more involved in research involving the human body and efforts to replicate the functioning of many of its systems.

Engineering Category Relating science concept to engineering

Keywords Brain, Computer, Muscles, Sensors, Biotech, LEGO

Educational Standards

- Science: Missouri 2005 Strand 8.1.B. a (grade 3,4,5)
 - Describe how new technologies have helped scientists make better observations and measurements for investigations (e.g., telescopes, electronic balances, electronic microscopes, x-ray technology, computers, ultrasounds, computer probes such as thermometers)

Missouri 2005 Strand 3.2.C.g (grade 8)

- Explain the interactions between nervous and muscular systems when an organism responds to a stimulus

Pre-Requisite Knowledge

- Knowledge of parts of a computer
- Understanding of the senses of the human body
- Basic knowledge of types of sensors seen on robots
- Knowledge of brain functions and the major parts of the brain.

Learning Objectives

After this lesson, students should be able to:

- Begin to visualize the human body from the perspective of an engineer- as a functioning system of interacting elements, much as the systems in a robot.
- Compare body functions and related structures to systems within a robot.
- Describe how human body response to a stimulus is like a robot response to its sensors

Introduction / Motivation

NOTE: This section is meant for the teacher to impart information to the students. This information can be used along with the powerpoint slides provided for this lesson.

PART 1: A Human is a Robot

- **HUMAN BODY AND ITS COMPONENTS**

Sensors

Your sensory organs (eyes, ears, nose and skin) provide much needed information to make decisions.

- There are five senses that we all are familiar with
 - Your eyes allow you to see the world.
 - Your ears allow you to hear sounds.
 - Your skin lets you feel objects through touch.
 - Your nose lets you smell the many scents present in the world.
 - Your tongue lets you taste.
- There are also other sensors in the body that we don't notice directly.
 - Sensors in the inner ear give the body information about balance
 - Sensors in our muscles that let the brain know our body position.

Human Body itself

Various parts of the body contribute to the effective day to day functions.

- Your heart provides much of the energy to keep you going by pumping oxygenated blood to all organs and removing harmful gases out of the system.
- Your muscles allow you to move around by providing a force against your bones that causes motion.
- The full functioning of the human body requires all of its components, kind of like a robot. For example, when you are eating, sensors in your eyes send messages through your nervous system to your brain, which allows you to see the food. The brain then sends a message to the muscles in your arms and hands for you to move your fork and pick up the food, then transfer it to your mouth. Taste sensors in your tongue will then send messages through your nervous system to your brain, telling it whether the

food tastes good or not, which allows the brain to decide whether it should tell your muscles to get more.

NOTE: This section utilizes a LEGO NXT Mindstorm Kit. Prior to the class, the teacher is required to make a LEGO NXT Taskbot based on instructions provided with the kit. This basic information to make a Taskbot is also provided with this material along with instructions to program the LEGO NXT Taskbot.

- **ROBOT AND ITS COMPONENTS**

Sensors

- A sensor is a device that measures a physical quantity and transmits this measurement so that a computer, instrument, or observer can read it.
- Some sensors simply detect the presence of a stimulus –
 - Example: A sound sensor that detects the presence of a sound.
- Other sensors can actually discern relative values of a stimulus
 - Example: A sound sensor that detects the number of decibels present in a sound.
- Sensors are used in everyday objects such as touch-sensitive elevator buttons and lamps, which dim or brighten by touching the base. Applications include cars, machines, aerospace, medicine, manufacturing and robotics

Robot itself, e.g., LEGO NXT Robot (Taskbot)

- In addition to the sensors and computer, the robot has a ‘body’ consisting of a chassis, motors, and wheels
- A robot uses all its components to function reliably, i.e., it receives input from a sensor and reacts to it. For example a LEGO taskbot can be programmed to ‘backoff’ when it nears a wall. This is implemented by using a touch sensor which informs the robotic computer that it is near a wall. The robot then makes the decision to reverse its motors so that it moves backwards. A LEGO taskbot can be programmed in this manner to be autonomous much as a human being.

NOTE: This table is included in the powerpoint presentation version of this lesson.

	Human	NXT Robot
Parts	The main parts of the human body include the brain, nerves, muscles, bones, and sensors/receptors of the body.	The main parts of an NXT robot include the computer brick, the wires, the motors, the Lego building pieces, and the NXT sensors

Decision making	The human brain makes decisions about what the body will do next	The NXT computer brick reads the program its running to find out what to do next
Sending information	<p>The brain sends signals through the nerves of the body to tell parts of the body what to do.</p> <p>Sensors in the body send signals to the brain to give it information about what they experience. (Ears send signals to the brain if they hear a sound. This signal also tells the brain whether the sound was loud or soft, high pitched or low pitched)</p>	<p>The NXT computer brick sends signals through its wires to the motors to tell the robot where to go/ what to do. It also can send signals to its lamp to turn it on or off.</p> <p>Sensors of the NXT send signals through its wires to the NXT computer brick to give it information. (The touch sensor tells the brick whether something has bumped it or not)</p>

NOTE: This table compares the concept of Movement between humans and NXT Robots. This table is included in the powerpoint presentation version of this lesson.

Example: Movement	Humans	Robots (e.g., NXT)
Step 1:	Brain decides to walk	NXT computer brick reads program command to move
Step 2	Brain sends signals through the nerves to the muscles commanding them to move	NXT computer brick sends signals through the wires to the motors, commanding them to move.
Step 3:	Muscles contract, making the body move	Motors rotate, causing the robot to move
Step 4:	Brain decides to stop	NXT computer brick reads program command to stop
Step 5:	Brain sends signals through nerves to the muscles commanding them to stop	NXT computer brick sends signals through the wires to the motors, commanding them to stop.
Step 6:	Muscles stop contracting	Motors stop moving

PART 2: The Brain is a Computer (Optional advanced lesson)

Computer

- What is a computer made up of (refer figure below for numbers listed in parenthesis)?
 - There is a hard disk (3), power supply (1), a processor (10), memory (6), wires (2), keyboard, a mouse and a monitor (11).
- What can we do with a computer?
 - They help us perform every day activities such as doing homework (calculators, word processing), playing video games, running software programs, communication (chat, email, cell phones), vehicles, traffic regulation, aircraft, space vehicles and satellites, just to name a few.

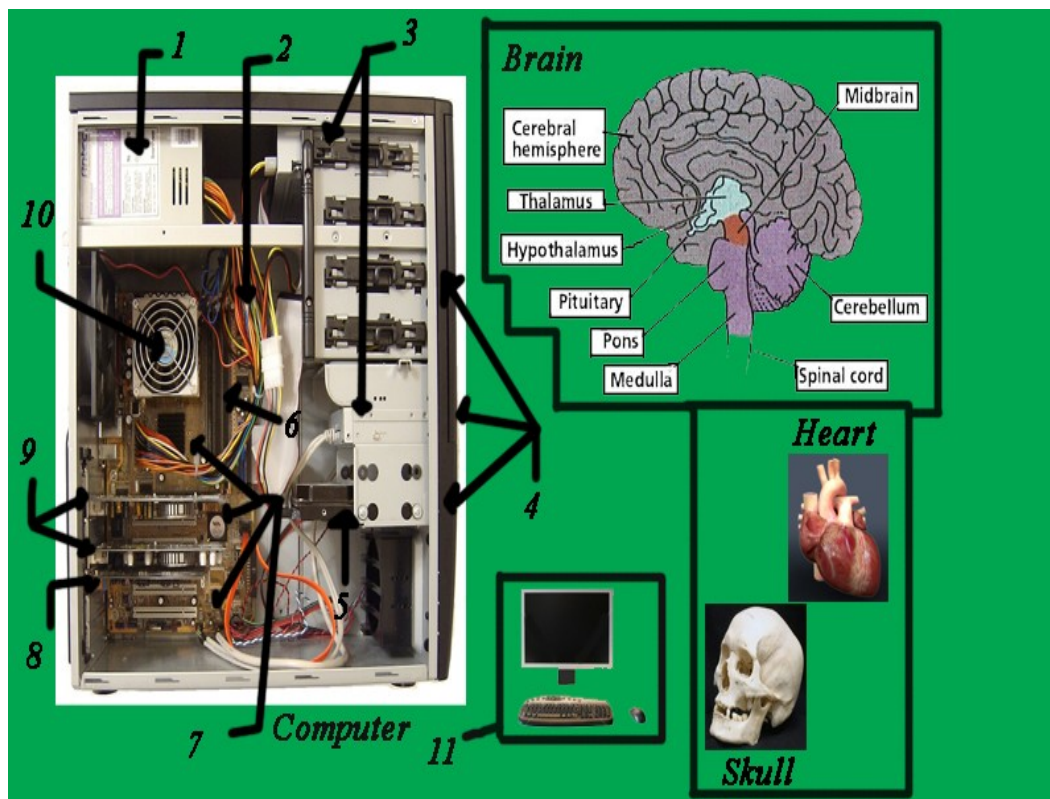


Image 2

ADA Description: Picture of the inside of a computer and relating it to drawings of the brain, heart and skull

Caption: none

Image file name: computer_part_brain_heart_skull.jpg

Source/Rights: None

Brain

The spinal cord sends information back and forth from the senses to the brain and vice versa. Finally, the brain integrates this information, thus, providing you with a complete picture of your surroundings. All your thoughts, functions and memories originate in the brain. The brain is the most important organ of our nervous system. **REFLEX!**

Word	Definition
Cerebrum	The largest part of the human brain, associated with higher brain function such as thought and action.
Medulla	It is responsible for maintaining vital body functions such as breathing and heart rate.
Midbrain	It is involved in functions such as vision, hearing, eye movement, and body movement.
Pons	It is involved in motor control and sensory analysis.
Thalamus	The structure has sensory and motor functions. Almost all sensory information enters this structure.
Hypothalamus	The structure is involved in functions including homeostasis, emotion, thirst, hunger, circadian rhythms, and control of the autonomic nervous system.
Cerebellum	This structure is associated with regulation and coordination of movement, posture, and balance.
RAM	Random access memory responsible for storing information that the computer is currently processing.
CPU	Central processing unit used by the computer to execute instructions.

NOTE: This table is included in the powerpoint presentation version of this lesson.

<u>Brain-related Structure</u>	<u>Function</u>	<u>Computer-related-Structure</u>
<i>Glucose provided by blood</i>	Supplies energy necessary to perform functions	<i>Electricity provided by Power Supply</i>
<i>Nervous System</i>	Relays information between center and periphery	<i>Wiring</i>
<i>Skull</i>	Protects delicate systems	<i>Case</i>
<i>Cerebrum</i>	Data Storage	<i>Hard Drive</i>
<i>Cerebrum</i>	Short-term memory	<i>RAM</i>
<i>Hypothalamus and Cerebellum</i>	Maintains homeostasis and involuntary functions	<i>Motherboard</i>
<i>Pons</i>	Regulates Involuntary function controller	<i>Motherboard</i>
<i>Midbrain, Thalamus</i>	Relays information from sensory input to necessary location	<i>Motherboard</i>

<i>Cerebrum</i>	Converts data to a visual image	<i>Graphics card</i>
<i>Medulla</i>	Regulates vital involuntary functions	<i>CPU and Operating System</i>
<i>Blood Supply</i>	Cooling Agent	<i>Fan</i>
<i>Sensory organs, muscles allowing us to move</i>	Interactions with the world	<i>Monitor, keyboard, mouse, speaker, microphone, camera</i>
<i>Cerebrum</i>	Thought	<i>None</i>

Lesson Background & Concepts for Teachers

Teachers should be familiar with the basic parts of a computer like hard disk, motherboard, power supply and the sensors on an LEGO NXT robot, and parts of the brain. The How to build a LEGO NXT taskbot document and LEGO NXT software tutorial explains how to put together a LEGO NXT taskbot and the basic programming required for this lesson. Many components and functions of the human brain and body can be related to the components and functions of a computer and the sensors on an LEGO NXT robot. Different parts of the computer are used for memory storage, processing, etc., just as different parts of the brain perform those tasks. Sensors on an LEGO NXT robot allow it to interact with the environment similar to the ways the human body uses its senses. There is a connection between how engineers design computer components and robotic sensors and the parts of the brain, body, and senses that they are related to.

Supplementary information:

Interior components that make up a computer:

http://www.kids-online.net/learn/c_n_1.html

NXT robots and sensors:

<http://mindstorms.lego.com/eng/Overview/default.aspx>

Parts of the brain:

<http://serendip.brynmawr.edu/bb/kinser/Structure1.html>

Human body systems:

http://www.stcms.si.edu/hbs/hbs_student.htm

Associated Activities

TE Lesson Activity: Understanding human movement and Movement in Robots- How does it compare to movement by humans?

Lesson Closure

Part 1: Human is a Robot:

- Sensors on an NXT robot provide similar functions to the senses in our human bodies.

- Ultrasonic and light sensors are like our eyes.
- Sound sensors are like our ears.
- Touch sensors provide feeling like our hands and feet.

Engineers are always trying to develop sensors to be more like the senses in our bodies. There are also sensors that measure temperature, pressure, etc, like we can through feeling things with sensors in our skin. Engineers sometimes get design ideas for computers and robots from our own brains and bodies, and this makes them have a lot of similarities. Because of this the brain is like a computer.

Part 2: Brain is a computer:

The brain is like a computer. Many brain functions are similar to computer functions.

- There are parts of the brain that store information like memory in a computer.
- There is part of the brain that does calculations like a computer processor.
- The input and output components of a computer, like the monitor, speakers, mouse, and keyboard, provide a way to interact similar to your eyes, ears, mouth, hands, and feet.
- The heart is a power supply for the body like a computer has a power supply to make it run.
- There are many wires that connect the parts inside a computer just like a spinal cord sends information to different parts of the body.

Assessment

Pre-Lesson Assessment

Ask students about their knowledge of brain anatomy, computer parts, and NXT sensors.

Post-Lesson Assessment

Ask students about what they learned during the lesson. Ask for other examples of similarities between the brain and computers. Ask students what they might now want to learn about the brain and computers beyond the lesson.

Post-Activity Assessment

Use the jeopardy powerpoint. Alternatively could use the written format of post activity assessment. Solutions for the post activity assessment (written format) have also been provided.

Lesson Extension Activities

None

Additional Multimedia Support

- Are we like Robots? (ppt)

References

Barnard, Tommy Michael. Kids Online. Accessed March 3, 2009. http://www.kids-online.net/learn/c_n_1.html

LEGO.com. MINDSTORMS Overview. The LEGO Group. Accessed March 3, 2009. <http://mindstorms.lego.com/eng/Overview/default.aspx>

Brain Structures and Their Functions. By Serendip. Last Modified June 3, 2005. Accessed March 3, 2009. <http://serendip.brynmawr.edu/bb/kinser/Structure1.html>

Appendix C.2

How do human sensors work?

Subject Area(s): Life Science, Biology, Science and Technology

Grade Level: 5 (4-8)

Time Required: 45 min

Summary. This lesson highlights the similarities between human sensors and their engineering counterparts. This allows students to view the human body as a working system, and from the perspective of an engineer. Humans have recreated most of the human sensors in robots – eyes, ears, and sensors for temperature, touch, and smell.

Engineering Connection. A major component of biological engineering and neuroscience is the ability to see the human body as a functioning, controlled, system, similar to a robot. In particular, various parts of a computer are designed and function similar to the human body. Engineers get inspiration from human body systems to develop sensors and devices. More and more findings are showing that mathematical principles similar to those used in robotics are extremely useful or even necessary for a complete understanding of the functioning of the human body. With such fields as biological engineering, systems neurobiology, and biological engineering, engineers are becoming more and more involved in research involving the human body and in efforts to replicate the functioning of many of its systems, such as sensors and robots.

Engineering Category. Relating science concept to engineering

Keywords. Human body, brain, robot, sensor, neuroscience, LEGO

Educational Standards

- Science: Missouri 2005 Strand 8.1.B. a (grade 3,4,5)
 - Describe how new technologies have helped scientists make better observations and measurements for investigations (e.g., telescopes, electronic balances, electronic microscopes, x-ray technology, computers, ultrasounds, computer probes such as thermometers)
- Missouri 2005 Strand 3.2.C.g (grade 8)
 - Explain the interactions between nervous and muscular systems when an organism responds to a stimulus
- Missouri 2005 Strand 1.2.A.f,g (grade 6)
 - Identify receivers of visible light energy (e.g., eye, photocell)

- Recognize that an object is “seen” only when the object emits or reflects light to the eye

Missouri 2005 Strand 7.1.B.a (grade 4-8)

- Make qualitative observations using the 5 senses

Pre-Requisite Knowledge

- Knowledge of the parts of a computer
- Understanding of the senses of the human body
- Basic knowledge of types of sensors seen on robots

Learning Objectives

After this lesson, students should be able to:

- Begin to visualize the human body sensors from the perspective of an engineer
- Compare body sensory functions and related them to electronic sensors in a robot.
- Describe how human body sensors response to a stimuli is like a robot response to its sensors

Introduction / Motivation

NOTE: This section is meant for the teacher to impart information to the students. This information can be used along with the powerpoint slides provided for this lesson.

Various parts of the body contribute to the effective day to day functions. The focus of this lesson will be the interaction between the sensory organs of the body and the brain, and how similar the human organs are to sensors that are utilized in robots.

Is the fascinating engineering invention of a robot similar to a human? We explore this in the lesson plan, and provide engineering connections to the human body.

Sensors

- A sensor is a device that measures a physical quantity and transmits this measurement so that a computer, instrument, or observer can read it.
- Some sensors simply detect the presence of a stimulus –
 - Example: A sound sensor that detects the presence of a sound.
- Other sensors can actually discern relative values of a stimulus
 - Example: A sound sensor that detects the number of decibels in a sound.
- Sensors are used in everyday objects such as touch-sensitive elevator buttons and lamps, which dim or brighten by touching the base. Applications include cars, machines, aerospace, medicine, manufacturing and robotics

Human Sensors

Your sensory organs (eyes, ears, nose and skin) provide much needed information to make decisions. They work in a manner very similar to the working of sensors of an robot. Your brain uses the information that it receives from your sensory organs to make more informed decisions.

- There are five senses that we all are familiar with
 - Your eyes allow you to see the world.
 - Your ears allow you to hear sounds.
 - Your skin lets you feel objects through touch.
 - Your nose lets you smell the many scents present in the world.
 - Your tongue lets you taste.
- There are also other sensors in the body that we don't notice directly.
 - Sensors in the inner ear give the brain information about balance
 - Sensors in our muscles that let the brain know our body position.

Signal Transmission- Nervous system.

When the sensors of the human body detect a stimulus, they send this information through the nervous system to the brain. The nervous system contains two main parts. One is called the *peripheral nervous system*, which is a series of branches of single *nerves*. There are nerves that connect to every sensor in your body. They send signals to other nerves, which send signals to more nerves until the signal reaches the second part of the nervous system: the *central nervous system*. The central nervous system consists of your spinal cord and your brain. The spinal cord is made up of bundles of nerves that are surrounded by bones for protection. Once a signal from a sensor reaches the spinal cord, it is send up the cord until the brain, where the brain decides what to do based on the information received.

How do human sensors work?

1. How do our eyes work?

Have nice pictures/schematics to illustrate how each works, and then do the same for the engineering counterpart

<http://www.aoa.org/x6024.xml>

<http://www.cyh.com/HealthTopics/HealthTopicDetailsKids.aspx?p=335&np=152&id=1730>

http://wiki.answers.com/Q/Compare_the_parts_of_a_camera_to_the_human_eye

- Light is *refracted* or made to change directions by the *cornea*, the outermost part of the eye.
- This light is directed through the pupil, which is a hole through which it can pass. The surrounding muscular tissue contained in the *iris*, which is the colored part of the eye, controls the size of the pupil.

- The light that enters the back of the eye through the pupil is redirected by the eye's *lens*, which directs the light to nerves in the back of the eye that convert light into electrical signals. There are two main types of such nerves. Cones, which are concentrated in the middle of the eye, detect details and colors in good light. Rods, which are concentrated in the sides of the eye, detect the presence of objects in bad light.
- Cones and rods send electrical signals through the *optic nerve* to the brain.

2. How do our ears work?

<http://www.cyh.com/HealthTopics/HealthTopicDetailsKids.aspx?p=335&np=152&id=1463>

- Sounds that you hear are made up of *sound waves*, which are disturbances in the air, which vibrates. These vibrations travel through the air, as vibrating air causes air next to it to vibrate.
- Sound waves enter your ear canal and cause your eardrum to vibrate.
- The vibration of your eardrum is passed on through three structures called the hammer, anvil, and stirrup to a fluid-filled structure called the *cochlea*.
- Different pitches of sound cause different parts of the cochlea to vibrate.
- When the fluid in the cochlea vibrates, it moves little hairs that connect to nerve cells and send an electrical signal to the brain.

3. How do we feel using our skin?

http://www.medindia.net/know_ur_body/skin.asp

- Your skin contains millions of highly sensitive nerve endings that are able to detect several different types of stimulation. These include pressure, temperature, and pain.
- When these specialized receptors are stimulated, they send a signal through the nervous system to the brain, which then interprets it.

4. How do we smell using our nose?

<http://www.howstuffworks.com/question139.htm>

<http://videos.howstuffworks.com/howstuffworks/461-how-smell-works-video.htm>

- First, small particles of almost everything around us are present in the air. For example, when you open a pizza box, particles of the pizza enter the air around you, and enter your nose when you breathe in.
- These particles come into contact with a set of nerve endings in your upper nasal passage. These nerve endings send signals through other nerves to your brain, which is able to make sense of the smell
- You are able to distinguish between hundreds of different smells, while dogs can distinguish thousands.

5. How do we taste using our tongue?

<http://health.howstuffworks.com/taste.htm>

- Your tongue has several sensory receptors called taste buds that are able to detect one of five different flavors: sweet, salty, bitter, sour, and a taste called *umami*.
 - Umami is a flavor that is said to be present in many high-protein foods, such as meats, cheeses, tomatoes, and mushrooms, and is generally described as being a savory, meaty taste.
- These receptors are comprised of cells called *gustatory receptor cells*. These cells have hairs that detect taste from the food that you eat. These cells then send information through the nervous system to the brain, which detects the information as taste.
- Flavor is much more than just taste. It comprises taste, smell, texture of food, and even other sensations such as pain when you eat something spicy. Eating food with your nose blocked shows a marked decrease in flavor, even though the taste is the same.

NOTE: This table is included in the powerpoint presentation version of this lesson.

Human sensor	Equivalent Robot sensor
Eyes	Light sensor, Ultrasonic sensor
Ears	Sound sensor
Skin	Touch sensor
Smell	None
Taste	None

Lesson Background & Concepts for Teachers

Teachers should be familiar with the parts of a computer, the sensors on a robot (e.g. LEGO NXT Taskbot), and parts of the brain. Many components and functions of the human brain and body can be related to the components and functions of a computer and the sensors on a robot. Different parts of the computer are used for memory storage, processing, etc., just as different parts of the brain perform those tasks. Sensors on a robot allow it to interact with the environment similar to the ways the human body uses its senses. There is a connection between how engineers design computer components and robotic sensors and the parts of the brain, body, and senses that they are related to.

Supplementary information:

Human body systems: http://www.stcms.si.edu/hbs/hbs_student.htm

Parts of the brain: <http://serendip.brynmawr.edu/bb/kinser/Structure1.html>

NXT robots and sensors: <http://mindstorms.lego.com/eng/Overview/default.aspx>

Interior components that make up a computer: http://www.kids-online.net/learn/c_n_1.html

Associated Activities

None

Lesson Closure

The brain is like a computer. Many brain functions are similar to computer functions.

- The input and output components of a computer, like the monitor, speakers, mouse, and keyboard, provide a way to interact similar to your eyes, ears, mouth, hands, and feet.
- Sensors on a robot provide similar functions to the senses in our human bodies.
 - Ultrasonic and light sensors are like our eyes.
 - Sound sensors are like our ears.
 - Touch sensors provide feeling like our hands and feet.

Engineers are always trying to develop sensors to be more like the senses in our bodies. There are also sensors that measure temperature, pressure, etc, like we can through feeling things with sensors in our skin. Engineers sometimes get design ideas for computers and robots from our own brains and bodies, and this makes them have a lot of similarities. Because of this the brain is like a computer.

Assessment

Pre-Lesson Assessment

How do human sensors work – pre-assessment sheet (doc)

Post-Lesson Assessment

Post lesson assessment several formats.

- a. How do human sensors work – post-assessment sheet (doc)
- b. How do human sensors work– jeopardy format (ppt)

Lesson Extension Activities

None

Additional Multimedia Support

How do human sensors work powerpoint can be projected in class to teach the lesson.

References

Barnard, Tommy Michael. Kids Online. Accessed March 3, 2009. http://www.kids-online.net/learn/c_n_1.html

LEGO.com. MINDSTORMS Overview. The LEGO Group. Accessed March 3, 2009. <http://mindstorms.lego.com/eng/Overview/default.aspx>

Brain Structures and Their Functions. By Serendip. Last Modified June 3, 2005. Accessed March 3, 2009. <http://serendip.brynmawr.edu/bb/kinser/Structure1.html>

Appendix C.3

Development of LEGO Robotics Camp and Activities

Abstract

The InSITE (Incorporating Science, Industrial Technology, and Engineering) Team at the University of Missouri–Columbia supported by a National Science Foundation grant brings engineering graduate students into the classroom in surrounding schools in Mid-Missouri. These graduate student fellows increase children’s interests in science, industrial technology, and engineering through innovative, hands-on engineering design projects designed to challenge students in a fun and educational approach. Intern graduate students are given the ability to practice and refine skills in pedagogy and team-building. Teachers benefit by working with an engineering graduate student, an expert in engineering concepts, and who can help incorporate engineering standards into their curriculum. In just our second year we have had overwhelming success and positive feedback from all that’s involved including the fellows, teachers, students, and the community. In an effort to sustain this program for future years we have put together a plan to run a robotics camp throughout the year as a profit generating approach to fund graduate and undergraduate students for the continuation of this program in local schools. This paper will describe the foundation for our plan for the future development and implementation of the sustainable program.

Introduction

As the National Science Foundation website states, the GK-12 Fellowship program is designed to:

“... provides funding to graduate students in NSF- supported science, technology, engineering, and mathematics (STEM) disciplines to acquire additional skills that will broadly prepare them for professional and scientific careers in the 21st century. Through interactions with teachers in K-12 schools, graduate students can improve communication and teaching skills while enriching STEM instruction in K-12 schools. Through this experience graduate students can gain a deeper understanding of their own scientific research. In addition, the GK-12 program provides institutions of higher education with an opportunity to make a permanent change in their graduate programs by incorporating GK-12 like activities in the training of their STEM graduate students. Expected outcomes include improved communication, teaching and team building skills for the fellows; professional development opportunities for K-12 teachers; enriched learning for K-12 students; and strengthened partnerships between institutions of higher education and local school districts.”

Graduate fellows at the University of Missouri-Columbia come from backgrounds in Electrical/Computer Engineering, Mechanical Engineering, and Biological Engineering and most are currently working on their PhD degrees. They currently spend about 10

hours in a classroom at a local school each week observing lessons, aiding the teachers, and teaching lessons. We hope to increase awareness and content of engineering in K-12 education, an area that has been presently lacking in the United States.

We have currently focused our efforts on middle school grades 6 – 9, but have ventured into both the elementary school and the high school. Our program is closely based off the work of Tufts University in Massachusetts, where they run an educational outreach program involving both the GK-12 Program and STOMP (Student Teacher Outreach Mentorship Program). They have been working for several years on not only educational outreach, but also product development like the Robolab software, a service component involving workshops for teachers and camps for kids, and an engineering education section compiling research on their efforts. They have been some of the pioneers in using LEGO Mindstorms as a gateway to teaching engineering principles in the classroom.

We have also chosen to use the LEGO Mindstorm Robotics Kits as a tool in the classroom to base hands-on engineering design projects for lessons to teach engineering concepts. These lessons are fun and provide the students with experience implementing the engineering design process as stated by the Massachusetts Department of Education (Massachusetts Dept of Ed). They work in teams and concentrate on solving problems that have real-world applications. It is said that the LEGO materials are a great platform for introducing young children (ages 5-8) to science and engineering concepts (LEGO Engineering Website). Our goal here is to spark interest among children to pursue a career in engineering and use skills in math and science to gain an understanding of how to use engineering.

Many of the teachers in our school have little background in engineering concepts and the importance of the engineering design process. With the help from engineering graduate fellows working along side the teacher new lessons and an enhanced curriculum can be developed. Tufts has documented the fellow's role with the teacher is said to be that of a support mechanism, providing help with hands-on projects, resolving technical issues with equipment, answering engineering questions, doing research on topics, and helping to brainstorm activities (Portsmore - STOMP).

As stated in the above synopsis of the NSF GK-12 project the focus of this program really is on developing the fellow's skills in pedagogy and team-building. It is an experience for the fellow that provides opportunities for them to practice communication and teaching skills. The work of the InSITE team at the University of Missouri-Columbia has made a significant impact on the professional development of the fellow, the educational system, and the community as a whole. The NSF grant will support 3 years of funding for this project and it is our job to find a sustainable support structure to implement this program in the future. This paper will document our work thus far in creating a profitable LEGO Robotics Camp to fund graduate and undergraduate students to go into the classroom after the grant is over and describe future considerations in implementing this plan.

Current Work

The objective of the InSITE LEGO Robotics Camp is to create a profit generating support structure to fund graduate and undergraduate students as to sustain the NSF GK-12 program in local schools in Mid-Missouri. The plan is to run camps during the summer and during winter and spring recess for 3 day segments giving parents options for childcare. The length of the camp might be longer during the summer. The best date will be selected during the two recesses considering dates that children will be out of school and parents might still have to work and away from potential travel days around the holidays. The dates must be finalized at least 3 months prior to the camp. It will most likely last for 6 hours (9:00 am – 3:00 pm) and be held at the University of Missouri-Columbia Campus. We will target children in grades 4th – 7th, but will probably offer an advanced camp over the summer for grades 8th – 12th. The cost for 3 day camp will be \$300 and includes lunch and a CD containing materials from the camp, the students programs, and pictures. The cost was based on similar camps taking place around the country and on estimates of our profit goal.

Further information on current camps can be found on the programs website at <http://ww.missouri.edu/~engk12/>. The camp will focus on learning about LEGO Engineering by building and programming robots using LEGO Mindstorms in fun, hands-on, real-world problem solving activities. Instructors will be graduate and undergraduate students in engineering at the University with professional experience in robotics. Students of all abilities are welcome to learn by working in small groups to design and build working robots and program it to perform tasks. The proceeds from the camp will benefit the sustainability of the InSITE program in local schools in Mid-Missouri by providing equipment and funding for engineering students expertise in the classroom. The University of Missouri-Columbia, National Science Foundation, and the Schools will not gain any monetary profit from these camps.

Engineering students taking part in running the camps and visiting classrooms at local schools will be compensated for their time through an account setup with the University of Missouri-Columbia titled “InSITE Robotics Team.” To enable the InSITE robotics camp to be able to hold LEGO camps across the year and to generate revenue for the program, it is essential to setup a formal account for the camp that will be responsible to collect funds. In this regard, we sought help from the accounting and the grants department at the University of Missouri-Columbia. We filed a formal application to the department of accounts indicating the need and the purpose for obtaining and running such an account. The account shall be a place to deposit cheques obtained from students who attend these camps. The money generated through these means will be expended for purposes such as advertising for future camps, buying equipment and other articles necessary to run such future camps. Also, the income generated will be used to compensate for salaries for those who work and act as trainers during the camp. Under no circumstances will any funds be diverted for personal usage. Under the able guidance of Satish Nair, Dianne Robinson and Monica Frank efforts to set up an account for these purposes is underway.

We plan to advertise for these positions and pay approximately \$10.00 per hour and work around 10-20 hours per week with around 5-6 students in the program. The actual numbers will depend on the amount of profit generated from the camps and will have to be carefully budgeted. Engineering student workers will need to have experience working with robotics using the LEGO Mindstorms and take part in a short workshop to aid in developing teaching skills and going over logistics for the camp and classroom activities. Continuing student workers will take part in meetings to discuss successes and failures, ways of improving the camp, and continued training.

Other logistics include obtaining resources for the camp which include securing a room, kits, computers, and funding. All resources are based on approximately 24-36 children attending the camp and 5-6 instructors. In our efforts so far the University of Missouri-Columbia has been very helpful in providing a room in the engineering building on campus to run the camp for no charge. We would require a space with a common area and two rooms to split the 24-36 children based on ability level that would include tables to work on, a whiteboard, and a media projector. Equipment requirements would be 15 LEGO Mindstorm kits which can be borrowed from Jim Fisher, Electronic technician, Electrical and Computer Engineering Department. Additionally 13 Laptops would be needed that include in the Robolab and Science Investigator software and the room would need to have enough outlets to accommodate this many computers. Laptops could be borrowed from the Educational Department. Our contact is Dr. John Lannin (lanninj@missouri.edu). Initial funding might come from the current NSF GK-12 Project to pay for advertising, equipment, and other miscellanies. We have developed the following financial plan listing our expected incomes and expenses.

Item	Income	Expenses	Total Profit
Camp Fee (24 students at \$300 ea.)	\$7,200.00		
Food (\$5 day for 3 days, 24 students)		\$360.00	
Instructors Pay (\$10 hour for 7 hours for 3 days, 4 instructors)		\$840.00	
Advertising (Printing, Newspaper)		\$60.00	
Misc. (Napkins, Plates, Cups)		\$20.00	
Insurance		\$100.00	
Batteries		\$20.00	
Total	\$7,200.00	\$1,400.00	\$5,800.00

The current estimates based on 24 children attending would generate profits near \$5,000 for a single 3 day camp and running this camp 5 times a year (winter, spring, and 3 during the summer) would generate a yearly profit of \$25,000. This could help fund approximately 6-8 graduate and undergraduate students around 10 hours a week in the local schools for the school year (36 weeks). Other logistics include providing lunch, advertisings, and a schedule for the camp. We thought the best option for lunch would be pizza, sub sandwiches, and hamburgers. The estimated cost would be about \$5.00 a person which would be provided to the children and instructors. It should be noted that we should provide special arrangements for any participant who needs them. Napkins, plates, and cups would be included in miscellanies expenses and should cost about \$20.00. Other expenses that may arise will be added to the misc. category.

We have also developed a distribution plan for advertising for the camp and for instructors. We plan to begin advertising for the event as early as three months before the date. We will need instructor confirmations 2 months prior to the event and will take registrations from participants up to 1 month before the event. The advertisement for instructors will be posted around the engineering building and will also be directed to certain classes and individuals involved in robotics. We will target the schools in our target age range for the camp in local schools around Mid-Missouri, contacting teachers and principals to help in supporting us. Approximately 5 color flyers for the camp will be supplied to each school along with as many registration forms that are requested which will need to remain in the office of the school and picked up by the student or parent individually. Unfortunately no email will be able to be sent out to parents as this is not a school sponsored program. The schools and teachers can make announcements and instruct the student where they get further information on our camp. We have also planned on advertising in the community (i.e. newspaper, television, radio, stores, etc.). In all cases we would like to direct them to our website link containing again a printable flyer, registration form, and further information on the camp and our program. A copy of the flyer and registration form is contained in the appendix of this document.

The preliminary schedule of the camp is below:

Day 1

- 8:30 – 9:00 Instructors arrive to setup room and help with kids arriving (laptops on and working, kits out, plan for day, registration, payments)
- 9:00 – 9:20 Introductions of instructors, plans for the week (Presentation – Intro to LEGO Robotics and Engineering)
- 9:20 – 9:40 Introduction to LEGO pieces, Building skills, questions (group students based on 3 levels i.e. beginner, moderate, advanced)
- 9:40 – 10:30 First Design Challenge – Simple Build (like a structure for example) (No programming or RCX)
- 10:30 – 11:00 Present build to class – Talk about what they did, good things, and how they can improve
- 11:00 – 12:00 Build a sturdy car
- 12:00 – 12:30 Lunch
- 12:30 – 1:00 Present cars to class (again talk about good things, and improvements)
- 1:00 – 1:30 Introduction to Robolab, Pilot, trouble shooting
- 1:30 – 2:50 Build a car to do something, Design Challenge, Make turns, go forward then back up
- 2:50 – 3:00 Recap day, clean up and adjourn

Day 2

- 9:00 – 9:30 Robolab and Sensors, inventor
- 9:30 – 11:30 Design Challenge – with sensors
- 11:30 – 12:00 Share Designs
- 12:00 – 12:30 Lunch
- 12:30 – 1:00 Gears
- 1:00 – 2:50 Design Challenge – Gears

2:50 – 3:00 Recap day, clean up and adjourn

Day 3

9:00 – 9:30 Robolab – Jumps and Lands, Loops

9:30 – 12:00 Begin Final Design Challenge – Obstacle Course

12:00 – 12:30 Lunch

12:30 – 2:30 Finish and have competition of Final Design Challenge – Maybe have parents come at 2:00 to watch

2:30 – 3:00 Present Awards, Clean up, Adjourn

The schedule will be revised for each camp depending on feedback and instructor suggestions. Also we want to provide more than what is offered in only the classroom setting and don't want to mimic any of the same lessons that the children might have already done. There will also be a few versions depending on the ability level of the children with more advanced or easier challenges within each activity. This is only a preliminary schedule and the final schedule will be made 1 month prior to the camp and be posted on the website with additional information based on input from the instructors.

Additional considerations for the camp are targeting local schools PTAs (Parents Teachers Associations) and local business (suggestions from Craig Adams and Sara Torres) to gain sponsorship to provide funding to children who might not be able to afford the price but have considerable interest in LEGO engineering. We could have teachers nominate outstanding students and select children based on interest and need. Many teachers have made us aware that the price might be too high for the children in their school to afford. Another issue is that we will need to provide insurance for the children while they are on the Universities campus.

The objective of the InSITE Lego Camp is to encourage further and continuing involvement of the students and the fellows in sustaining interest of schools in the Mid-MO area in robotics and similar projects. The camp intends to target elementary and middle school kids with the focus remaining to incorporate a scientific approach to playing with robots. Highly competent students from the university with an engineering background are hired to be organizers and staff during this camp. Besides, an effort is also made to include people who have the background of dealing with kids.

It was decided about a month before the camp planned for December 2006 to cancel it and wait until either Spring Recess 2007 and/or the summer of 2007. The decision was made because of lack of time left to ensure a successful camp. This document includes the work accomplished thus far and acts as the foundation for a support mechanism to sustain the GK-12 InSITE Program for many years.

Difficulties

Many of the difficulties encountered in setting up the first camp arose in the last few months before the camp was to take place. The flyer was delayed from its expected date to be posted by about 2 weeks and two of the major coordinators were not going to be in town during the event. We also ran into problems with our account not being fully setup.

Lastly there were more implications involving the local schools connection with this event that had to be figured out than expected. These difficulties will be taken care of in the near future, as we now know that it will take more time and planning to run a successful camp.

Future

While significant progress has been made in the creation of InSITE LEGO Robotics Camp as a sustainable support structure for the GK-12 Program, our future plans are to set up a time table with deadlines to have certain tasks accomplished. As well we would like to work with teachers and administrators in the local schools to adhere to all rules involving using names and advertising. Lastly we would like to get the community involved in sponsoring needing children to attend the camp, making this open to all children that are interested.

Acknowledgements

The authors would like to thank all supporters of our program including participating teachers in local schools, the University of Missouri-Columbia, and engineering students and coordinators involved in the GK-12 program.

References

Portsmore, Meredith; Rogers, Chris; Pickering, Melissa. **STOMP: Student Teacher Outreach Mentorship Program.** Tufts University. *Proceedings of the 2003 American Society for Engineering Education Annual Conference & Exposition.*

Massachusetts Department of Education, **Technology/Engineering Curriculum Frameworks** - Spring 2001 http://www.jets.org/programs/nedc/nedc_edp.pdf

LEGO Engineering Website. **Center for Engineering Educational Outreach, Tufts University and LEGO Education.** 2006. <http://www.legoengineering.com/>

FIGURES

The poster features a background of a blue circuit board with various components and text like 'Crystal LAM', 'CS9000', and 'K1AGSD00'. A yellow LEGO Mindstorms robot is on the right, and a red LEGO logo is on the left. The text is in various colors and fonts, including red and white with black outlines.

University of Missouri

InSITE LEGO Robotics Camp

Spring Recess / Summer 2007
3-Day Camp

Students will build and program robots in fun, hands-on, real world problem-solving activities using LEGO Mindstorms. Cost: \$300 (includes lunch)

**For More Information contact:
Ashwin Mohan at 573-884-1430 or
Craig Weilbaecher at 573-884-9158**

**Send registration and payment to:
InSITE Robotics Team
University of Missouri-Columbia
135 Engineering Building West
Columbia, MO 65211
Registration and payment due by:
To be announced**

**Download a registration form at:
<http://www.missouri.edu/~engk12>**



GK12 Fellows Program

University of Missouri InSITE LEGO Robotics Camp

Come learn about LEGO engineering by building and programming robots using LEGO Mindstorms in fun, hands-on, real world problem solving activities. Instructors will be MU engineering students with professional experience in robotics. Students of all ability levels are welcome to learn by working in small groups to design and build a working robot and program it to perform tasks.

Date & Time: December 20 - 22, 2006
9:00 am - 3:00 pm

Location: University of Missouri Columbia
Laffere Engineering Building (East)
Time Capsule Room

Open to: Grades 4th - 7th

Cost: \$300 (Includes Lunch and CD)

More Information at: <http://www.missouri.edu/~eng12/>

Contacts:

Ashwin Mohan 573-882-1430 amgc5@mizzou.edu
 Craig Weibaecher 573-884-9158 cwwe06@mizzou.edu
 Dr. Satish Nair 573-882-2964 NairS@missouri.edu

Send Registration and Payment to:

InSITE Robotics Team
 University of Missouri-Columbia
 135 Engineering Building West
 Columbia, MO 65211

Registration and Payment due:
 December 8, 2006

Proceeds:

Currently engineering students from MU have been put in local classrooms in grades 6th - 9th as part of the Engineering GK-12 Fellowship Program sponsored by the National Science Foundation. Proceeds will benefit the sustainability of this program in years to come providing equipment and engineering expertise in the classroom.

"Space is limited and will be on a first-come, first-served basis"



The program is partially supported by the National Science Foundation GK-12 Fellow Program and the University of Missouri-Columbia. No profit will be taken from the proceeds of this camp.

Detach this Portion and Send with Payment

Students Name _____ Gender _____ Grade _____
 School _____ Teacher _____
 Street Address _____ Apt. _____
 City & State _____ Zip Code _____ Telephone _____
 Parent/Guardian Name _____ Daytime Telephone _____
 Parent/Guardian Email _____ Emergency Telephone _____

TABLES

Teacher Survey

Questions

Is this the right age group to target?

What length in days/time is appropriate?

Are your kids able to afford this price?

With the holiday, what would be the best date to hold the camp?

What kinds of experience would you want your kids to get out of this?

About how many students do you think would be interested in this camp?

Comments/Suggestions?

Summary

- 11 said age target is good, 2 suggested adding 7th grade, 1 thinks upper grades
- 8 agreed with 9 -3 time and 3 days, a few said start a little earlier and end later for working parents, some said 4 days
- 5 yes responses to price, 10 no responses, (some said both), Scholarships!!
- Almost all (7) said Dec 20 – 22, 1 said after Christmas, 1 said Dec 21 – 23
- Experience – read below, but most said fun, hands-on, learning, programming
- I counted about 60 kids would seem interested from just these schools
- Suggestions - Scholarships, P.T.A., ways to bring cost down

Distribution Plan for Flyer

Print 250 Copies (Registration Form) 100 Copies (Flyer)

Millcreek – 50 and 5

Gentry – 40 and 5

Smithton – 40 and 5

Lange – 40 and 5

Hallsville - 20 and 5

Moberly – 20 and 5

Others – xx and 5

Radio Stations

101.5

102.3

106.1

106.9

TV

KOMU

Local

Walmart

Toys-R-Us

Columbia Mall

How to run the LEGO Camps

Typical Dates: Thanks giving: Nov (3rd week), Winter Break: Dec (3rd or 4th week), Spring Break: March (3rd week), Summer: May (4th week), June and July (all weeks)

Also,

Obtain DATES for Fall and Spring at the end of summer (Check CPS website) **AND**
Obtain DATES for Summer in November –Program Coordinator

Avoid:

Mizzou Football game weeks (homecoming etc.)

2 Months Prior to Camp:

- Update Website with camp dates –Webmaster
- Upload revised flyer on website – Webmaster
- Send email to mailing list –Program Coordinator
- Update the Excel sheet (create new sheet with camp dates/fields) –Program Coordinator
- Confirm Room (W 1004 Laffere) –Program Coordinator
- Send out email to instructors with camp dates – Program Coordinator
- Put out an advertisement on Wednesday and Sunday in the Columbia Tribune. – Program Coordinator

1 Month Prior to Camp

- Update participant list based on entries and drop off checks to Claudia Lynch (only if 5 or more have registered for a camp) –Program Coordinator
- Put out an advertisement in the Missourian if intake is low–Program Coordinator
- Send a reminder out to the camp instructors –Program Coordinator
- Confirm Room reservation (Preferred W1004, **Or** Lafferre hall/ Ketcham Auditorium) **Or** Kauffman Camps (MU Stotler or Black Culture Center)– Program Coordinator

2 Weeks Prior

- Update participant list based on entries and drop off checks to Claudia Lynch (only if 5 or more have registered for a camp) –Program Coordinator
- Finalize camp schedule and distribute tasks to instructors –Program Coordinator
- Get paper work done for Insurance–Program Coordinator
- If camp is FULL, send email to instructors to meet a week in advance to discuss any changes, etc –Program Coordinator
- Take inventory (For 3 day camps: 1.5” folders, CD, sleeves, Certificates, print outs) –Program Coordinator + Main Instructor
- Arrange items to make a taskbot in individual kits, sensors need to be sorted out along with their pieces –Main Instructor + Camp workers

1 Week Prior

- If Camp has more than 5 entries, send confirmation email to parents –Program Coordinator

- Arrange for keys, cart, and supplies (2x4's, black tape, tape measure etc) – Program Coordinator
- Organize LEGO kits –Program Coordinator
- Buy snacks and drinks from Walmart for One day camp (typically chewy bars and Tropicana juice) – Program Coordinator
- Prepare check-in sheet–Program Coordinator
- Ensure camera is available –Program Coordinator
- Ask Shirley/Claudia to order Pizza for day 1 of the camp. Usually 2-3 slices per participant + instructors –Program Coordinator

First Day of the camp (Things to do)

- Main Instructor and camp workers to arrive 1 hour prior to start
- Setup room so that a table has no more than 2-3 students.
- Arrange 1 kit and laptop per team/table
- Main instructor to greet parents and Check the kid in.
- Ensure to have a camera around and take lot of pictures
- Have extra copies of Photo release forms
- Take lunch orders for other two days (Heavenly Ham and Jimmy Johns) and give it to Shirley/Claudia. Save all receipts –Program Coordinator

Final Day of the camp

- Update pictures folder and burn CD's –Main Instructor
- Interface with parents and ensure that they are 'satisfied' with all aspects of the camp. Announce future camp dates and inform that they will be on a mailing list – Program Coordinator

After the camp

- Send a thank you email to parents and get their response to the camp–Program Coordinator

NOTES:

1. Lunch order: Shakespeares Pizza/ Papa Johns: Usually 3 slices per person, Ask to make 10 slices per pizza, Typically Pepperoni, Meat lovers, Cheese, Veggie
2. Heavenly Ham boxed lunches: Sheets available with Shirley/Claudia.
3. Jimmy Johns: Get order from all the kids by going to the online menu during lunch hour.
4. Usually order bottled water with the lunches
5. Take stock of paper plates, napkins, CD's, Pencils, Print outs etc before start of camp.

How to run the Annual ROBOTICS CHALLENGE

4 Months Prior to Challenge: (November)

1. Need to obtain dates for the event (Check websites or call CPS, and other private schools to check for holidays, also, check community calendars for other events that might create conflicts for parents & kids) – Program Manager & Fellows
2. Decide on the age group, maximum number of students and the grades that will be targeted. Ideally, 1-3, 4-6 – Fellows
3. Prepare outline of course, type of challenge, sensors to be used, material required to replicate course, and point system – Fellows
4. Make the course drawing and get approval from committee and teachers - Fellows
5. Set deadline for registration and team size - Fellows
6. Confirm the space/location for conducting the event, time, intake number prior to preparing the flyer – Program Manager
7. Update the Robotics Challenge event document, course challenge, point system and send out via email to schools (be as specific as possible about the rules and point system) - Program Manager and Fellows
8. Update Programming rubric and develop a rubric for the course - Fellows
9. Prepare the flyer and provide, email address, phone number of contact person – Program Manager
10. Update the website with Flyer, and registration form – Program Manager
11. Inform Teachers and ask them to spread the word – Program Manager

1 Month Prior to Challenge (February)

1. Prepare the challenge course and make any corrections required. Any change in course or the scoring should be communicated to the participants - Fellows
2. Prepare Excel sheet with all pertinent information. Fields should include name, school, Teams, contact information, etc – Program Manager
3. Send a reminder email teachers and inform them about any additional information required (number of teams and participants) - Program Manager
4. Organize for categories to be awarded. Organize for gifts to be given – Program Manager

2 Weeks Prior to Challenge (March)

1. Advertise the camp. Contact Jan Fales or Laura Forbes at MU – Program Manager
2. Distribute tasks to volunteers and reconfirm location - Program Manager + Fellows

1 Week Prior to Challenge:

1. Arrange for timers, microphone, rope to cordon area, print outs, certificates, and ASEE print out - Program Manager + Fellows
2. Reminder email to participants with final date, venue, registration and event start times – Program Manager
3. Get name labels printed off for Fellows and Students – Program Manager
4. Prepare the sign up sheet – Program Manager

5. Organize for camera – Program Manager
6. Organize for snacks, drinks, and gift cards – Program Manager
7. Print out rubric for programming judges – Fellows
8. Organize for post it pads, pens and scrap paper for judges – Program Manager
9. Transport course(s) to the challenge location - Fellows

During the Challenge:

1. Arrive one hour prior to start of event - All
2. Set up course - Fellows
3. Post the relevant flyers – Program Manager
4. Set up registration desk, and emcee microphone - Fellows
5. Project rules and cordon area near course - Emcee
6. Discuss the event with judges and arrange meeting prior to giving away prizes
7. Recognize all who participated - Emcee

After the Challenge:

1. Send a thank you email to parents and teachers for supporting the event – S.Nair
2. Update Robotics Challenge Document
3. Collect pictures and upload on website

Appendix D

Publications, Conferences and Other Presentations

Book Chapter

- **Mohan, A;** Pendyam, S; Li, G; Kalivas, P; and Nair, S.S. Computational models of neuronal networks – Modeling neuroplasticity in Glu transmission due to cocaine. Chapter in *New Research on Neuronal Networks*, Yoshida and Sato (Eds.), Nova Science Publishers, New York, pp. 65–107, 2008. ISBN: 978–1–60456–561–4.

Refereed Journal Articles

- Pendyam, S*; **Mohan, A***; Kalivas, P; and Nair, S.S. Computational model of extracellular glutamate in the nucleus accumbens incorporates neuroadaptations by chronic cocaine. *Neuroscience*, vol. 158, pp: 1266–1276, 2009. (* – Authors contributed equally to the research).
- **Mohan, A;** Pendyam, S; Kalivas, P; and Nair, S.S. Molecular diffusion model of neurotransmitter homeostasis around synapses supporting gradients. Submitted to *Neural Computation*.
- Pendyam, S; **Mohan, A;** Kalivas, P; and Nair, S.S. Role of perisynaptic parameters in neurotransmitter homeostasis – A computational study of a general synapse. Submitted to *Journal of Neurocomputing*.
- **Mohan, A;** Merle, D.M; Jackson, C; Lannin, J; and Nair, S.S. Professional skills in the engineering curriculum. *IEEE Transactions in Engineering Education*. (In press).

In preparation

- **Mohan, A***; Ramaswamy, K*; Catanho, M; Nair, S.S; and Cocroft, R. Computational model of information transfer in a group–living insect predicts underlying rules for emergent behavior. (* – Authors contributed equally to the research).
- **Mohan, A;** Chen, Y; Li, G; Quirk, G; and Nair, S.S. Computational model predicts formation of distinct groups of neurons in the basal amygdale with fear conditioning.
- **Mohan, A;** Franklin, C; Merle, D.M; Lannin, J; and Nair, S.S. An evaluation of graduate student perceptions of the professional and soft skills: A comparative study between engineering, education and biology.
- **Mohan, A;** Franklin, C; Lannin, J; and Nair, S.S. Teaching professional skills to graduate students.

Conference papers and abstracts

- **Mohan, A;** Pendyam, S; Enke, B; Kalivas, P; and Nair S.S. Stochastic model of glutamatergic PFC–NAc synapse predicts cocaine – induced changes in receptor

occupancy. Proceedings of the Dynamic Systems and Control Conference, Hollywood, CA, 2009.

- Borduin, R; Ramaswamy, K; **Mohan, A**; Cocroft, R; and Nair, S.S. Modeling the rapid transmission of information within a social group of insects—Emergent patterns in the antipredator signals. Proceedings of Dynamic Systems and Control Conference, Ann Arbor, MI, pp.1–7, 2008.
- **Mohan, A**; Gall, J; and Nair, S.S. Glutamate dynamics in the PFC–NAc synapse. Proceedings of ASME International Mechanical Engineering Congress and Exposition, Chicago, IL, pp.767–772, 2006.

Posters presentations by Mohan A

- **Mohan, A**; Pendyam, S; Kalivas, P; and Nair, S.S. Molecular diffusion model of glutamatergic PFC–NAc synapse during cocaine pathology predicts receptor occupancy. 39th Society of Neuroscience (SFN) Annual Meeting, Chicago, IL, November, 15–20, 2009.
- **Mohan, A**; Pendyam, S; Enke, B; Kalivas, P; and Nair, S.S. Stochastic model of glutamatergic PFC–NAc synapse during cocaine pathologies predicts receptor occupancy. Missouri life sciences week, Columbia, MO, April, 13–18, 2009. (Poster Abstract. W85).
- Pendyam, S; **Mohan, A**; Kalivas, P; and Nair, S.S. Molecular diffusion model of glutamate homeostasis and nucleus accumbens to study geometric configurations of perisynaptic glia and tortuosity. 38th SFN Annual Meeting, Washington, DC, November, 15–20, 2008. (Poster Abstract. 242.22/J5).
- Gall, J; Kalivas, P; and Nair, S.S. Modeling glutamate homeostasis in PFC–NAc synapse. 36th SFN Annual Meeting, Atlanta, GA, October, 14–18, 2006. (Poster Abstract. 189.23/MM92).

VITA

Ashwin Mohan was born December 24th, 1978 in Chennai, India. He received his Bachelors of Engineering (B.E.) from the University Of Mumbai, India in 2001. He received his Master of Science in Electrical Engineering and Doctorate of Philosophy in Electrical and Computer Engineering from the University of Missouri-Columbia in 2004 and 2009 respectively. His academic background includes Computational Neuroscience, Biologically realistic modeling, Nonlinear systems, Intelligent Control, Instrumentation and Process Control. His personal interests include music, travel, arts and photography.